The multifaceted role of AdipoRon, an adiponectin receptor agonist: tackling myosteatosis, sarcopenia and aging

Camille Selvais

Supervisor: Pr. Sonia Brichard

Endocrinology, Diabetes and Nutrition Unit (EDIN)
Institute of Experimental and Clinical Research (IREC)
Université catholique de Louvain

JURY MEMBERS

Supervisor

Pr. Sonia Brichard
Endocrinology, Diabetes and Nutrition Unit, Institute of Experimental and Clinical Research, Université Catholique de Louvain, Brussels, Belgium.

Jury president

Pr. Jean-Christophe Jonas
Endocrinology, Diabetes and Nutrition Unit, Institute of Experimental and Clinical Research, Université Catholique de Louvain, Brussels, Belgium.

Internal jury members

Pr. Isabelle Leclercq
Hepato-Gastroenterology Unit, Institute of Experimental and Clinical Research, Université Catholique de Louvain, Brussels, Belgium.

Pr. Louise Deldicque
Cellular and Molecular Division, Institute of Neuroscience, Université Catholique de Louvain, Brussels, Belgium.

Pr. Philippe Gailly
Cellular and Molecular Division, Institute of Neuroscience, Université Catholique de Louvain, Brussels, Belgium.

External jury members

Dr. Benoit Viollet
National Institute of Health and Medical Research, Institut Cochin, Paris, France.

Pr. Marco Sandri
Department of Biomedical Sciences, University of Padova, Padova, Italy.

Remerciements

Tout d'abord, merci Professeure Sonia Brichard pour votre encadrement fidèle et votre confiance au cours de ces années de doctorat. Vous m'avez appris à structurer mes idées, à prendre du recul (to see the big picture), à prioriser, à déléguer, à transmettre clairement mes résultats par écrit et à l'oral, ainsi qu'à affiner mon regard critique. Vous m'avez guidée avec flexibilité et disponibilité dans divers projets, aussi bien scientifiques qu'artistiques, et vous m'avez offert l'environnement idéal pour réaliser mon doctorat dans les meilleures conditions. Je tiens à vous remercier aussi chaleureusement que l'était votre « ça va ma belle ? » ou votre petite tape de la main sur mon épaule.

Merci à vous, membres du jury, Professeur Jonas, Professeure Deldicque, Professeur Gailly et Professeure Leclercq, pour vos conseils, vos mots d'encouragement et votre réactivité tout au long de ce travail. Merci Docteur Viollet et Professeur Sandri d'avoir accepté et pris le temps d'évaluer ce travail de thèse. Merci Professeure Leclercq pour votre collaboration dans nos projets de recherche et l'accueil que vous m'avez réservé, à de multiples occasions, dans le laboratoire GAEN.

Merci à la dream team ! Merci, Michel, de m'avoir formée, coachée et d'avoir supervisé mon travail sans faille depuis le début. Tu as accepté « l'étudiante qui ne connaissait rien du labo » pour un stage mémoire et tu m'as transmis généreusement, toujours, tes connaissances. Merci de m'avoir redonné confiance quand il le fallait et de m'avoir supportée. Ta façon d'aborder les choses avec une grande sagesse (et de l'humour comme il faut) a été d'un énorme soutien. Merci Laurence, pour toute l'aide fournie sur les différents projets, tant sur le plan scientifique, administratif, technique que moral. Ton empathie et ta sensibilité ont été des gardiennes de ma santé mentale au cours de toutes ces années. Tu es à toi seule, le baromètre émotionnel le plus performant que je connaisse ; un seul regard et tout est dit. Tes marques de soutien « de rien du tout » (comme tu dis) ont souvent eu l'effet explosif de bombes de réconfort. Merci Maya, quelle chance d'avoir pu travailler avec toi. Ton expertise, ton goût pour l'exploration de nouvelles techniques, ta bienveillance, ton énergie et ton enthousiasme ont donné un réel coup de boost au projet. Ces heures interminables passées dans le noir au microscope ont été illuminées par le soleil que tu es. Merci Romain pour tous ces

moments de rire. On ne tombera jamais d'accord pour savoir si oui ou non « la France est le plus beau pays du monde » mais on sera d'accord tous les deux pour dire que tu es l'expert du comique de répétition (« je répète… ») et de l'art de relativiser. Merci de m'avoir aidée avec beaucoup de bonne volonté et d'avoir été un collègue attentionné et à l'oreille attentive. Merci Nicolaaas pour ta bonne humeur permanente et tes divers coups de main. Merci aux super étudiantes, Laura, Alice, Marie et Chloé. Vous avez rejoint le laboratoire pour un an et votre engagement dans les projets a contribué à leurs avancées. Vos personnalités propres et attachantes ont embelli les expériences menées ensemble.

Merci à tous les collègues du pôle EDIN pour les chouettes moments passés ensemble.

Merci Justine, Maxime, Camille, Corinne du pôle GAEN pour votre collaboration et le partage de votre expertise (et les sorties, aussi :-)).

Merci Caroline et Aurélie pour vos conseils pour l'acquisition des images. Merci Professeure Many et Professeur Van den Bergh pour votre aide dans l'interprétation des images de microscopie électronique. Merci Véronique pour la formation technique pour les marquages histologiques. Merci Olivier pour ta collaboration pour les tests comportementaux.

Merci à mes amies de toujours, Claire, Charlotte, Eléna, Mélanie, et les ami(e)s SBIM, Sophie, Justine, Paola, Mehdi, pour le soutien durant ces 5 années de thèse.

Merci Nathalie d'avoir organisé ces sorties sportives au grand air qui ont oxygéné mon cerveau.

Merci à ma famille, papa, maman, pour votre soutien permanent, et les bro' aussi bien sûr, Antonia, Simon, Maïté, Cécile, Tanguy et Louis.

Last but not least, merci João et Fado, d'être mon tendre cocon d'amour, si joyeux, si chaleureux et si réconfortant. Merci João de m'avoir épaulée tout au long de ce parcours doctoral et d'être mon merveilleux partenaire de vie, quel que soit le projet.

Table of contents

Chapter 1: Introduction 1

Part I: Skeletal muscle 3

1. Functions 3

2. Structure 4

Part II: Obesity and ectopic lipid deposition 8

1. Definition and prevalence 8

2. Myosteatosis 8

3. NAFLD 12

Part III: Aging 15

1. Hallmarks of aging in the skeletal muscle 15

2. Sarcopenia 33

3. Obesity as an accelerator of the aging process? 37

Part IV: Adiponectin and AdipoRon 39

1. Adiponectin 39

2. AdipoRon 52

Chapter 2: Aims of the work 69

Context 71

Objectives 72

Study 1 72

Study 2 73

Chapter 3: Results 75

Study 1 77

Study 2 135

Chapter 4: General discussion and perspectives 179

Part I: Discussion 181

1. Bridging the gaps in age-related research and sarcopenia 181

2. Hallmarks of aging under Adiponectin/AdipoRon spotlight 183

3. Potential of AdipoRon in preventing sarcopenia and preserving health .. 187

4. Other interventions for aging and sarcopenia 192

5. General conclusion 194

Part II: Perspectives 196

1. Further explorations of AdipoRon in pre-clinical research 196

2. Other ApN receptors agonists 197

3. Other potential effects of ApN mimics in aging 198

Annexes 207

Annex 1: List of Abbreviations 209

Annex 2: Additional publication 212

Annex 3 238

CHAPTER 1: INTRODUCTION

CHAPTER 1: INTRODUCTION

The following introduction is organized into four sections. The first explores the structure and function of skeletal muscle. The second focuses on obesity and ectopic lipid deposition in skeletal muscle and liver. The third delves into the aging process, investigating the hallmarks of aging and sarcopenia. Finally, the last section reports on adiponectin properties in skeletal muscle and highlights the therapeutic potential of AdipoRon, an adiponectin receptor agonist.

PART I: SKELETAL MUSCLE

The skeletal muscle is one of the most dynamic and plastic tissues of the human body, comprising approximately 40% of total body weight in healthy individuals. It stands as an essential organ, being responsible for a wide array of functions that are essential to our daily lives [1].

1. FUNCTIONS

Skeletal muscle transforms chemical energy into mechanical energy to generate strength and power, enabling movement, locomotion, and breathing. It provides structural stability to the body and helps maintain posture by working continuously against the force of gravity. Skeletal muscle also plays a critical role in energy metabolism, being a major site for glucose uptake and a significant reservoir of protein and glycogen. Its thermogenic effect helps to regulate body temperature [1]. Skeletal muscle is also considered as a secretory organ, because it produces and releases cytokines and peptides, called myokines, which act as autocrine, paracrine, or endocrine factors [2].

2. STRUCTURE

Skeletal muscle can be viewed as a biomechanical device comprising different interacting elements such as nerves for impulse transmission, vasculature for oxygenation, and metabolic machinery for maintaining cellular homeostasis [3]. This highly organized tissue is composed of individual muscle cells, or myofibers/muscle fibers, which assemble into bundles called fascicles. These fascicles collectively form the muscle tissue. Each of these layers is surrounded and supported by the extracellular matrix [3]. Generally, the size of a muscle is mostly determined by the number and size of individual muscle fibers, although infiltration by fat and connective tissue may alter this relationship [1].

2.1. PROTEIN CONTENT

Myofibers are enveloped by a cell membrane called sarcolemma. They are densely filled by myofibrils, which constitute the contractile machinery and are composed of repeating units of sarcomeres (Figure 1). Sarcomeres are made up of proteins filaments, with the most abundant ones being actin and myosin, collectively accounting for ~ 70–80 % of the total protein content of a single fiber. During concentric muscle contraction, these filaments slide past each other, which leads to sarcomere shortening and the generation of force and movement [1].

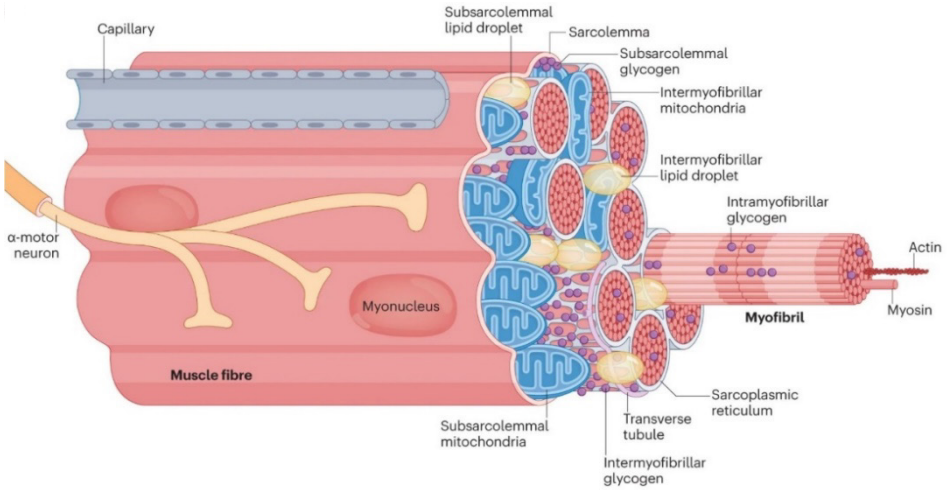

Figure 1. Skeletal muscle fiber structure. Smith J.A.B. et al. 2023 [5].

2.2. Organelles

Myofibrils are surrounded by the transverse tubular system (T-tubule) and the sarcoplasmic reticulum. The T-tubule system transmits the nerve action potential from the cell surface into its interior. The sarcoplasmic reticulum, positioned in close proximity to the T-tubule system, functions as a reservoir of calcium ions and controls their release and reuptake from the sarcoplasm, thereby regulating muscle contraction [1]. Mitochondria, that generate the energy needed for muscle actions when oxygen is available, are localized below the sarcolemma (subsarcolemmal) or between the myofibrils (intermyofibrillar, IMF) and form an interconnected reticulum [4] (Figure 1).

2.3. Energy depots

Free ATP in muscle is limited and fibers possess energy depots to maintain contractile activity, including creatine phosphate, glycogen and intramyocellular

lipids. Intramyocellular lipids are stored in lipid droplets (LDs) found in the intermyofibrillar or subsarcolemmal regions [5] (Figure 1).

2.4. Fiber type

Different types of fibers are typically found within the skeletal muscle and their proportion varies from one muscle to another [6, 7]. Myofibers can be classified based on their predominant metabolic pathway for energy production (oxidative or glycolytic), their contraction speed (fast or slow) and their degree of fatigue resistance during prolonged activation [7]. More commonly, fibers are classified based on the isoform of myosin heavy chain (MHC) primarily expressed, namely MHC-1, MHC-2a, MHC-2x, or MHC-2b, which are coded by the genes MYH7, MYH2, MYH1, and MYH4, respectively. In mice, there are four major types of muscle fibers, including slow type 1 fibers and fast type 2a, 2x, and 2b fibers (Table 1). In addition to 'pure' fibers that express only one type of MHC, there are other fibers that simultaneously express two MHC isoforms (1/2a, 2a/2x, 2x/2b) [7].

Type 1 fibers are slow-twitch, highly oxidative, and enduring due to their abundance of mitochondria. Type 2a fibers are fast-twitch fibers and rely primarily on oxidative metabolism, making them fatigue-resistant, also thanks to their mitochondrial content. Type 2b fibers are fast-twitch, glycolytic, and tire quickly because they have fewer mitochondria. Type 2x fibers exhibit intermediate properties between type 2a and 2b fibers [3, 7] (Table 1).

	Type 1	Type 2a	Type 2x	Type 2b
MHC isoform	MHC-1	MHC-2a	MHC-2x	MHC-2b
MYH gene	*MYH7*	*MYH2*	*MYH1*	*MYH4*
Metabolic type	Oxidative	Oxidative	Glycolytic	Glycolytic
Mitochondrial content	High	High	Low	Low
Fatigue resistance	High	High	Low	Very Low
Contraction speed	Slow	Fast	Fast	Very Fast

Table 1. Characteristics of the four major types of muscle fibers in mice.

Human muscles differ from those of mice in several aspects [8]. In mice, muscles are primarily composed of type 2x and 2b fibers, followed by type 2a fibers, while type 1 fibers are relatively rare and are mainly found in oxidative muscles such as the soleus. In contrast, human muscles contain a much higher proportion of type 1 fibers, followed by type 2a fibers, and with a lower proportion of type 2x fibers [7].

Mitochondrial content varies depending on the fiber type and the species. For example, in mice, the abundance of mitochondria and the activity of oxidative enzymes are highest in type 2a muscle fibers (followed by type 1 > 2x > 2b), while in humans, they are higher in type 1 fibers. Additionally, slow type 1 fibers have a higher lipid content in human muscles, whereas in murine muscles, these are the type 2a fibers [6, 7, 9].

PART II: OBESITY AND ECTOPIC LIPID DEPOSITION

1. DEFINITION AND PREVALENCE

Obesity is characterized by an excessive accumulation of body fat that may impair health and by a Body mass index (BMI) greater than 30 kg/m². According to the World Health Organization [10], the prevalence of obesity has nearly tripled worldwide since 1975 and continue to grow at a pandemic rate [11]. In 2016, 39% of adults worldwide were overweight, and 13% were obese [10]. In Belgium, these numbers are even higher, with more than 50% of adults being overweight and 15% being obese [12]. Obesity increases the risk of metabolic diseases, such as insulin resistance and type 2 diabetes mellitus, fatty liver disease, cardiovascular diseases, and also some types of cancer. Obesity therefore reduces both the quality of life and life expectancy, and represents a significant economic burden [11].

Rather than adiposity itself, body fat distribution is an important risk factor for obesity-related disorders. Central obesity (waist circumference) is included in the diagnostic criteria for metabolic syndrome, emphasizing that an excess of intra-abdominal fat, rather than subcutaneous fat, is associated with adverse outcomes [13].

2. MYOSTEATOSIS

Plasma non-esterified free fatty acids concentrations (NEFA) are chronically elevated in obese individuals, mainly due to the impaired ability of insulin to inhibit lipolysis [13]. The excessive supply of NEFA and the decrease of fatty oxidation in the muscle result in an accumulation of intramyocellular lipids (IMCL) [14]. The term 'myosteatosis' is used to describe the excess of fat in the Skeletal muscle [15] and includes lipids accumulated between muscles or myofibers (extramyocellular

lipids, EMCL) as well as those inside the muscle fibers (IMCL) [15]. There is a positive relationship between IMCL and insulin-resistance in obesity and type 2 diabetes [15-18], while myosteatosis negatively correlates with muscle mass and strength. Importantly, myosteatosis is also a negative prognostic factor for cancer, cardiovascular disease, or Non-alcoholic Fatty Liver Disease (NAFLD) [15, 19]. Computed tomography is the most widely used imaging technique to indirectly assess myosteatosis. Muscle density is expressed in Hounsfield Unit. A low density expressed in HU indicates a high degree of myosteatosis. The drawback of this technique is that it does not allow for the differentiation between EMCL and IMCL [15, 19].

2.1. Muscle lipid metabolism

The translocation of fatty acids from plasma into myofibers predominantly occurs via transport proteins, including fatty acid translocase/cluster of differentiation 36 (FAT/CD36), fatty acid binding protein (FABP) and fatty acid transport protein (FATP). FAT/CD36 is the predominant transporter and its protein levels are upregulated in response to contraction, high-fat diet (HFD), obesity and type 2 diabetes [14, 16, 20-22]. Depending on metabolic demands, NEFA are directed either to the mitochondria or stored as triacyglycerol (TAG) in LDs [14, 16]. LDs serve as an energy reservoir for exercise and are responsible for the trafficking of FA between the different cellular compartments [14]. In response to contraction, TAG can be hydrolyzed by three distinct lipases, namely monoacylglycerol lipase, adipose triglyceride lipase, and hormone-sensitive lipase. This process results in an increased fatty acids flux into the cytosol and mitochondria, where they subsequently undergo β-oxidation, contributing to ATP synthesis [14].

LDs consists of a hydrophobic core primarily composed of TAG and sterol esters, enveloped by a phospholipid monolayer. They are covered with proteins that

influence their structural and signaling properties. Among them, the perilipins (PLIN) have been the most investigated. PLIN2 is thought to be involved in LD growth and lipolysis inhibition: its overexpression increases LD accumulation, while its knockdown reduces it and promotes fat oxidation in cultured myotubes. In contrast, PLIN5, which is more abundant on LDs of trained individuals, appears to facilitate the interaction between LDs and mitochondria. LD-mitochondrial tethering may help fatty acid oxidation by releasing fatty acids in close proximity to the mitochondria [17, 18, 23].

2.2. IMCL, INSULIN RESISTANCE AND THE ATHLETE PARADOX

Skeletal muscle is an important organ for whole-body glucose homeostasis, being responsible for approximately 80% of insulin-stimulated glucose uptake in postprandial state. The increase of body weight in obesity is accompanied with an increase in skeletal muscle insulin resistance, which markedly reduces the insulin-stimulated glucose uptake [24, 25].

As mentioned above, IMCL are implicated in muscle insulin resistance. However, endurance athletes have similar, if not higher, IMCL content than obese patients with type 2 diabetes, while maintaining high insulin sensitivity. This phenomenon is described as the "athlete's paradox" and is explained by a more nuanced appraisal of muscle LDs, related to their size, density, localization, dynamics, and lipid species composition [17, 26, 27] (Figure 2). First, LD size is inversely correlated to insulin sensitivity and physical fitness [17, 28]. In fact, smaller LDs exhibit a relatively greater surface area for lipase action and, thus, potentially have a greater capacity to mobilize lipids [29]. Secondly, density plays a controversial role in insulin action [17, 28]; yet, it seems to be increased in athletes. Third, the subcellular localization of LD is important, since LDs located just below the surface membrane (subsarcolemmal or peripheral) exert a more deleterious effect on insulin

sensitivity than central ones [17, 26, 30]. The latter provide fuel to central mitochondria, which have a greater respiratory activity and are more specialized to meet the high energy demand required for contraction [31]. By contrast, peripheral LDs supply subsarcolemmal mitochondria, which are involved in membrane-related processes [17] (Figure 2). Finally, beyond triglycerides, specific complex lipids within the muscle may be more deleterious than others. For instance, diacylglycerol (DAG), long chain acyl-CoA (LCA-COA), and ceramides may accumulate in muscle when the triglyceride turnover rate is low, thereby impairing insulin signaling [26, 32]. As for the mechanisms involved, the accumulation of DAG and LCA-COA promotes the activation of serine kinases, which phosphorylate and inactivate insulin receptor substrate proteins, while ceramides dephosphorylate Akt, a key effector of the metabolic effects of insulin. C16:0 and C18:0 ceramide species are considered the most potent in decreasing insulin sensitivity. Taken together, these events disrupt the normal insulin signaling cascade and eventually reduce glucose transporter type 4 (GLUT4) translocation and glucose uptake [16, 25]. It is important to note that, despite these generalities, different isomeric forms may have distinct effects on cellular signaling. At this level of complexity, it should further be added that the localization of these lipid species may plays a role in promoting decreased insulin sensitivity [26]. Returning to the "athlete's paradox" endurance athletes have a high number of smaller central LDs with elevated turnover rate in type I (oxidative) fibers while obese and diabetic patients have larger peripheral LDs with low turnover rate in type II (glycolytic) fibers [17, 18, 32, 33].

Of note, besides being associated with adverse metabolic outcomes, large LDs could also affect muscle contractile capacity [34]. In myofibers isolated from obese subjects, there is also an inverse relationship between IMCL content and fiber contraction, power and force development, raising the possibility of a vicious circle between IMCL accumulation and functional muscle impairment, thereby further worsening obesity [35].

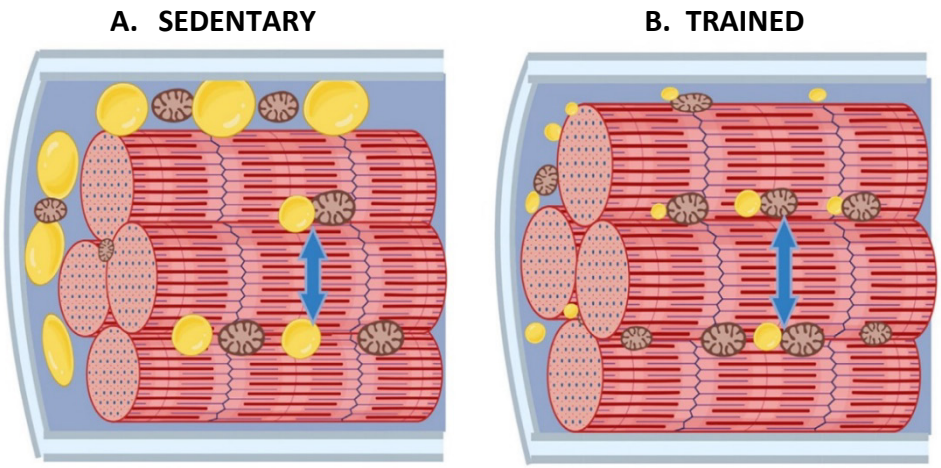

Figure 2. Schematic of lipid distribution within the skeletal muscle of sedentary (A) and trained (B) individuals. Trained humans (B) exhibit smaller LD (in yellow), increased LD number and density, higher IMF (indicated by blue arrows) LD, fewer SS LD and greater LD-mitochondria contact when compared to sedentary humans (A). Seibert J.T. et al. 2020 [17].

3. NAFLD

Lipid deposit occurs not only in the Skeletal muscle, but also in other tissues like the liver [36]. Nonalcoholic fatty liver disease (NAFLD) is the hepatic complication of obesity and the most common chronic liver disease in the world. NAFLD encompasses a spectrum of diseases, ranging from steatosis/NAFL to nonalcoholic steatohepatitis (NASH) [19, 37, 38]. NAFL diagnosis requires more than 5% of

hepatic steatosis. One out of four individuals develops NAFL, and 20% of them will develop NASH. NASH is characterized by steatosis (>5%), hepatocyte injury (ballooning) and lobular inflammation on histology. NASH can potentially progress to cirrhosis and hepatocellular carcinoma, and require liver transplant [39] (Figure 3).

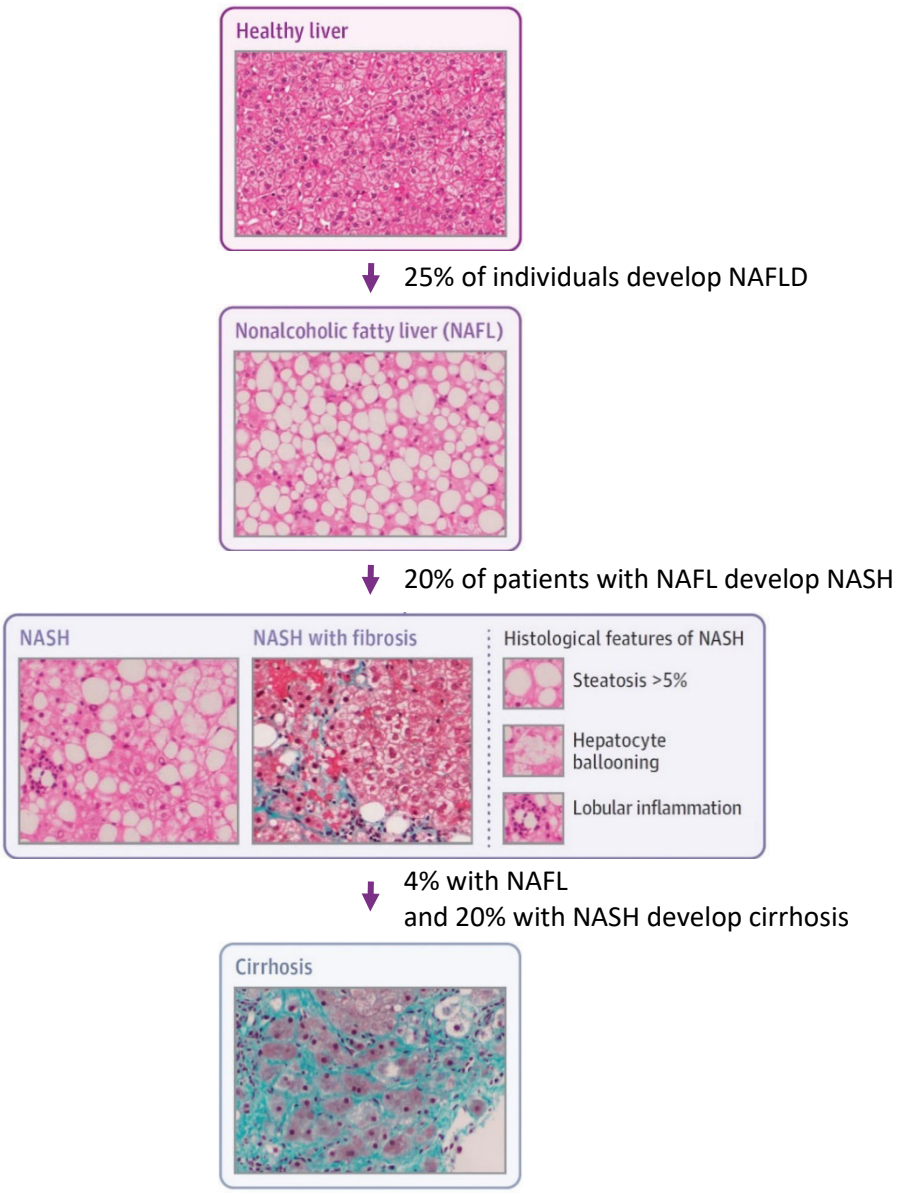

Figure 3. Histological features and epidemiology of non-alcoholic steatohepatitis. Adapted from Sheka A.C. et al. 2020 [39].

PART III: AGING

Over the last century, life expectancy at birth has increased by 30 years, marking one of humanity's greatest achievements [40]. However, adding more years to life is a mixed blessing if it is not accompanied by adding more life to years [41]. Aging is characterized by a progressive loss of physiological integrity, leading to impaired function and increased vulnerability to death. Cellular damage accumulate and this deterioration is the primary risk factor for major human pathologies, including cancer, diabetes, cardiovascular disorders, musculoskeletal and neurodegenerative diseases [42]. Efforts are now focused on addressing these aging-related diseases in order to both extend and improve healthspan [40].

1. HALLMARKS OF AGING IN THE SKELETAL MUSCLE

Cellular and molecular hallmarks have been identified as contributors to the aging process. They are interconnected with each other and together determine the aging phenotype [42, 43]. Each of these hallmarks of aging is considered as a point-of-entry for exploration of the aging process and for the development of new anti-aging medicines [43].

Some of them are addressed below, with specific emphasis on skeletal muscle: loss of proteostasis, disabled macroautophagy, mitochondrial dysfunction, deregulated nutrient sensing, cellular senescence and chronic inflammation.

1.1. LOSS OF PROTEOSTASIS

The loss of proteostasis with aging, i.e. impaired protein homeostasis, leads to the accumulation of misfolded, oxidized or ubiquitinylated proteins that often form protein aggregates [43]. Reported reasons for proteostasis imbalance are the decline of protein quality control mechanisms of folded proteins by molecular

chaperones, endoplasmic reticulum stress, oxidative stress and decreased autophagy [44]. Protein aggregates may exert several adverse effects on cell function (lysosome and DNA damage, disruption of the membrane system and calcium (Ca) homeostasis, and induction of reactive oxygen species (ROS)), thereby accelerating in many ways aging [44].

1.1.1. TUBULAR AGGREGATES (TAGS)

Described in both mice and human muscles, tubular aggregates are an abnormal accumulation of sarcoplasmic reticulum tubes. By Electronic microscopy, they appear as straight, single- or double-walled tubules, regularly organized into tight aggregates with a honeycomb-like para-crystalline order [45, 46]. In humans, the presence of TAgs defines a clinically heterogenous group of disorders termed "TAgs myopathies" characterized by muscle weakness [46]. TAg abundance in old mice is accompanied by impaired ability to restore internal Ca^{2+} stores from extracellular space, which could contribute to muscle impairment [45].

1.1.2. PROTEIN DEGRADATION PATHWAYS

The major cellular systems of protein clearance are the ubiquitin-proteasome pathway and the autophagy-lysosome pathway. They play key roles to maintain protein quality, regulate protein turnover, support muscle growth and repair and adapt to physiological conditions [44].

A) THE UBIQUITIN PROTEASOME SYSTEM (UPS)

The degradation via the UPS consists of two main processes: (1) the marking of the substrate protein with the covalent attachment of multiple ubiquitin molecules, and (2) the subsequent breakdown of the tagged protein by the 26S proteasome. Three enzymes regulate the ubiquitination: the ubiquitin-activating enzyme (E1), ubiquitin-conjugating enzyme (E2), and ubiquitin ligase (E3). The first activates

ubiquitin molecules, the second facilitates their transfer to target proteins, and the third provides substrate specificity by recognizing specific proteins [47, 48]. Once a sufficient number of ubiquitin molecules have been attached to target protein, the ubiquitin chain is recognized by the 26S proteasome. The protein is unfolded and fed into the proteasome, where it is broken down into smaller peptides [48] (Figure 4).

Atrogin-1 and MuRF-1, both E3 ligases, are widely used markers of proteolysis. They are markedly induced in all types of atrophy [49], but studies in sarcopenic muscle have revealed inconsistent results, mainly based on mRNA levels [47]. However, it seems that the ubiquitin/proteasome system is reduced during aging. These results suggest that sarcopenia, a disorder characterized by the accelerated loss of muscle mass, quality, and function, primarily occurring with aging, is not likely caused by excessive protease-dependent degradation [50-52]. In line with this, chronic inhibition of atrogin-1 and MuRF1 in knockout mice induces muscle mass and/or force loss, indicating that the activity of these ubiquitin ligase is required to preserve muscle function during aging in mice [53].

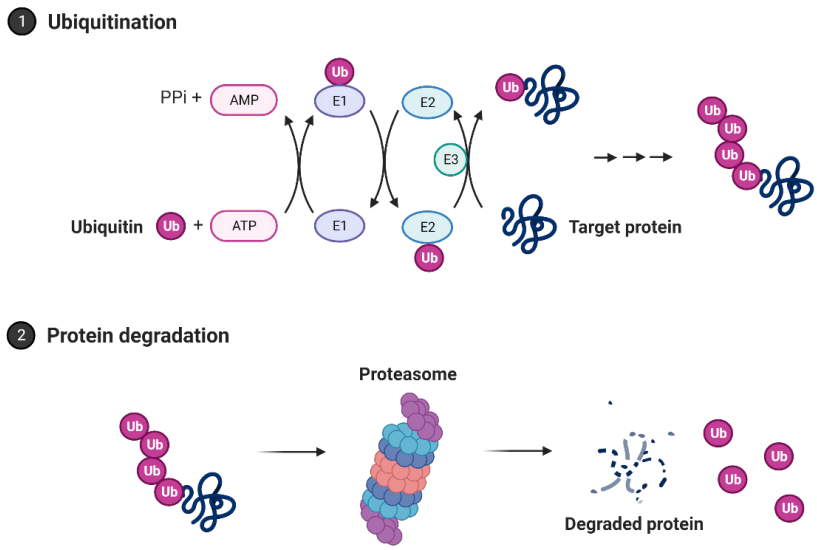

Figure 4. Protein degradation mediated by ubiquitin proteasome system. Adapted from Murton A.J. et al. 2008 and drawn by Selvais C.M. with BioRender [48].

B) The autophagy-lysosome system

Autophagy is another catabolic process which plays a crucial role in cellular physiology by facilitating lysosomal degradation and recycling of intracellular macromolecules and organelles [54]. It allows adaptation to metabolic stress, removal of dangerous cargo (e.g., protein aggregates, damaged organelles, intracellular pathogens), renovation during differentiation and development, and prevention of genomic damage [55]. Because autophagy also involves non-protein structures, this mechanism and its failure with aging are described separately in the following section (Disabled autophagy), thus illustrating the various interactions that exist between the different hallmarks [43].

1.2. Disabled autophagy

1.2.1. Overview of the autophagy process

We will focus in this work on macroautophagy, the mechanism involving the degradation of cytosolic material via sequestration into double-membrane vesicles called autophagosomes, which subsequently fuse with lysosomes [54]. Macroautophagy, which will be hereafter termed autophagy, comprises several steps (Figure 5) regulated by a family of autophagy-related genes (ATG):

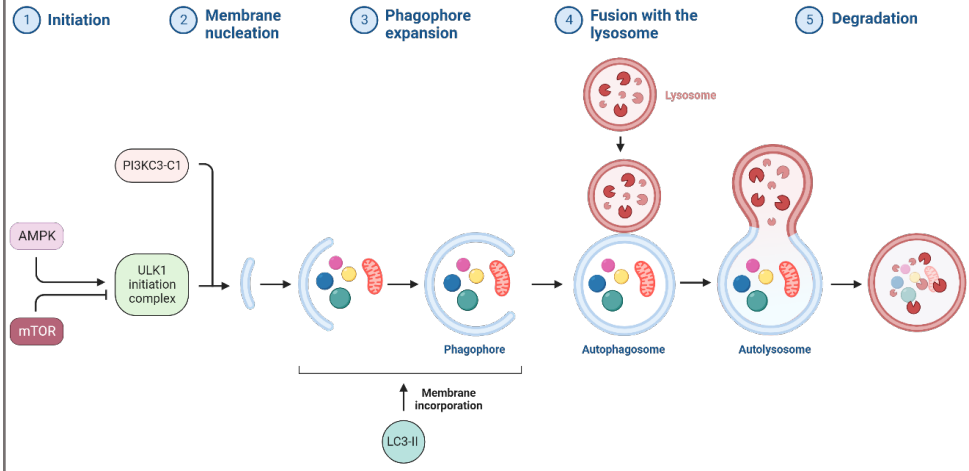

Figure 5. The macroautophagy process. Adapted from Hansen M. et al. 2018 and drawn by Selvais C.M. with BioRender [54].

1) **Initiation**. Through phosphorylation, specific signals like AMP-activated protein kinase (AMPK), activate the Unc-51-like kinase 1 (ULK1) complex, which, in turn, regulates the initiation of autophagy [56]. Conversely, mammalian target of rapamycin (mTOR) prevents ULK1 activation [57].

2) **Membrane nucleation and formation of a double membrane structure, the phagophore.** The formation of class III phosphatidylinositol-3 kinase (PI3KC3)

complexe I, which includes beclin-I as one of its components, is an essential event at this nucleation stage.

3) **Phagophore elongation and sequestration of cytoplasmic cargo**. Microtubule-associated protein 1A/1B-light chain 3 protein (LC3)-II is incorporated into the phagophore membranes. LC3-II can recognize structures to be degraded and serves as an autophagic marker. Initially, LC3 is cleaved by the protease ATG4 to form LC3-I (the cytosolic form). Next, ATG7 plays a critical role by facilitating the activation of LC3-I, allowing it to be conjugated to phosphatidylethanolamine to form LC3-II (the lipidated form).

4) **Fusion of the autophagosome** (the fully enclosed phagophore) **with the lysosome** to form an autolysosome.

5) **Digestion** of sequestered cargo by the acidic lysosomal hydrolases. Amino acids and fatty acids are released back to the cytoplasm and are reused for cellular metabolism [54, 58, 59].

1.2.2. SELECTIVE AND NON-SELECTIVE AUTOPHAGY

Autophagy can be 'non-selective', i.e. associated with the indiscriminate engulfment of cytosolic components, or 'selective', i.e. degrading specific targets such as protein aggregates (aggrephagy), damaged organelles (mitophagy)… Non-selective autophagy occurs in response to nutrient starvation and is commonly referred to as bulk autophagy. Selective autophagy is importantly involved in cellular quality control. Therefore, autophagy is considered as a pathway both for restoring intracellular nutrient supply during starvation and as an important quality control mechanism to protect the cell against damage caused by toxic macromolecules and damaged organelles [60].

In the selective autophagy process, cargo receptors serve as adapters to recognize specific structures that need to be degraded (referred as 'cargo'). Ubiquitylation, mediated by different E3 ligases, is a major factor for target recognition. Cargo receptors cluster on the surface of the target and simultaneously bind the phagophore through their LC3-interacting region (LIR) which interact with LC3-II, thereby tethering the cargo and marking it for engulfment in the autophagosome. Ubiquitin-binding protein p62/sequestosome 1 (p62) is a prominent example of cargo receptor. p62 is consumed along with the cargo during degradation, and its accumulation is, therefore, inversely correlated with autophagic activity [54, 60, 61]. The cargo itself may also contain an LIR motif and interact directly with LC3 [55].

1.2.3. MITOPHAGY

Mitophagy is a type of selective autophagy that eliminates dysfunctional or superfluous mitochondria, thereby fine-tuning mitochondrial number and preserving energy metabolism [62]. The most extensively studied mitophagy pathway is ubiquitin-dependent and involves Phosphatase and tensin homolog (PTEN)-induced kinase 1 (PINK1) and the E3 ligase Parkin. In healthy and functional mitochondria, PINK1 is imported into the inner mitochondrial membrane and degraded. However, when a mitochondrion becomes depolarized (loses its electrochemical gradient), PINK1 stabilizes on the outer mitochondrial membrane, which stimulates the recruitment of Parkin from the cytosol and its activation. Parkin then ubiquitinates various mitochondrial proteins. Poly-ubiquitinated proteins are phosphorylated by PINK1. Adapter proteins, such as p62, recognize phosphorylated poly-ubiquitin chains and initiate the formation of the autophagosome through binding with LC3-II (Figure 6). Parkin is not the sole ubiquitin ligase to regulate mitophagy; other proteins such as Gp78, SMURF1,

MUL1, and more, are involved in generating ubiquitin chains and triggering the recruitment of cargo receptor, including p62. In addition to ubiquitin-dependent mitophagy, certain mitochondrial proteins (Nix, Bnip3, FUNDC1) serve as mitophagy receptors, interacting directly with LC3 through their LIR motifs [62, 63].

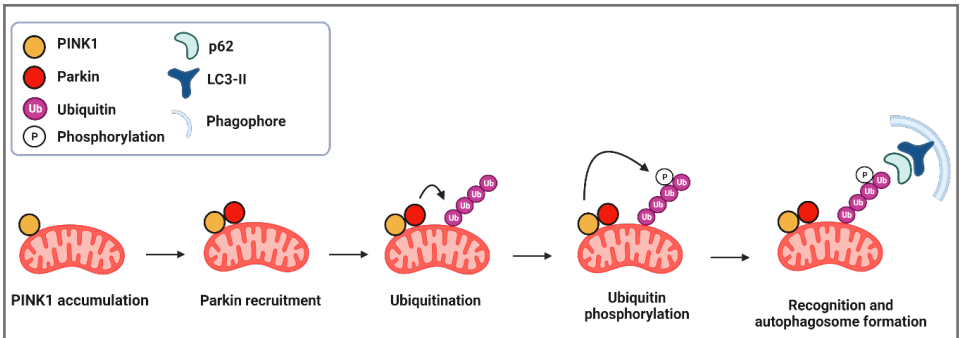

Figure 6. The PINK1-Parkin pathway of mitophagy. Dysfunctional/damaged mitochondria represented in red. Adapted from Palikaras K. et al. 2018 [62] and drawn by Selvais C.M. with BioRender.

1.2.4. AUTOPHAGY IN AGING

Autophagy declines during aging in the skeletal muscle of mice [64-67] and humans [65]. However, recent research increasingly highlights that autophagy is crucial for longevity by specifically targeting dysfunctional cellular components and preventing their accumulation [54]. Accordingly, in the skeletal muscle, autophagy is required to preserve muscle mass and myofiber integrity. Muscle-specific inhibition of autophagy (Atg7 deletion) in mice induces muscle atrophy, force loss and weakness, reticulum distension, oxidative stress, aberrant structures, and accumulation of abnormal mitochondria [68]. It also exacerbates the age-related deterioration of synaptic structure and function, and reduces survival [65]. Moreover, defective autophagy in physiologically aged or young satellite cells from mice causes entry into senescence and results in altered regenerative capacity [67].

Conversely, stimulation or re-establishment of autophagy improves the neuromuscular synaptic function, enhances muscle mass [65] and restores regenerative functions of satellite cells [67]. Mitophagy is also known to be impaired in aged skeletal muscle, leading to progressive accumulation of defective mitochondria [63, 69]. In light of this, perturbation of mitophagy in parkin-deficient mice induces several aging-like features, including contractile and impaired mitochondrial dysfunction [63, 70], while parkin overexpression in old mice attenuates the loss of muscle mass and strength, oxidative stress and increase mitochondrial activity [71].

In summary, ubiquitin-proteasome pathway and the autophagy-lysosome system are critical for maintaining muscle quality, and their chronic inhibition or decrease with aging is detrimental to muscle health.

1.3. MITOCHONDRIAL DYSFUNCTION

Mitochondria play an essential role in the cell, participating in multiple cellular processes such as ATP production through oxidative phosphorylation (OXPHOS). The majority of mitochondrial proteins are encoded by nuclear DNA (nDNA), synthesized in the cytosol, and then imported into mitochondria. However, mitochondria are unique in that they harbor their own genome (mtDNA), which encodes for 13 protein-coding genes, 22 transfer RNAs and 2 ribosomal RNAs genes. These proteins are indispensable for mitochondrial function, because they are critical components of respiratory chain subunits [51, 72, 73].

1.3.1. MITOCHONDRIAL REGULATION

Mitochondria are highly dynamic organelles that are constantly being synthesized (mitochondrial biogenesis), recycled (mitophagy) and remodeled (fusion, fission).

This turnover promotes the maintenance of a healthy mitochondrial pool and adaptation to energy requirements (Figure 7). These control mechanisms are described below, except for mitophagy, which has already been described in the previous hallmark.

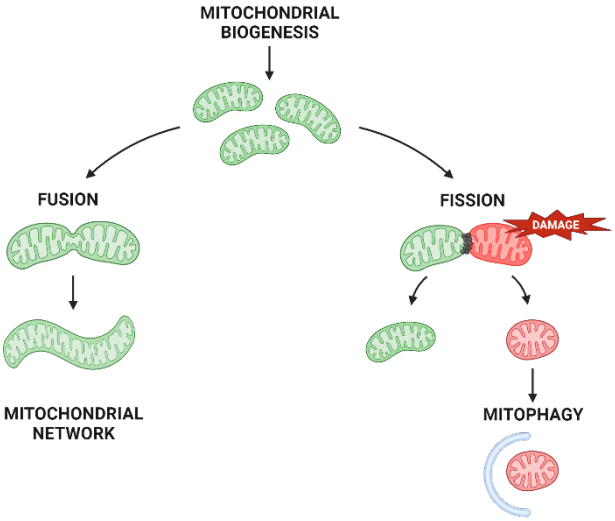

Figure 7. Overview of the mechanisms regulating mitochondria. Adapted from Romanello V. 2021 [85], and drawn by Selvais C.M. with BioRender.

A) MITOCHONDRIAL BIOGENESIS

Mitochondrial biogenesis is a coordinated process involving the expression of genes from both the nuclear and mitochondrial genomes, with peroxisome proliferator-activated receptor gamma coactivator 1-alpha (PGC-1α) acting as its master regulator. Different metabolic sensors like Calcium/Calmodulin-Dependent Protein Kinase (CaMK), AMPK and Sirtuin 1 (SIRT1) stimulate PGC-1α [74]. PGC-1α, in turn,

coactivates numerous transcription factors such as the nuclear respiratory factor 1 and 2 (NRF-1/2) and the estrogen-related receptor α (ERRα), to upregulate the expression of nuclear genes encoding mitochondrial proteins [75, 76]. Subsequently, several mitochondrial proteins are expressed and transported into the mitochondria [74], including the mitochondrial transcription factor A (TFAM), which plays a pivotal role in regulating the transcription and replication of mtDNA [77]. This interplay between mtDNA and nDNA ensures the synchronized expression of proteins encoded by each genome (Figure 8).

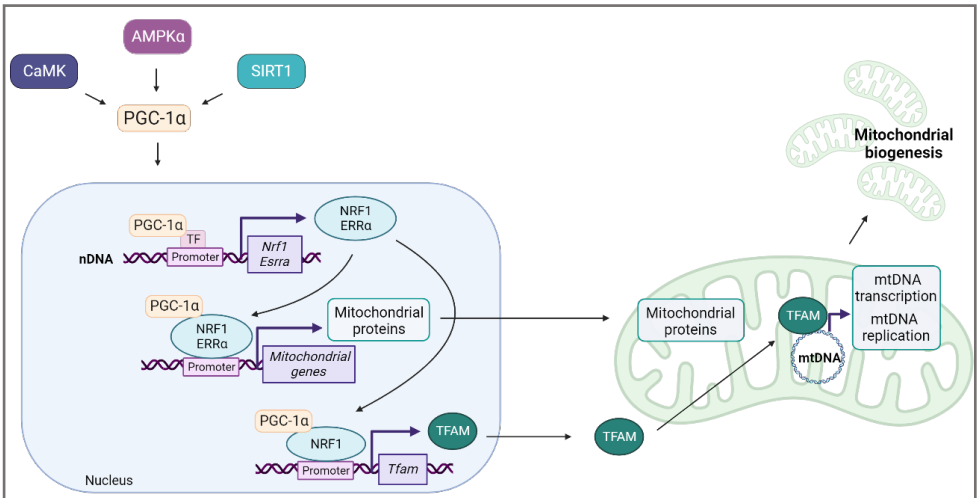

Figure 8. Regulation of mitochondrial biogenesis by PGC-1α. Figure drawn by Selvais C.M. with BioRender.

B) Fusion and fission

Mitochondria are constantly being reshaped by fission and fusion events. On one hand, fusion increases interconnection between mitochondria and lead to an elongated mitochondrial network. It allows mtDNA, metabolites, protein mixing within the network and prevent focal accumulation of mutant DNA, promoting DNA integrity. It also increases the bioenergetic capacity of the cell. Mitofusin 1/2 and

optical atrophy 1 (OPA1) are the proteins involved in mitochondrial fusion of the outer and inner mitochondrial membrane, respectively. On the other end, fission fragments the network, which allow segregation of dysfunctional, damaged or unnecessary components and their removal via mitophagy. Mitochondrial fission depends on the joint work of the dynamin-related protein1 (Drp1), the mitochondrial fission factor (Mff) and fission protein 1 (Fis1) [4, 63, 76, 78]. The balance between fusion and fission is essential for muscle health, as their up or downregulation by genetic manipulations disrupt it [4, 63].

1.3.2. MITOCHONDRIAL DYSFUNCTION WITH AGING

During the aging process, mitochondrial dysfunction in the skeletal muscle comprises different features, including reduced mitochondrial respiration and ATP production, altered mitochondrial morphology, increased oxidative stress and mtDNA damage [72, 73, 79, 80].

The generation of ROS mainly occurs within mitochondria as by-products of oxidative phosphorylation. Skeletal muscle thus naturally generates a great amount of ROS. Aging is characterized by an imbalance between the production of ROS and the antioxidant defenses [81, 82], which leads to oxidative stress. Excessive exposure to ROS disrupts many cellular structures such as membranes, lipids, proteins, and DNA [83].

With regard to the mitochondrial morphology, two different populations of mitochondria are observed: the subsarcolemmal (SS) mitochondria, which are located just underneath the sarcolemma, close to the nutrient-delivering capillaries and have a large globular shape, and the IMF mitochondria, which are more compact and located between the contractile filaments. IMF mitochondria directly support myofibrillar contraction by providing ATP to the contractile filaments. The specialization of SS mitochondria, however, is not well understood. SS

mitochondria have a greater abundance of complex IV, while IMF mitochondria possess higher levels of complex V (ATP synthase). Consequently, it is believed that SS mitochondria specialize in generating a membrane potential that is subsequently transferred through the reticulum into the IMF mitochondrial network. The IMF mitochondria, in turn, support rapid ATP production and diffusion to myofibrillar ATPases [5, 76, 84]. Skeletal muscle mitochondria have been reported to be abnormally enlarged in aged muscles [85], with vacuolization of the matrix and damaged cristae [73], particularly in the case of SS mitochondria [80].

Muscle mitochondrial capacity is decreased with aging [79, 86]. Although it is still unclear how aging exactly alters mitochondrial function in skeletal muscle, disruption of the regulatory mechanisms cited above could play a role. Mitochondrial biogenesis is blunt with aging. This may be due to decreased responsiveness of AMPK signaling [87, 88] and PGC-1α expression in skeletal muscle [89-91]. In older mice, muscle-specific knockout of PGC-1α accelerates the deterioration of mitochondrial function [92]. The impact of aging on mitochondrial content is, however, controversial. Mitochondrial content is sometimes reported to be reduced, sometimes not [78]. Similarly, the changes in mitochondrial dynamics in the aged skeletal muscle remain unclear, as conflicting data exist in the field (Leduc-Gaudet et al., 2021). Anyway, it has been shown that an imbalance between fusion and fission, one way or the other, alters muscle function [4]. Moreover, as discussed in the previous hallmark, mitophagy is decreased [63, 69].

In summary, the decline in mitochondrial biogenesis, coupled with the impairment of mitochondrial removal, suggests altered mitochondrial turnover with aging, ultimately resulting in the accumulation of dysfunctional organelles [78].

1.4. Deregulated nutrient sensing

The nutrient-sensing network responds to nutrients levels to maintain energy homeostasis, by fine-tuning anabolic and catabolic pathways. It includes extracellular ligands, their receptors and the intracellular signaling cascades. Two key nutrient-sensing pathways are the insulin/ insulin-like growth factor 1 (IGF1)-Akt-mTOR signaling pathway and the AMPK pathway [42, 43] (Figure 9).

1.4.1. Insulin/IGF1-AKT-mTOR pathway

Insulin and IGF1 are anabolic factors essential for maintaining overall body and muscle growth. By binding to their receptor (insulin receptor and IGF1 receptor), they initiate a cascade of phosphorylation events that modulate various proteins, enzymes, and transcription factors. This signaling pathway plays a pivotal role in regulating key cellular processes such as protein synthesis, protein degradation, cellular proliferation, survival, glucose uptake, and energy production. Notably, insulin/IGF1 signaling converges on the central kinase mTOR, which integrates a multitude of signals and is the master of cellular growth regulation. mTOR assembles with other proteins into two distinct complexes: mTORC1 complex, containing Raptor, and mTORC2 complex, containing Rictor. These complexes have different roles, with mTORC2 involved in glucose and lipid homeostasis, while mTORC1 predominantly governs anabolic processes, including protein synthesis. Through its downstream effectors, ribosomal protein S6 kinase beta-1 (p70S6K1) and eukaryotic translation initiation factor 4E-binding protein 1 (4EBP1), mTOR regulates the protein synthesis [93, 94]. Simultaneously, mTOR inhibits protein catabolism by blocking autophagy via ULK1 and the ubiquitin proteasome system [57, 95] (Figure 9).

Multiple studies have investigated the effects of the lack of mTOR signaling in mice [94, 96-98]. They have shown myopathy and impairment in protein synthesis,

highlighting the importance of mTOR for muscle growth, development, and survival. Paradoxically, overactivation of mTOR has also been proved to be detrimental. Sustained activation of mTORC1 in TSC1-deficient muscle mice caused a late-onset myopathy related to impaired autophagy. This was largely reversible by rapamycin, a potent inhibitor of mTORC1 [99].

Chronic activation of mTOR has been reported in the skeletal muscle of aged mice, human [100], and rats [101], while mTOR inhibitor treatments show protective effects on the muscle [100, 101]. For example, a late long-term treatment of rapamycin in old mice preserves muscle size, function and neuromuscular junction integrity [102], and extend lifespan [103]. Hence, while mTOR plays a crucial role in regulating muscle growth during development, sustained mTOR activation in later life seems to produce the contrary effect.

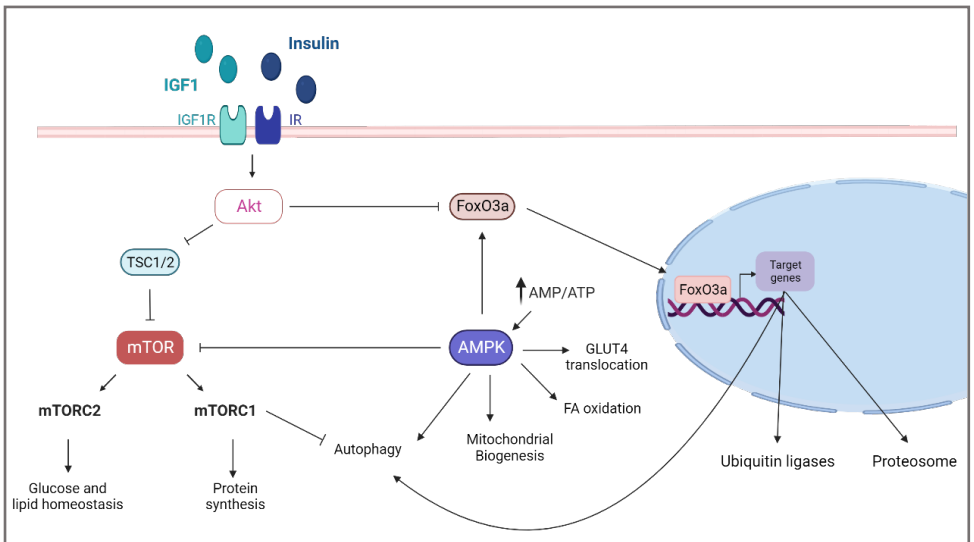

Figure 9. Overview of mTOR/AMPK signaling pathways. Adapted from Sartori R. et al. 2021 [93], and drawn by Selvais C.M. with BioRender.

1.4.2. AMPK PATHWAY

While mTOR signals a state of nutrient abundance, AMPK responds to energy depletion and nutrient scarcity. AMPK is mostly activated by elevation of the AMP/ATP and ADP/ATP ratios, but also by the upstream kinases liver kinase B1 (LKB1) and Ca^{2+}/calmodulin-dependent protein kinase kinase beta (CAMKK). Once activated, AMPK counterbalances mTOR signaling by inhibiting mTOR activity, thereby reducing protein synthesis. Moreover, AMPK regulates muscle protein degradation, which serves as a source of amino acids that can be used for energy production by various other organs. AMPK phosphorylates forkhead box protein O3a (FoxO3a), which controls the transcription of the E3 ligases MAFbx and MuRF1 and several proteins of the autophagic machinery [104]. AMPK is also an important regulator of autophagy and mitophagy through its direct phosphorylation of ULK1 [104, 105]. Conversely, mTOR phosphorylation of ULK1 on Ser757 disrupts the interaction between AMPK and ULK1 [57]. AMPK has an additional important role in the regulation of mitochondrial homeostasis by controlling mitochondrial biogenesis. Indeed, AMPK phosphorylates and activates PGC-1α [106]. Activation of AMPK also stimulates fatty acid oxidation through inhibition of acetyl-coenzyme A carboxylase 2 (ACC2) and FAT/CD36 translocation to the plasma membrane, and decreases inflammation. Finally, AMPK increases skeletal muscle glucose uptake by facilitating GLUT4 translocation [104, 107] (Figure 9). AMPK thus integrates and mediates several longevity pathways, and its activation is reported to extend lifespan in model organisms [87, 108].

As mentioned earlier, the responsiveness of AMPK signaling seems to be blunted with aging in skeletal muscle [87, 88] and PGC-1α expression declines [89-91]. However, AMPK seems to be essential for maintaining muscle integrity and mitochondrial function during aging. Aged mice lacking muscle AMPK exhibit a significant myopathy characterized by reduced muscle function, mitochondrial

dysfunction, and accumulation of the autophagy/mitophagy proteins p62 and parkin [109].

1.5. SENESCENCE

Cellular senescence is a cell state characterized by cell-cycle arrest and the acquisition of a senescence-associated secretory phenotype (SASP). Senescent cells exhibit elevated expression of cell cycle-inhibitory proteins, collectively known as cyclin-dependent kinase inhibitors. Among these, $p16^{INK4A}$ (p16) and $p21^{Cip1}$ (p21) are central in the accumulation of senescent cells during aging, ensuring long-lasting maintenance of proliferative arrest. Senescent cells secrete a wide spectrum of proinflammatory cytokines, chemokines, proteases, and other factors, which can act in a paracrine or endocrine manner and contribute to age-related dysfunction and chronic low-grade inflammation [110-112]. Senescence can be induced by diverse stress stimuli including DNA damage, telomere shortening, metabolic and mitochondrial dysfunction, and inflammation [110]. The accumulation of senescent cells increases in multiple tissues with aging [113] and in the context of obesity and diabetes [114], and shorten both healthspan and lifespan [113, 115]. In the skeletal muscle of aged mice, senescent cells increase drastically after injury and produce factors that trigger inflammation and fibrosis, blocking regeneration [116, 117]. The elimination of senescent cells [113, 118, 119] or suppression of the SASP [120], can alleviate or delay multiple chronic age-related conditions, demonstrating the therapeutic potential of targeting senescent cells. For example, oral treatment with senolytic drugs in aged mice relieves physical dysfunction and increases survival [115].

1.6. CHRONIC INFLAMMATION

Advancing age is accompanied by chronic, low-grade and systemic inflammation. This process, known as inflammaging, is recognized as a risk factor for several age-related diseases, including cardiovascular and neurodegenerative diseases, cancer, type 2 diabetes, and sarcopenia [121]. Inflammaging arises from multiple derangements that stem from all the other hallmarks [43]. Importantly, senescent cells, which accumulate in different organs with age, contribute to systemic inflammation via their SASP [110]. Targeting them with senolytics represents therefore a potential anti-aging strategy. Treatment with Dasatinib and Quercetin has shown to suppress the age-related increase in the expression of pro-inflammatory cytokines in the adipose tissue of mice [122] and humans [115]. The anti-diabetic drug metformin is also being considered for its potential to inhibit inflammatory cytokines by blocking NFkB [123-125].

2. SARCOPENIA

2.1. DEFINITION, PREVALENCE AND DIAGNOSIS

Sarcopenia is a progressive and generalized skeletal muscle disorder characterized by the accelerated loss of muscle mass, quality and function. It commonly occurs as an age-related process and is associated with adverse outcomes, including an increased risk of falls, frailty, institutionalization and mortality [126]. Estimating the prevalence of sarcopenia is challenging due to variations in classifications, cut-off points [127] and the high number of undiagnosed cases [126]. The diagnosis requires the assessment of muscle mass, strength and physical performance. The latter refers to an individual's ability to carry out physical tasks necessary for independent daily living. It involves the function of the whole body rather than that of a single organ and is considered as a critical measure for assessing the severity of sarcopenia [126].

2.2. BODY COMPOSITION CHANGES WITH AGING

Typically, changes in body composition with age are characterized by an increase in body fat until the seventh decade of life [128], coupled with a decrease in muscle mass beginning in the fourth decade [129, 130]. The loss of mass reaches 1-2% per year and a loss of strength is also observed, estimated at 1.5-5 % per year [130]. Moreover, adipose tissue is redistributed, with decreased subcutaneous adipose tissue, increased intra-abdominal visceral depots, and increased fat deposition in heart, liver and skeletal muscle. This redistribution during aging is correlated with an increased risk of metabolic abnormalities, particularly insulin resistance [15, 131, 132].

2.3. Pathophysiology of sarcopenia

Sarcopenia is a complex condition and not yet fully understood. Several intrinsic and extrinsic factors may contribute. Intrinsic factors include neurodegeneration, muscle loss of fibers, chronic inflammation, hormonal changes, mitochondrial dysfunction, oxidative stress, altered regeneration and reduced autophagy. Nutritional status and physical activity levels are described as extrinsic factors [51, 133-136] (Figure 10).

The neuromuscular degeneration

The integrity of the neuromuscular system is compromised with aging and is thought to be a major factor contributing to sarcopenia. Different components of this system fail, leading to loss of muscle mass and function. Indeed, there is a continuous reorganization of motor units with a loss of alpha-motoneurons. This loss promotes lateral sprouting of the neighboring motoneurons, which reinnervate the denervated muscle fibers. As a result, the number of fibers innervated by one motoneuron increases. However, the total muscle fiber number decrease, suggesting that the process of reinnervating denervated fibers remains incomplete [51, 133, 137]. Additionally, the neuromuscular junction becomes less organized and degenerates, with morphological changes including increased presynaptic branching, more dispersed postsynaptic endplate areas, and a reduction in the coupling of the presynaptic vesicles and postsynaptic receptors [51, 137, 138]. Finally, muscle function is impaired, notably due to the loss of muscle fibers and the loss of motor units [51].

Intramyocellular dysfunction

Besides the aging-related loss of muscle fibers, qualitative changes occur at the muscle fiber level and may have a significant impact on overall muscle function and

sarcopenia. With aging, the decrease in muscle mass and strength tend to be dissociated, with the decline of muscle strength being faster than the decrease of muscle mass, suggesting a decrease in muscle quality [73]. Qualitative changes of the fibers include, among others, accumulation of dysfunctional mitochondria and proteins and oxidative stress. These changes have already been described in the previous section “hallmarks of aging”. Autophagy, for example, is required to clear the cell of dysfunctional organelles and altered proteins, but is decreased with aging. The loss of autophagy exacerbates mitochondrial dysfunction and oxidative stress and alters neuromuscular synaptic function. ROS modify actin and myosin and disrupt their interaction, which impacts muscle contraction [65]. The regeneration capacity is also impaired. Satellite cell populations in resting muscle decline with age, as does their regenerative potential [139]. This event exemplifies another hallmark of aging in skeletal muscle, known as “stem cell exhaustion” [43]. Moreover, fibrosis is an important contributor to poor muscle quality in the elderly. Infiltration with connective tissue disrupts the muscle structural integrity, compromises muscle function and regenerative process, and promotes muscle weakness, stiffness and susceptibility to re-injury [140, 141]. Lastly, myosteatosis increases with aging, reduces muscle quality, and correlated with muscle weakness [15, 142].

HORMONAL CHANGES

Changes in hormone production and sensitivity occur with age. The main anabolic hormones (growth hormone (GH)/insulin-like growth factor-I (IGF-1), testosterone, estrogens) decrease and catabolic hormones such as cortisol increase [143]. Insulin sensitivity is impaired. These hormonal changes impact muscle mass, regeneration and metabolic homeostasis [143, 144]. It is of note that aging-related alterations, such as mitochondrial dysfunction, accumulation of IMCL, oxidative stress and

inflammation, contribute to exacerbate insulin resistance in skeletal muscle, thereby increasing the risk of elderly to develop type 2 diabetes [145].

Inflammation

Overtime, the chronic low-grade inflammation that accompanies aging may render the muscle more vulnerable to developing sarcopenia, potentially by provoking protein degradation, impaired regeneration, mitochondrial dysregulation, and insulin resistance [146]. High circulating levels of TNF-α have been associated with an 8-fold increased risk of sarcopenia in elderly subjects [147], while its pharmacological blockade prevented sarcopenia and extended survival in aged mice [148]. Moreover, circulating MCP-1 has been described as a measure of biological rather than chronological age both in mice and in humans. In mice, MCP-1 levels were significantly higher in progeroid animals than in control ones, and in elderly humans, were higher in frail individuals compared to non-frail [149].

Lifestyle

Physical inactivity, defined by not reaching the recommended levels of weekly physical activity (at least 150 min of moderate-intensity aerobic activity per week), is now recognized as the fourth leading cause of death and has been demonstrated to be a contributor to many chronic diseases, including sarcopenia [150]. Sedentary behavior and immobilization have been associated with a higher risk of sarcopenia [151, 152] while physical activity is considered as a preventive intervention [129, 153]. Inadequate nutrition may also play a role. It has been reported that food intake falls by around 25% between 40 and 70 years of age. Low food intake put older people at risk of inadequate nutrient intake which may contribute to the decline of muscle strength and physical capabilities [154]. Added to these behaviors is the important fact that anabolic resistance is a common feature of aging.

Anabolic resistance is defined by a blunted response in muscle protein synthesis rates to common anabolic stimuli in skeletal muscle tissue, such as dietary protein and exercise [155, 156].

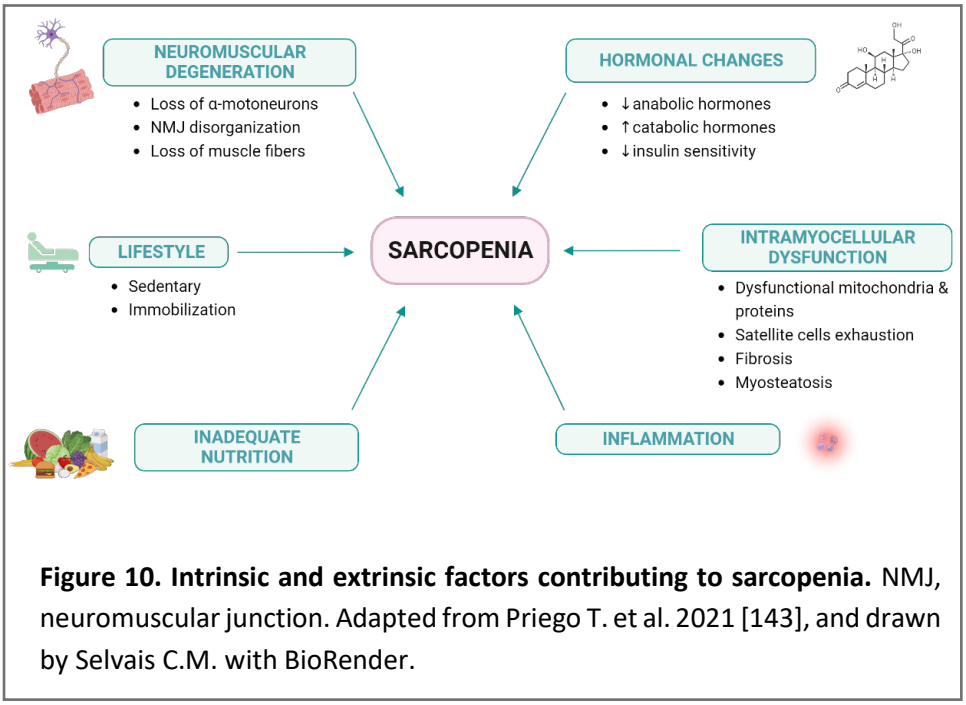

Figure 10. Intrinsic and extrinsic factors contributing to sarcopenia. NMJ, neuromuscular junction. Adapted from Priego T. et al. 2021 [143], and drawn by Selvais C.M. with BioRender.

3. Obesity as an accelerator of the aging process?

A number of molecular and cellular processes are disrupted in obese patients in a manner similar to aging. Obesity triggers chronic, low-grade inflammation, ectopic lipid accumulation, and dysregulation of adipokines. Pathways participating to nutrient sensing are disturbed. Skeletal muscle, liver and adipose tissue become resistant to insulin actions, which exacerbates fat accumulation and muscle loss and increases the risk for the development of type 2 diabetes [157]. In skeletal muscle, AMPK activity is inhibited [158], while mTOR is overactivated [159].The presence of IMCL induces lipotoxicity and inflammation, impairs regeneration and promotes fibrosis [126, 160, 161]. Mitochondria become dysfunctional and senescent cells

accumulate in various organs [114, 162]. Finally, obesity increases the risk of developing a range of diseases that bear resemblance to age-related conditions. It could exacerbate their early onset, leading to premature disability and death [11, 163, 164]. Considering all these effects, it has been suggested that obesity promotes an aging-like phenotype [157, 163, 165].

Sarcopenic obesity is a misdiagnosed and high-risk condition. It designates the coexistence of excess adiposity and low muscle mass and function [161]. This syndrome is predominantly observed in an aging population that is at risk of synergistic complications from both sarcopenia and obesity [160]. Diagnosis for sarcopenic obesity should include assessment of skeletal muscle function and body composition, where the presence of excessive adiposity and low skeletal muscle mass confirm the diagnosis [161]. One challenge is that excess adiposity often conceals the depletion of muscle mass in the clinical setting. Clinicians may mistakenly associate sarcopenia with leanness, and low muscle mass could remain unnoticed in obese patients [19, 126].

PART IV: ADIPONECTIN AND ADIPORON*

1. ADIPONECTIN (APN)

1.1. STRUCTURE

Adiponectin (ApN) is a hormone abundantly secreted by adipocytes [13]. In humans, ApN is a protein consisting of 244 amino acids encoded by the ADIPOQ gene, with a molecular weight of approximately 30 kDa [167]. ApN is synthesized as a monomeric peptide composed of four domains: a signal sequence, a short variable region, a collagen-like domain and a globular domain [168, 169]. ApN monomers can assemble into complexes of up to 18 mers (Figure 11)[170]. Consequently, ApN circulates in the bloodstream as low-molecular-weight form (LMW, trimer), middle-molecular-weight form (MMW, hexamer) and high-molecular-weight form (HMW, 12–18 mers) [171]. Not only the total levels of ApN, but also the distribution of its various forms contribute to the biological effects of the hormone. HMW ApN elicits the most potent insulin-sensitizing effects [172]. ApN could also be cleaved into a smaller globular fragment (gApN) by leukocyte elastases secreted from activated monocytes and neutrophils [173, 174].

* Some portions of this section have been adapted from a review article 166. Abou-Samra, M., et al., *Adiponectin and Its Mimics on Skeletal Muscle: Insulin Sensitizers, Fat Burners, Exercise Mimickers, Muscling Pills … or Everything Together?* Int J Mol Sci, 2020. **21**(7). in which I contributed as a co-author.

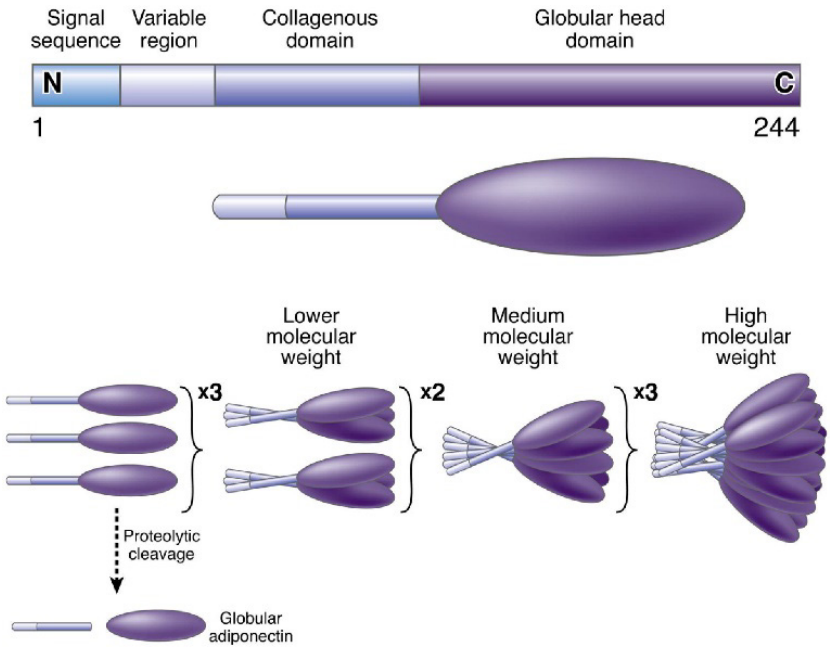

Figure 11. ApN structure. Badman M.K. & Flier J.S. 2007 [170].

1.2. PRODUCTION AND SECRETION

ApN gene expression by adipocytes is controlled by a number of transcription factors. PPARγ (peroxisome proliferator-activated receptor gamma), C/EBPα (CAAT/enhancer-binding protein alpha), and SREBP (sterol regulatory element-binding protein) promote ApN gene transcription, while NFAT (nuclear factor of activated T-cells) and CREB (cAMP response element-binding protein) act as transcriptional repressors. ApN multimerization involves post-translational modifications such as hydroxylation, glycosylation, and disulfide bond formation, and is regulated by enzymes within the endoplasmic reticulum, namely Ero1-Lα, DsbA-L, ERp44 [175].

Besides being an adipokine, ApN can also be secreted by the skeletal muscle as a myokine [176, 177]. Although it is mainly secreted by adipocytes under normal conditions, ApN may be produced in skeletal muscle of mice submitted to stressful challenges. Acute lipopolysaccharides (LPS) injection or low-grade inflammation (genetic or nutritional induced obesity) enhanced ApN expression in muscle of challenged mice [176, 178, 179]. ApN up-regulation was also reproduced in cultured murine or human myotubes in response to pro-inflammatory cytokines, ROS inducers or triglycerides [176, 178]. This led to the hypothesis that muscle ApN could be a local protective mechanism to counteract excessive inflammatory reaction, ectopic fat deposit, and oxidative damage.

ApN is found in plasma at high concentrations (~ µg/mL; at least 3 orders of magnitude higher than other hormones). Unlike most adipokines that increase with higher adiposity, circulating ApN levels are negatively correlated with the BMI and are decreased (< 4.0 µg/mL) in obesity and patients meeting the criteria for the metabolic syndrome [13]. The mechanisms underlying the downregulation of ApN production are related to the low-grade chronic inflammatory state and the enhanced oxidative stress that prevail in obesity; expression and secretion of ApN in adipocytes are inhibited by oxygen species and pro-inflammatory cytokines (TNF-α, ILs, …)[175]. Inversely, weight loss in obese humans [180] or exercise [181] increase ApN plasma concentration.

1.3. ApN receptors

AdipoR1 and AdipoR2 are the major ApN receptors in vivo [182]. They contain seven transmembrane domains but differ structurally and functionally from G-protein coupled receptors. AdipoR1 is mainly expressed in skeletal muscle, whereas AdipoR2 is predominantly expressed in the liver [183]. AdipoR1 is tightly linked to

activation of AMPK pathways, while AdipoR2 seems to be associated with activation of peroxisome proliferator-activated receptor (PPAR)-α pathways [182, 184]. AdipoR1 is a high-affinity receptor for gApN but can also bind full-length ApN. AdipoR2 shows intermediate affinity for both the globular and the full-length forms [183]. T-cadherin is an additional binding partner for MMW and HMW isoforms of ApN. T-cadherin is a glycosylphosphatidylinositol-anchored cadherin, lacking transmembrane and cytosolic domains, and is expressed in the heart, aorta, and skeletal muscle. In these tissues, ApN may stimulate exosome production to potentially enhance whole-body metabolism. This receptor further mediates cardiovascular protection and skeletal muscle regeneration by HMW ApN [185].

Obesity is not only accompanied by low levels of ApN (hypoadiponectinemia), but also by reduced expression of adiponectin receptors, AdipoR1 and AdipoR2 [186]. In ob/ob mice, the expression of AdipoR1/R2 is significantly diminished in both skeletal muscle and adipose tissue, which is associated with decreased activation of AMPK by ApN [187]. Furthermore, individuals with a family history of type 2 diabetes also exhibit decreased expression of AdipoR1 in skeletal muscle [188].

1.4. Pleiotropic effects

ApN, by binding to its receptors AdipoR1 or AdipoR2, exerts a wide range of biological effects on several target tissues. ApN is known for its insulin-sensitizing, anti-atherogenic, anti-inflammatory, and antioxidant properties. In the liver, ApN stimulates fatty-acid oxidation [189] and reduces glucose production, thereby exerting an insulin-sensitizing effect on this organ [190]. In adipose tissue, ApN also exerts insulin-sensitizing properties through its anti-inflammatory action combined to an increase of glucose uptake [191, 192]. ApN shows anti-atherosclerotic and cardio-protective effects by inducing the production of nitric oxide in endothelial cells [193], and by acting as anti-inflammatory and anti-apoptotic agent on the

cardiovascular system [194]. Figure 12 summarizes the diverse effects of ApN on different tissues [166]. ApN effects on skeletal muscle are detailed in the following section.

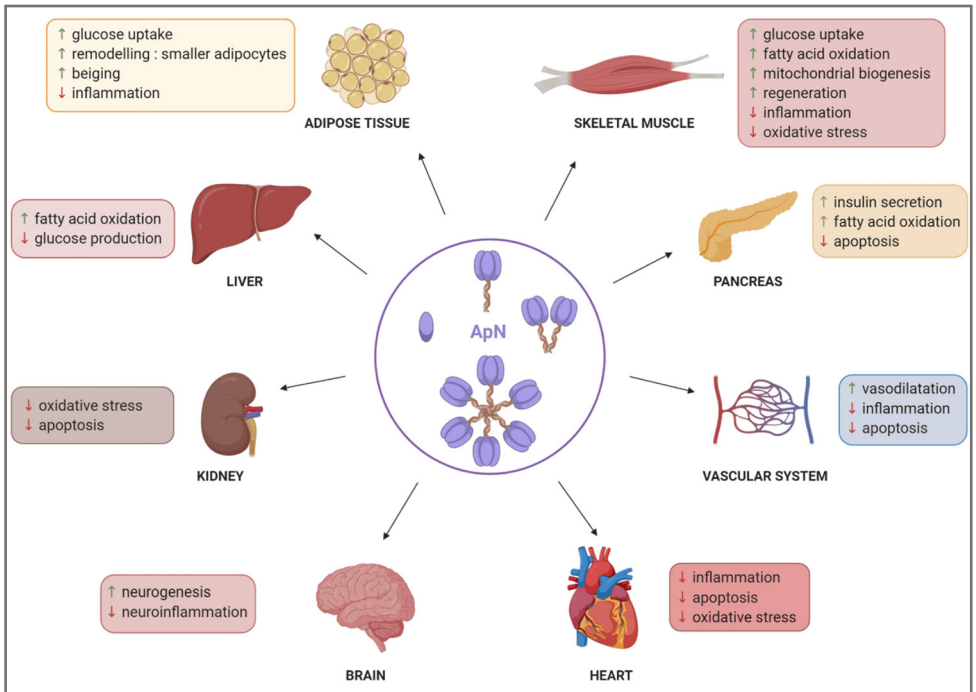

Figure 12. Pleiotropic effects of adiponectin. ApN, adiponectin as globular, trimeric, hexameric or multimeric forms (starting from left symbol and going in a clockwise direction). Abou-Samra M. et al. 2020 [166].

1.5. ApN effects on Skeletal muscle

Skeletal muscle is an important target where ApN regulates energy metabolism, mitigates oxidative stress and inflammation, and promotes regeneration [171]. These properties have been investigated in vivo, utilizing mice that either received ApN, overexpressed it, or were deficient in ApN/AdipoR. Most of these data have been confirmed in vitro using human muscle cells.

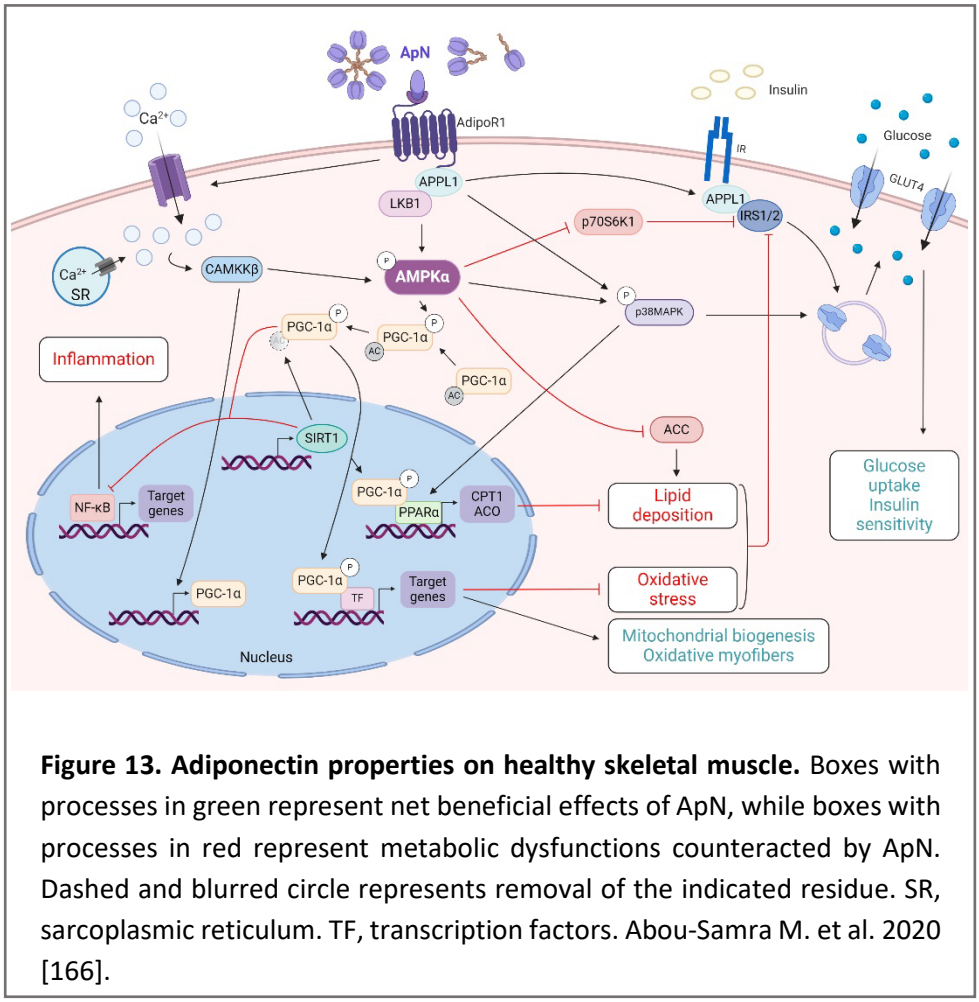

Figure 13. Adiponectin properties on healthy skeletal muscle. Boxes with processes in green represent net beneficial effects of ApN, while boxes with processes in red represent metabolic dysfunctions counteracted by ApN. Dashed and blurred circle represents removal of the indicated residue. SR, sarcoplasmic reticulum. TF, transcription factors. Abou-Samra M. et al. 2020 [166].

1.5.1. Fuel partitioning and metabolic effects

A) AdipoR1-AMPK-SIRT1-PGC-1α pathway and mitochondrial biogenesis

ApN exerts its metabolic effects on the skeletal muscle mainly by activating the AMPK signaling pathway (Figure 13). As described previously, AMPK plays a critical role in systemic energy balance. It is activated after phosphorylation by distinct upstream kinases such as LKB1 or CAMKKβ. When ApN links to AdipoR1, it induces

the binding of the adaptor protein APPL1, which functions as an anchoring protein tethering LKB1 [195]. ApN also induces extracellular Ca^{2+} influx [184] and Ca^{2+} release from the sarcoplasmic reticulum [195], thereby activating CAMKKβ, which leads to increased expression of PGC-1α [184]. Both LKB1 and CAMKKβ fully activate AMPK. Next, P-AMPK phosphorylates PGC-1α and indirectly increases the expression of a deacetylase, SIRT1. SIRT1 then completely activates PGC-1α by deacetylation. In turn, PGC-1α increases the activity of several transcriptions factors (TF), thus stimulating the expression of target genes leading to an increase of mitochondrial biogenesis and a shift towards an oxidative metabolism [184].

B) FATTY ACID OXIDATION

AMPK is also implicated in the sequential activation of p38 mitogen-activated protein kinase (MAPK) and PPARα (Figure 13). By this mechanism, ApN increases the transcriptional activity of PPARα and the expression of its target genes, involved in fatty-acid transport into the mitochondria (carnitine palmitoyltransferase 1, CPT1) and oxidation (Acyl-CoA Oxidase, ACO) [196]. Eventually, AMPK further increases fatty-acid oxidation by inhibiting acetyl-CoA carboxylase 2 (ACC2) through phosphorylation. ACC is the enzyme that catalyzes the committed step in fatty-acid synthesis. A decrease in ACC activity reduces the levels of intracellular malonyl-CoA, an allosteric inhibitor of CPT1. Hence, CPT1 can assume the transfer of long-chain fatty acids from the cytosol into the mitochondria, where they are oxidized [197].

C) INSULIN-SENSITIZING ACTION

ApN exerts a core protective effect against the metabolic syndrome through its insulin-sensitizing action. Its expression is reduced in HFD-induced obese mice, leading to insulin-resistance. However, administration of ApN effectively lowers blood sugar levels and reduces insulin resistance [198]. Similarly, ApN-transgenic (ApN-Tg) mice are more sensitive to insulin [192], while ApN-KO mice are more

resistant [199]. Finally, ApN-Tg ob/ob mice (obese mice overexpressing ApN) showed partial attenuation of insulin resistance and diabetes [200].

In the skeletal muscle, ApN can modulate insulin sensitivity through a variety of mechanisms (Figure 13). First, ApN activates AMPK signaling and P-AMPK inhibits p70S6K1, an enzyme that inactivates the insulin receptor substrate-1 (IRS-1) through phosphorylation on serine residues, thereby blocking the insulin signaling cascade [201]. Second, activation of PGC-1α enhances the expression of several oxidative-stress detoxification enzymes and molecules involved in fatty-acid oxidation [75, 202]. As both oxidative stress and increased triglyceride content are linked to insulin resistance by inhibitory phosphorylation in IRS-1, ApN further acts as a sensitizing agent [203]. Third, ApN induces the translocation of GLUT4 to the plasma membrane, thereby promoting glucose uptake [183, 204]. This translocation results from stimulating p38 MAPK via either AMPK [183, 196] or interaction with APPL1. Alternatively, interaction between APPL1 and Rab5 (a small GTPase) may also contribute. Eventually, APPL1 promotes IRS-1 binding to the insulin receptor and enhances insulin signaling [205].

1.5.2. Control of inflammation and oxidative stress

ApN appears to be necessary to control inflammation and oxidative stress in skeletal muscle. ApN-deficient mice display higher susceptibility to oxidative stress, inflammation, and apoptosis; all these abnormalities are exacerbated by acute (LPS) or chronic (obesogenic diet) inflammatory challenge and corrected by local electro-transfer of the ApN gene [179, 206]. Mice with muscle-specific disruption of AdipoR1 also exhibited a local decrease in oxidative-stress-detoxifying enzymes [184]. Moreover, ApN disclosed strong anti-inflammatory properties in human myotubes when submitted to an inflammatory challenge [207, 208]. ApN could also

put a brake on local inflammation by functioning as a direct regulator of macrophage phenotype favoring the switch from a pro-inflammatory M1-like state to an anti-inflammatory M2-like state, as shown in vivo and in vitro. M2 cells are known to secrete the anti-inflammatory cytokine IL-10 and down-regulate the production of pro-inflammatory cytokines [209].

Mechanistically, the anti-inflammatory effects of ApN in human "healthy" myotubes were linked to activation of the AdipoR1-AMPK-SIRT1-PGC-1α pathway [207, 208]. The AMPK pathway is known to inhibit inflammation and oxidative stress by repressing the activity of the transcription factor, nuclear factor kappa B (NF-κB), a key inducer of inflammatory responses. Indeed, both PGC-1α and SIRT1 could repress NF-κB [210] (Figure 13). Moreover, a strong microRNA candidate, mir-711, has also been identified by the laboratory for mediating the anti-inflammatory action of ApN on mouse and human skeletal muscles. ApN up-regulated the expression of miR-711, which, in turn, also repressed NF-κB as well as the inflammasome complex [211, 212]. Eventually, as mentioned earlier, PGC-1α is also a regulator of cellular oxidant–antioxidant homeostasis by stimulating gene expression of several antioxidant enzymes such as superoxide dismutase-2, catalase, and glutathione peroxidase [75].

1.5.3. Tissue repair and regeneration

After acute injury, skeletal muscle has a remarkable capacity to initiate a rapid and extensive regeneration, which is always associated with an inflammatory reaction that varies in intensity [213]. Evidence points out that a controlled and efficient inflammation is necessary for an optimal muscle recovery [214]. Regeneration of skeletal muscle also depends on the satellite cells, which are kept in a quiescent state in a healthy muscle [213].

After injury, immune cells, including M1 macrophages, are recruited to the lesion site where they produce and release elastases that cleave native ApN into its globular ApN form (gApN) [174]. As gApN expression is low in the bloodstream, it is likely that most gApN is locally produced by muscle (satellite cells, differentiating myoblasts…) and acts in an autocrine or paracrine manner as a tissue regenerating hormone [215]. Both M1 macrophages and gApN play essential roles in the activation of satellite cells and the initiation of muscle regeneration [214, 215]. Once activated, satellite cells will migrate, proliferate and give rise to myoblasts that differentiate into myotubes, which then fuse to restore damaged fibers or generate new one [213].

ApN appears to regulate several steps of the repair process by activating different signaling pathways, including p38MAPK and AMPK [215], and different myogenic TF such as Myf5, MyoD, Myogenin, and Mrf4 [207]. First, up-regulation of Myf5 by ApN in skeletal muscle [207] allows the activation of satellite cells and their commitment to regenerate the skeletal muscle [216]. gApN also elicits a specific motility program in satellite cells by allowing them to produce specific metalloproteases, which can degrade the extracellular matrix surrounding muscle fibers, thus driving a proteolytic migration to reach the injury site [217]. Second, gApN induces the expression of MyoD that allows myoblast proliferation and differentiation [207, 218]. Third, ApN can coordinate the last step of skeletal muscle regeneration. Indeed, it activates the expression of two key factors of muscle differentiation, Myogenin and Mrf4 [207], which are essential for provoking cell fusion into multinucleated myotubes [216] (Figure 14).

There is an interplay among the 3 major functions of ApN in skeletal muscle. ApN plays a crucial role in coordinating resolution of inflammation and energy metabolism for an efficient muscle regeneration. ApN promotes the conversion of M1 to M2 macrophages, thereby favoring the resolution of inflammation [209]. Meanwhile, ApN enhances PGC-1α expression and activity, which promotes oxidative metabolism to respond to the high energy demand for sustaining tissue-healing and regeneration [219]. Thus, controlled accumulation of immune cells and increased energy metabolism are essential for appropriate muscle tissue remodeling [214].

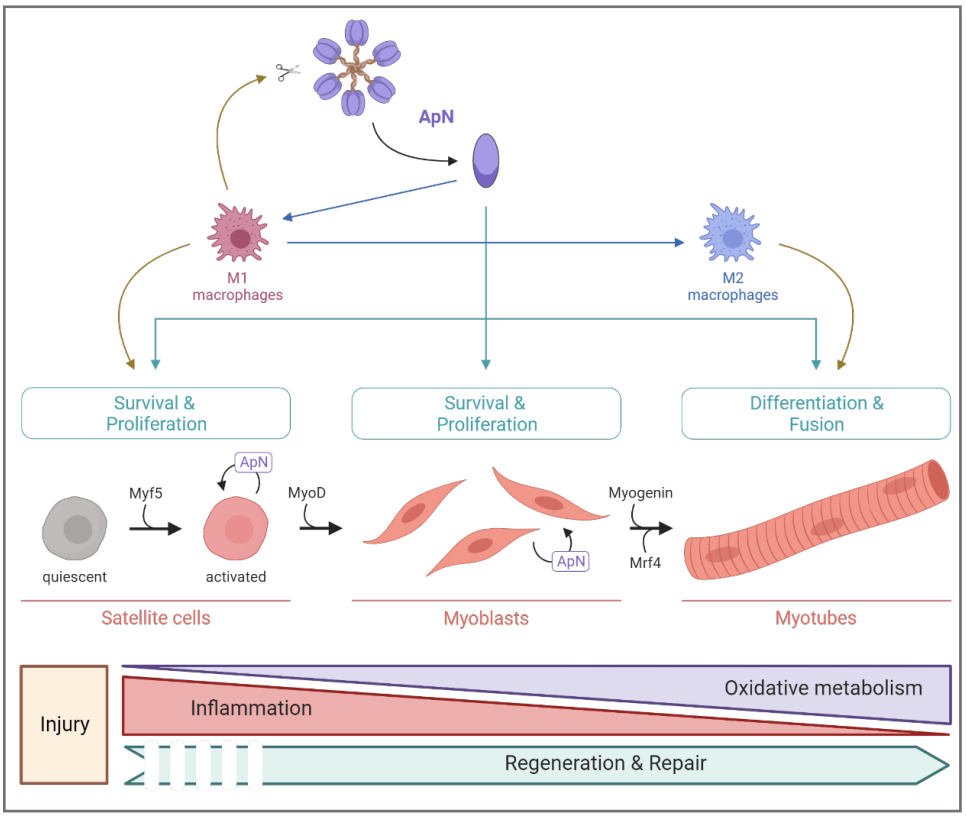

Figure 14. Pro-myogenic properties of Adiponectin. This figure summarizes the multiple beneficial effects of ApN on several steps of muscle regeneration (boxes in green), while highlighting an important interplay among 3 major processes, including resolution of inflammation, energy metabolism, and muscle repair. Green arrows represent the direct pro-myogenic effects of ApN. Blue arrows represent an indirect pro-myogenic effect of ApN by inducing a shift from pro-inflammatory M1 to anti-inflammatory M2 macrophages, for a resolution of inflammation and activation of the tissue-healing process. Pink arrows represent an indirect pro-myogenic effect of ApN by stimulating non-muscle stem cells and driving their commitment towards the skeletal muscle lineage. Brown arrows represent the different effects of macrophages. Abou-Samra M. et al. 2020 [166].

1.5.4. AUTOPHAGY

ApN could also activates autophagy, although limited research has been conducted on this topic to date in the skeletal muscle. In vitro, treatment of myoblasts with gApN promotes autophagy via AMPK, leading to increased cell viability and protection against apoptosis. When AMPK or autophagy are inhibited, these effects of ApN treatment are lost [220]. Another study has demonstrated a similar autophagic response, indicating that ApN (non-globular in this case) activates autophagic flux through AMPK, which in turn phosphorylates ULK1 at Ser555 [221]. AMPK, in addition to activating ULK1 [105], could also indirectly promote autophagy by inhibiting mTOR [109, 222]. In vivo, ApN knockout mice display reduced expression of the autophagic markers LC3-II and beclin-I [220]. Moreover, the knockdown of AdipoR1 prevents the expression of certain markers of autophagy that are typically increased with exercise [223].

1.6. ApN as a protector for the skeletal muscle?

In the context of skeletal muscle, our previous researches have demonstrated the powerful protective effects of ApN in mdx mice, a model with a severe muscle disease (Duchenne Muscular Dystrophy, DMD). ApN attenuates muscle inflammation and oxidative stress while enhancing the myogenic program, resulting in reduced muscle damage and improved force and endurance. These beneficial effects are mainly mediated through the AdipoR1-AMPK-PGC-1α pathway [166, 207].

This protective action of ApN on skeletal muscle is also evident in a model of accelerated senescence. Specifically, chronic exercise training in these mice ameliorates age-related muscle alterations in strength, endurance, muscle mass, and myofiber size, while also increasing circulating levels of ApN. However, these exercise-induced muscular benefits are compromised upon the blockade of ApN or AdipoR1 using specific antibodies. Such interventions suppress exercise-triggered AMPK activation, reduce PGC-1α, and result in enhanced mitochondrial damage. These observations suggest that exercise training may exert beneficial effects on muscle through the ApN-AdipoR1 axis, thereby underscoring the potent protective role of ApN in skeletal muscle [224].

1.7. ApN as an anti-aging therapy?

ApN appears to be a significant player in the regulation of healthspan and lifespan. In murine models for example, ApN knockout mice have a notably shortened lifespan, whether fed a regular chow diet or a HFD. Furthermore, these mice exhibit worsened age-related glucose and lipid metabolism disorders [225, 226]. Likewise, AdipoR1/AdipoR2 knockout mice have a shortened lifespan compared to wild-type mice, under both normal and HFD [227]. In contrast, mice that overexpress ApN

show an extended healthspan and median lifespan, along with enhanced systemic insulin sensitivity and reduced age-related tissue inflammation and fibrosis in adipose tissue, kidney and liver [225].

In humans, plasma ApN levels are higher among centenarians than in elderly individuals. These levels correlate with a favorable metabolic phenotype, including good lipid profile and insulin sensitivity [228, 229]. In geriatric patients, those who are sarcopenic exhibit lower levels of ApN and higher inflammatory markers (C-reactive protein) compared to their non-sarcopenic counterparts [230]. Lastly, low circulating levels of ApN also prevail in patients with obesity, sarcopenic obesity, and in those with the metabolic syndrome, and is inversely correlated with insulin resistance [13, 160].

All together, these results support a role of ApN as potent protector of skeletal muscle and an essential regulator of healthspan and lifespan.

2. AdipoRon

2.1. ApN therapeutic hurdles

Given its numerous beneficial pleiotropic effects, ApN has attracted considerable interest, raising hopes for its utilization as a therapeutic agent in the treatment of several diseases [231]. One strategy to enhance ApN effects is the utilization of recombinant bioactive ApN. However, its large-scale production faces several challenges. First, ApN is difficult to produce in its full-length form and requires several post-translational modifications to form higher-order structures. Furthermore, ApN circulates at high concentrations in the plasma (µg/ml) and has a rapid turnover, necessitating repeated administration over time. Finally, being a peptide, ApN needs to be injected to exert its effects, further complicating its

administration [231]. In this context, the development ApN mimics that can specifically bind to AdipoR was eagerly awaited. Several short peptides and small molecules have now been identified to target AdipoRs and mimic some of ApN effects [166].

2.2. AdipoRon

Among these agonists, AdipoRon has been the most extensively studied to date. AdipoRon was identified in 2013 by Okada-Iwabu et al. This orally active synthetic small molecule binds to both AdipoR1 and AdipoR2 at low µM concentration and recapitulates the effects of ApN both in vitro and in vivo. In C2C12 cells, AdipoRon increases AMPK activation and PGC-1α expression, resulting in mitochondrial biogenesis. In vivo, it activates the AMPK and PPAR-α pathways, improving glucose and lipid metabolism, as well as insulin sensitivity in mice fed with a HFD. In these mice, AdipoRon also improves exercise endurance. Moreover, AdipoRon ameliorates diabetes of db/db mice and extends their lifespan. More specifically in the skeletal muscle, AdipoRon increases mitochondrial biogenesis, reduces tissue triglyceride content and oxidative stress. In the liver, AdipoRon decreases lipid content, oxidative stress and inflammation [227].

AdipoRon has thus been first proposed for the treatment of type 2 diabetes and other obesity-related disorders in mice [227, 232-236]. Since then, its beneficial effects have also been demonstrated in other non-metabolic conditions including cancer [237, 238], depression [233], anxiety [239], and Alzheimer's disease [240].

Our team has recently demonstrated the beneficial and protective effects of AdipoRon on dystrophic skeletal muscle in mdx mice and human DMD myotubes. An 8-week oral treatment significantly mitigated skeletal muscle inflammation,

oxidative stress, and damage, while markedly enhancing regeneration and endurance capacity. AdipoRon acted mainly through AdipoR1-AMPK signaling [241].

To date, AdipoRon has not been tested in humans. However, a recent study by Iwabu *et al* has confirmed the effectiveness of AdipoRon on the human receptor AdipoR1 [242]. They generated muscle AdipoR1-humanized mice and demonstrated that AdipoRon could still exert its beneficial effects in the absence of murine AdipoR1-AdipoR2 receptors. This study has translational implications since it suggests that AdipoRon also exerts its effects through human AdipoR1 and may, therefore, be effective for clinical application.

By mimicking the potent pleiotropic beneficial effects of ApN, AdipoRon may offer an effective therapeutic approach for the prevention and treatment of age-related complications, and may promote healthy longevity. Specifically, its short- and long-term effects on aging muscle should be investigated, especially given the current lack of pharmacological approaches to mitigate the age-related loss of muscle mass, quality and function.

REFERENCES

1. Frontera, W.R. and J. Ochala, *Skeletal muscle: a brief review of structure and function.* Calcif Tissue Int, 2015. **96**(3): p. 183-95.
2. Pedersen, B.K. and M.A. Febbraio, *Muscles, exercise and obesity: skeletal muscle as a secretory organ.* Nat Rev Endocrinol, 2012. **8**(8): p. 457-65.
3. Mukund, K. and S. Subramaniam, *Skeletal muscle: A review of molecular structure and function, in health and disease.* Wiley Interdiscip Rev Syst Biol Med, 2020. **12**(1): p. e1462.
4. Romanello, V. and M. Sandri, *The connection between the dynamic remodeling of the mitochondrial network and the regulation of muscle mass.* Cell Mol Life Sci, 2021. **78**(4): p. 1305-1328.
5. Smith, J.A.B., et al., *Exercise metabolism and adaptation in skeletal muscle.* Nat Rev Mol Cell Biol, 2023. **24**(9): p. 607-632.
6. Bloemberg, D. and J. Quadrilatero, *Rapid determination of myosin heavy chain expression in rat, mouse, and human skeletal muscle using multicolor immunofluorescence analysis.* PLoS One, 2012. **7**(4): p. e35273.
7. Schiaffino, S. and C. Reggiani, *Fiber types in mammalian skeletal muscles.* Physiol Rev, 2011. **91**(4): p. 1447-531.
8. Schiaffino, S., *Muscle fiber type diversity revealed by anti-myosin heavy chain antibodies.* Febs j, 2018. **285**(20): p. 3688-3694.
9. Gouspillou, G., et al., *The relationship between muscle fiber type-specific PGC-1α content and mitochondrial content varies between rodent models and humans.* PLoS One, 2014. **9**(8): p. e103044.
10. Organization, W.H. *Obesity and overweight*. 2021; Available from: https://www.who.int/news-room/fact-sheets/detail/obesity-and-overweight.
11. Blüher, M., *Obesity: global epidemiology and pathogenesis.* Nat Rev Endocrinol, 2019. **15**(5): p. 288-298.
12. Mertens, E., D. Sagastume, and J.L. Peñalvo, *Quantification of disparities in the distribution of lifestyle and metabolic risk factors, prevalence of non-communicable diseases and related mortality: the Belgian Health Interview Surveys 1997-2018.* BMJ Open, 2021. **11**(11): p. e053260.
13. Maury, E. and S.M. Brichard, *Adipokine dysregulation, adipose tissue inflammation and metabolic syndrome.* Mol Cell Endocrinol, 2010. **314**(1): p. 1-16.
14. Morales, P.E., J.L. Bucarey, and A. Espinosa, *Muscle Lipid Metabolism: Role of Lipid Droplets and Perilipins.* J Diabetes Res, 2017. **2017**: p. 1789395.
15. Correa-de-Araujo, R., et al., *Myosteatosis in the Context of Skeletal Muscle Function Deficit: An Interdisciplinary Workshop at the National Institute on Aging.* Front Physiol, 2020. **11**: p. 963.
16. Coen, P.M. and B.H. Goodpaster, *Role of intramyocelluar lipids in human health.* Trends Endocrinol Metab, 2012. **23**(8): p. 391-8.
17. Seibert, J.T., et al., *Muscle Lipid Droplets: Cellular Signaling to Exercise Physiology and Beyond.* Trends Endocrinol Metab, 2020. **31**(12): p. 928-938.

18. Gemmink, A., P. Schrauwen, and M.K.C. Hesselink, *Exercising your fat (metabolism) into shape: a muscle-centred view.* Diabetologia, 2020. **63**(8): p. 1453-1463.
19. Nachit, M. and I.A. Leclercq, *Emerging awareness on the importance of skeletal muscle in liver diseases: time to dig deeper into mechanisms!* Clin Sci (Lond), 2019. **133**(3): p. 465-481.
20. Bonen, A., et al., *Triacylglycerol accumulation in human obesity and type 2 diabetes is associated with increased rates of skeletal muscle fatty acid transport and increased sarcolemmal FAT/CD36.* Faseb j, 2004. **18**(10): p. 1144-6.
21. Zhang, L., et al., *Role of fatty acid uptake and fatty acid beta-oxidation in mediating insulin resistance in heart and skeletal muscle.* Biochim Biophys Acta, 2010. **1801**(1): p. 1-22.
22. Fritzen, A.M., A.M. Lundsgaard, and B. Kiens, *Tuning fatty acid oxidation in skeletal muscle with dietary fat and exercise.* Nat Rev Endocrinol, 2020. **16**(12): p. 683-696.
23. Benador, I.Y., et al., *Mitochondria Bound to Lipid Droplets: Where Mitochondrial Dynamics Regulate Lipid Storage and Utilization.* Cell Metab, 2019. **29**(4): p. 827-835.
24. Wu, H. and C.M. Ballantyne, *Skeletal muscle inflammation and insulin resistance in obesity.* J Clin Invest, 2017. **127**(1): p. 43-54.
25. Abdul-Ghani, M.A. and R.A. DeFronzo, *Pathogenesis of insulin resistance in skeletal muscle.* J Biomed Biotechnol, 2010. **2010**: p. 476279.
26. Bergman, B.C. and B.H. Goodpaster, *Exercise and Muscle Lipid Content, Composition, and Localization: Influence on Muscle Insulin Sensitivity.* Diabetes, 2020. **69**(5): p. 848-858.
27. Selvais, C.M., et al., *Fiber Type and Subcellular-Specific Analysis of Lipid Droplet Content in Skeletal Muscle.* J Vis Exp, 2022(184).
28. Nielsen, J., et al., *Lipid droplet size and location in human skeletal muscle fibers are associated with insulin sensitivity.* Am J Physiol Endocrinol Metab, 2017. **313**(6): p. E721-e730.
29. Bosma, M., *Lipid droplet dynamics in skeletal muscle.* Exp Cell Res, 2016. **340**(2): p. 180-6.
30. Nielsen, J., et al., *Increased subsarcolemmal lipids in type 2 diabetes: effect of training on localization of lipids, mitochondria, and glycogen in sedentary human skeletal muscle.* Am J Physiol Endocrinol Metab, 2010. **298**(3): p. E706-13.
31. Ferreira, R., et al., *Subsarcolemmal and intermyofibrillar mitochondria proteome differences disclose functional specializations in skeletal muscle.* Proteomics, 2010. **10**(17): p. 3142-54.
32. Barrett, J.S., et al., *High intramuscular triglyceride turnover rates and the link to insulin sensitivity: influence of obesity, type 2 diabetes and physical activity.* Appl Physiol Nutr Metab, 2022. **47**(4): p. 343-356.
33. Daemen, S., et al., *Distinct lipid droplet characteristics and distribution unmask the apparent contradiction of the athlete's paradox.* Mol Metab, 2018. **17**: p. 71-81.
34. Andrich, D.E., et al., *Altered Lipid Metabolism Impairs Skeletal Muscle Force in Young Rats Submitted to a Short-Term High-Fat Diet.* Front Physiol, 2018. **9**: p. 1327.

35. Choi, S.J., et al., *Intramyocellular Lipid and Impaired Myofiber Contraction in Normal Weight and Obese Older Adults.* J Gerontol A Biol Sci Med Sci, 2016. **71**(4): p. 557-64.
36. Rasouli, N., et al., *Ectopic fat accumulation and metabolic syndrome.* Diabetes Obes Metab, 2007. **9**(1): p. 1-10.
37. Samuel, V.T. and G.I. Shulman, *Nonalcoholic Fatty Liver Disease as a Nexus of Metabolic and Hepatic Diseases.* Cell Metab, 2018. **27**(1): p. 22-41.
38. Younossi, Z., et al., *Global burden of NAFLD and NASH: trends, predictions, risk factors and prevention.* Nat Rev Gastroenterol Hepatol, 2018. **15**(1): p. 11-20.
39. Sheka, A.C., et al., *Nonalcoholic Steatohepatitis: A Review.* Jama, 2020. **323**(12): p. 1175-1183.
40. Olshansky, S.J., *From Lifespan to Healthspan.* Jama, 2018. **320**(13): p. 1323-1324.
41. Organization, W.H. *Decade of healthy ageing: baseline report*. 2020; Available from: https://www.who.int/publications/i/item/9789240017900.
42. López-Otín, C., et al., *The hallmarks of aging.* Cell, 2013. **153**(6): p. 1194-217.
43. López-Otín, C., et al., *Hallmarks of aging: An expanding universe.* Cell, 2023. **186**(2): p. 243-278.
44. Wen, J.H., et al., *Cellular Protein Aggregates: Formation, Biological Effects, and Ways of Elimination.* Int J Mol Sci, 2023. **24**(10).
45. Brady, S., et al., *Tubular Aggregates and Cylindrical Spirals Have Distinct Immunohistochemical Signatures.* J Neuropathol Exp Neurol, 2016. **75**(12): p. 1171-1178.
46. Boncompagni, S., et al., *Long-Term Exercise Reduces Formation of Tubular Aggregates and Promotes Maintenance of Ca(2+) Entry Units in Aged Muscle.* Front Physiol, 2020. **11**: p. 601057.
47. Hughes, D.C., et al., *Ubiquitin Ligases in Longevity and Aging Skeletal Muscle.* Int J Mol Sci, 2022. **23**(14).
48. Murton, A.J., D. Constantin, and P.L. Greenhaff, *The involvement of the ubiquitin proteasome system in human skeletal muscle remodelling and atrophy.* Biochim Biophys Acta, 2008. **1782**(12): p. 730-43.
49. Cohen, S., J.A. Nathan, and A.L. Goldberg, *Muscle wasting in disease: molecular mechanisms and promising therapies.* Nat Rev Drug Discov, 2015. **14**(1): p. 58-74.
50. Edström, E., et al., *Atrogin-1/MAFbx and MuRF1 are downregulated in aging-related loss of skeletal muscle.* J Gerontol A Biol Sci Med Sci, 2006. **61**(7): p. 663-74.
51. Larsson, L., et al., *Sarcopenia: Aging-Related Loss of Muscle Mass and Function.* Physiol Rev, 2019. **99**(1): p. 427-511.
52. Koyuncu, S., et al., *Rewiring of the ubiquitinated proteome determines ageing in C. elegans.* Nature, 2021. **596**(7871): p. 285-290.
53. Sandri, M., et al., *Signalling pathways regulating muscle mass in ageing skeletal muscle: the role of the IGF1-Akt-mTOR-FoxO pathway.* Biogerontology, 2013. **14**(3): p. 303-23.
54. Hansen, M., D.C. Rubinsztein, and D.W. Walker, *Autophagy as a promoter of longevity: insights from model organisms.* Nat Rev Mol Cell Biol, 2018. **19**(9): p. 579-593.

55. Levine, B. and G. Kroemer, *Biological Functions of Autophagy Genes: A Disease Perspective.* Cell, 2019. **176**(1-2): p. 11-42.
56. Hurley, J.H. and L.N. Young, *Mechanisms of Autophagy Initiation.* Annu Rev Biochem, 2017. **86**: p. 225-244.
57. Kim, J., et al., *AMPK and mTOR regulate autophagy through direct phosphorylation of Ulk1.* Nat Cell Biol, 2011. **13**(2): p. 132-41.
58. Xia, Q., et al., *The Role of Autophagy in Skeletal Muscle Diseases.* Front Physiol, 2021. **12**: p. 638983.
59. Parzych, K.R. and D.J. Klionsky, *An overview of autophagy: morphology, mechanism, and regulation.* Antioxid Redox Signal, 2014. **20**(3): p. 460-73.
60. Vargas, J.N.S., et al., *The mechanisms and roles of selective autophagy in mammals.* Nat Rev Mol Cell Biol, 2023. **24**(3): p. 167-185.
61. Johansen, T. and T. Lamark, *Selective autophagy mediated by autophagic adapter proteins.* Autophagy, 2011. **7**(3): p. 279-96.
62. Palikaras, K., E. Lionaki, and N. Tavernarakis, *Mechanisms of mitophagy in cellular homeostasis, physiology and pathology.* Nat Cell Biol, 2018. **20**(9): p. 1013-1022.
63. Leduc-Gaudet, J.P., et al., *Mitochondrial Dynamics and Mitophagy in Skeletal Muscle Health and Aging.* Int J Mol Sci, 2021. **22**(15).
64. Sakuma, K., et al., *p62/SQSTM1 but not LC3 is accumulated in sarcopenic muscle of mice.* J Cachexia Sarcopenia Muscle, 2016. **7**(2): p. 204-12.
65. Carnio, S., et al., *Autophagy impairment in muscle induces neuromuscular junction degeneration and precocious aging.* Cell Rep, 2014. **8**(5): p. 1509-21.
66. Zhou, J., et al., *Changes in macroautophagy, chaperone-mediated autophagy, and mitochondrial metabolism in murine skeletal and cardiac muscle during aging.* Aging (Albany NY), 2017. **9**(2): p. 583-599.
67. García-Prat, L., et al., *Autophagy maintains stemness by preventing senescence.* Nature, 2016. **529**(7584): p. 37-42.
68. Masiero, E., et al., *Autophagy is required to maintain muscle mass.* Cell Metab, 2009. **10**(6): p. 507-15.
69. Drake, J.C. and Z. Yan, *Mitophagy in maintaining skeletal muscle mitochondrial proteostasis and metabolic health with ageing.* J Physiol, 2017. **595**(20): p. 6391-6399.
70. Gouspillou, G., et al., *Protective role of Parkin in skeletal muscle contractile and mitochondrial function.* J Physiol, 2018. **596**(13): p. 2565-2579.
71. Leduc-Gaudet, J.P., et al., *Parkin overexpression protects from ageing-related loss of muscle mass and strength.* J Physiol, 2019. **597**(7): p. 1975-1991.
72. Kauppila, T.E.S., J.H.K. Kauppila, and N.G. Larsson, *Mammalian Mitochondria and Aging: An Update.* Cell Metab, 2017. **25**(1): p. 57-71.
73. Peterson, C.M., D.L. Johannsen, and E. Ravussin, *Skeletal muscle mitochondria and aging: a review.* J Aging Res, 2012. **2012**: p. 194821.
74. Hock, M.B. and A. Kralli, *Transcriptional control of mitochondrial biogenesis and function.* Annu Rev Physiol, 2009. **71**: p. 177-203.
75. Kang, C. and L. Li Ji, *Role of PGC-1α signaling in skeletal muscle health and disease.* Ann N Y Acad Sci, 2012. **1271**(1): p. 110-7.

76. Hood, D.A., et al., *Maintenance of Skeletal Muscle Mitochondria in Health, Exercise, and Aging.* Annu Rev Physiol, 2019. **81**: p. 19-41.
77. Picca, A. and A.M. Lezza, *Regulation of mitochondrial biogenesis through TFAM-mitochondrial DNA interactions: Useful insights from aging and calorie restriction studies.* Mitochondrion, 2015. **25**: p. 67-75.
78. Romanello, V. and M. Sandri, *Mitochondrial Quality Control and Muscle Mass Maintenance.* Front Physiol, 2015. **6**: p. 422.
79. Grevendonk, L., et al., *Impact of aging and exercise on skeletal muscle mitochondrial capacity, energy metabolism, and physical function.* Nat Commun, 2021. **12**(1): p. 4773.
80. Leduc-Gaudet, J.P., et al., *Mitochondrial morphology is altered in atrophied skeletal muscle of aged mice.* Oncotarget, 2015. **6**(20): p. 17923-37.
81. Gomes, M.J., et al., *Skeletal muscle aging: influence of oxidative stress and physical exercise.* Oncotarget, 2017. **8**(12): p. 20428-20440.
82. Scicchitano, B.M., et al., *The physiopathologic role of oxidative stress in skeletal muscle.* Mech Ageing Dev, 2018. **170**: p. 37-44.
83. Pizzino, G., et al., *Oxidative Stress: Harms and Benefits for Human Health.* Oxid Med Cell Longev, 2017. **2017**: p. 8416763.
84. Willingham, T.B., P.T. Ajayi, and B. Glancy, *Subcellular Specialization of Mitochondrial Form and Function in Skeletal Muscle Cells.* Front Cell Dev Biol, 2021. **9**: p. 757305.
85. Romanello, V., *The Interplay between Mitochondrial Morphology and Myomitokines in Aging Sarcopenia.* Int J Mol Sci, 2020. **22**(1).
86. Andreux, P.A., et al., *Mitochondrial function is impaired in the skeletal muscle of pre-frail elderly.* Sci Rep, 2018. **8**(1): p. 8548.
87. Salminen, A. and K. Kaarniranta, *AMP-activated protein kinase (AMPK) controls the aging process via an integrated signaling network.* Ageing Res Rev, 2012. **11**(2): p. 230-41.
88. Reznick, R.M., et al., *Aging-associated reductions in AMP-activated protein kinase activity and mitochondrial biogenesis.* Cell Metab, 2007. **5**(2): p. 151-6.
89. Ghosh, S., et al., *Reduction in reactive oxygen species production by mitochondria from elderly subjects with normal and impaired glucose tolerance.* Diabetes, 2011. **60**(8): p. 2051-60.
90. Kang, C., et al., *Exercise training attenuates aging-associated mitochondrial dysfunction in rat skeletal muscle: role of PGC-1α.* Exp Gerontol, 2013. **48**(11): p. 1343-50.
91. Chabi, B., et al., *Mitochondrial function and apoptotic susceptibility in aging skeletal muscle.* Aging Cell, 2008. **7**(1): p. 2-12.
92. Gill, J.F., et al., *Peroxisome proliferator-activated receptor γ coactivator 1α regulates mitochondrial calcium homeostasis, sarcoplasmic reticulum stress, and cell death to mitigate skeletal muscle aging.* Aging Cell, 2019. **18**(5): p. e12993.
93. Sartori, R., V. Romanello, and M. Sandri, *Mechanisms of muscle atrophy and hypertrophy: implications in health and disease.* Nat Commun, 2021. **12**(1): p. 330.
94. Vainshtein, A. and M. Sandri, *Signaling Pathways That Control Muscle Mass.* Int J Mol Sci, 2020. **21**(13).

95. Zhao, J., et al., *mTOR inhibition activates overall protein degradation by the ubiquitin proteasome system as well as by autophagy.* Proc Natl Acad Sci U S A, 2015. **112**(52): p. 15790-7.
96. Bentzinger, C.F., et al., *Skeletal muscle-specific ablation of raptor, but not of rictor, causes metabolic changes and results in muscle dystrophy.* Cell Metab, 2008. **8**(5): p. 411-24.
97. Zhang, Q., et al., *Lack of muscle mTOR kinase activity causes early onset myopathy and compromises whole-body homeostasis.* J Cachexia Sarcopenia Muscle, 2019. **10**(1): p. 35-53.
98. Risson, V., et al., *Muscle inactivation of mTOR causes metabolic and dystrophin defects leading to severe myopathy.* J Cell Biol, 2009. **187**(6): p. 859-74.
99. Castets, P., et al., *Sustained activation of mTORC1 in skeletal muscle inhibits constitutive and starvation-induced autophagy and causes a severe, late-onset myopathy.* Cell Metab, 2013. **17**(5): p. 731-44.
100. Tang, H., et al., *mTORC1 underlies age-related muscle fiber damage and loss by inducing oxidative stress and catabolism.* Aging Cell, 2019. **18**(3): p. e12943.
101. Joseph, G.A., et al., *Partial Inhibition of mTORC1 in Aged Rats Counteracts the Decline in Muscle Mass and Reverses Molecular Signaling Associated with Sarcopenia.* Mol Cell Biol, 2019. **39**(19).
102. Ham, D.J., et al., *The neuromuscular junction is a focal point of mTORC1 signaling in sarcopenia.* Nat Commun, 2020. **11**(1): p. 4510.
103. Miller, R.A., et al., *Rapamycin-mediated lifespan increase in mice is dose and sex dependent and metabolically distinct from dietary restriction.* Aging Cell, 2014. **13**(3): p. 468-77.
104. Kjøbsted, R., et al., *AMPK in skeletal muscle function and metabolism.* Faseb j, 2018. **32**(4): p. 1741-1777.
105. Egan, D.F., et al., *Phosphorylation of ULK1 (hATG1) by AMP-activated protein kinase connects energy sensing to mitophagy.* Science, 2011. **331**(6016): p. 456-61.
106. Jäger, S., et al., *AMP-activated protein kinase (AMPK) action in skeletal muscle via direct phosphorylation of PGC-1alpha.* Proc Natl Acad Sci U S A, 2007. **104**(29): p. 12017-22.
107. Mounier, R., et al., *Expanding roles for AMPK in skeletal muscle plasticity.* Trends Endocrinol Metab, 2015. **26**(6): p. 275-86.
108. Burkewitz, K., Y. Zhang, and W.B. Mair, *AMPK at the nexus of energetics and aging.* Cell Metab, 2014. **20**(1): p. 10-25.
109. Bujak, A.L., et al., *AMPK activation of muscle autophagy prevents fasting-induced hypoglycemia and myopathy during aging.* Cell Metab, 2015. **21**(6): p. 883-90.
110. Khosla, S., et al., *The role of cellular senescence in ageing and endocrine disease.* Nat Rev Endocrinol, 2020. **16**(5): p. 263-275.
111. Tchkonia, T., et al., *Cellular senescence and the senescent secretory phenotype: therapeutic opportunities.* J Clin Invest, 2013. **123**(3): p. 966-72.
112. Di Micco, R., et al., *Cellular senescence in ageing: from mechanisms to therapeutic opportunities.* Nat Rev Mol Cell Biol, 2021. **22**(2): p. 75-95.
113. Zhang, L., et al., *Cellular senescence: a key therapeutic target in aging and diseases.* J Clin Invest, 2022. **132**(15).

114. Palmer, A.K., et al., *Cellular Senescence in Type 2 Diabetes: A Therapeutic Opportunity.* Diabetes, 2015. **64**(7): p. 2289-98.
115. Xu, M., et al., *Senolytics improve physical function and increase lifespan in old age.* Nat Med, 2018. **24**(8): p. 1246-1256.
116. Glass, D.J., *Senescent cells damage the body throughout life.* Nature, 2023. **613**(7942): p. 30-31.
117. Moiseeva, V., et al., *Senescence atlas reveals an aged-like inflamed niche that blunts muscle regeneration.* Nature, 2023. **613**(7942): p. 169-178.
118. Chaib, S., T. Tchkonia, and J.L. Kirkland, *Cellular senescence and senolytics: the path to the clinic.* Nat Med, 2022. **28**(8): p. 1556-1568.
119. Baker, D.J., et al., *Clearance of p16Ink4a-positive senescent cells delays ageing-associated disorders.* Nature, 2011. **479**(7372): p. 232-6.
120. Xu, M., et al., *JAK inhibition alleviates the cellular senescence-associated secretory phenotype and frailty in old age.* Proc Natl Acad Sci U S A, 2015. **112**(46): p. E6301-10.
121. Dugan, B., J. Conway, and N.A. Duggal, *Inflammaging as a target for healthy ageing.* Age Ageing, 2023. **52**(2).
122. Islam, M.T., et al., *Senolytic drugs, dasatinib and quercetin, attenuate adipose tissue inflammation, and ameliorate metabolic function in old age.* Aging Cell, 2023. **22**(2): p. e13767.
123. Moiseeva, O., et al., *Metformin inhibits the senescence-associated secretory phenotype by interfering with IKK/NF-κB activation.* Aging Cell, 2013. **12**(3): p. 489-98.
124. Li, X., et al., *Inflammation and aging: signaling pathways and intervention therapies.* Signal Transduct Target Ther, 2023. **8**(1): p. 239.
125. Birch, J. and J. Gil, *Senescence and the SASP: many therapeutic avenues.* Genes Dev, 2020. **34**(23-24): p. 1565-1576.
126. Cruz-Jentoft, A.J. and A.A. Sayer, *Sarcopenia.* Lancet, 2019. **393**(10191): p. 2636-2646.
127. Petermann-Rocha, F., et al., *Global prevalence of sarcopenia and severe sarcopenia: a systematic review and meta-analysis.* J Cachexia Sarcopenia Muscle, 2022. **13**(1): p. 86-99.
128. Villareal, D.T., et al., *Obesity in older adults: technical review and position statement of the American Society for Nutrition and NAASO, The Obesity Society.* Obes Res, 2005. **13**(11): p. 1849-63.
129. Cruz-Jentoft, A.J., et al., *Sarcopenia: revised European consensus on definition and diagnosis.* Age Ageing, 2019. **48**(4): p. 601.
130. Keller, K. and M. Engelhardt, *Strength and muscle mass loss with aging process. Age and strength loss.* Muscles Ligaments Tendons J, 2013. **3**(4): p. 346-50.
131. Ou, M.Y., et al., *Adipose tissue aging: mechanisms and therapeutic implications.* Cell Death Dis, 2022. **13**(4): p. 300.
132. Kuk, J.L., et al., *Age-related changes in total and regional fat distribution.* Ageing Res Rev, 2009. **8**(4): p. 339-48.

133. Venturelli, M., C. Reggiani, and F. Schena, *Beyond the current knowledge on sarcopenia: new insight on neuromuscular factors.* Aging Clin Exp Res, 2022. **34**(5): p. 1183-1185.
134. Bauer, J., et al., *Sarcopenia: A Time for Action. An SCWD Position Paper.* J Cachexia Sarcopenia Muscle, 2019. **10**(5): p. 956-961.
135. Kim, T.N. and K.M. Choi, *Sarcopenia: definition, epidemiology, and pathophysiology.* J Bone Metab, 2013. **20**(1): p. 1-10.
136. Cruz-Jentoft, A.J., et al., *Sarcopenia: European consensus on definition and diagnosis: Report of the European Working Group on Sarcopenia in Older People.* Age Ageing, 2010. **39**(4): p. 412-23.
137. Hunter, S.K., H.M. Pereira, and K.G. Keenan, *The aging neuromuscular system and motor performance.* J Appl Physiol (1985), 2016. **121**(4): p. 982-995.
138. Li, L., W.C. Xiong, and L. Mei, *Neuromuscular Junction Formation, Aging, and Disorders.* Annu Rev Physiol, 2018. **80**: p. 159-188.
139. Sousa-Victor, P., L. García-Prat, and P. Muñoz-Cánoves, *Control of satellite cell function in muscle regeneration and its disruption in ageing.* Nat Rev Mol Cell Biol, 2022. **23**(3): p. 204-226.
140. Wood, L.K., et al., *Intrinsic stiffness of extracellular matrix increases with age in skeletal muscles of mice.* J Appl Physiol (1985), 2014. **117**(4): p. 363-9.
141. Mahdy, M.A.A., *Skeletal muscle fibrosis: an overview.* Cell Tissue Res, 2019. **375**(3): p. 575-588.
142. Petersen, K.F., et al., *Mitochondrial dysfunction in the elderly: possible role in insulin resistance.* Science, 2003. **300**(5622): p. 1140-2.
143. Priego, T., et al., *Role of hormones in sarcopenia.* Vitam Horm, 2021. **115**: p. 535-570.
144. Ikeda, K., K. Horie-Inoue, and S. Inoue, *Functions of estrogen and estrogen receptor signaling on skeletal muscle.* J Steroid Biochem Mol Biol, 2019. **191**: p. 105375.
145. Shou, J., P.J. Chen, and W.H. Xiao, *Mechanism of increased risk of insulin resistance in aging skeletal muscle.* Diabetol Metab Syndr, 2020. **12**: p. 14.
146. Wang, T., *Searching for the link between inflammaging and sarcopenia.* Ageing Res Rev, 2022. **77**: p. 101611.
147. Li, C.W., et al., *Circulating factors associated with sarcopenia during ageing and after intensive lifestyle intervention.* J Cachexia Sarcopenia Muscle, 2019. **10**(3): p. 586-600.
148. Sciorati, C., et al., *Pharmacological blockade of TNFα prevents sarcopenia and prolongs survival in aging mice.* Aging (Albany NY), 2020. **12**(23): p. 23497-23508.
149. Yousefzadeh, M.J., et al., *Circulating levels of monocyte chemoattractant protein-1 as a potential measure of biological age in mice and frailty in humans.* Aging Cell, 2018. **17**(2).
150. Kerr, N.R. and F.W. Booth, *Contributions of physical inactivity and sedentary behavior to metabolic and endocrine diseases.* Trends Endocrinol Metab, 2022. **33**(12): p. 817-827.
151. Smith, L., et al., *The Association Between Sedentary Behavior and Sarcopenia Among Adults Aged ≥65 Years in Low- and Middle-Income Countries.* Int J Environ Res Public Health, 2020. **17**(5).

152. Gao, Q., et al., *Associated Factors of Sarcopenia in Community-Dwelling Older Adults: A Systematic Review and Meta-Analysis.* Nutrients, 2021. **13**(12).
153. Steffl, M., et al., *Relationship between sarcopenia and physical activity in older people: a systematic review and meta-analysis.* Clin Interv Aging, 2017. **12**: p. 835-845.
154. Robinson, S., C. Cooper, and A. Aihie Sayer, *Nutrition and sarcopenia: a review of the evidence and implications for preventive strategies.* J Aging Res, 2012. **2012**: p. 510801.
155. Paulussen, K.J.M., et al., *Anabolic Resistance of Muscle Protein Turnover Comes in Various Shapes and Sizes.* Front Nutr, 2021. **8**: p. 615849.
156. Bauer, J., et al., *Evidence-based recommendations for optimal dietary protein intake in older people: a position paper from the PROT-AGE Study Group.* J Am Med Dir Assoc, 2013. **14**(8): p. 542-59.
157. Salvestrini, V., C. Sell, and A. Lorenzini, *Obesity May Accelerate the Aging Process.* Front Endocrinol (Lausanne), 2019. **10**: p. 266.
158. Steinberg, G.R., et al., *Tumor necrosis factor alpha-induced skeletal muscle insulin resistance involves suppression of AMP-kinase signaling.* Cell Metab, 2006. **4**(6): p. 465-74.
159. Khamzina, L., et al., *Increased activation of the mammalian target of rapamycin pathway in liver and skeletal muscle of obese rats: possible involvement in obesity-linked insulin resistance.* Endocrinology, 2005. **146**(3): p. 1473-81.
160. Batsis, J.A. and D.T. Villareal, *Sarcopenic obesity in older adults: aetiology, epidemiology and treatment strategies.* Nat Rev Endocrinol, 2018. **14**(9): p. 513-537.
161. Donini, L.M., et al., *Definition and Diagnostic Criteria for Sarcopenic Obesity: ESPEN and EASO Consensus Statement.* Obes Facts, 2022. **15**(3): p. 321-335.
162. Chaib, S., T. Tchkonia, and J.L. Kirkland, *Obesity, Senescence, and Senolytics.* Handb Exp Pharmacol, 2022. **274**: p. 165-180.
163. Tam, B.T., J.A. Morais, and S. Santosa, *Obesity and ageing: Two sides of the same coin.* Obes Rev, 2020. **21**(4): p. e12991.
164. Bhaskaran, K., et al., *Association of BMI with overall and cause-specific mortality: a population-based cohort study of 3·6 million adults in the UK.* Lancet Diabetes Endocrinol, 2018. **6**(12): p. 944-953.
165. Ahima, R.S., *Connecting obesity, aging and diabetes.* Nat Med, 2009. **15**(9): p. 996-7.
166. Abou-Samra, M., et al., *Adiponectin and Its Mimics on Skeletal Muscle: Insulin Sensitizers, Fat Burners, Exercise Mimickers, Muscling Pills … or Everything Together?* Int J Mol Sci, 2020. **21**(7).
167. Whitehead, J.P., et al., *Adiponectin--a key adipokine in the metabolic syndrome.* Diabetes Obes Metab, 2006. **8**(3): p. 264-80.
168. Hu, E., P. Liang, and B.M. Spiegelman, *AdipoQ is a novel adipose-specific gene dysregulated in obesity.* J Biol Chem, 1996. **271**(18): p. 10697-703.
169. Maeda, K., et al., *cDNA cloning and expression of a novel adipose specific collagen-like factor, apM1 (AdiPose Most abundant Gene transcript 1).* Biochem Biophys Res Commun, 1996. **221**(2): p. 286-9.

170. Badman, M.K. and J.S. Flier, *The adipocyte as an active participant in energy balance and metabolism.* Gastroenterology, 2007. **132**(6): p. 2103-15.
171. Kadowaki, T., et al., *Adiponectin and adiponectin receptors in insulin resistance, diabetes, and the metabolic syndrome.* J Clin Invest, 2006. **116**(7): p. 1784-92.
172. Pajvani, U.B., et al., *Complex distribution, not absolute amount of adiponectin, correlates with thiazolidinedione-mediated improvement in insulin sensitivity.* J Biol Chem, 2004. **279**(13): p. 12152-62.
173. Fruebis, J., et al., *Proteolytic cleavage product of 30-kDa adipocyte complement-related protein increases fatty acid oxidation in muscle and causes weight loss in mice.* Proc Natl Acad Sci U S A, 2001. **98**(4): p. 2005-10.
174. Waki, H., et al., *Generation of globular fragment of adiponectin by leukocyte elastase secreted by monocytic cell line THP-1.* Endocrinology, 2005. **146**(2): p. 790-6.
175. Liu, M. and F. Liu, *Transcriptional and post-translational regulation of adiponectin.* Biochem J, 2009. **425**(1): p. 41-52.
176. Delaigle, A.M., et al., *Induction of adiponectin in skeletal muscle by inflammatory cytokines: in vivo and in vitro studies.* Endocrinology, 2004. **145**(12): p. 5589-97.
177. Krause, M.P., et al., *Adiponectin is expressed by skeletal muscle fibers and influences muscle phenotype and function.* Am J Physiol Cell Physiol, 2008. **295**(1): p. C203-12.
178. Delaigle, A.M., et al., *Induction of adiponectin in skeletal muscle of type 2 diabetic mice: In vivo and in vitro studies.* Diabetologia, 2006. **49**(6): p. 1311-23.
179. Jortay, J., et al., *Local induction of adiponectin reduces lipopolysaccharide-triggered skeletal muscle damage.* Endocrinology, 2010. **151**(10): p. 4840-51.
180. Bruun, J.M., et al., *Regulation of adiponectin by adipose tissue-derived cytokines: in vivo and in vitro investigations in humans.* Am J Physiol Endocrinol Metab, 2003. **285**(3): p. E527-33.
181. Becic, T., C. Studenik, and G. Hoffmann, *Exercise Increases Adiponectin and Reduces Leptin Levels in Prediabetic and Diabetic Individuals: Systematic Review and Meta-Analysis of Randomized Controlled Trials.* Med Sci (Basel), 2018. **6**(4).
182. Yamauchi, T., et al., *Targeted disruption of AdipoR1 and AdipoR2 causes abrogation of adiponectin binding and metabolic actions.* Nat Med, 2007. **13**(3): p. 332-9.
183. Yamauchi, T., et al., *Cloning of adiponectin receptors that mediate antidiabetic metabolic effects.* Nature, 2003. **423**(6941): p. 762-9.
184. Iwabu, M., et al., *Adiponectin and AdipoR1 regulate PGC-1alpha and mitochondria by Ca(2+) and AMPK/SIRT1.* Nature, 2010. **464**(7293): p. 1313-9.
185. Rubina, K.A., et al., *Revisiting the multiple roles of T-cadherin in health and disease.* Eur J Cell Biol, 2021. **100**(7-8): p. 151183.
186. Yamauchi, T. and T. Kadowaki, *Adiponectin receptor as a key player in healthy longevity and obesity-related diseases.* Cell Metab, 2013. **17**(2): p. 185-96.
187. Tsuchida, A., et al., *Insulin/Foxo1 pathway regulates expression levels of adiponectin receptors and adiponectin sensitivity.* J Biol Chem, 2004. **279**(29): p. 30817-22.

188. Civitarese, A.E., et al., *Adiponectin receptors gene expression and insulin sensitivity in non-diabetic Mexican Americans with or without a family history of Type 2 diabetes.* Diabetologia, 2004. **47**(5): p. 816-20.
189. Yamauchi, T., et al., *Adiponectin stimulates glucose utilization and fatty-acid oxidation by activating AMP-activated protein kinase.* Nat Med, 2002. **8**(11): p. 1288-95.
190. Combs, T.P. and E.B. Marliss, *Adiponectin signaling in the liver.* Rev Endocr Metab Disord, 2014. **15**(2): p. 137-47.
191. Ge, Q., et al., *Adipokines identified as new downstream targets for adiponectin: lessons from adiponectin-overexpressing or -deficient mice.* Am J Physiol Endocrinol Metab, 2011. **301**(2): p. E326-35.
192. Bauche, I.B., et al., *Overexpression of adiponectin targeted to adipose tissue in transgenic mice: impaired adipocyte differentiation.* Endocrinology, 2007. **148**(4): p. 1539-49.
193. Chen, H., et al., *Adiponectin stimulates production of nitric oxide in vascular endothelial cells.* J Biol Chem, 2003. **278**(45): p. 45021-6.
194. Shibata, R., et al., *Adiponectin protects against myocardial ischemia-reperfusion injury through AMPK- and COX-2-dependent mechanisms.* Nat Med, 2005. **11**(10): p. 1096-103.
195. Zhou, L., et al., *Adiponectin activates AMP-activated protein kinase in muscle cells via APPL1/LKB1-dependent and phospholipase C/Ca2+/Ca2+/calmodulin-dependent protein kinase kinase-dependent pathways.* J Biol Chem, 2009. **284**(33): p. 22426-22435.
196. Yoon, M.J., et al., *Adiponectin increases fatty acid oxidation in skeletal muscle cells by sequential activation of AMP-activated protein kinase, p38 mitogen-activated protein kinase, and peroxisome proliferator-activated receptor alpha.* Diabetes, 2006. **55**(9): p. 2562-70.
197. Marcinko, K. and G.R. Steinberg, *The role of AMPK in controlling metabolism and mitochondrial biogenesis during exercise.* Exp Physiol, 2014. **99**(12): p. 1581-5.
198. Yamauchi, T., et al., *The fat-derived hormone adiponectin reverses insulin resistance associated with both lipoatrophy and obesity.* Nat Med, 2001. **7**(8): p. 941-6.
199. Maeda, N., et al., *Diet-induced insulin resistance in mice lacking adiponectin/ACRP30.* Nat Med, 2002. **8**(7): p. 731-7.
200. Yamauchi, T., et al., *Globular adiponectin protected ob/ob mice from diabetes and ApoE-deficient mice from atherosclerosis.* J Biol Chem, 2003. **278**(4): p. 2461-8.
201. Wang, C., et al., *Adiponectin sensitizes insulin signaling by reducing p70 S6 kinase-mediated serine phosphorylation of IRS-1.* J Biol Chem, 2007. **282**(11): p. 7991-6.
202. Civitarese, A.E., et al., *Role of adiponectin in human skeletal muscle bioenergetics.* Cell Metab, 2006. **4**(1): p. 75-87.
203. Houstis, N., E.D. Rosen, and E.S. Lander, *Reactive oxygen species have a causal role in multiple forms of insulin resistance.* Nature, 2006. **440**(7086): p. 944-8.
204. Tomas, E., et al., *Enhanced muscle fat oxidation and glucose transport by ACRP30 globular domain: acetyl-CoA carboxylase inhibition and AMP-activated protein kinase activation.* Proc Natl Acad Sci U S A, 2002. **99**(25): p. 16309-13.

205. Ruan, H. and L.Q. Dong, *Adiponectin signaling and function in insulin target tissues.* J Mol Cell Biol, 2016. **8**(2): p. 101-9.
206. Jortay, J., et al., *Adiponectin and skeletal muscle: pathophysiological implications in metabolic stress.* Am J Pathol, 2012. **181**(1): p. 245-56.
207. Abou-Samra, M., et al., *Involvement of adiponectin in the pathogenesis of dystrophinopathy.* Skelet Muscle, 2015. **5**: p. 25.
208. Lecompte, S., et al., *Skeletal muscle secretome in Duchenne muscular dystrophy: a pivotal anti-inflammatory role of adiponectin.* Cell Mol Life Sci, 2017. **74**(13): p. 2487-2501.
209. Ohashi, K., et al., *Adiponectin promotes macrophage polarization toward an anti-inflammatory phenotype.* J Biol Chem, 2010. **285**(9): p. 6153-60.
210. Salminen, A., J.M. Hyttinen, and K. Kaarniranta, *AMP-activated protein kinase inhibits NF-κB signaling and inflammation: impact on healthspan and lifespan.* J Mol Med (Berl), 2011. **89**(7): p. 667-76.
211. Boursereau, R., et al., *New targets to alleviate skeletal muscle inflammation: role of microRNAs regulated by adiponectin.* Sci Rep, 2017. **7**: p. 43437.
212. Boursereau, R., et al., *Downregulation of the NLRP3 inflammasome by adiponectin rescues Duchenne muscular dystrophy.* BMC Biol, 2018. **16**(1): p. 33.
213. Baghdadi, M.B. and S. Tajbakhsh, *Regulation and phylogeny of skeletal muscle regeneration.* Dev Biol, 2018. **433**(2): p. 200-209.
214. Dufresne, S.S., J. Frenette, and N.A. Dumont, *[Inflammation and muscle regeneration, a double-edged sword].* Med Sci (Paris), 2016. **32**(6-7): p. 591-7.
215. Fiaschi, T., et al., *Adiponectin as a tissue regenerating hormone: more than a metabolic function.* Cell Mol Life Sci, 2014. **71**(10): p. 1917-25.
216. Zammit, P.S., *Function of the myogenic regulatory factors Myf5, MyoD, Myogenin and MRF4 in skeletal muscle, satellite cells and regenerative myogenesis.* Semin Cell Dev Biol, 2017. **72**: p. 19-32.
217. Fiaschi, T., et al., *Globular adiponectin activates motility and regenerative traits of muscle satellite cells.* PLoS One, 2012. **7**(5): p. e34782.
218. Fiaschi, T., et al., *Globular adiponectin induces differentiation and fusion of skeletal muscle cells.* Cell Res, 2009. **19**(5): p. 584-97.
219. Eming, S.A., T.A. Wynn, and P. Martin, *Inflammation and metabolism in tissue repair and regeneration.* Science, 2017. **356**(6342): p. 1026-1030.
220. Gamberi, T., et al., *Activation of autophagy by globular adiponectin is required for muscle differentiation.* Biochim Biophys Acta, 2016. **1863**(4): p. 694-702.
221. Liu, Y., et al., *Adiponectin stimulates autophagy and reduces oxidative stress to enhance insulin sensitivity during high-fat diet feeding in mice.* Diabetes, 2015. **64**(1): p. 36-48.
222. Gwinn, D.M., et al., *AMPK phosphorylation of raptor mediates a metabolic checkpoint.* Mol Cell, 2008. **30**(2): p. 214-26.
223. Chen, Y.L., et al., *Physical exercise attenuates age-related muscle atrophy and exhibits anti-ageing effects via the adiponectin receptor 1 signalling.* J Cachexia Sarcopenia Muscle, 2023. **14**(4): p. 1789-1801.

224. Inoue, A., et al., *Exercise restores muscle stem cell mobilization, regenerative capacity and muscle metabolic alterations via adiponectin/AdipoR1 activation in SAMP10 mice.* J Cachexia Sarcopenia Muscle, 2017. **8**(3): p. 370-385.
225. Li, N., et al., *Adiponectin preserves metabolic fitness during aging.* Elife, 2021. **10**.
226. Otabe, S., et al., *Overexpression of human adiponectin in transgenic mice results in suppression of fat accumulation and prevention of premature death by high-calorie diet.* Am J Physiol Endocrinol Metab, 2007. **293**(1): p. E210-8.
227. Okada-Iwabu, M., et al., *A small-molecule AdipoR agonist for type 2 diabetes and short life in obesity.* Nature, 2013. **503**(7477): p. 493-9.
228. Arai, Y., K. Kamide, and N. Hirose, *Adipokines and Aging: Findings From Centenarians and the Very Old.* Front Endocrinol (Lausanne), 2019. **10**: p. 142.
229. Atzmon, G., et al., *Adiponectin levels and genotype: a potential regulator of life span in humans.* J Gerontol A Biol Sci Med Sci, 2008. **63**(5): p. 447-53.
230. Can, B., et al., *Serum markers of inflammation and oxidative stress in sarcopenia.* Aging Clin Exp Res, 2017. **29**(4): p. 745-752.
231. Holland, W.L. and P.E. Scherer, *Cell Biology. Ronning after the adiponectin receptors.* Science, 2013. **342**(6165): p. 1460-1.
232. Kim, Y., et al., *The Adiponectin Receptor Agonist AdipoRon Ameliorates Diabetic Nephropathy in a Model of Type 2 Diabetes.* J Am Soc Nephrol, 2018. **29**(4): p. 1108-1127.
233. Nicolas, S., et al., *Adiporon, an adiponectin receptor agonist acts as an antidepressant and metabolic regulator in a mouse model of depression.* Transl Psychiatry, 2018. **8**(1): p. 159.
234. Hong, K., et al., *Adiponectin Receptor Agonist, AdipoRon, Causes Vasorelaxation Predominantly Via a Direct Smooth Muscle Action.* Microcirculation, 2016. **23**(3): p. 207-20.
235. Wang, Y., et al., *Hepatoprotective effects of AdipoRon against d-galactosamine-induced liver injury in mice.* Eur J Pharm Sci, 2016. **93**: p. 123-31.
236. Zhang, Y., et al., *AdipoRon, the first orally active adiponectin receptor activator, attenuates postischemic myocardial apoptosis through both AMPK-mediated and AMPK-independent signalings.* Am J Physiol Endocrinol Metab, 2015. **309**(3): p. E275-82.
237. Messaggio, F., et al., *Adiponectin receptor agonists inhibit leptin induced pSTAT3 and in vivo pancreatic tumor growth.* Oncotarget, 2017. **8**(49): p. 85378-85391.
238. Akimoto, M., et al., *Antidiabetic adiponectin receptor agonist AdipoRon suppresses tumour growth of pancreatic cancer by inducing RIPK1/ERK-dependent necroptosis.* Cell Death Dis, 2018. **9**(8): p. 804.
239. Sun, F., et al., *Adiponectin modulates ventral tegmental area dopamine neuron activity and anxiety-related behavior through AdipoR1.* Mol Psychiatry, 2019. **24**(1): p. 126-144.
240. Ng, R.C., et al., *Chronic oral administration of adipoRon reverses cognitive impairments and ameliorates neuropathology in an Alzheimer's disease mouse model.* Mol Psychiatry, 2021. **26**(10): p. 5669-5689.
241. Abou-Samra, M., et al., *AdipoRon, a new therapeutic prospect for Duchenne muscular dystrophy.* J Cachexia Sarcopenia Muscle, 2020. **11**(2): p. 518-533.

242. Iwabu, M., et al., *AdipoR agonist increases insulin sensitivity and exercise endurance in AdipoR-humanized mice.* Commun Biol, 2021. **4**(1): p. 45.

CHAPTER 2: AIMS OF THE WORK

CHAPTER 2: AIMS OF THE WORK

CONTEXT

Over the last century, life expectancy at birth has steadily increased [1]. Sarcopenia occurs commonly as an age-related process and is characterized by the accelerated loss of muscle mass, quality and function. Sarcopenia is associated with adverse outcomes such as falls, institutionalization and mortality. Preventive and therapeutic strategies are therefore vital [2].

Beyond physical impairment and sarcopenia, muscle disturbances would lead to insulin resistance and the metabolic syndrome [3]. Particularly, obesity, whose prevalence has tremendously risen in recent decades [4], accelerates the aging process [5]. Obesity is also characterized by the loss of muscle quality, function, and endurance capacity. Two additional burdens involve ectopic lipid deposition in the liver and the skeletal muscle, namely, nonalcoholic fatty liver disease (NAFLD) and myosteatosis [6, 7].

ApN is regarded as a unique and salutary adipokine, known for its beneficial metabolic effects that may increase longevity and protect against age-related diseases. Plasma ApN levels are high among centenarians, while they are low in cases of obesity. ApN overexpression increases lifespan in mice whereas complete deficiency of ApN in knockout mice shortens it. In the muscle and the liver, ApN exerts insulin-sensitizing and fat-burning properties through its major receptors AdipoR1 and AdipoR2 [8]. Our research has previously demonstrated that ApN protects the muscle of dystrophic mice by reducing inflammation, oxidative stress and improving regeneration. This, in turn, leads to improvements in force and endurance [9].

OBJECTIVES

This thesis aimed to explore whether oral treatment with an agonist of ApN receptors, AdipoRon, could protect the skeletal muscle during the aging process and promote healthy aging.

STUDY 1

We examined the effect of long-term (~1 year) treatment with AdipoRon in middle-aged obese mice with a normal genetic background. These mice were rendered obese through chronic excess of caloric intake to simulate our Western lifestyle habits and the high prevalence of obesity. We investigated whether AdipoRon could slow down muscle dysfunction and reduce myosteatosis and degenerative muscle markers in these middle-aged obese mice. The effects of AdipoRon were also assessed in the liver, and more specifically on the NAFLD.

We showed that long-term AdipoRon treatment activates the AMPK signaling pathway in the skeletal muscle and enhances muscle endurance in obese middle-aged mice. AdipoRon protects the skeletal muscle and the liver from the adverse metabolic and degenerative effects of ageing and calorie excess.

During this study, a comprehensive protocol for the quantification and analysis of intramyocellular lipids was developed. This protocol enables their measurement and the assessment of lipid droplet morphology in a fiber-type specific manner.

Research article 1:

Selvais CM, Davis-López de Carrizosa MA, Nachit M, Versele R, Dubuisson N, Noel L, Gillard J, Leclercq IA, Brichard SM, Abou-Samra M. AdipoRon enhances healthspan in middle-aged obese mice: striking alleviation of myosteatosis and

muscle degenerative markers. J Cachexia Sarcopenia Muscle. 2023 Feb;14(1):464-478.

Methodological article:

Selvais CM, De Cock LL, Brichard SM, Davis-López de Carrizosa MA. Fiber Type and Subcellular-Specific Analysis of Lipid Droplet Content in Skeletal Muscle. J Vis Exp. 2022 Jun 8;(184). See annex 2.

STUDY 2

In this second part, we investigated whether a late and shorter AdipoRon treatment could actually reverse sarcopenia and hallmarks of aging in older mice. To this end, old mice were treated with AdipoRon for 3 months. Their muscle mass, quality and function were characterized in detail. The mechanisms underlying AdipoRon protection and its effects on inflammaging were further explored.

We found that AdipoRon treatment results in notable improvements in muscle mass, quality, and function in old mice, effectively counteracting sarcopenia. AdipoRon increases the activation of AMPK signaling and autophagy and mitochondrial function. AdipoRon also reduces fibrosis and inflammaging.

Research article 2:

Selvais CM, Davis-López de Carrizosa MA, Versele R, Dubuisson N, Noel L, Brichard SM, Abou-Samra M. Thwarting sarcopenia: Exploring AdipoRon in aging skeletal muscle as a healthspan-extending shield. Submitted.

REFERENCES

1. Olshansky, S.J., *From Lifespan to Healthspan.* Jama, 2018. **320**(13): p. 1323-1324.
2. Cruz-Jentoft, A.J. and A.A. Sayer, *Sarcopenia.* Lancet, 2019. **393**(10191): p. 2636-2646.
3. Shou, J., P.J. Chen, and W.H. Xiao, *Mechanism of increased risk of insulin resistance in aging skeletal muscle.* Diabetol Metab Syndr, 2020. **12**: p. 14.
4. Blüher, M., *Obesity: global epidemiology and pathogenesis.* Nat Rev Endocrinol, 2019. **15**(5): p. 288-298.
5. Tam, B.T., J.A. Morais, and S. Santosa, *Obesity and ageing: Two sides of the same coin.* Obes Rev, 2020. **21**(4): p. e12991.
6. Correa-de-Araujo, R., et al., *Myosteatosis in the Context of Skeletal Muscle Function Deficit: An Interdisciplinary Workshop at the National Institute on Aging.* Front Physiol, 2020. **11**: p. 963.
7. Nachit, M. and I.A. Leclercq, *Emerging awareness on the importance of skeletal muscle in liver diseases: time to dig deeper into mechanisms!* Clin Sci (Lond), 2019. **133**(3): p. 465-481.
8. Abou-Samra, M., et al., *Adiponectin and Its Mimics on Skeletal Muscle: Insulin Sensitizers, Fat Burners, Exercise Mimickers, Muscling Pills … or Everything Together?* Int J Mol Sci, 2020. **21**(7).
9. Abou-Samra, M., et al., *Involvement of adiponectin in the pathogenesis of dystrophinopathy.* Skelet Muscle, 2015. **5**: p. 25.

CHAPTER 3: RESULTS

CHAPTER 3: RESULTS

STUDY 1

AdipoRon enhances healthspan in middle-aged obese mice: Striking alleviation of myosteatosis and muscle degenerative markers

Camille M. Selvais[1], Maria A. Davis-López de Carrizosa[1,3], Maxime Nachit[2], Romain Versele[1], Nicolas Dubuisson[1], Laurence Noel[1], Justine Gillard[2], Isabelle A. Leclercq[2], Sonia M. Brichard[1] and Michel Abou-Samra[1].

[1] Endocrinology, Diabetes and Nutrition Unit, Institute of Experimental and Clinical Research, UCLouvain, Brussels, Belgium;

[2] Hepato-Gastroenterology Unit, Institute of Experimental and Clinical Research, UCLouvain, Brussels, Belgium;

[3] Departamento de Fisiología, Facultad de Biología, Universidad de Sevilla, Seville, Spain.

Corresponding author:

Camille Selvais

E-mail : camille.selvais@uclouvain.be

Tel: 32-2-7649576

ABSTRACT

BACKGROUND

Obesity among older adults has increased tremendously. Obesity accelerates aging and predisposes to age-related conditions and diseases, like loss of endurance capacity, insulin resistance and features of the metabolic syndrome. Namely, ectopic lipids play a key role in the development of non-alcoholic fatty liver disease (NAFLD) and myosteatosis, two severe burdens of aging and metabolic diseases. Adiponectin (ApN) is a hormone, mainly secreted by adipocytes, which exerts insulin-sensitizing and fat-burning properties in several tissues including the liver and the muscle. Its overexpression also increases lifespan in mice. In this study, we investigated whether an ApN receptor agonist, AdipoRon (AR) could slown muscle dysfunction, myosteatosis and degenerative muscle markers in middle-aged obese mice. The effects on myosteatosis were compared to those on NAFLD.

METHODS

Three groups of mice were studied up to 62 weeks of age: one group received normal diet (ND), another high-fat diet (HFD) and the last HFD combined with AR given orally for almost 1 year. An additional group of young mice under a ND was used. Treadmill tests and micro-computed tomography (CT) were carried out *in vivo*. Histological, biochemical and molecular analyses were performed on tissues *ex vivo.* Bodipy staining was used to assess intramyocellular lipid (IMCL) and lipid droplet morphology.

RESULTS

AR did not markedly alter diet-induced obesity. Yet, this treatment, rescued exercise endurance in obese mice (up to 2.4-fold, $P<0.05$), an event that preceded

the improvement of insulin sensitivity. Dorsal muscles and liver densities, measured by CT, were reduced in obese mice (-42% and -109%, respectively, *P*<0.0001), suggesting fatty infiltration. This reduction tended to be attenuated by AR. Accordingly, AR significantly mitigated steatosis and cellular ballooning at liver histology, thereby decreasing the NALFD activity score (-30%, *P*<0.05). AR also strikingly reversed IMCL accumulation either due to aging in oxidative fibers (types 1/2a, soleus) or to HFD in glycolytic ones (types 2x/2b, extensor digitorum longus) (-50% to -85%, *P*<0.05 or less). Size of subsarcolemmal lipid droplets, known to be associated with adverse metabolic outcomes, was reduced as well. Alleviation of myosteatosis resulted from improved mitochondrial function and lipid oxidation. Meanwhile, AR halved aged-related accumulation of dysfunctional proteins identified as tubular aggregates and cylindrical spirals by electron microscopy (*P*<0.05).

CONCLUSION

Long-term AdipoRon treatment promotes “healthy aging” in obese middle-aged mice by enhancing endurance and protecting skeletal muscle and liver against the adverse metabolic and degenerative effects of aging and caloric excess.

KEYWORDS

Adiponectin – Myosteatosis – Intramyocellular lipids – Aging – Non-alcoholic fatty liver disease – Endurance

INTRODUCTION

As society ages, the incidence of physical limitations is dramatically increasing. An important cause of physical limitations is the age-related loss of skeletal muscle mass, referred to as sarcopenia. Muscle function is impaired as well, and the endurance capacity declines [1]. Beyond physical performance, muscles play also a crucial role in insulin sensitivity and fuel homeostasis. Muscle disturbances may thus contribute to insulin resistance and metabolic syndrome [1].

Obesity among older adults aged 65 and over has increased noticeably over the last decades on all continents and its prevalence is reaching 35% in the US where it is expected to at least double by 2050 [2]. Obesity accelerates aging and predisposes an individual to age-related conditions and diseases. Thus, obesity and aging go hand in hand with loss of muscle mass, function and endurance capacity, insulin resistance and features of the metabolic syndrome [3]. Two additional burdens associated with this syndrome involve ectopic lipid deposition in the liver and the skeletal muscle, namely non-alcoholic fatty liver disease (NAFLD)/steatohepatitis (NASH) and myosteatosis, whose rising prevalence tends to parallel that of obesity and aging [4, 5].

Adiponectin (ApN) is a hormone, mainly secreted by the adipose tissue, which is known to be tightly linked to the metabolic syndrome. ApN exerts insulin-sensitizing, fat-burning and anti-inflammatory actions, thereby effectively counteracting several facets of this syndrome. Liver and muscle are two of its main target tissues. The ApN receptor, AdipoR2 is predominantly expressed in the liver, whereas AdipoR1 is predominantly expressed in the skeletal muscle. In the liver, ApN stimulates fatty-acid oxidation and reduces glucose production [6]. In skeletal muscle, we have shown that ApN does also exert powerful protective effects in mdx

mice, a model with a severe muscle disease (Duchenne Muscular Dystrophy). Thus, ApN reduces muscle inflammation and oxidative stress, and enhances the myogenic program, thereby decreasing muscle damage while increasing force/endurance [6, 7]. Importantly, overexpression of ApN in transgenic mice prolongs life span [8] while complete deficiency of ApN in knockout mice shortens it [9].

ApN has a complex three-dimensional structure and must be injected to produce its effects [6]. The development of novel molecules that mimic the beneficial effects of ApN is therefore relevant. AdipoRon is an orally active synthetic agonist of ApN receptors, which, based on data in animal models, has been proposed for the treatment of type 2 diabetes and other obesity-related disorders [10-12]. Relevant for translational applications, AdipoRon remains efficient in AdipoR1-humanized mice [13]. We have recently shown that, like ApN, AdipoRon protects the skeletal muscle of mdx mice [14]. However, its potential beneficial properties on aging muscle have been scarcely addressed [15]. It is also unknown whether this molecule does effectively prolong life span in normal (wild type) mice. An effect on longevity has been observed in a mouse model with a severe form of genetic diabetes; hence, the marked alleviation of diabetes provoked by AdipoRon was, in this case, a major confounding factor [10].

The overall aim of this work was to explore whether AdipoRon could promote healthy aging in middle-aged obese mice on a normal genetic background. Mice were rendered obese by chronic excess of caloric intake in order to mimic our western-life style habits and the high prevalence of obesity in the elderly. Some of these mice were concomitantly treated with AdipoRon for ~1 year. Herein, we investigated whether an ApN receptor agonist, AdipoRon could slow down muscle dysfunction, myosteatosis and degenerative muscle markers in middle-aged obese mice. The effects on myosteatosis were compared to those on NAFLD.

METHODS

Experimental design and animals

Male C57BL/6J mice were divided into three groups and studied up to 62 weeks of age. They are referred to as old (O) mice (Figure 1a). Two of these groups received a high-fat diet (HFD): mice in one HFD group were orally treated with AdipoRon (AR) for ~ 1 year (30 mg/kg/day scaled up to 50 mg/kg/day; O-HFD+AR), while mice in the other group were left untreated (O-HFD). HFD groups were compared to O mice kept on a normal diet (O-ND). An additional group of young (12-week-old) mice under a normal diet (Y-ND) was also studied. Mice were subjected to Treadmill Exhaustion Tests at 32 and 56 weeks of age and to micro-computed tomography (CT) at 59 weeks. Histological, biochemical and molecular analyses were performed on tissues *ex vivo*. Mice were purchased from Janvier Labs, Genest, France and AdipoRon from Bio-Techne, Minnesota, USA. Please see the Supporting Information for detailed experimental procedures.

RESULTS

Long-term administration of AdipoRon protects against impaired glycemia, dyslipidemia and improves endurance

The body weight of O-HFD mice steadily increased and was twice that of O-ND animals at the end of study (Figure 1b). In line with others [10], AdipoRon did not markedly alter obesity and only stabilized the body weight at the end of the protocol. Likewise, daily energy intake, which was ~ 60% higher under HFD, was not modified by AdipoRon (Figure S1). Yet, AdipoRon, when administered at the highest dose (50 mg/kg/day), progressively decreased fasting blood glucose levels, which were moderately elevated in HFD-fed mice, to reach O-ND values (Figure 1c). The insulin resistance index was attenuated as well (Figure 1d). Moreover, AdipoRon decreased plasma cholesterol levels induced by HFD, possibly through increased efflux, without modifying other circulating lipids (Table S1). Plasma ApN levels were decreased in old mice compared to young ones (O-ND vs. Y-ND) and this decrease was further amplified in obese mice when data were normalized by white fat mass (i.e., expressed per “secretion unit”; [16]) (Table S1).

We next evaluated the effect of AdipoRon on muscle function by using an uphill treadmill exhaustion test. This test was performed twice, with each time a protocol adapted to age and obesity of the mice (Figure 1e, see supporting information). At 32 weeks, exercise endurance capacity, expressed as work, was reduced in O-HFD mice compared to O-ND ones and was corrected by AdipoRon. At 56 weeks, work of O-HFD was drastically reduced (73 % vs. O-ND), while it was partially rescued by AdipoRon. Thus, AdipoRon was able to partially or totally rescue exercise endurance of middle-aged obese mice. This already occurs at the low dose of

AdipoRon (30 mg/kg/day), which did affect neither glucose homeostasis nor the body weight (compare Figure 1e *left* panel vs. b, c).

Effects of AdipoRon on body composition, and liver and muscle density

We measured *in vivo* the body composition of mice as well as liver and muscle density by micro-CT. Whole body fat mass, which was markedly increased in O-HFD mice, was reduced by 20% under AdipoRon treatment (Figure S1b), in line with the decreased subcutaneous fat measured *ex vivo* (Table S1). However, AdipoRon did not significantly alter total lean mass (Figure S1c), in agreement with the unchanged dorsal muscle area, an index of muscle mass [17] (Figure S1d) and the unchanged weight of several muscles sampled *ex vivo* (Table S1). Dorsal muscle density was decreased in HFD mice, suggesting fatty infiltration (Figure 1f, *left*). However, this decrease tended to be less pronounced under AdipoRon treatment, a result confirmed *a posteriori* by lipid dosage of dorsal muscle (Figure S1e). Likewise, liver density was reduced in both groups of HFD-mice but this reduction also tended to be attenuated by AdipoRon (Figure 1f, *right*). These data suggest therefore that AdipoRon treatment lessens hepatic steatosis and myosteatosis induced by HFD.

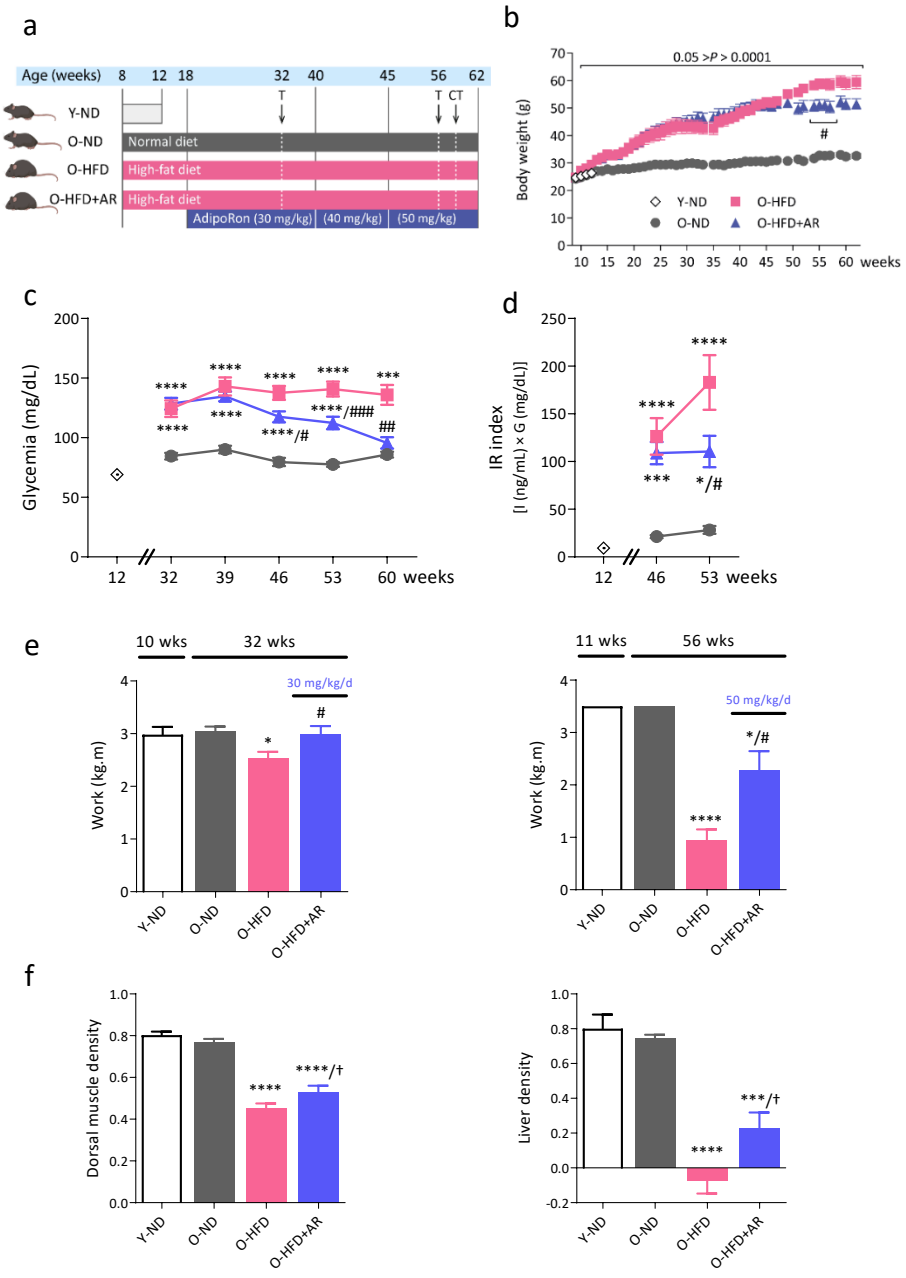

Figure 1. Chronic administration of AdipoRon improves insulin sensitivity, endurance and enhances CT scan muscle and liver densities in middle-aged obese mice. (a) Experimental protocol. Four groups of mice were studied. Three groups were studied up to 62 weeks of age and are referred to as old (O) mice. Two of these groups received a high-fat diet (HFD) from 8 weeks. One HFD group was orally

treated with AdipoRon (AR), starting from 18 weeks (30 mg/kg/day scaled up to 50 mg/kg/day; O-HFD+AR), while the other one was left untreated (O-HFD). Both groups were compared to O mice kept on a normal diet (O-ND). An additional group of young (12-week-old) mice under a normal diet (Y-ND) was also used for comparison. At the indicated times, mice were submitted to treadmill exhaustion test (T) or micro-computed tomography (CT). **(b-d)** Evolution of body weight, glycemia and insulin resistance index during the study. **(e)** Mice were submitted to an uphill treadmill exhaustion test at different ages, with each time a protocol adapted to mice conditions. Endurance capacity was expressed as work to consider the differences in body weight (kg) over the distance covered (m). **(f)** Micro-CT evaluation of dorsal muscle and liver density, a decrease in density reflecting fatty infiltration. Data are means ± SEM for 6 Y-ND, and 9-12 mice in the other 3 groups. Statistical analysis was performed using a mixed-effects analysis (b) or one-way ANOVA followed by Tukey's test to compare the 3 groups of O mice (c-f). Comparisons between Y-ND and O-ND were carried out using unpaired two-tailed *t*-test. $^{*}P < 0.05$, $^{***}P < 0.001$, $^{****}P < 0.0001$ vs. O-ND mice. $^{\dagger}P \leq 0.07$, $^{\#}P < 0.05$, $^{\#\#}P < 0.01$, $^{\#\#\#}P < 0.001$ vs. O-HFD mice.

AdipoRon reduces the severity of NAFLD

To further investigate the effects of AdipoRon on the liver, several parameters including steatosis, hepatocellular ballooning and inflammation were quantified on histological sections using the NAFLD activity score (NAS score) (Figure 2a, b). O-ND mice had almost normal liver histology (NAS = 0.4). O-HFD mice were diagnosed with non-alcoholic steatohepatitis (NASH) (i.e., NAS ≥ 3 with at least 1 point in each sub-score) as they exhibited steatosis (>2), inflammation (>2) and ballooning (>1). By contrast, O-HFD+AR mice did not reach NASH stage: they had lower scores of steatosis (<2), inflammation (<2) and ballooning (<1). Strikingly, only 3 out of 10 O-HFD+AR mice presented ballooning versus 7 out of 8 in untreated HFD ones. The protective effect of AdipoRon on steatosis was corroborated by liver lipid dosage and liver weight (Figure 2c; Table S1). These data indicate that AdipoRon partially

protected against liver fatty infiltration and mitigated the severity of NAFLD in diet-induced obese mice.

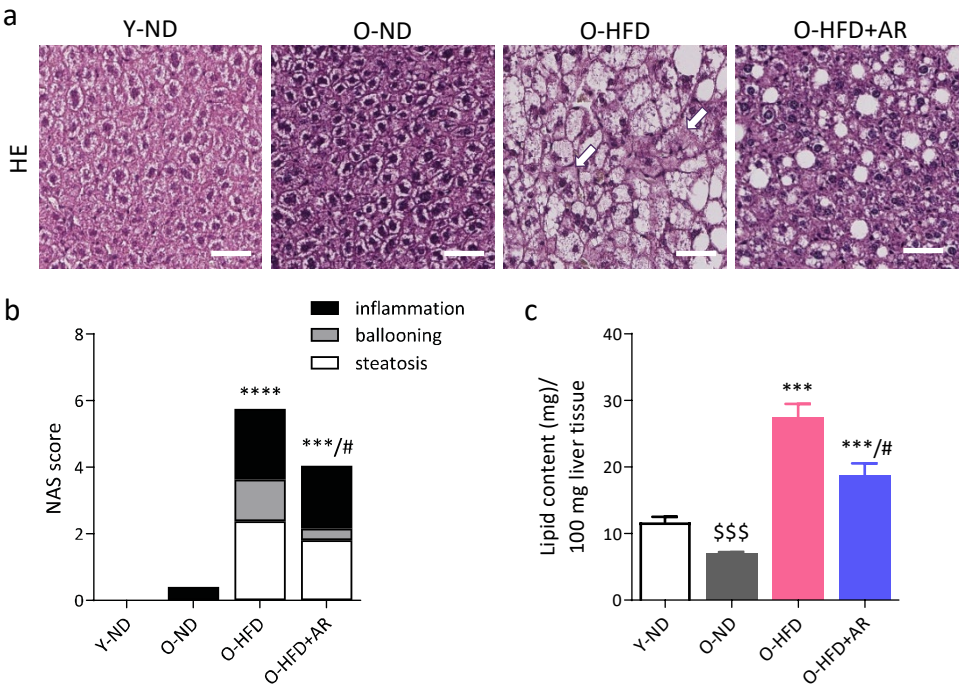

Figure 2. Chronic administration of AdipoRon reduces the severity of non-alcoholic fatty liver disease (NAFLD) in middle-aged obese mice. (a) Representative hematoxylin and eosin-stained liver sections from the different groups of mice. Arrows indicate hepatocellular ballooning, scale bar = 50 µm. **(b)** Histological NAFLD activity score (NAS) calculated on sections like those shown in A. **(c)** Lipid content in liver (biochemical measure). Data are means ± SEM for 6 Y-ND, and 8-10 mice in the other 3 groups. Unless otherwise specified, statistical analysis was performed using one-way ANOVA followed by Tukey's test (comparing 3 groups of O-mice) or by unpaired two-tailed *t*-test (Y-ND vs. O-N). $^{\$\$\$}P < 0.001$ vs. Y-ND mice. $^{***}P < 0.001$, $^{****}P < 0.0001$ vs. O-ND mice. $^{\#}P < 0.05$ vs. O-HFD mice.

AdipoRon drastically blunts diet- or age- induced accumulation of Intramyocellular lipids

We next examined the effects of AdipoRon on myosteatosis and more specifically on the excessive accumulation of intramyocellular lipids (IMCLs) that leads to insulin resistance in obesity and type 2 diabetes [18, 19]. This accumulation being fiber type-dependent, we quantified IMCL content and analyzed lipid droplet (LD) morphology in the soleus, a slow-twitch oxidative muscle and in the *extensor digitorum longus* (EDL), a fast-twitch glycolytic one. We performed fiber typing and LD staining on serial muscle cryosections.

Total number of fibers in each muscle was similar between the four groups of mice (data not shown). Fiber typing was carried out by immunofluorescence staining of different MyHCs isoforms (Figure 3a). As expected, the soleus contained a large proportion of slow-oxidative type 1 (blue, ~38%) and 2a fibers (green, ~50%), whereas the EDL was mainly composed of fast-glycolytic type 2b (black, ~65%) and 2x (red, ~17%) fibers (Figure 3a, b). There was also a small proportion of hybrid fibers. Overall, the proportion of fiber types in each muscle did not significantly differ between the 4 groups of mice (Figure 3b). Thus, AdipoRon did not induce a fiber switch towards a more oxidative phenotype in middle-aged obese mice, unlike in mdx mice [14]. Fiber size, assessed by both cross-sectional area or minimum Feret's diameter, was also roughly similar in the different groups (not shown).

Next, we quantified by Bodipy staining IMCL content and LD size on a fiber type and subcellular (peripheral vs. central)-specific basis (Figures 3c, 4). The overall lipid content was higher in the peripheral (subsarcolemmal) region than at the center of the myofiber. Peripheral IMCL accumulation has been associated with insulin resistance [18, 19] and could also exert a mechanical stress on sarcolemma. As

shown on Figure 3c, the plasma membrane presented scalloped edges (arrows) due to the presence of large subsarcolemmal LDs. In type 1 and type 2a fibers of soleus, IMCL content (expressed as % stained area) was significantly increased in O-ND mice compared to Y-ND ones (both centrally and peripherally) and was not significantly modified by HFD (Figure 4a). However, when compared to HFD-fed mice, AdipoRon reduced total IMCL content in both fiber types. In EDL (type 2x and type 2b fibers), IMCL content of O-ND mice was roughly similar to that of Y-ND mice (except for the periphery in 2x fibers) (Figure 4b). By contrast, this content was significantly increased by HFD in both fiber types (compare O-HFD vs. O-ND mice). AdipoRon drastically reduced HFD-induced IMCL accumulation in both types of fibers and in both regions. Moreover, it tended or reduced LD size in soleus (especially in 2a fibers) and in EDL in both fiber types, both centrally and peripherally (Figure 4c, d). Taken together, these results indicate that AdipoRon strikingly reversed IMCL accumulation either due to aging in oxidative fibers or to HFD in glycolytic ones. It reduced LD size as well.

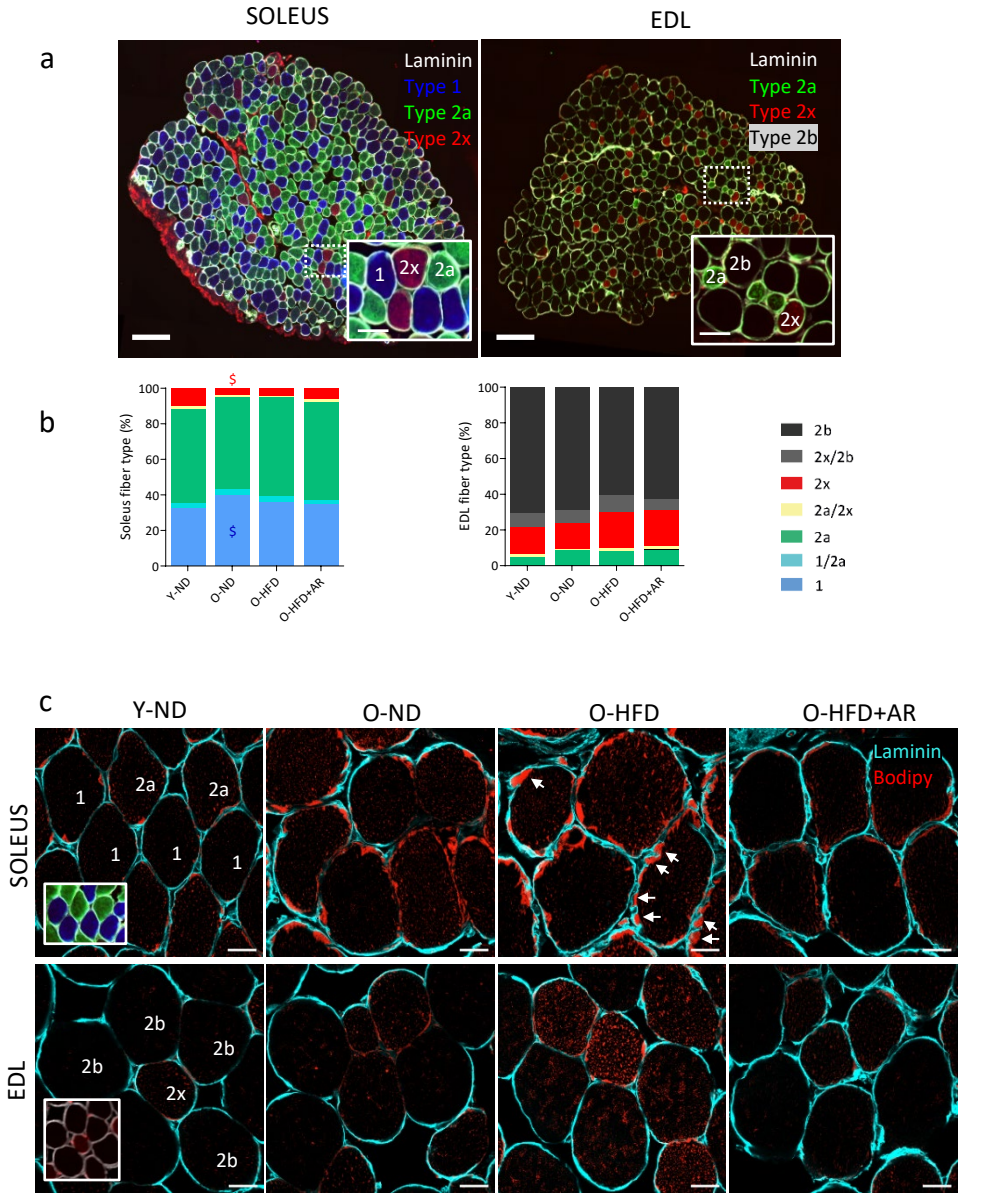

Figure 3. Effects of AdipoRon on fiber type composition and lipid infiltration in soleus and EDL from middle-aged obese mice. Fiber typing and bodipy staining were performed on serial muscle cross-sections in an oxidative (soleus) and a glycolytic (EDL) muscle. **(a)** Fiber typing was carried out by immunofluorescence staining of different myosin heavy chains isoforms (MyHCs). Type 1 fibers were

labeled in blue, type 2a in green, 2x in red while 2b were nonlabeled (black). Laminin antibody was used to delineate basal membrane (white). Representative sections for each group are shown. Scale bar = 200 µm. *Insets:* Higher magnification of immunostaining images (scale bar = 50 µm). **(b)** Fiber type proportion for each muscle in the 4 groups of mice. Data are means for 6 mice per group. Statistical analysis was performed using one-way ANOVA followed by Tukey's test (comparing 3 groups of O-mice) or by unpaired two-tailed *t*-test (Y-ND *vs*. O-ND). $^{\$}P < 0.05$ vs. Y-ND mice. **(c)** Bodipy staining of lipids (red) on muscle cross-sections to quantify IMCL content on a fiber type specific-basis. Laminin was colored in cyan. Peripheral (subsarcolemmal, SS) lipid droplets (LDs) are usually more abundant than central ones. Arrows indicate scalloped edges of sarcolemma facing large SS LDs. Representative sections for 6 mice per group are shown. Scale bar = 20 µm.

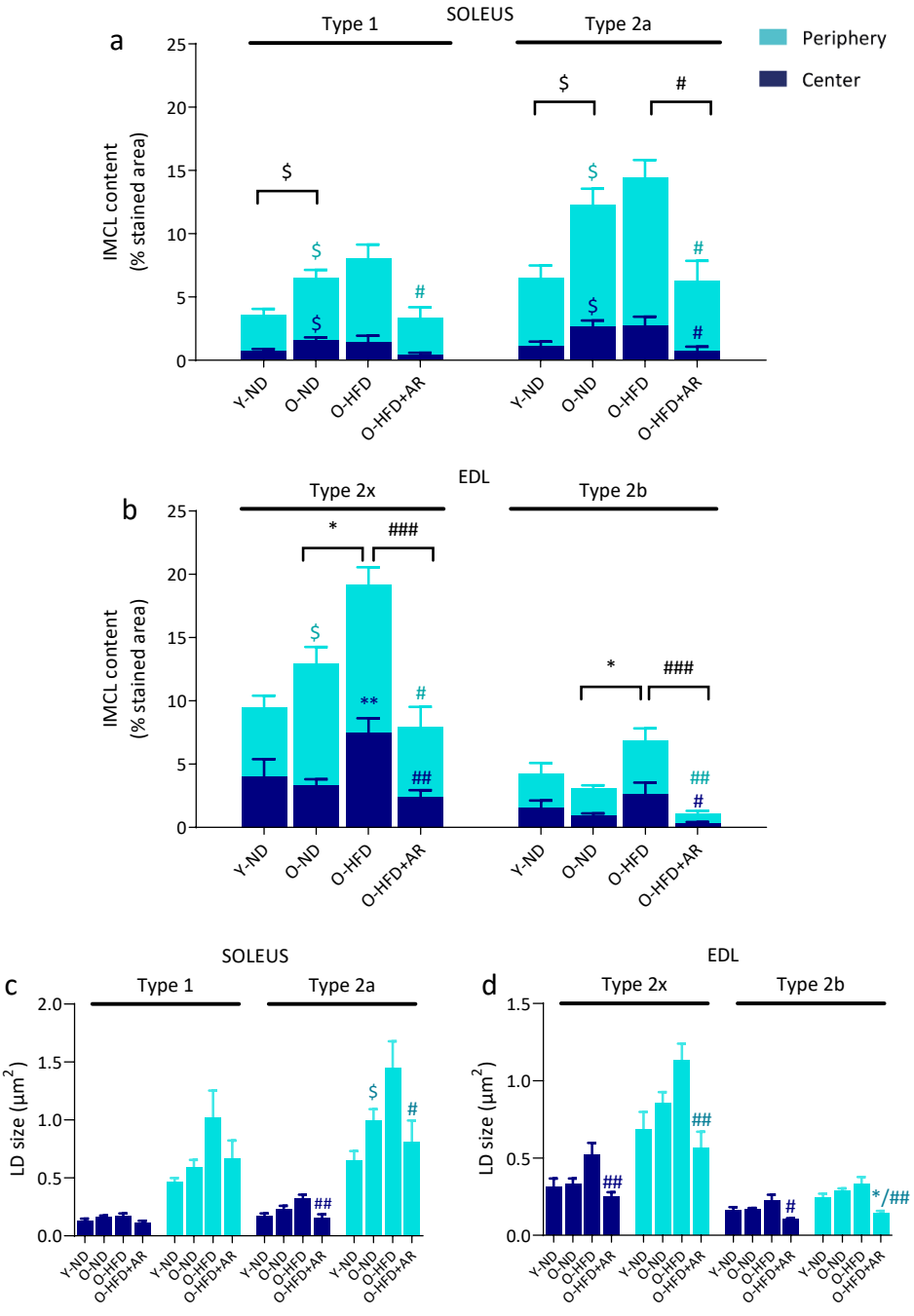
a
SOLEUS
Type 1
Type 2a
Periphery
Center
IMCL content
(% stained area)
Y-ND
O-ND
O-HFD
O-HFD+AR
b
EDL
Type 2x
Type 2b
c
LD size (µm²)
d

Figure 4. AdipoRon drastically blunts diet- or age- induced accumulation of intramyocellular lipids (IMCL) in middle-aged obese mice. (a) IMCL content of soleus in peripheral and central subcellular regions in type 1 and 2a fibers stained by Bodipy and **(b)** IMCL content of EDL in subcellular regions in type 2x and 2b fibers. IMCL content in each region was expressed as % of stained area normalized to total fiber area. Symbols for differences among central regions are in dark blue, among peripheral regions in turquoise blue, and those for the total content in black. **(c)** LD size in peripheral and central subcellular regions in type 1 and 2a fibers from soleus and **(d)** in type 2x and 2b fibers from EDL. Data are means ± SEM for 5 mice per group. Statistical analysis was performed using one-way ANOVA followed by Tukey's test (comparing 3 groups of O-mice) or by unpaired two-tailed *t*-test (Y-ND vs. O-ND). $^{\$}P < 0.05$ vs. Y-ND mice. $^{*}P < 0.05$, $^{**}P < 0.01$ vs. O-ND mice. $^{\#}P < 0.05$, $^{\#\#}P < 0.01$, $^{\#\#\#}P < 0.001$ vs. O-HFD mice.

We then analyzed whether AdipoRon enhanced fatty acid oxidation by stimulating the AMP-activated protein kinase (AMPK)-peroxisome proliferator-activated receptor γ coactivator-1α (PGC-1α/*Ppargc1a*) axis (Figure S2)[6]. The phosphorylated and active form of AMPK (P-AMPK) and protein levels of PGC-1α doubled under AdipoRon when compared to the other two groups of O-mice. The expression of relevant target genes of this transcriptional co-activator was (or tended to be) increased by AdipoRon, including those involved in fatty acid oxidation or energy dissipation (represented by dark blue boxes, part 1 on Figure S2). Thus, AdipoRon enhanced (or tended to enhance) mRNA abundance of medium-chain acyl-CoA dehydrogenase (*Acadm*), acyl-CoA oxidase (*Acox*) and uncoupling protein 3 (*Ucp3*) (Figure 5b).

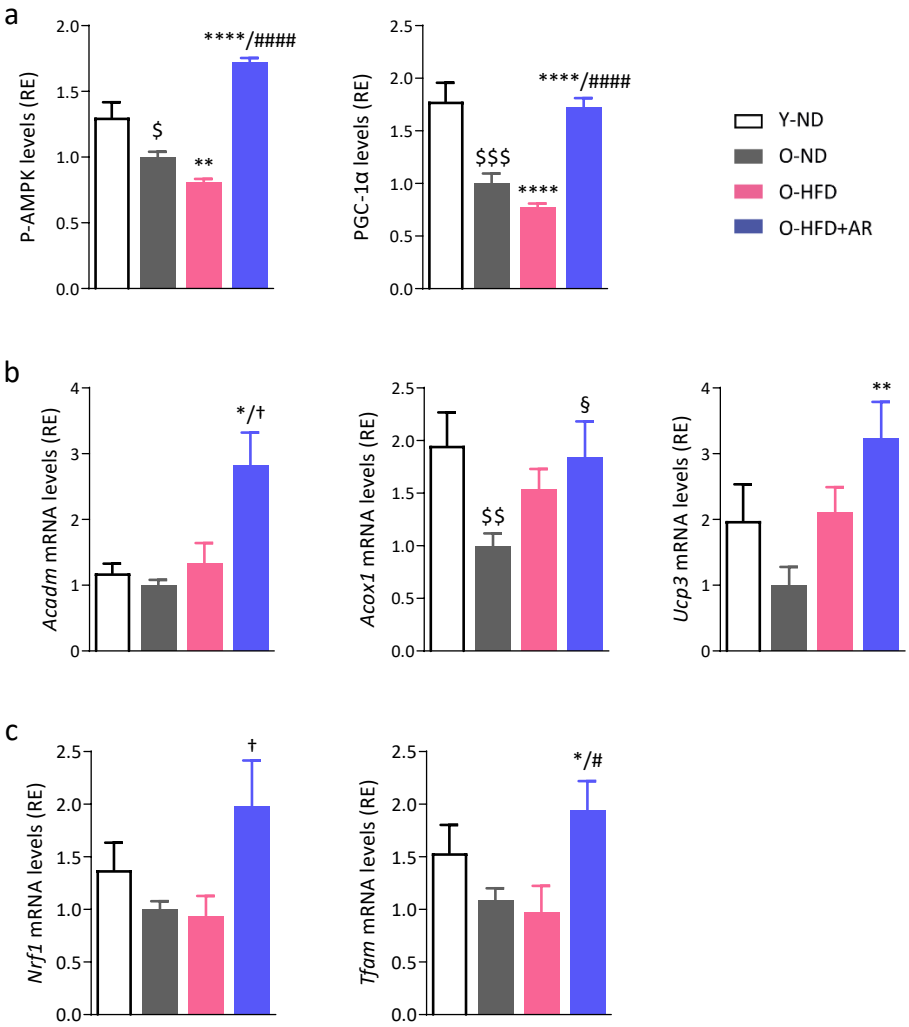

Figure 5. AdipoRon increases or tends to increase the expression of genes involved in fatty acid oxidation, mitochondrial biogenesis and function in soleus of middle-aged obese mice. (a) AMPK activity and **protein levels of PGC-1α (gastrocnemius)**, early signaling events of the cascade leading to enhancing effects on mitochondria. **(b)** mRNA levels of medium-chain acyl-CoA dehydrogenase (*Acadm*) and Acyl-CoA oxidase 1 (*Acox1)* implicated in fatty acid oxidation and uncoupling protein 3 (*Ucp3)* in energy dissipation. **(c)** mRNA levels of nuclear respiratory factor-1 (*Nrf1)*, a target gene of PGC-1α and of mitochondrial transcription factor A *(Tfam)*. mRNA levels were normalized to cyclophilin, and the subsequent ratios presented as relative expression compared with O-ND values.

The active phosphorylated form of AMPKα (P-AMPK) and PGC-1α protein levels were quantified by ELISA and absorbance data were presented as relative expression compared with O-ND values. Data are means ± SEM for 6 Y-ND, and 8-10 mice in the other 3 groups (a-c). Statistical analysis was performed by one-way ANOVA followed by Tukey's test (comparing 3 groups of O-mice) or by unpaired two-tailed *t*-test (Y-ND *vs*. O-ND). $^{\$}P < 0.05$, $^{\$\$}P < 0.01$, $^{\$\$\$}P < 0.001$ vs. Y-ND mice. $^{\S}P = 0.059$, $^{*}P < 0.05$, $^{**}P < 0.01$, $^{****}P < 0.0001$ vs. O-ND mice. $^{\dagger}P \leq 0.08$, $^{\#}P < 0.05$, $^{\#\#\#\#}P < 0.0001$ vs. O-HFD mice.

AdipoRon improves muscle mitochondrial function

PGC-1α also promotes mitochondrial biogenesis and function via the transcriptional regulation of nuclear transcription factors such as nuclear respiratory factor-1 (NRF-1)(part 2 on Figure S2). Expression of NRF-1 tended to be increased by AdipoRon (Figure 5c). Moreover, AdipoRon doubled the expression of mitochondrial transcription factor A (*Tfam*), downstream of NRF1, which binds to mitochondrial DNA (mtDNA) and activates mitochondrial biogenesis and function [20] (Figures 5c and S2).

Myofiber mitochondrial content was assessed by immunodetection of the Translocase of Outer Mitochondrial Membrane 20 (TOMM20) in soleus and EDL, in a fiber- and subcellular-specific way (Figures 6 and S2). As described [21], in soleus, type 2a fibers, which are more oxidative than type 1, have a higher mitochondrial content (Figure 6a, b; compare the % stained area between the 2 fiber types). Likewise, in EDL, type 2x fibers have more mitochondria than 2b, which are more glycolytic and whose mitochondrial content was barely detectable [21] (Figure 6a, b). Mitochondria were usually more abundant in the subsarcolemmal region. In soleus, total mitochondrial content rose under HFD (mainly due to an increase in subsarcolemmal mitochondria) in line with other reports [22] but this content was not influenced by the treatment. Mitochondria content decreased with age in 2x fibers (Figure 6b). Overall, there was no major change in mitochondrial content

induced by AdipoRon in any muscle. Yet, as shown in Figures 6c and S3, (immuno)fluorescence co-labeling (TOMM20/Bodipy) revealed physical contacts between LDs and mitochondria, which may facilitate the trafficking of fatty acids released from LDs to mitochondria, where they are oxidized. Transmission Electron Microscopy (TEM) confirmed such close contacts (Figure 6c).

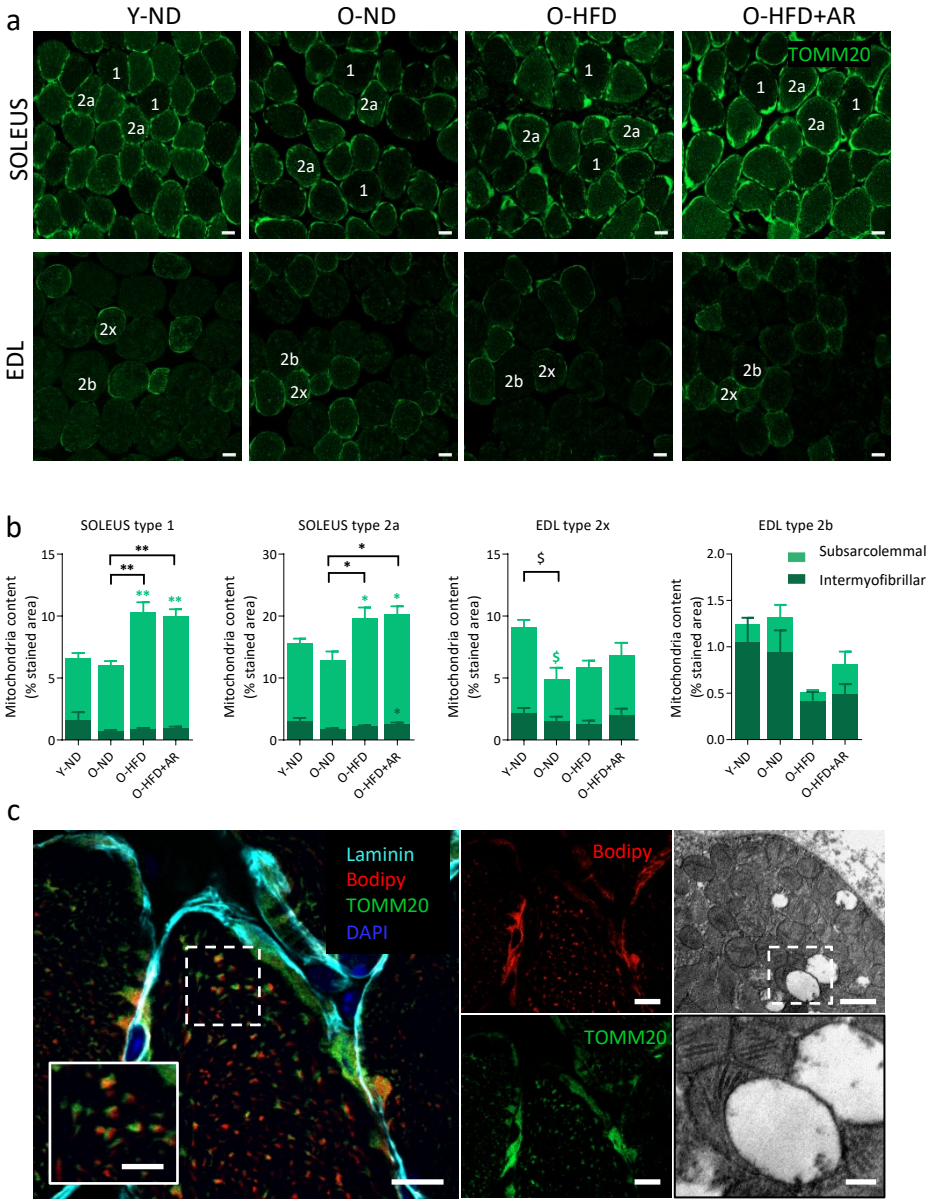

Figure 6. Quantification of mitochondrial content in muscle of middle-aged obese mice treated or not with AdipoRon. (a) Mitochondrial content was assessed by immunodetection of the Translocase of Outer Mitochondrial Membrane 20 (TOMM20) in soleus and EDL from the 4 groups of mice on a fiber dependent manner. Representative images for each group are shown. Scale bar = 20 µm.

(b) Quantification of mitochondrial content in peripheral (subsarcolemmal) and central (intermyofibrillar) subcellular regions for each fiber type in soleus or EDL. Mitochondrial content in each region was expressed as % of stained area normalized to total fiber area. Data are means ± SEM for 5-6 mice per group. Statistical analysis was performed by one-way ANOVA (comparing 3 groups of O-mice) or by unpaired two-tailed t-test (Y-ND vs. O-ND). $^{\$}P < 0.05$ vs. Y-ND mice. $^{*}P < 0.05$, $^{**}P < 0.01$ vs. O-ND mice. Symbols for differences among central regions are in dark green, among peripheral regions in light green, and those for the total content in black. **(c)** Lipid droplet (LD)-mitochondrion contacts. *Left,* Confocal fluorescence micrographs of soleus from an O-HFD mouse: LDs were stained with Bodipy in red, mitochondria with anti-TOMM20 in green, the edge of the fiber with anti-laminin in cyan and nuclei with DAPI in blue. Some mitochondria co-localized with LDs when channels were merged. Scale bar = 10 µm. Inset: Higher magnification (scale bar = 5 µm). *Right,* Transmission electron micrograph of rectus femoris from an O-HFD+AR mouse illustrating LD-mitochondrion contact. Scale bar = 1 µm (*top right*) and 0.25 µm (inset, *bottom right*).

Because mitochondrial content did not increase with AdipoRon, while the treatment significantly reduced LD accumulation, we tested the hypothesis that AdipoRon mainly enhanced mitochondrial function. We measured the activity of two respiratory enzymes: Cytochrome C oxidase (COX), whose catalytic subunits are partly encoded by mtDNA, and succinate dehydrogenase (SDH), which is entirely encoded by nuclear cDNA (Figure S2). For COX, the proportion of dark fibers indicating high activity was increased in O-HFD+AR compared to the other groups of old mice (+34% vs. O-ND and +26% vs. O-HFD), while the proportion of pale fibers was decreased (Figure 7a, b). In addition, COX activity was reduced in O-ND mice compared with Y-ND, reflecting impaired mitochondrial activity with aging. By contrast, SDH activity was roughly similar between the different groups of mice (Figure 7c, d). As mtDNA integrity is essential for the successful synthesis of active COX, these results indicate that mitochondrial function, which is impaired with aging, was improved and even corrected with AdipoRon.

Because abnormal mitochondrial ultrastructure is associated with impaired mitochondrial function, we qualitatively analyzed mitochondrial morphology by TEM in each group of mice. Figure 7e illustrates mitochondria and LDs in the subsarcolemmal region of the rectus femoris. The two groups of untreated old mice showed a greater abundance of aberrant mitochondria (painted in pale green): swollen mitochondria, organelles with disrupted cristae, vacuoles-like structure formation and reduced electron density of the matrix, while AdipoRon treatment alleviated these abnormalities (normal mitochondria in dark green, see annex 3 for uncolored images).

AdipoRon reduces aged-related tubular aggregate and cylindrical spiral formation

Tubular aggregates (TAg) and cylindrical spirals (CS) were observed in rectus femoris of middle-aged mice. These are two distinct ultrastructural abnormalities that share similar histochemical staining characteristics [23]. By bright field microscopy, they appear as pale or slightly basophilic inclusions with hematoxylin-eosin, bright red ones with Gomori Trichrome (Figure 8a) or unstained with COX or SDH detection (see Figure 7a, c). By electron microscopy, TAg may display different forms, the most typical being straight single-walled or double-walled tubules, regularly organized in tightly packed aggregates with a para-crystalline order, while CS appear as accumulations of spiral lamellae (Figure 8b).

These abnormal structures (bright red inclusions) were quantified on Gomori sections from the 4 groups of mice (Figure 8c). They were almost absent in young mice but were much more abundant in old ones. Strikingly, AdipoRon reduced by almost 50% the accumulation of these aging-related structures in myofibers. Because these structures represent intracellular bins for dysfunctional

accumulation of proteins, we instigated autophagy-related players (Figures 8d and S4). Autophagy marker Light Chain 3 (LC3) II/I ratio was unchanged in the 4 groups of mice. However, p62 expression was reduced by 53% in O-HFD+AR mice compared to O-ND, suggesting that AdipoRon stimulates autophagy. Moreover, AdipoRon enhanced the phosphorylation of UNC-51 like kinase (ULK1) at Ser555 (~40% vs. other O-mice), in line with the fact that AMPK phosphorylates and activates this autophagy marker [24].

AdipoRon and muscle inflammation

Lastly, we studied the potential anti-inflammatory effect of AdipoRon on the muscle. AdipoRon reduced by ~20% NF-κB activity, assessed by the active and phosphorylated form of the p65-subunit (Figure S5). However, the other markers of inflammation (TNFα, IL1-β, CD68) or oxidative stress (peroxiredoxin 3 and hydroxy-2-nonenal), measured either at the mRNA or protein level, were extremely low or undetectable and were not influenced by AdipoRon (not shown).

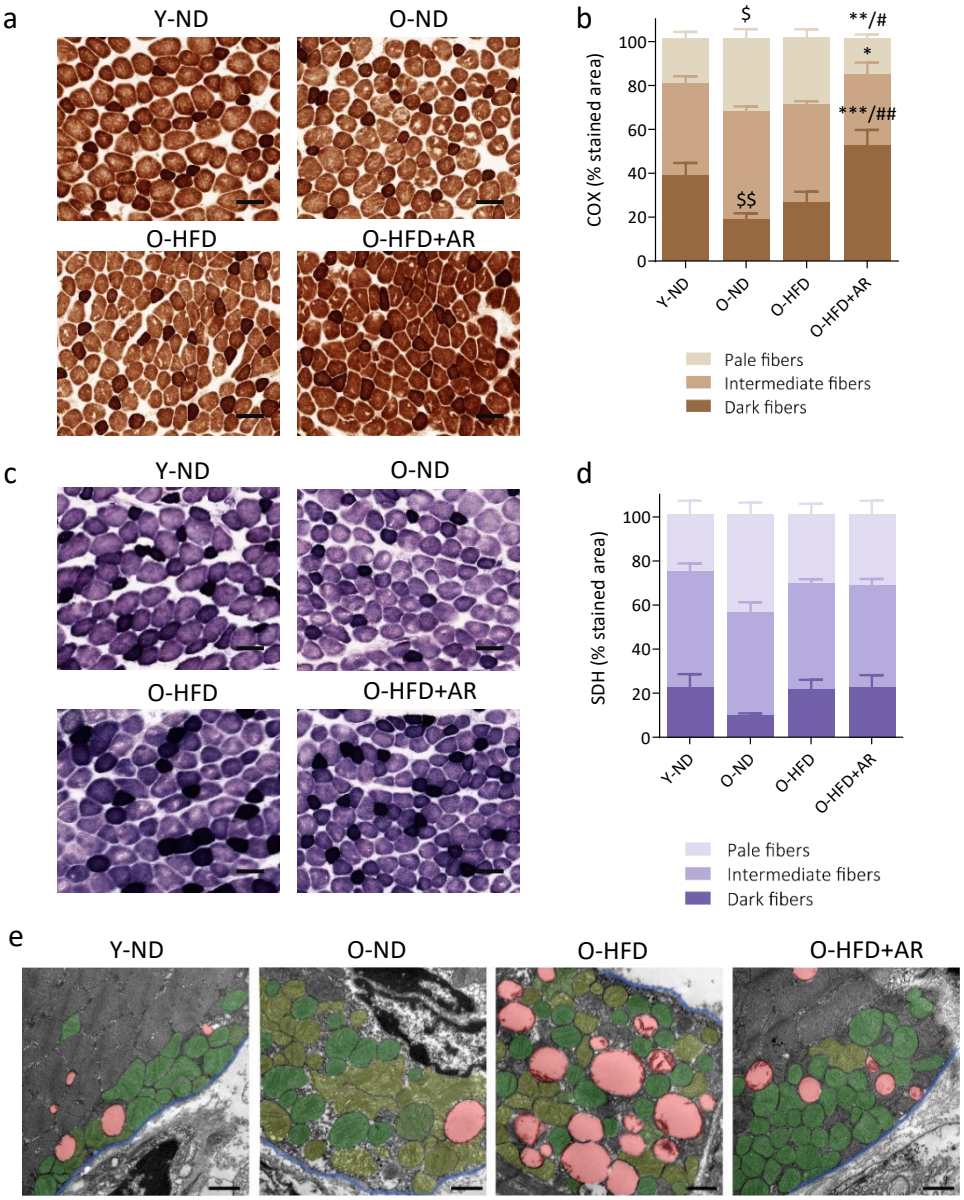

Figure 7. Chronic administration of AdipoRon enhances mitochondrial function and protection in muscle of middle-aged obese mice. (a, c) Histochemistry staining of COX and SDH activity in the rectus femoris of the 4 groups mice, the darkest color being associated with the highest activity. Representative images of both stainings for each group are shown. Scale bar = 100 µm. **(b, d)** Quantification of COX and SDH activity. Activity was expressed as % of stained area normalized to the cross-

sectional area of the muscle, for each of the 3 staining intensities (set up as corresponding to pale, intermediate or dark color). Data are means ± SEM for 4-6 mice per group. Statistical analysis was performed by one-way ANOVA (comparing 3 groups of O-mice) or by unpaired two-tailed *t*-test (Y-ND *vs*. O-ND). $^{\$}P < 0.05$, $^{\$\$}P < 0.01$ vs. Y-ND mice. $^{*}P < 0.05$, $^{**}P < 0.01$, $^{***}P < 0.001$ vs. O-ND mice. $^{\#}P < 0.05$, $^{\#\#}P < 0.01$ vs. O-HFD mice. **(e)** Transmission electron micrographs of mitochondria in the subsarcolemmal region of rectus femoris in the 4 groups of mice. For sake of clarity, abnormal mitochondria are false-colored in pale green, while normal mitochondria are colored in dark green, LDs in red and the blue line delimits the sarcolemma. Representative images of each group are shown. Scale bar = 1 µm.

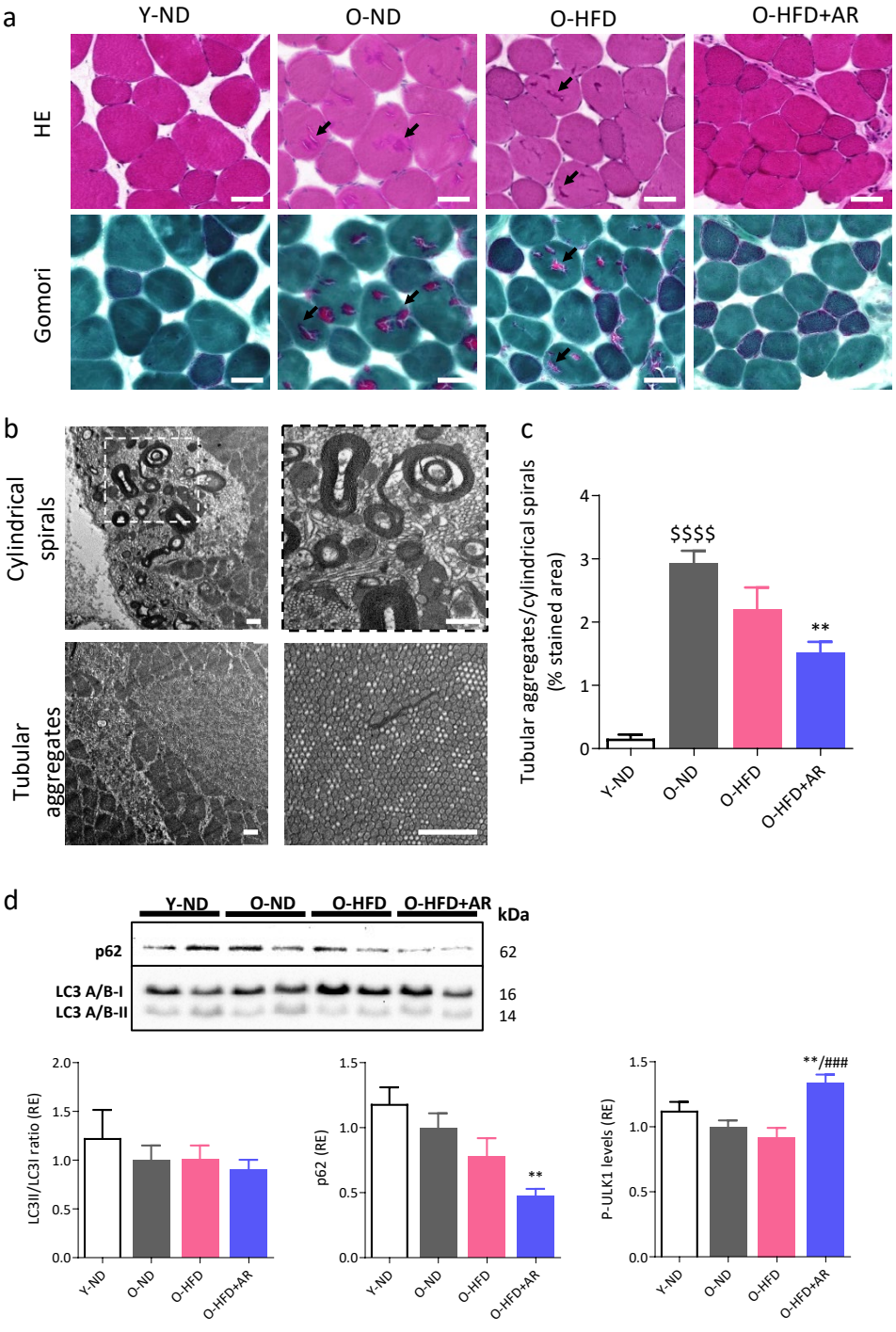
a
Y-ND
O-ND
O-HFD
O-HFD+AR
HE
Gomori
b
Cylindrical spirals
Tubular aggregates
c
Tubular aggregates/cylindrical spirals (% stained area)
$$$$
**
Y-ND
O-ND
O-HFD
O-HFD+AR
d
Y-ND
O-ND
O-HFD
O-HFD+AR
kDa
p62
62
LC3 A/B-I
LC3 A/B-II
16
14
LC3II/LC3I ratio (RE)
p62 (RE)
**
P-ULK1 levels (RE)
**/###

Figure 8. Chronic administration of AdipoRon reduces aged-related tubular aggregate (TAg) and cylindrical spiral (CS) formation in muscle of middle-aged obese mice. (a) TAg and CS (indicated by arrows) appear in rectus femoris from the different groups of mice as pale or slightly basophilic inclusions with hematoxylin-eosin (HE) and bright red ones with Gomori Trichrome. Scale bars = 50 µm. **(b)** Confirmation of these structures by transmission electron microscopy. Scale bars = 1 µm. **(c)** Quantification of TAg/CS abundance expressed as % of stained area (bright red inclusions) normalized to the cross-sectional area of the muscle after Gomori Trichrome. Data are means ± SEM for 6 mice per group. **(d)** Effects of AdipoRon on autophagy markers in muscle from the 4 groups of mice. LC3II/LC3I ratio and p62 were analyzed by Western blotting and the phosphorylated form (Ser555) of ULK1 by ELISA. p62 levels were normalized to Ponceau S staining (shown in Figure S4). Results were then presented as relative expression compared to O-ND values. Data are means ± SEM for 6-10 mice per group. Statistical analysis was performed by one-way ANOVA followed by Tukey's test (comparing 3 groups of O-mice) or by unpaired two-tailed *t*-test (Y-ND *vs*. O-ND). $^{\$\$\$\$}P < 0.0001$ vs. Y-ND mice. $^{**}P < 0.01$ vs. O-ND mice. $^{\#\#\#}P < 0.001$ vs. O-HFD mice.

DISCUSSION

Long-term administration of AdipoRon improves exercise endurance, attenuates ectopic lipid deposit and reduces degenerative markers in the muscle of obese and middle-aged mice. Thus, AdipoRon administration close to 1 year promotes healthy aging in mice on a normal genetic background. These findings extend the effects observed in mice with a genetic defect (db/db) where the marked alleviation of the severe diabetic status by AdipoRon was a major confounding factor [10]. This is the longest treatment with AdipoRon ever reported so far. Its persisting effects indicate that there is no habituation to this compound. This long treatment was also well tolerated and safely promotes beneficial effects.

Plasma ApN levels were low in old mice compared to young ones (O-ND vs. Y-ND). Likewise, in a "classical" population of geriatric patients, those who were also more likely to be functionally dependent had lower plasma ApN levels than the others [25]. Conversely, in most studies, plasma ApN levels were higher among centenarians than in elderly individuals and those levels correlated with a preferable metabolic phenotype [26]. Hence, there could be a rationale for therapeutic correction of ApN in aging.

By reducing ectopic lipids in both liver and muscle, AdipoRon protects obese and middle-aged mice against burdens associated with the metabolic syndrome: NASH and myosteatosis. NAFLD is the most common chronic liver disease in the world due to the rising prevalence of obesity and aging. NAFLD encompasses steatosis and NASH. NASH is the severe form of NAFLD with lobular inflammation and hepatocyte ballooning; this stage has a clear potential of progression to cirrhosis and hepatocellular cancer [17]. Herein, in spite of receiving HFD for more than 1 year, mice treated with AdipoRon exhibit NAFLD that does not progress into NASH,

as assessed by the NAS score. These data extend the decreased hepatic lipid content measured by chemical extraction after 2 weeks of AdipoRon in HFD mice or db/db mice [10] and the lessening of liver injury caused by toxic agents under AdipoRon [12].

The protective effects of AdipoRon against myosteatosis have been poorly studied so far [10]. Yet, myosteatosis is emerging as a public health problem. It increases with age and obesity and is recognized to negatively correlate with muscle mass, strength, and mobility, and disrupts metabolism (insulin resistance, diabetes) [4]. It is also a negative prognostic factor for cancer [27], cardiovascular disease [28] or NAFLD [17]. IMCLs are predominantly stored in LDs to serve as metabolic fuel during physical exercise. However, when lipid supply exceeds demand, or when mitochondria become dysfunctional, IMCLs are also implicated in muscle insulin resistance as in obesity and type 2 diabetes [29, 30]. Yet, endurance athletes have similar, if not higher, IMCL content than obese patients with type 2 diabetes, while maintaining high insulin sensitivity. This “athlete’s paradox” is explained by a more nuanced appraisal of muscle LDs, including localization and size [19, 29]. Peripheral LDs exert a more deleterious effect on insulin sensitivity than central ones, which are more dedicated to produce fuel for contraction [19, 29]. LD size also plays a role on overall metabolism as this parameter is inversely correlated to insulin sensitivity and physical fitness [18, 29]. In fact, smaller LDs exhibit a relatively larger surface area for lipase action and thus, potentially have a greater capacity to mobilize lipids [29]. By using Bodipy staining, we quantified IMCL content and analyzed LD size and subcellular distribution in a fiber-specific manner. Our study highlights a differential impact of aging and dietary fat overload on IMCL content according to fiber-type. Thus, aging promotes accumulation of IMCLs in oxidative fibers while dietary fat overload promotes such an accumulation in glycolytic ones. The latter observation

is concordant with the elevated fatty acid content observed in EDL, but not in soleus, after 5 weeks of HFD administration to mice [31]. The lower impact of HF overload on soleus may be explained by the concomitant upregulation of mitochondrial content in oxidative fibers [22](see figure 6b), which may partly cope with lipid excess. A novel and important finding is that AdipoRon strikingly reversed IMCL accumulation whether due to aging in oxidative fibers (types 1 and 2a) or to HFD in glycolytic ones (types 2x and 2b). This correction occurs in both subcellular regions. The size of LDs, especially subsarcolemmal ones was reduced as well.

Besides being associated with adverse metabolic outcomes, large LDs could also affect muscle contractile capacity as previously suggested [32]. Herein, we proposed that large subsarcolemmal LDs could exert a mechanical stress on plasma membrane as supported by scalloped edges of sarcolemma. Other mechanisms could also contribute to impair contractility: inhibition of sarco/endoplasmic reticulum Ca^{2+}-ATPase (SERCA) or of mitochondrial function by fatty acid metabolites for instance [31]. Even in single-myofiber isolated from obese older or normal weight subjects, there was an inverse relationship between IMCL content and fiber contraction, power, and force development, raising the possibility of a vicious circle between IMCL accumulation and functional muscle impairment, thereby further worsening obesity [33]. Taken together, our data show that AdipoRon potently protects against myosteatosis caused by aging or calorie excess. As total number of fibers in each muscle and cross-sectional area for each fiber type were similar between the 4 groups of mice, this raises the possibility that the true contractile mass was actually higher in AdipoRon mice due to lower IMCL accumulation. When comparing the protection afforded by AdipoRon against ectopic lipid deposit in the liver and the skeletal muscle, the alleviation of steatosis was more drastic in the muscle where the correction was complete.

We next examined the mechanisms underlying the marked reduction of myosteatosis and focused on mitochondrial biogenesis and function, which are known to be stimulated by AdipoRon [10]. The mitochondrial content, assessed by TOMM20 staining was not modified by AdipoRon, while COX activity was enhanced. As mtDNA integrity is essential for synthesis of active COX, these results suggest that mitochondrial function is impaired with aging [34], but then markedly improved with AdipoRon. Consistently, the expression of genes involved in fatty acid oxidation or energy dissipation was - or tended to be - increased as well, in line with a previous report [10]. The beneficial effects of AdipoRon on mitochondrion are reinforced by TEM analysis indicating that there were less damaged - presumably less dysfunctional- mitochondria in the muscle of AR-treated mice than in age-matched untreated groups. Comparing these results with those of TOMM20, we assume that some damaged mitochondria could still remain immunoreactive for TOMM20. Taken together, these data indicate that AdipoRon protects against the decline of mitochondrial function due to aging.

By using TEM, we fortuitously found the presence of tubular aggregates (TAg) and cylindrical spirals (CS) in glycolytic myofibers of middle-aged mice [35, 36]. These structures correspond to abnormal accumulation of sarcoplasmic reticulum (SR) components. Immunohistochemical studies showed that TAg derive from the whole SR, while CSs derive merely from the longitudinal one [23, 35]. In humans, the presence of TAg defines a clinically heterogenous group of disorders termed TA myopathies (TAM) characterized by muscle weakness, while CSs have been implicated in some rare familial muscle disorders [23, 35]. As yet, the presence of TAg or CS has not been studied in the elderly but TAg virtually identical to those of TAM patients have been found in aging mice [36]. TAg abundance in old mice is accompanied by impaired ability to restore internal Ca^{2+} stores from extracellular

space, which could contribute to muscle weakness. Herein, an original finding is that AdipoRon strikingly reduced the accumulation of TAg and CS in middle-aged mice and improved exercise endurance. In line with this observation, long-term regular exercise counteracted TAg formation in aged mice, while improving capability of fibers to use extracellular Ca^{2+}[36].

Because AdipoRon reduced damaged mitochondria as well as TAg and CS, we speculated that this mimic could stimulate autophagy in the muscle of middle-aged obese mice. Different lines of evidence indicate that autophagy declines with aging, while autophagy stimulation may have beneficial effects on lifespan [37]. We found no changes in autophagy markers in our two groups of middle-aged mice that did not receive AdipoRon. However, such changes are usually observed in older mice (~24 months) [38]. Yet, AdipoRon activated the phosphorylation (Ser555) of ULK1, an autophagy marker under the control of AMPK [24]. It also markedly decreased the p62 protein, a receptor for cargo including protein aggregates destined for clearance [37]. Taken together, these data suggest that autophagy clearance was actually stimulated by AdipoRon in the muscle, in line with other studies [39, 40].

AdipoRon is known to increase exercise endurance [10]. Here, we extend these data to severely obese and middle-aged mice. Improved endurance was linked to preserved mitochondrial function, higher lipid oxidation and alleviation of myosteatosis. Reduced accumulation of dysfunctional SR proteins and potential improved capability of fibers to use extracellular Ca^{2+} could contribute as well. Conversely, prevention of muscle dysfunction in aged mice thanks to endurance training was attenuated by neutralizing antibodies against ApN or AdipoR1 [41]. The better performance of AR-mice was not due to a higher motivation of these mice: a panel of behavioral tests did not demonstrate any attitude differences

between our HFD-mice treated or not (not shown), unlike data obtained in a mouse model of depression.

In conclusion, long-term AdipoRon treatment enhances muscle endurance in obese middle-aged mice and protects the skeletal muscle and the liver from the adverse metabolic and degenerative effects of aging and calorie excess. By promoting "healthy aging", AdipoRon could hence serve as a crucial step towards enhancing both healthspan and lifespan.

Acknowledgements

This work was supported by grants from UCL University (Research project FSR 2017), Société Francophone du Diabète/Abott Diabetes Care 2020 and Fund for Scientific Research– FNRS (Research Credit 35275437, 2019). M.A.-S is Chargé de Recherches and C.M.S. has received a fellowship from the FRIA. M.A.D.-L.d.C. received a fellowship from the Wallonie-Bruxelles International Excellence Program.

We are grateful to Caroline Bouzin and the IREC imaging platform for the use of the equipment and their aid, to Pr. Philippe Gailly and Dr. Olivier Schakman for providing the necessary equipment and the know-how for the in vivo functional tests. We thank Camille Pichon for her involvement in the analysis of micro-CT scans; Marie-Christine Many and Peter Van den Bergh for their help in the interpretation of TEM images; Véronique Van Den Berge for her technical support; Laura De Cock, Alice Monnier and Marie Clerbois for their participation in mice experiments and tissue analysis. We also thank Greetje Vande Velde (MoSAIC, KU Leuven) for providing the micro-CT scan and the microscopy department (CITIUS, Universidad de Sevilla) for their technical support for transmission electron microscopy.

Ethical guidelines and consent

All authors certify that they comply with the ethical guidelines for authorship and publishing in the Journal of Cachexia, Sarcopenia and Muscle [42].

All procedures conducted in mice were approved by the Ethical Committee for Animal Experimentation from the Medical Sector at Université Catholique de Louvain (2019/UCL/MD/013).

Conflict of interest

Authors declare that no conflict of interest exists.

References

1. Tieland, M., I. Trouwborst, and B.C. Clark, *Skeletal muscle performance and ageing.* J Cachexia Sarcopenia Muscle, 2018. **9**(1): p. 3-19.
2. Fakhouri, T.H., et al., *Prevalence of obesity among older adults in the United States, 2007-2010.* NCHS Data Brief, 2012(106): p. 1-8.
3. Tam, B.T., J.A. Morais, and S. Santosa, *Obesity and ageing: Two sides of the same coin.* Obes Rev, 2020. **21**(4): p. e12991.
4. Correa-de-Araujo, R., et al., *Myosteatosis in the Context of Skeletal Muscle Function Deficit: An Interdisciplinary Workshop at the National Institute on Aging.* Front Physiol, 2020. **11**: p. 963.
5. Alqahtani, S.A. and J.M. Schattenberg, *NAFLD in the Elderly.* Clin Interv Aging, 2021. **16**: p. 1633-1649.
6. Abou-Samra, M., et al., *Adiponectin and Its Mimics on Skeletal Muscle: Insulin Sensitizers, Fat Burners, Exercise Mimickers, Muscling Pills … or Everything Together?* Int J Mol Sci, 2020. **21**(7).
7. Abou-Samra, M., et al., *Involvement of adiponectin in the pathogenesis of dystrophinopathy.* Skelet Muscle, 2015. **5**: p. 25.
8. Otabe, S., et al., *Overexpression of human adiponectin in transgenic mice results in suppression of fat accumulation and prevention of premature death by high-calorie diet.* Am J Physiol Endocrinol Metab, 2007. **293**(1): p. E210-8.
9. Li, N., et al., *Adiponectin preserves metabolic fitness during aging.* Elife, 2021. **10**.
10. Okada-Iwabu, M., et al., *A small-molecule AdipoR agonist for type 2 diabetes and short life in obesity.* Nature, 2013. **503**(7477): p. 493-9.
11. Zhang, Y., et al., *AdipoRon, the first orally active adiponectin receptor activator, attenuates postischemic myocardial apoptosis through both AMPK-mediated and AMPK-independent signalings.* Am J Physiol Endocrinol Metab, 2015. **309**(3): p. E275-82.
12. Wang, Y., et al., *Hepatoprotective effects of AdipoRon against d-galactosamine-induced liver injury in mice.* Eur J Pharm Sci, 2016. **93**: p. 123-31.
13. Iwabu, M., et al., *AdipoR agonist increases insulin sensitivity and exercise endurance in AdipoR-humanized mice.* Commun Biol, 2021. **4**(1): p. 45.
14. Abou-Samra, M., et al., *AdipoRon, a new therapeutic prospect for Duchenne muscular dystrophy.* J Cachexia Sarcopenia Muscle, 2020. **11**(2): p. 518-533.
15. Balasubramanian, P., et al., *Adiponectin receptor agonist AdipoRon improves skeletal muscle function in aged mice.* Elife, 2022. **11**.
16. Jortay, J., et al., *Adiponectin and Skeletal Muscle: Pathophysiological Implications in Metabolic Stress.* The American Journal of Pathology, 2012. **181**(1): p. 245-256.
17. Nachit, M., et al., *Myosteatosis rather than sarcopenia associates with non-alcoholic steatohepatitis in non-alcoholic fatty liver disease preclinical models.* J Cachexia Sarcopenia Muscle, 2021. **12**(1): p. 144-158.
18. Nielsen, J., et al., *Lipid droplet size and location in human skeletal muscle fibers are associated with insulin sensitivity.* Am J Physiol Endocrinol Metab, 2017. **313**(6): p. E721-e730.

19. Bergman, B.C. and B.H. Goodpaster, *Exercise and Muscle Lipid Content, Composition, and Localization: Influence on Muscle Insulin Sensitivity.* Diabetes, 2020. **69**(5): p. 848-858.
20. Picca, A., et al., *Fueling Inflamm-Aging through Mitochondrial Dysfunction: Mechanisms and Molecular Targets.* Int J Mol Sci, 2017. **18**(5).
21. Schiaffino, S. and C. Reggiani, *Fiber types in mammalian skeletal muscles.* Physiol Rev, 2011. **91**(4): p. 1447-531.
22. Hancock, C.R., et al., *High-fat diets cause insulin resistance despite an increase in muscle mitochondria.* Proc Natl Acad Sci U S A, 2008. **105**(22): p. 7815-20.
23. Brady, S., et al., *Tubular Aggregates and Cylindrical Spirals Have Distinct Immunohistochemical Signatures.* Journal of Neuropathology & Experimental Neurology, 2016. **75**(12): p. 1171-1178.
24. Bujak, A.L., et al., *AMPK activation of muscle autophagy prevents fasting-induced hypoglycemia and myopathy during aging.* Cell Metab, 2015. **21**(6): p. 883-90.
25. Can, B., et al., *Serum markers of inflammation and oxidative stress in sarcopenia.* Aging Clinical and Experimental Research, 2017. **29**(4): p. 745-752.
26. Arai, Y., K. Kamide, and N. Hirose, *Adipokines and Aging: Findings From Centenarians and the Very Old.* Front Endocrinol (Lausanne), 2019. **10**: p. 142.
27. Aleixo, G.F.P., et al., *Myosteatosis and prognosis in cancer: Systematic review and meta-analysis.* Crit Rev Oncol Hematol, 2020. **145**: p. 102839.
28. Miljkovic, I., et al., *Greater Skeletal Muscle Fat Infiltration Is Associated With Higher All-Cause and Cardiovascular Mortality in Older Men.* J Gerontol A Biol Sci Med Sci, 2015. **70**(9): p. 1133-40.
29. Seibert, J.T., et al., *Muscle Lipid Droplets: Cellular Signaling to Exercise Physiology and Beyond.* Trends Endocrinol Metab, 2020. **31**(12): p. 928-938.
30. Gemmink, A., P. Schrauwen, and M.K.C. Hesselink, *Exercising your fat (metabolism) into shape: a muscle-centred view.* Diabetologia, 2020. **63**(8): p. 1453-1463.
31. Ciapaite, J., et al., *Fiber-type-specific sensitivities and phenotypic adaptations to dietary fat overload differentially impact fast- versus slow-twitch muscle contractile function in C57BL/6J mice.* J Nutr Biochem, 2015. **26**(2): p. 155-64.
32. Andrich, D.E., et al., *Altered Lipid Metabolism Impairs Skeletal Muscle Force in Young Rats Submitted to a Short-Term High-Fat Diet.* Front Physiol, 2018. **9**: p. 1327.
33. Choi, S.J., et al., *Intramyocellular Lipid and Impaired Myofiber Contraction in Normal Weight and Obese Older Adults.* J Gerontol A Biol Sci Med Sci, 2016. **71**(4): p. 557-64.
34. Chistiakov, D.A., et al., *Mitochondrial aging and age-related dysfunction of mitochondria.* Biomed Res Int, 2014. **2014**: p. 238463.
35. Xu, J.W., et al., *Cylindrical Spirals in Skeletal Muscles Originate From the Longitudinal Sarcoplasmic Reticulum.* J Neuropathol Exp Neurol, 2016. **75**(2): p. 148-55.
36. Boncompagni, S., et al., *Long-Term Exercise Reduces Formation of Tubular Aggregates and Promotes Maintenance of Ca(2+) Entry Units in Aged Muscle.* Front Physiol, 2020. **11**: p. 601057.

37. Hansen, M., D.C. Rubinsztein, and D.W. Walker, *Autophagy as a promoter of longevity: insights from model organisms.* Nature Reviews Molecular Cell Biology, 2018. **19**(9): p. 579-593.
38. Huang, D.D., et al., *Nrf2 deficiency promotes the increasing trend of autophagy during aging in skeletal muscle: a potential mechanism for the development of sarcopenia.* Aging (Albany NY), 2020. **12**(7): p. 5977-5991.
39. Liu, Y., et al., *Adiponectin stimulates autophagy and reduces oxidative stress to enhance insulin sensitivity during high-fat diet feeding in mice.* Diabetes, 2015. **64**(1): p. 36-48.
40. Ahlstrom, P., et al., *Adiponectin improves insulin sensitivity via activation of autophagic flux.* J Mol Endocrinol, 2017. **59**(4): p. 339-350.
41. Inoue, A., et al., *Exercise restores muscle stem cell mobilization, regenerative capacity and muscle metabolic alterations via adiponectin/AdipoR1 activation in SAMP10 mice.* J Cachexia Sarcopenia Muscle, 2017. **8**(3): p. 370-385.
42. von Haehling, S., et al., *Ethical guidelines for publishing in the Journal of Cachexia, Sarcopenia and Muscle: update 2019.* J Cachexia Sarcopenia Muscle, 2019. **10**(5): p. 1143-1145.

Supplementary information

SUPPLEMENTARY METHODS

Animals

Male C57BL/6J mice (Janvier Labs, Genest, France) were divided into three groups and studied up to 62 weeks of age (O, old mice): control Normal Diet group (O-ND), High-Fat Diet group (O-HFD) and HFD group treated with AR (O-HFD+AR) (*n* = 9-12 mice/group). The O-ND mice were fed a standard diet (Carfil quality, Oud-Turnhout, Belgium), while the O-HFD and O-HFD+AR mice were fed a diet with a high content of saturated fatty acids (60% kcal from fat) (D12492, Brogaarden, Lynge, Denmark) starting from 8 weeks of age. Throughout the protocol, drinking water was replaced by solidified water for all mice (Solid Drink, Triple A Trading, Tiel, The Netherlands) and renewed daily. In the treated group (O-HFD+AR), AdipoRon (Bio-Techne, Minnesota, USA) was incorporated into the solid drink. Treatment started at 18 weeks of age at a dose of 30 mg/kg/day, which then gradually increased to 50 mg/kg/day at 45th week of age and maintained until the end of the study. A fourth group of young mice under a normal diet (Y-ND) was also used.

Animals were maintained under the same standard-rearing conditions, i.e. constant temperature (22°C) and humidity (40-60%), with a fixed 12h light – 12h dark cycle (lights on from 7 a.m. to 7 p.m.). Each animal body weight and food consumption were closely monitored and measured once a week. *In vivo* functional tests were performed and several blood samples were collected to assess physical capacity and glucose homeostasis, respectively. Blood glucose and insulin levels were sampled after overnight fasting at several time points. Body composition was also measured by micro-CT scan at 59 weeks of age.

Y-mice were euthanized at 12 weeks of age and O-mice were euthanized at 62 weeks of age, as described [1]. Blood samples were collected after sacrifice and stored at -20°C for later analysis. Different skeletal muscles from the upper and lower limbs were collected and weighed, as well as liver, subcutaneous, epididymal and brown adipose tissues. Organs and tissues were either directly processed and studied in some experiments, while others were stored at -80°C for subsequent analysis.

In vivo functional testing

Mice were subjected to a *Treadmill Exhaustion Test* to assess their endurance and their resistance to fatigue. In this test, mice ran to exhaustion on a treadmill. An electric grid, placed at the back of the treadmill, delivered small electric shocks of a constant intensity (0.2 mA) to motivate the mice to run. The day before testing, mice were trained to run for 10 minutes at a speed of 3 m/min, which then gradually increased to reach a speed of 12 m/min. A first Treadmill Exhaustion Test was performed at 32 weeks of age in old mice and at 10 weeks of age in Y-ND ones, where mice ran on a treadmill with a 10° upward incline. The initial speed was set at 5m/min for the first 5 minutes and 10 m/min for the next 5 minutes. The speed was then increased by 1.8 m/min every 3 minutes until exhaustion. A second testing was later performed at 56 weeks of age in old mice and at 11 weeks of age in Y-ND, where mice ran on a treadmill inclined at 5°, with a speed fixed at 13,2 m/min after a three minutes warm-up. The maximum time period for this second test was set at 90 minutes.

After each test, the work (W, kg.m) performed by each animal was used to adjust the vertical distance covered (d, meters) to the body weight (BW, kg). It was

thus calculated using the following formula: W (kg.m) = BW (kg) x d (m) x sin (sinus of the treadmill inclination angle, °) [2].

Micro-computed tomography

At 59 weeks of age, micro-CT was performed on mice anaesthetized with isoflurane to monitor changes in body composition, skeletal muscle, and liver fatty infiltration. Data of Y-ND mice were obtained at 20 weeks of age in C57BL/6J mice from another cohort (J. Gillard and I. Leclercq). Scanning and analysis of reconstructed images were performed as previously described by Nachit *et al.*[3]. Muscle density (Hounsfield units, HU) and surface (mm^2) were measured in the dorsal muscle, i.e. erector *spinae/quadratus lumborum* and psoas muscles, at L4 and L5. Virtual liver biopsy was performed by placing a 3D cylindrical region of interest (±1.3 cm^3) in the liver avoiding large vessels, and the mean density (HU) of the entire volume was automatically computed. In each animal, dorsal muscle and liver density were normalized to spleen density (an internal invariant control). The muscle-to-spleen ratio and the liver-to-spleen ratio are referred to as the muscle and the liver density, respectively.

Quantification of metabolic circulating parameters

Blood glucose was measured using a glucometer (Freestyle Precision Neo, Abbott, Wavre, Belgium). Plasma insulin (Crystal Chem, Illinois, USA) and adiponectin levels were quantified by ELISA (Abcam, Amsterdam, Netherlands). The insulin resistance index was calculated as Insulin (ng/mL) × Glycemia (mg/dL)[4]. Plasma cholesterol, triglycerides and NEFAS were measured by commercial kits (all three from Diasys, Connecticut, USA). Kits were based on colorimetric methods and were used following the manufacturers' instructions.

Bright-field histochemistry and morphometry

Liver samples were fixed in 10% formalin for 24 h and then embedded in paraffin. Sections of 5 µm were stained with hematoxylin (Labconsult, Brussels, Belgium) and eosin (Sigma-Aldrich, Overijse, Belgium) (HE) and used for histological evaluation of the liver and NAFLD activity score (NAS), blindly assessed as per Kleiner *et al*., 2005 [5]. Non-alcoholic steatohepatitis diagnosis was defined according to the SAF algorithm; thus, samples with NAS ≥ 3 with at least 1 point in each sub-score (i.e. steatosis, inflammation, and ballooning) were considered as NASH while those with at least 1 point in steatosis were considered as NAFL [6].

Rectus femoris from quadriceps muscles were embedded in optimal cutting temperature compound (Gentaur, Kampenhout, Belgium) and frozen in isopentane chilled with liquid nitrogen (VWR International, Leuven, Belgium). 10 µm transversal cryosections were stained with HE. In addition, Gomori Trichrome (Kyvobio, Evere, Belgium) staining was used to quantify tubular aggregates and cylindrical spirals. Finally, COX and SDH staining were performed to evaluate mitochondrial respiratory function as previously described [7]. For each staining, all slides were processed simultaneously. Whole muscle sections were scanned using a slide scanner (SCN400, Leica Biosystems, Machelen, Belgium), and quantification was made using Fiji/ImageJ software (NIH, Maryland, USA) [8]. For analysis of COX and SDH, the images were converted to grayscale (8-bit, 0-255). By setting 3 different thresholds, the percentage of muscle area covered by 3 different intensities of staining (pale, intermediate or dark) was quantified in intracellular regions. To quantify tubular aggregates and cylindrical spirals in the rectus femoris, the percentage of cross-sectional area covered with bright red abnormal Gomori Trichrome inclusions was calculated using FIJI/ImageJ software.

(Immuno)fluorescence

Cryosections of soleus and EDL muscles were obtained as described above, and the staining for fiber typing and LDs quantification with Bodipy was performed on serial transverse sections immediately after cutting.

Fiber type

Muscle sections were immunolabeled for the different myosin heavy chains (MyHCs), as described [9]. Briefly, mouse primary antibodies were directed against MyHC-1 (IgG2b, BA-D5), MyHC-2a (IgG1, SC-71), MyHC-2x (IgM, 6H1) (Developmental Studies Hybridoma Bank, University of Iowa, IA) and rat primary antibody against laminin α-2 chain (Sigma-Aldrich) (1:10, 1:10, 1:5, 1:1000, respectively). The corresponding secondary antibodies used were: goat anti-mouse IgG2b Alexa Fluor (AF) 405 (1:500, Sigma-Aldrich), goat anti-mouse IgG1 AF488 (1:500, Thermo Fisher Scientific, Merelbeke, Belgium), goat anti-mouse IgM AF568 (1:1000, Abcam) and goat anti-rat AF647 (1:500, Thermo Fisher Scientific), respectively. Images were captured using an epifluorescence microscope (Axio Imager Z1/ApoTome1, Zeiss, Zaventem). Excitation filters for DAPI (405 nm), FITC, TRITC, and Cy5 were selected to detect type 1, 2a, 2x fibers, and laminin, respectively. Type 2b fibers were recognized as unlabeled fibers (black sarcoplasm surrounded by laminin). Analysis of the fiber type of each muscle was performed using the Cell Counter tool of Fiji/ImageJ software. Results are presented as the % of fibers of each type, out of the total number of fibers in the muscle section. Myofibers morphometry (cross-sectional area and minimum Feret's diameter) were calculated from laminin staining.

Lipid droplet (LD) quantification

Muscle sections were immunolabeled for laminin as explained above. The slides were also stained with Bodipy-558/568 C12 (1 µg/mL, Thermo Fisher

Scientific) to identify LD [9]. Images were captured using confocal microscope with a 40x/1.4 NA oil immersion objective. Bodipy and laminin were excited using a 561 nm and a 640 nm diode laser line, respectively. Analysis of LDs was performed in a fiber type-dependent manner by using a customized macro developed internally using Fiji/ImageJ. Briefly, myofiber area and minimum Feret diameter were calculated based on laminin labeling. After applying a fixed detection threshold, the Fiji's "analyze particles" tool was used to quantify the percentage of area covered by the signal above the threshold and the average particle size. To distinguish between peripheral or central LDs, the peripheral region was identified as a ring beneath the cell border whose thickness (in µm) was 1/6 of the minimum Feret diameter and the central region as the remainder of the cell [10]. For each fiber type and for each muscle sample, between 10 and 15 fibers were analyzed.

Mitochondria quantification

For each animal, a third serial cryosection of the soleus and EDL was incubated with a rabbit anti-TOMM20 primary antibody (1:1000, Abcam) followed by a goat anti-rabbit secondary antibody AF488 (1:300, Thermo Fisher Scientific). Images were captured using confocal microscope with a 20x/0.8 NA objective. TOMM20-AF488 labeled mitochondria were excited using a 488 nm diode laser line. Quantification of the percentage of myofiber surface covered with TOMM20-labeled mitochondria was performed in a fiber-type-dependent manner applying a fixed threshold and with the Fiji/ImageJ "analyze particles" tool. As for LD quantification, the center and the periphery of the fiber were studied separately. For each fiber type and for each muscle sample, at least 20 fibers were analyzed.

LD and mitochondria co-labeling

Cryosections (soleus) were co-labeled for LD, mitochondria, laminin, and nuclei using Bodipy, anti-TOMM20 and anti-laminin antibodies, and 4',6-diamidino-

2-phenylindole (DAPI, 0.5 µg/mL, Thermo Fisher Scientific), respectively. The staining protocol followed was similar to those described above and images were acquired with the same confocal microscope.

Transmission electron microscopy

For electron microscope analysis, a piece of the rectus femoris muscle was cut and fixed for 2 h in a solution of 2.5% glutaraldehyde in 0.1 M cacodylate buffer (pH 7.4). Samples were post-fixed for 1 h at 4°C in 1% osmium tetroxide and then incubated with 2% uranyl acetate for 2 h at RT. Muscles were embedded in resin (Araldite) and transverse and longitudinal ultrathin sections were cut (70 nm thick) with an ultramicrotome (UC7, Leica Biosystems) and mounted on copper grids to be visualized with the MET LIBRA 120 (Zeiss).

RNA extraction and real-time quantitative PCR (RT-qPCR)

RNA was isolated from mouse skeletal muscles with TriPure reagent (Sigma-Aldrich). 0.5 µg of total RNA were reverse transcribed, and 40 ng total RNA equivalents were amplified using an iCycler iQ real-time PCR detection system (Bio-Rad Laboratories, Nazareth, Belgium) as described [1]. RT-qPCR primers for mouse cyclophilin were used as reported [11]. New mouse primer sequences were designed for acyl-CoA dehydrogenase medium chain (*Acadm*, forward, 5'-ACTGCCCGCAAGTTTGCCAGA-3'; reverse, 5'-TGTGCGCGTTGATCAAGCCGA-3'), acyl-CoA oxidase 1 (*Acox1*, forward, 5'-TCTTCTTGAGACAGGGCCCA-3'; reverse, 5'-GTTCCGACTAGCCAGGCATG-3'), uncoupling protein 3 (*Ucp3*, forward, 5'-CTTGGCTAGACGCACAGCTTC-3'; reverse, 5'-AATGGGCCTGGTTCCTTTGC-3'), nuclear respiratory factor 1 (*Nrf1*, forward, 5'-ACAGATAGTCCTGTCTGGGGAAA-3'; reverse, 5'-TGGTACATGCTCACAGGGATCT-3'), and mitochondrial transcription factor A (*Tfam*, forward, 5'-AGGCACCGTATTGCGTGAGA-3'; reverse, 5'-AGACAAGACTGATAGACGAGGGG-3'). The threshold cycles (Ct) were measured in

separate tubes and in duplicate. The identity and purity of the amplified product were checked by electrophoresis on agarose minigels, and analysis of the melting curve was carried out at the end of the amplification. To ensure the quality of the measurements, each plate included a negative control for each set of primers.

Protein extraction, ELISA, and Western Blot

Gastrocnemius muscle samples were homogenized in a lysis buffer supplemented with 1% protease/phosphatase inhibitor cocktail (both from Cell Signaling Technology, BIOKE, Leiden, The Netherlands) and 10 mM NaF (Merck Life Science, Overijse, Belgium). Proteins were quantified using the Bradford method and were stored at -80°C. 25-150 µg of total protein extracts were used for each analysis. Three ELISA assays were used to specifically detect and quantify the active phosphorylated form of AMP-activated protein kinase alpha (P-AMPK), the active phosphorylated form of the p65 subunit of nuclear factor kappa B (NF-κB) (P-p65) and the active phosphorylated form (Ser555) of UNC-51 like kinase 1 (ULK1) (all from Cell Signaling Technology). Another ELISA kit was also used to detect PGC-1α (MyBioSource, Vancouver, Canada). Kits were based on colorimetric methods and were carried out following manufacturer's instructions. Immunoblotting was performed as reported [12] by using rabbit monoclonal antibodies directed against the ubiquitin-binding protein p62 and LC3A-I/II (both from Cell signalling Technology), both markers of autophagy. Signals were revealed by enhanced chemiluminescence, then quantified and normalized to those of Ponceau stain [13] using ImageJ.

Other biochemical analysis

Lipids were extracted from 50 mg of liver and from 100 mg of dorsal muscle using methanol and chloroform, and total lipids were quantitated using the

vanillin–phosphoric acid reaction. Results were normalized on weighted liver/dorsal muscle [14].

Statistical analysis

Results are means ± SEM for the indicated number of mice. Comparisons between the three groups of old mice (O-ND, O-HFD, and O-HFD+AR) were carried out by one-way ANOVA followed by Tukey's test. A mixed effects model for repeated measures was used to compare the 3 groups over time (Prism 9; Graphpad Software, San Diego, CA). Comparisons between Y-ND and O-ND were assessed by two-tailed unpaired Student's *t*-test (Prism 9). Differences were considered statistically significant at $P < 0.05$. Yet, we mentioned *P* values of ANOVA post-test, which were slightly larger than 0.05 (in this case, unpaired Student's *t*-test between the two implicated groups was always below this threshold), when it seems to be relevant into the physiological context.

REFERENCES RELATED TO METHODS

1. Abou-Samra, M., et al., *AdipoRon, a new therapeutic prospect for Duchenne muscular dystrophy.* J Cachexia Sarcopenia Muscle, 2020. **11**(2): p. 518-533.
2. Avila, J.J., S.K. Kim, and M.P. Massett, *Differences in Exercise Capacity and Responses to Training in 24 Inbred Mouse Strains.* Front Physiol, 2017. **8**: p. 974.
3. Nachit, M., et al., *Myosteatosis rather than sarcopenia associates with non-alcoholic steatohepatitis in non-alcoholic fatty liver disease preclinical models.* J Cachexia Sarcopenia Muscle, 2021. 12(1): p. 144-158.
4. Jortay, J., et al., *Adiponectin and Skeletal Muscle: Pathophysiological Implications in Metabolic Stress.* The American Journal of Pathology, 2012. 181(1): p. 245-256.
5. Kleiner, D.E., et al., *Design and validation of a histological scoring system for nonalcoholic fatty liver disease.* Hepatology, 2005. 41(6): p. 1313-21.
6. Bedossa, P., et al., *Histopathological algorithm and scoring system for evaluation of liver lesions in morbidly obese patients.* Hepatology, 2012. 56(5): p. 1751-9.
7. Ross, J.M., *Visualization of mitochondrial respiratory function using cytochrome c oxidase/succinate dehydrogenase (COX/SDH) double-labeling histochemistry.* J Vis Exp, 2011(57): p. e3266.
8. Schindelin, J., et al., *Fiji: an open-source platform for biological-image analysis.* Nature Methods, 2012. 9(7): p. 676-682.
9. Selvais, C.M., et al., *Fiber Type and Subcellular-Specific Analysis of Lipid Droplet Content in Skeletal Muscle.* J Vis Exp, 2022(184).
10. Strauss, J.A., et al., *Divergence exists in the subcellular distribution of intramuscular triglyceride in human skeletal muscle dependent on the choice of lipid dye.* Histochemistry and Cell Biology, 2020. **154**(4): p. 369-382.
11. Abou-Samra, M., et al., *Potential Therapeutic Action of Adiponectin in Duchenne Muscular Dystrophy.* Am J Pathol, 2017. **187**(7): p. 1577-1585.
12. Abou-Samra, M., et al., *Involvement of adiponectin in the pathogenesis of dystrophinopathy.* Skelet Muscle, 2015. **5**: p. 25.
13. Sander, H., et al., *Ponceau S waste: Ponceau S staining for total protein normalization.* Anal Biochem, 2019. **575**: p. 44-53.
14. Bligh, E.G. and W.J. Dyer, *A rapid method of total lipid extraction and purification.* Can J Biochem Physiol, 1959. **37**(8): p. 911-7.

Table S1. Additional circulating parameters and organ weights in the four groups of mice at the end of the study.

	Y-ND	O-ND	O-HFD	O-HFD+AR
Circulating parameters				
Cholesterol (g/l)	0.8 ± 0.02	0.8 ± 0.05	1.9 ± 0.15 ****	1.5 ± 0.09 $^{****/\#}$
Triglycerides (g/l)	1.0 ± 0.12	0.8 ± 0.05	0.9 ± 0.07	0.8 ± 0.05
NEFAs (mg/dl)	29.5 ± 2.9	43.0 ± 3.0 $^{\$}$	38.9 ± 3.8	41.3 ± 4.2
ApN (µg/ml)	3.3 ± 0.3	2.7 ± 0.1 *	2.7 ± 0.1	2.9 ± 0.2
ApN (µg/ml)/fat mass (g)	7.9 ± 0.4	2.8 ± 0.3 $^{\$\$\$\$}$	0.6 ± 0.1 ***	0.7 ± 0.1 ***
Body weight (g)	26.3 ± 0.7	32.6 ± 0.9 $^{\$\$\$}$	59.4 ± 2.4 ****	51.5 ± 1.9 $^{****/\#}$
Adipose tissue weight (g)				
Subcutaneous	0.22 ± 0.01	0.45 ± 0.06 $^{\$\$}$	3.8 ± 0.41 ***	2.69 ± 0.21 $^{****/\sim}$
Epididymal	0.20 ± 0.02	0.70 ± 0.06 $^{\$\$\$\$}$	1.59 ± 0.25 *	1.71 ± 0.19 **
Brown	0.06 ± 0.004	0.13 ± 0.01 $^{\$\$\$}$	0.25 ± 0.03 *	0.27 ± 0.04 **
Liver weight (g)	1.30 ± 0.05	1.49 ± 0.06 $^{\$}$	3.40 ± 0.33 **	2.71 ± 0.23 **
Skeletal muscle weight (mg)				
Soleus	19 ± 1	19 ± 1	22 ± 1 ^{x}	21 ± 1 *
EDL	11 ± 1	16 ± 2 $^{\$}$	16 ± 1	15 ± 1
Tibialis anterior	103 ± 2	99 ± 3	103 ± 4	104 ± 2
Gastrocnemius	311 ± 13	312 ± 7	327 ± 10	327 ± 6
Quadriceps	405 ± 11	401 ± 13	422 ± 13	397 ± 15
Biceps	33 ± 1	34 ± 1	38 ± 2	36 ± 1
Triceps	240 ± 9	258 ± 9	268 ± 8	263 ± 8

Circulating parameters were collected in fasted mice at the end of the study (at the age of 12 weeks for Y-ND and 62 weeks for the other 3 groups). ApN values per fat mass correspond to ApN values normalized for white fat mass (sum of subcutaneous and epididymal fat). Organ weights for adipose tissue or muscles refer to pairs of fat pads or skeletal muscles. NEFA, non-esterified fatty acids. Data are means ± SEM for 6 Y-ND, and 8-10 mice in the other 3 groups. Statistical analysis was performed using one-way ANOVA followed by Tukey's test to compare the 3 groups of O-mice. Comparisons between Y-ND and O-ND were carried out using unpaired two-tailed *t*-test. $^{\$}P < 0.05$, $^{\$\$}P < 0.01$, $^{\$\$\$}P < 0.001$, $^{\$\$\$\$}P < 0.0001$ vs. Y-ND mice. $^{x}P = 0.06$, $^{*}P < 0.05$, $^{**}P < 0.01$, $^{***}P < 0.001$, $^{****}P < 0.0001$ vs. O-ND mice. $^{\sim}P = 0.09$, $^{\#}P < 0.05$ vs. O-HFD mice.

SUPPLEMENTARY FIGURES

Fig. S1

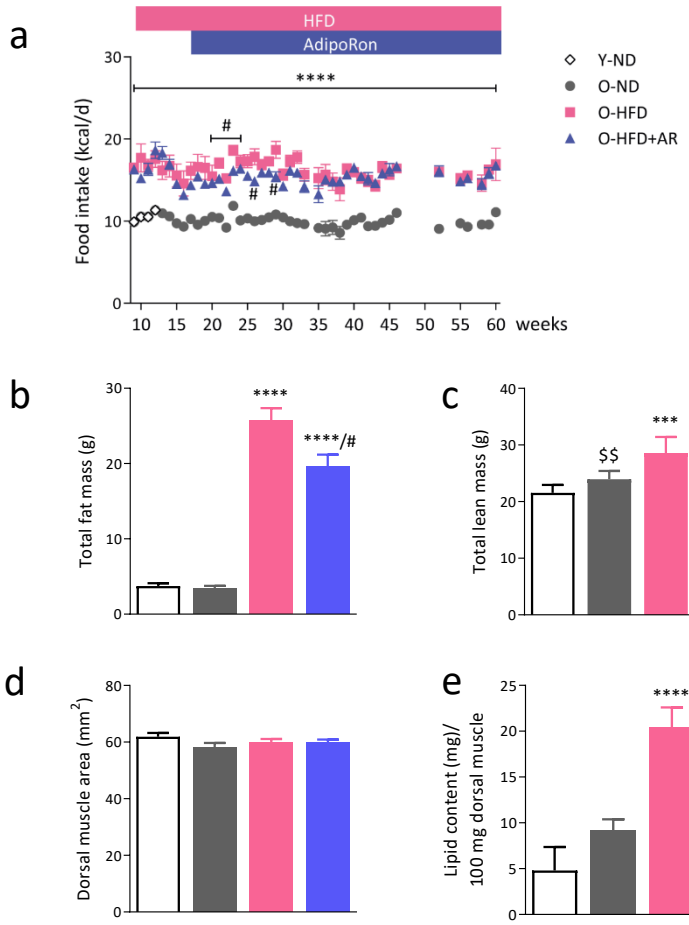

Figure S1. Effects of AdipoRon on food intake, CT scan parameters, and dorsal muscle lipid content in obese middle-aged mice. (a) Daily food intake measured throughout the study except when behavioral tests were performed (47-51 weeks) in the 4 groups of mice. **(b)** Total fat mass, **(c)** lean mass (muscles and organs) and **(d)** dorsal muscle area quantified by micro-CT scan**. (e)** Lipid content in dorsal muscle (biochemical measure). Data are means ± SEM for 6 Y-ND, and 9-10 mice in the other 3 groups. Statistical analysis was performed using a mixed-effects analysis (a) or one-way ANOVA followed by Tukey's test to compare the 3 groups of O mice (**b-e**). Comparisons between Y-ND and O-ND **(b-e)** were carried out using unpaired two-tailed *t*-test. $^{\$\$}P < 0.01$ vs. Y-ND mice. $^{*}P < 0.05$, $^{***}P < 0.001$, $^{****}P < 0.0001$ vs. O-ND mice. $^{\#}P < 0.05$ vs. O-HFD mice.

Fig. S2

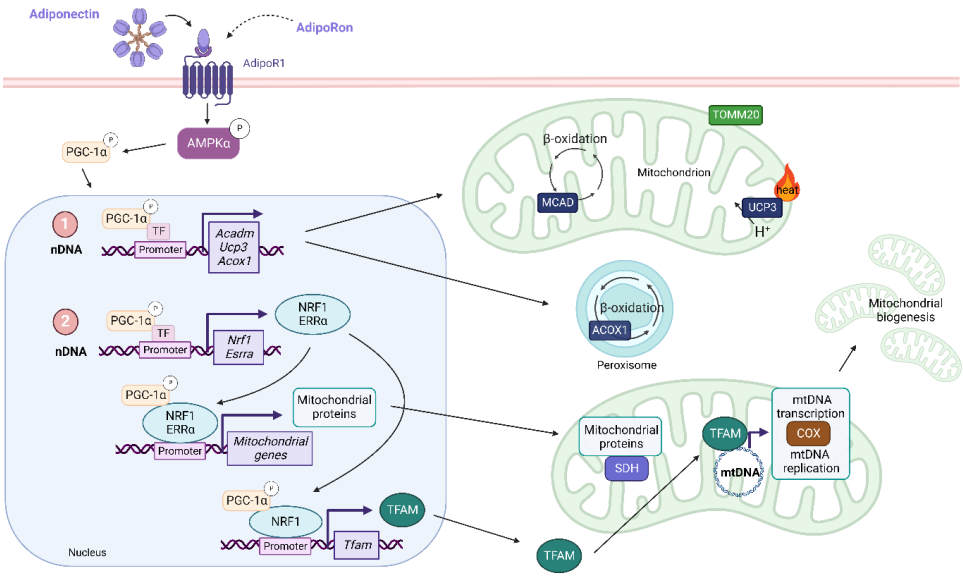

Figure S2. Proposed model for the effects of AdipoRon. Briefly, AdipoRon binds to AdipoR1 and activates the AMPK-PGC-1α axis therefore increasing the activity of several transcription factors involved in fatty acid oxidation (1) and mitochondrial biogenesis and function (2). (1) Medium-chain acyl-CoA dehydrogenase (*Acadm*, MCAD) is involved in mitochondrial FAO and uncoupling protein 3 (*Ucp3*, UCP3) in energy dissipation. Acyl-CoA oxidase 1 (*Acox1,* ACOX1) is implicated in peroxisomal fatty acid oxidation [1]. (2) Nuclear respiratory factor-1 (*Nrf1*, NRF-1) and estrogen-related receptor α (*Esrra*, ERRα) are two main transcription factors involved in mitochondrial biogenesis and function. They upregulate the expression of nuclear genes encoding mitochondrial proteins, including succinate dehydrogenase (SDH). NRF1 also increases the expression of mitochondrial transcription factor A (*Tfam*, TFAM), which binds to mitochondrial DNA (mtDNA) and activates transcription and replication of the mitochondrial genome [2]. Some catalytic subunits of cytochrome c oxidase (COX) are encoded by mtDNA. TOMM20 is a mitochondrial outer membrane translocase. Created with BioRender.com.

Fig. S3

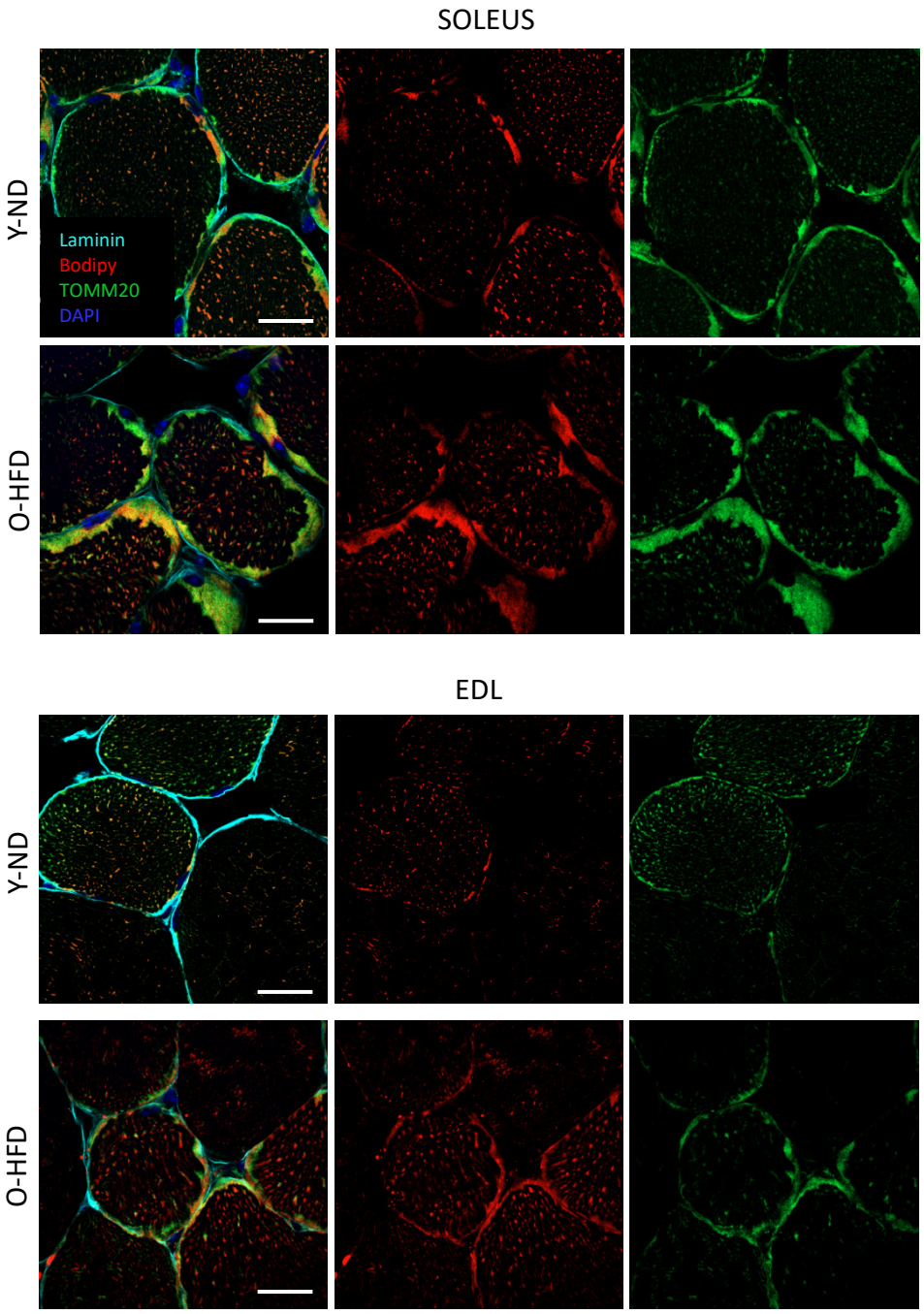

Figure S3. Illustrative comparison of mitochondria and lipid droplets in the soleus and EDL of Y-ND and O-HFD mice at high magnification. Confocal fluorescence micrographs of soleus and EDL from a Y-ND mouse and O-HFD mouse. LDs were stained with Bodipy in red, mitochondria with anti-TOMM20 in green, the edge of the fiber with anti-laminin in cyan and nuclei with DAPI in blue. Scale bar = 20 µm.

Fig. S4

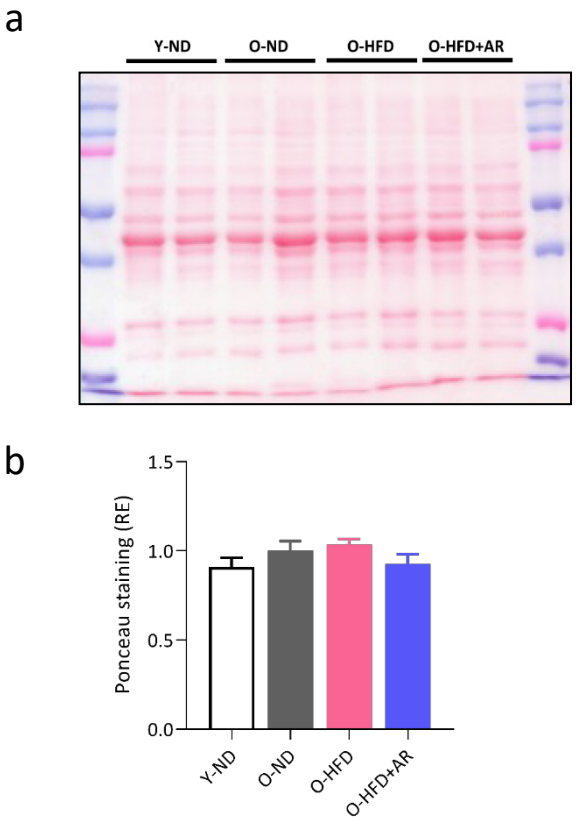

Figure S4. Representative Ponceau staining of Western blots shown in Figure 8d. (a) The full ponceau-staining membrane from Western blotting with Y-ND, O-ND, O-HFD, O-HFD+AR (two animals for each condition but representative for all the animals studied) . **(b)** Quantification of ponceau-staining expressed as relative expression compared to O-ND for 6-10 mice/group. RE: relative expression.

Fig. S5

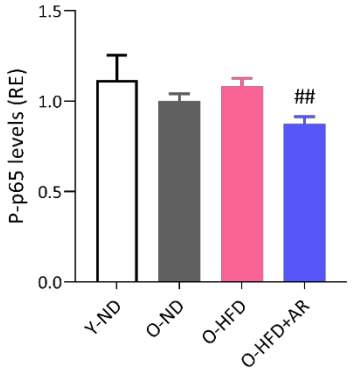

Figure S5. Effect of AdipoRon treatment on NF-κB activity. The active phosphorylated form of the p65 subunit of NF-κB (P-p65) was quantified by ELISA assay and absorbance data were presented as relative expression compared with O-ND values. Data are means ± SEM for 6 Y-ND, and 8-10 mice in the other 3 groups. Statistical analysis was performed using one-way ANOVA followed by Tukey's test (comparing 3 groups of O-mice) or by unpaired two-tailed *t*-test (Y-ND *vs.* O-ND). $^{\#\#}P < 0.01$ vs. O-HFD mice.

REFERENCES RELATED TO SUPPLEMENTARY FIGURE S2

1. Abou-Samra, M., et al., *Adiponectin and Its Mimics on Skeletal Muscle: Insulin Sensitizers, Fat Burners, Exercise Mimickers, Muscling Pills … or Everything Together?* Int J Mol Sci, 2020. **21**(7).
2. Picca, A., et al., *Fueling Inflamm-Aging through Mitochondrial Dysfunction: Mechanisms and Molecular Targets.* Int J Mol Sci, 2017. **18**(5).

STUDY 2

Thwarting Sarcopenia: Exploring AdipoRon in aging skeletal muscle as a healthspan-Extending Shield

Camille M. Selvais[1*], Maria A. Davis-López de Carrizosa[1,2†], Romain Versele[1†], Nicolas Dubuisson[1], Laurence Noel[1], Sonia M. Brichard[1] and Michel Abou-Samra[1].

[1] Endocrinology, Diabetes and Nutrition Unit, Institute of Experimental and Clinical Research, UCLouvain, Brussels, Belgium;

[2] Departamento de Fisiología, Facultad de Biología, Universidad de Sevilla, Seville, Spain.

†These authors have contributed equally to this work

***Corresponding author:**

Camille Selvais
E-mail: camille.selvais@uclouvain.be
Tel: 32-2-7649576

ABSTRACT

Sarcopenia is characterized by loss of muscle mass, quality and function, and is associated with adverse outcomes in aging. Recently, we demonstrated that long-term treatment with AdipoRon, an adiponectin receptor agonist, strikingly alleviated myosteatosis and muscle degenerative markers in middle-aged obese mice. Expanding on this, we aimed to ascertain if a shorter treatment with AdipoRon could effectively offset sarcopenia in older mice. We observed that AdipoRon remarkably inversed the loss of muscle mass by restoring the sarcopenia index and fiber count that were greatly diminished with age. Additionally, AdipoRon successfully saved muscle quality by halving the accumulation of tubular aggregates, which are age-related abnormal structures, and aberrant mitochondria. This action was mainly mediated by AMPK pathway and activation of autophagy. Futhermore, AdipoRon bolstered muscle function by rescuing mitochondrial activity and improving exercise endurance. Finally, AdipoRon markedly curbed muscle fibrosis and mitigated local/systemic inflammation. Conclusively, AdipoRon counteracts sarcopenia and various hallmarks of aging, thereby opening new therapeutic perspective to extend healthspan.

INTRODUCTION

The 30-year increase in life expectancy at birth over the last 100 years is one of humanity's greatest achievements. Efforts are now focused on addressing aging-related diseases in order to both extend and improve the healthspan [1]. Sarcopenia occurs commonly as an age-related process. It is a generalized skeletal muscle disorder characterized by the accelerated loss of muscle mass, quality and function. Sarcopenia is associated with adverse outcomes such as falls, frailty, institutionalization and mortality. Physical activity is currently the first therapeutic strategy to prevent sarcopenia but is not always feasible, and no specific drugs against it have been approved yet [2]. Preventive/therapeutic pharmacological approaches are therefore needed.

Adiponectin (ApN) is a hormone primarily secreted by adipocytes, exerting insulin-sensitizing, fat-burning and anti-inflammatory effects in various tissues, including the skeletal muscle. AdipoR1 and AdipoR2 are the major ApN receptors *in vivo*. AdipoR1 is the main receptor in skeletal muscle, while AdipoR2 is predominantly found in the liver [3]. With regard to skeletal muscle, we have previously shown that ApN exerts powerful protective effects in mdx mice, a model with a severe muscle disease (Duchenne Muscular Dystrophy). Indeed, ApN reduces muscle inflammation and oxidative stress, and enhances the myogenic program, thereby decreasing muscle damage while increasing force/endurance. This protection is mainly mediated through the AdipoR1-AMP-activated protein kinase (AMPK)-peroxisome proliferator-activated receptor coactivator-1α (PGC-1α) pathway [3, 4]. Importantly, ApN overexpression in transgenic mice prolongs lifespan and healthspan [5, 6], whereas ApN deficiency in knockout mice shortens them [6]. Thus, these results support a role of ApN as potent protector of skeletal muscle and an essential regulator of healthspan and lifespan.

ApN has a complex three-dimensional structure and thereby is difficult to produce and to administrate. In fact, it must be injected to produce its effects [3]. The development of novel molecules that mimic the beneficial effects of ApN and may easily be administered is therefore relevant. AdipoRon is an orally active synthetic agonist of ApN receptors, which, based on data in animal models, has been proposed for the treatment of type 2 diabetes and other obesity-related disorders [7-9]. Relevant for translational applications, AdipoRon remains efficient in AdipoR1-humanized mice [10]. We have demonstrated that, like ApN, AdipoRon protects the skeletal muscle of mdx mice [11]. So far, its potential beneficial properties on aging muscle have been scarcely addressed. We have recently shown that long-term AdipoRon treatment (1yr) enhanced endurance in middle-aged obese mice, and strikingly alleviated myosteatosis and muscle degenerative markers, thereby promoting healthy aging [12]. Short-term (6 wks) i.v. administration of AdipoRon has also been tested in older and non-obese mice. This treatment has been reported to enhance muscle function, together with a very slight increase in mitochondrial function. Yet, it was not established whether these old mice were actually sarcopenic (lack of young control group) and there was no conclusive evidence that AdipoRon reversed a potential loss of muscle mass (no muscle weight provided, decreased size for almost all fiber types) [13]. Therefore, studies unambiguously demonstrating a positive effect of AdipoRon on sarcopenia are warranted.

The aim of this work was thus to investigate whether AdipoRon treatment could actually reverse sarcopenia and hallmarks of aging in older mice. To this end, old mice were treated orally with AdipoRon for 3 months and their muscle mass, quality and function were characterized in detail, together with circulating pro-

inflammatory parameters. The mechanisms underlying AdipoRon protection were further explored, thereby significantly extending the scope of studies carried out to date [12, 13].

MATERIAL AND METHODS

Animals

18-month-old male C57BL/6J mice were obtained from The Jackson Laboratory (Bar Harbor, USA). From 20 months of age, mice were divided into two groups and studied until 23 months of age: a control group left untreated (O, old mice, *n*=10) and another group treated with AdipoRon (O-AR, *n*=9). During the study, 3 mice from the untreated O group developed large intra-abdominal tumors, while this was the case for only one in the treated O-AR group. All these mice were excluded from data analysis. Mice were fed a standard diet (Carfil quality, Oud-Turnhout, Belgium). Throughout the protocol, drinking water was replaced by solidified water for all mice (Solid Drink, Triple A Trading, Tiel, The Netherlands) and renewed daily. In the treated group (O-AR), AdipoRon (Bio-Techne, Minnesota, USA) was incorporated into the solid drink at a dose of 50 mg/kg/day for a total duration of 3 months. A third group of 3-month-old mice (Y, young mice) was also used.

Animals were maintained under the same standard-rearing conditions, i.e. constant temperature (22°C) and humidity (40-60%), with a fixed 12h light – 12h dark cycle (lights on from 7 a.m. to 7 p.m.). Each animal body weight and food consumption were closely monitored and measured once a week. Fasting blood glucose was measured at 22 months of age, and a functional treadmill test was performed at 22.5 months.

Y-mice were euthanized at 3 months of age and O-mice were euthanized at 23 months of age, as described [4]. Blood samples were collected after sacrifice and stored at -20°C for later analysis. Different skeletal muscles from the upper and lower limbs were collected and weighed, as well as liver, heart, subcutaneous, epididymal, brown adipose tissues and tibia. Tibia length was measured using a

caliper. Organs and tissues were either directly processed and studied in some experiments, or were stored at -80°C for subsequent analysis. Electron microscopy and immunofluorescence analyses were performed on 3 and 6 mice/group, respectively.

In vivo functional testing

Mice were subjected to a *Treadmill Exhaustion Test* to assess their endurance and their resistance to fatigue. In this test, mice ran to exhaustion on a treadmill. An electric grid, placed at the back of the treadmill, delivered small electric shocks of a constant intensity (0.2 mA) to motivate the mice to run. The day before testing, mice were trained to run for 10 minutes at a speed of 3 m/min, which then gradually increased to reach a speed of 12 m/min. Treadmill Exhaustion Test was performed at 22.5 months of age in old mice and at 10 weeks of age in Y ones, where mice ran on a treadmill with a 5° upward incline. The initial speed was set at 5m/min for the first 5 minutes and 10 m/min for the next 5 minutes. The speed was then progressively increased by 1.2 m/min to reach a maximum speed of 22.8 m/min. The maximum distance was set at 1200 m.

Quantification of circulating parameters

Blood glucose was measured using a glucometer (Freestyle Precision Neo, Abbott, Wavre, Belgium). Adiponectin levels were quantified by ELISA (Abcam, Amsterdam, Netherlands). Plasma cholesterol, triglycerides and NEFAS were measured by commercial kits (all three from Diasys, Connecticut, USA). These kits were based on colorimetric methods and were used following the manufacturers' instructions. Multiplex assays were also designed to measure plasma concentrations of TNF-α, MCP-1, IFN-ϒ, IL-6, IL-10, MIP-1α, MIP-1β, MIP-2, FGF21, eotaxin, GM-CSF, IL-2, IL-15, IL-1β and MIP-3α (Meso Scale Discovery, Rockville, USA).

Bright-field histochemistry and morphometry

Tibialis anterior muscles were embedded in optimal cutting temperature compound (Gentaur, Kampenhout, Belgium) and frozen in isopentane chilled with liquid nitrogen (VWR International, Leuven, Belgium). 10 µm transversal cryosections were stained with Hematoxylin-Eosin. In addition, Gomori Trichrome (Kyvobio, Evere, Belgium) and Picrosirius red (Abcam, Cambridge, UK) staining were used to quantify tubular aggregates and fibrosis, respectively. Finally, COX staining was performed to evaluate mitochondrial respiratory function as previously described [14]. For each staining, all slides were processed simultaneously. Whole muscle sections were scanned using a slide scanner (Pannoramic Scan II 3DHISTECH, Budapest, Hungary), and quantification was made using Fiji/ImageJ software (NIH, Maryland, USA) [15]. To quantify tubular aggregates, the percentage of cross-sectional area covered with bright pink abnormal Gomori Trichrome inclusions was calculated. Fibrotic tissue was quantified after setting a colour threshold and data obtained were expressed as the percentage of total section area. For analysis of COX, the images were converted to grayscale (8-bit, 0-255). By setting 3 different thresholds, the percentage of muscle area covered by 3 different intensities of staining (pale, intermediate or dark) was quantified in intracellular regions.

(Immuno)fluorescence

Cryosections of *tibialis anterior* were obtained as described above.

Fiber type

Muscle sections were immunolabeled for the different myosin heavy chains (MyHCs), as described [16]. Briefly, mouse primary antibodies were directed against MyHC-1 (IgG2b, BA-D5), MyHC-2a (IgG1, SC-71), MyHC-2x (IgM, 6H1)

(Developmental Studies Hybridoma Bank, University of Iowa, IA) and rat primary antibody against laminin α-2 chain (Sigma-Aldrich) (1:10, 1:10, 1:5, 1:1000, respectively). The corresponding secondary antibodies used were: goat anti-mouse IgG2b Alexa Fluor (AF) 405 (1:500, Sigma-Aldrich), goat anti-mouse IgG1 AF488 (1:500, Thermo Fisher Scientific, Merelbeke, Belgium), goat anti-mouse IgM AF568 (1:1000, Abcam) and goat anti-rat AF647 (1:500, Thermo Fisher Scientific), respectively. Images were captured using an epifluorescence microscope (Axio Imager Z1/ApoTome1, Zeiss, Zaventem). Excitation filters for DAPI (405 nm), FITC, TRITC, and Cy5 were selected to detect type 1, 2a, 2x fibers, and laminin, respectively. Type 2b fibers were recognized as unlabeled fibers (black sarcoplasm surrounded by laminin). Analysis of the fiber number and type was performed using the Fiji/ImageJ software. Results are presented as the total number of fibers over an entire cross-section and the number of fibers of each type. Minimum Feret's diameter was calculated from laminin staining.

Transmission electron microscopy

Electron microscopy analysis was conducted on the *gastrocnemius* muscles of 3 mice per group. This number of mice is commonly employed in TEM-based studies to investigate mitochondrial morphology and ultrastructure [17]. The red and oxidative part of the *gastrocnemius* muscle was cut and fixed for 2 h in a solution of 2.5% glutaraldehyde in 0.1 M cacodylate buffer (pH 7.4). Samples were post-fixed for 1 h at 4°C in 1% osmium tetroxide and then incubated with 2% uranyl acetate for 2 h at RT. Muscles were embedded in resin (Araldite) and transverse ultrathin sections were cut (70 nm thick) with an ultramicrotome (UC7, Leica Biosystems) and mounted on copper grids to be visualized with the MET LIBRA 120 (Zeiss).

Individual subsarcolemmal (SS) mitochondria from 3 Y, 3 O and 3 O-AR mice were manually traced on TEM cross-sectional images using the Fiji/ImageJ software to quantify the mitochondrion area (μm_2). On each image, the SS region was also traced and its area measured. The mitochondrial density was calculated by dividing the number of mitochondria by the SS area (N mitochondria/µm2 ratio). Around 45 images per group were analyzed, equivalent to 1117, 1604 and 1435 SS mitochondria sampled for Y, O and O-AR respectively. Mitochondria were classified as either "healthy" or "damaged". Damaged mitochondria showed at least one of the following characteristics: disarticulated cristae and vacuolization, reduced electron density of the matrix or swollen appearance [18, 19]. Mitochondria with an area greater than 0.78 µm2 were considered swollen (represent the 90th percentile for the mitochondrial area of Y mice)[20]. The percentage of abnormal mitochondria, calculated as the number of damaged mitochondria out of the total number of mitochondria, was also measured.

RNA extraction and real-time quantitative PCR (RT-qPCR)

RNA was isolated from *rectus femoris* (*quadriceps* muscles) with TriPure reagent (Sigma-Aldrich). 1 µg of total RNA were reverse transcribed, and 40 ng total RNA equivalents were amplified using an iCycler iQ real-time PCR detection system (Bio-Rad Laboratories, Nazareth, Belgium) as described [11]. RT-qPCR primers for mouse TATA-binding protein were ordered from Integrated DNA Technologies (Coralville, Iowa, USA). RT-qPCR primers for mouse Myogenin, Myogenic regulatory factor 4 (Mrf4), Myosin heavy chain 1 (Myh1) and Myh7 were used as reported [21]. The threshold cycles (Ct) were measured in separate tubes and in duplicate. The identity and purity of the amplified product were checked by electrophoresis on agarose minigels, and analysis of the melting curve was carried out at the end of the

amplification. To ensure the quality of the measurements, each plate included a negative control for each set of primers.

Protein extraction, ELISA, and Western Blot

Tibialis anterior and *triceps brachii* were used for protein analysis, the fiber type composition of these two muscles being highly similar [22, 23]. Muscle samples were homogenized in a lysis buffer supplemented with 1% protease/phosphatase inhibitor cocktail (both from Cell Signaling Technology, BIOKE, Leiden, The Netherlands) and 10 mM NaF (Merck Life Science, Overijse, Belgium). Proteins were quantified using the Bradford method and were stored at -80°C. 25-200 µg of total protein extracts were used for each analysis. Six ELISA assays were used to specifically detect and quantify the active phosphorylated form of AMP-activated protein kinase alpha (P-AMPK, Thr172), mammalian target of rapamycin (P-mTOR, Ser2448), UNC-51 like kinase 1 (P-ULK1, Ser555), beclin-1 (P-beclin-1, Ser 30), SMAD Family Member 2 (P-SMAD2, Ser 465/467) and the p65 subunit of nuclear factor kappa B (NF-κB) (P-p65) (all from Cell Signaling Technology). Other ELISA kits were also used to detect Atrogin-1, muscle-specific RING-finger protein 1 (MuRF1), adiponectin receptor 1 (AdipoR1), peroxisome proliferator-activated receptor gamma coactivator 1-alpha (PGC-1α), translocase of the outer mitochondrial membrane complex subunit 20 (TOMM20), p16 and p21 (all from MyBioSource, Vancouver, Canada). Kits were based on colorimetric methods and were carried out following manufacturer's instructions. Immunoblotting was performed as reported [4] by using rabbit monoclonal antibodies directed against the ubiquitin-binding protein p62, LC3A-I/II and Beclin-1 (all from Cell signalling Technology). Signals were revealed by enhanced chemiluminescence, then quantified and normalized to those of Ponceau stain [24] using ImageJ.

Statistical analysis

Results are expressed as means ± SEM for the indicated number of mice. Comparisons between the three groups of mice (Y, O, O-AR) were carried out by one-way ANOVA followed by Tukey's test (Prism 9; Graphpad Software, San Diego, CA). Differences were considered statistically significant at $P < 0.05$.

RESULTS

AdipoRon mitigates insulin resistance, rescues endurance and protects muscle mass

Three groups of mice were used. Two groups of old mice were studied from 20 up to 23 months of age. One of these two groups was orally treated with AdipoRon (O-AR, *n*=10), while the other was left untreated (O, *n*=9) (Figure 1a). During the study, 3 out of 9 mice from the untreated O group developed large intra-abdominal tumors, while this was the case for only 1 mouse out of 10 in the treated O-AR group. All these mice were excluded from data analysis. We additionally used young mice (Y) studied at 3 months of age.

At the end of the study, the body weight and the cumulative food intake of O mice were higher than Y mice (~30%). Treatment with AdipoRon did not affect these parameters (Figure 1b, c and Table S1). The IR index derived from 6h-fasting glycemia and insulinemia doubled in O mice compared to Y ones but decreased by 20% under AdipoRon (Figure 1d). Circulating lipid parameters as well as plasma ApN levels did not change between the three groups (Table S1). Using a treadmill exhaustion test, we evaluated the muscle function of O mice at 22.5 months of age. Endurance capacity, expressed as the distance covered until exhaustion, was markedly reduced in O mice compared to Y ones, while it was partially rescued by AdipoRon (+60% vs O mice)(Figure 1e).

Adipose tissue weights sampled from different sites did not change significantly between the three groups (Table S1). On the contrary, weights from some hind-limb muscles decreased with age [*tibialis anterior* (TA), Figure 1f, and *gastrocnemius* (G), Table S2)]. The sarcopenia index, calculated as the ratio of

skeletal muscle weight to tibia length [25], was significantly reduced in TA of O mice, but was restored in O-AR ones, suggesting a therapeutic protection of AdipoRon against sarcopenia (Figure 1g). Similar findings were even more strikingly observed for G muscle (Table S2), while in soleus, the decrease observed in O *vs.* Y mice was no longer significant under AR. To microscopically assess the potential effects of AdipoRon on sarcopenia, we performed fiber typing and muscle fiber size measurements on whole cryosections of TA. Fiber typing was carried out by immunofluorescence staining for the different myosin heavy chains isoforms (MyHCs) and by laminin staining for fiber size (Figure 1h). Total number of fibers was significantly decreased in O mice when compared to Y ones, but rescued in the O-AR group (Figure 1i). As expected, the TA contained a large number of fast-glycolytic type 2b fibers (dark), followed by 2x fibers (red), and a smaller number of slow-oxidative type 2a fibers (green) (Figure 1h, j). The number of 2x fibers was decreased in both groups of old mice. However, for each type, O-AR mice tended to have a higher number of fibers than O mice (Figure 1j). Although each trend did not reach significance, taken together, they are in line with the preserved total number of fibers observed in O-AR mice (Figure 1i). Fiber size was also measured using the Minimum Feret Diameter. Global fiber size was similar among the different groups (Figure 1k). Size distribution evidenced an increased number of fibers in the middle range of the distribution in O-AR mice (Figure 1l). Taken together, these results show that AdipoRon improves endurance and protects the muscle from sarcopenia by preserving the muscle from fiber loss.

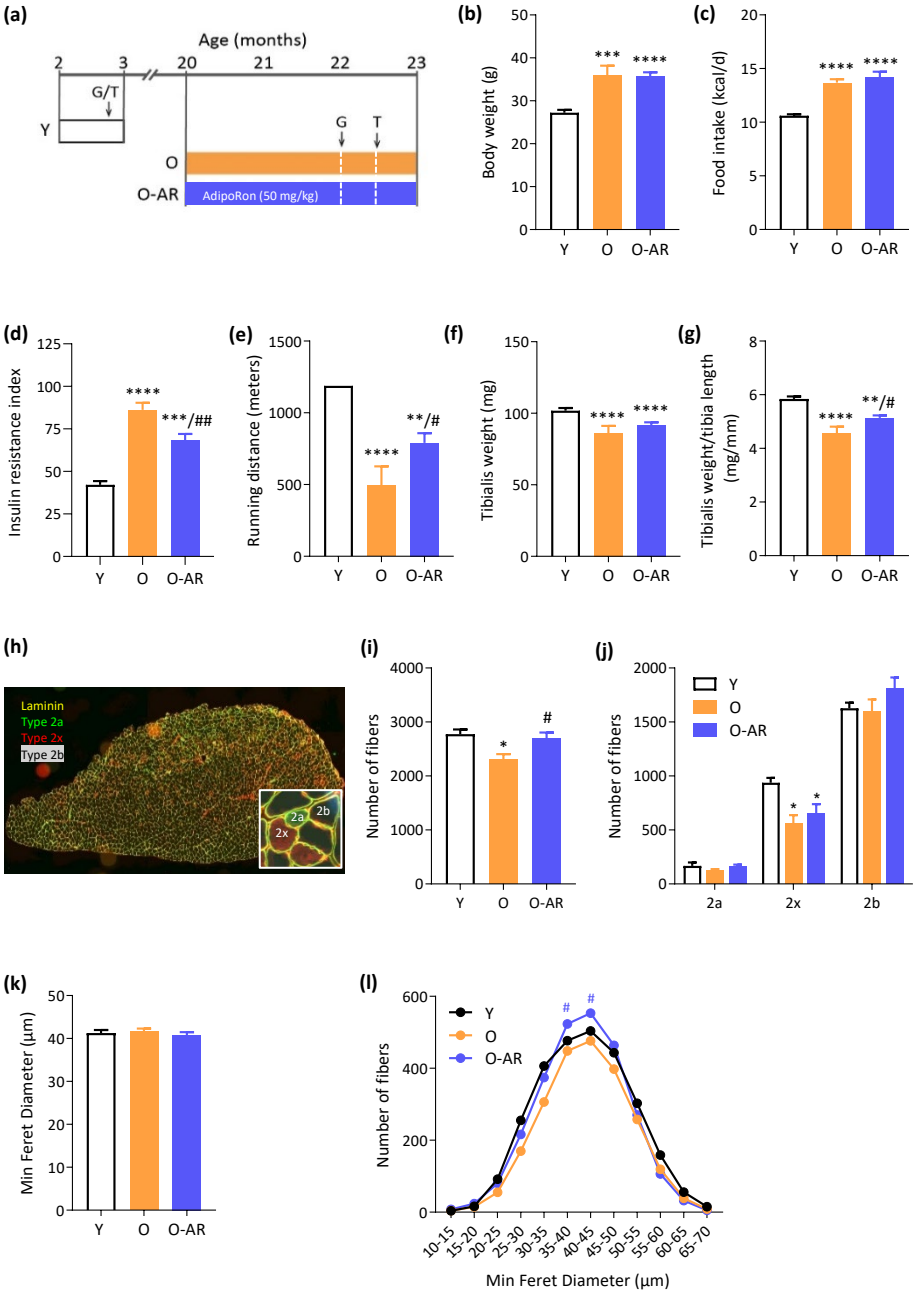

Figure 1. AdipoRon reduces insulin resistance, improves endurance and attenuates sarcopenia in O mice. (a) Experimental protocol. Three groups of mice were studied. Two groups were studied from 20 months to 23 months of age and are referred to as old (O) mice. One of the two groups was orally treated with

AdipoRon (AR) (50 mg/kg/day; O-AR), while the other one was left untreated (O). An additional group of young (3-months-old) mice was also used for comparison. At the indicated times, fasting glycemia was measured (G) and mice were submitted to treadmill exhaustion test (T). **(b)** Body weight at the end of the protocol. **(c)** Average food consumption over the whole study. **(d)** Insulin resistance index calculated as Insulin (ng/mL) × Glycemia (mg/dL) [26]. **(e)** Running distance covered (m) in an uphill treadmill exhaustion test. **(f)** Relative adipose tissues weight was calculated as the sum of subcutaneous and epididymal fat. **(g)** Sarcopenia index calculated as TA muscle weight normalized to tibia length. **(h)** Fiber typing was carried out by immunofluorescence staining of different MyHCs on a cross-section of TA muscle. Type 1 fibers were labeled in blue (none), type 2a in green, 2x in red while 2b were nonlabeled (black). Laminin antibody was used to delineate basal membrane (yellow). **(i)** Total number of fibers, **(j)** number of each fiber type, **(k)** global fiber size based on Minimum Feret Diameter and **(l)** fiber size distribution. All these data were quantified on whole cross-sections of TA. Data are means ± SEM for 6 Y, 6 O and 6-9 O-AR. Statistical analysis was performed using one-way ANOVA followed by Tukey's test to compare the 3 groups of mice. $^{*}P < 0.05$, $^{**}P < 0.01$, $^{***}P < 0.001$, $^{****}P < 0.0001$ vs. Y mice. $^{\#}P < 0.05$ vs. O mice.

AdipoRon reduces accumulation of tubular aggregates and promotes autophagy

Accumulation of abnormal structures related to aging and identified as tubular aggregates (TAgs), was detected in transverse sections of TA muscle. TAgs appear as pale or slightly basophilic inclusions with hematoxylin-eosin staining (Figure 2a, upper panels, white arrows) and as bright pink ones with Gomori trichrome (lower panels, white arrows). By electron microscopy, TAgs form straight, single- or double-walled tubules, regularly organized into tight aggregates with a honeycomb-like para-crystalline order (Figure 2c). These abnormal structures (bright pink inclusion) were quantified on Gomori sections of the three groups of mice. While they were absent in Y mice, these structures were abundant in O mice. Treatment with AdipoRon, however, more than halved TAgs accumulation compared with O mice (Figure 2b).

Since TAgs are a hallmark of dysregulated protein homeostasis, two key systems of protein clearance were studied: the ubiquitin-proteasome pathway and the autophagy-lysosome pathway [27]. In the ubiquitin-proteasome system, ubiquitin ligases such as Atrogin-1 and Muscle-specific RING finger protein 1 (MURF1) link ubiquitin chains to proteins that are to be degraded by the proteasome. These two protein levels were decreased in O and O-AR mice (~40% vs. Y mice) (Figure 2d). For the autophagy-lysosome system, the microtubule-associated protein light chain 3 (LC3) II/I ratio and p62 protein levels were measured [28]. LC3-I is converted to LC3-II during the early stages of autophagy, and an increase in LC3-II/LC3-I ratio indicates enhanced autophagic activity. In the O-AR group, the ratio was increased by 50% (Figure 2e), mainly due to the upregulation of LC3-II (Figure S1a). In contrast, p62 colocalizes with ubiquitinated protein aggregates and is degraded efficiently by autophagy. Therefore, accumulation of p62 is inversely correlated with autophagic activity. Expression of p62 rose by 65% in O mice compared with Y mice, but reverted to Y values in O-AR mice (Figure 2e). These data reveal that ubiquitin ligase levels are decreased with age, suggesting a downregulation of the ubiquitin-proteasome system, while AdipoRon enhances autophagy.

To unravel the mechanisms by which AdipoRon could increase autophagy, we studied the protein levels of the receptor and the activity of several downstream kinases known to be activated by ApN (Figure 3a). First, protein expression of the main muscle ApN receptor, AdipoR1, was decreased in O mice compared with Y ones (~35%), but restored by AdipoRon treatment (Figure 3b). Second, the phosphorylated, active form of AMPK (P-AMPK), which tended to be decreased in O mice, was overactivated in the O-AR group and even doubled when compared to the O group (Figure 3c). AMPK has been recognized as an activator of autophagy through phosphorylation and activation of UNC-51 like kinase (ULK1) [29] and

indirect inhibition of the mammalian target of rapamycin (mTOR) [30, 31] (Figure 3a). Accordingly, the active phosphorylated form of mTOR was increased in both groups of O mice compared to Y ones, but to a lesser extent in O-AR animals (40% and 25%, respectively) (Figure 3d). It should be noted that chronic activation of mTOR in muscle may be catabolic, rather than anabolic [32]. AdipoRon also enhanced the phosphorylation and activation of ULK1 (30%) (Figure 3e). Eventually, both AMPK and ULK1 target Beclin-1 for autophagy activation (Figure 3a) [33]: the phosphorylated and active form of Beclin-1 in the O-AR group was doubled when compared to O mice (Figure 3f, S2). Taken together, these results show that AdipoRon activates autophagy in skeletal muscle, which could certainly contribute to its protective role against the abnormal accumulation of TAgs.

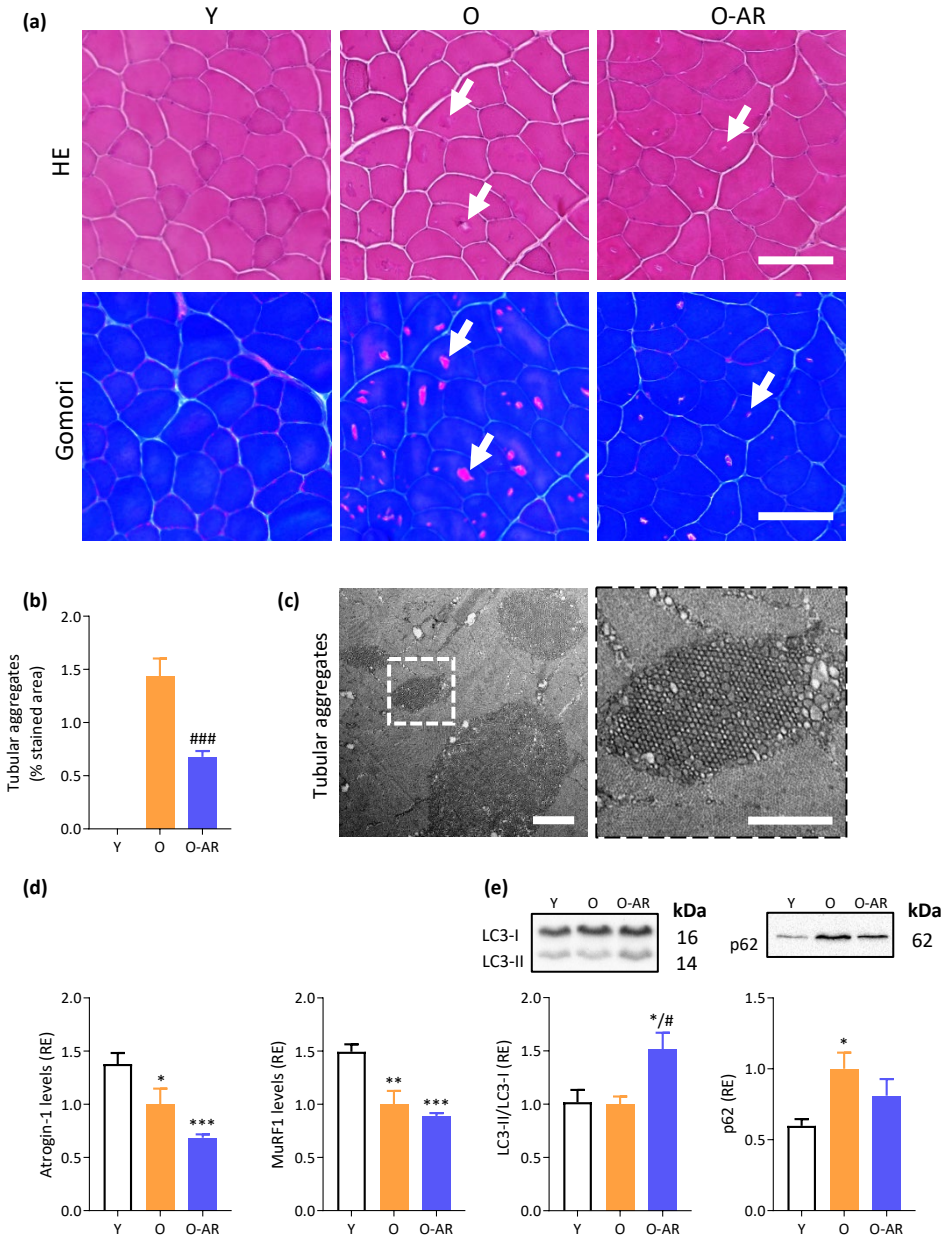

Figure 2. AdipoRon reduces age-related accumulation of tubular aggregates (TAgs). (a) TAgs (indicated by arrows) appear as pale or slightly basophilic inclusions with hematoxylin-eosin (HE) and bright pink ones with Gomori Trichrome on serial cross-section of TA. Scale bars = 100 µm. **(b)** Quantification of TAg abundance after Gomori Trichrome expressed as % of stained area (i.e. bright pink inclusions areas

normalized to the cross-sectional area of the muscle). **(c)** Characteristic honeycomb appearance of TAgs by transmission electron microscopy. Scale bar = 2 µm, Inset scale bar = 1 µm. **(d)** Protein levels of Atrogin-1 and MURF1 were measured by ELISA. **(e)** LC3-II/LC3-I ratio and p62 were analyzed by Western blotting. p62 levels were normalized to Ponceau S staining (shown in Figure S1b). Results are presented as relative expression compared to O values (d,e). Data are means ± SEM for 6 Y, 6 O and 9 O-AR. Statistical analysis was performed using unpaired two-tailed *t*-test to compare O and O-AR (b) or one-way ANOVA followed by Tukey's test to compare the 3 groups of mice (d,e). $^{*}P < 0.05$, $^{**}P < 0.01$, $^{***}P < 0.001$ vs. Y mice. $^{\#}P < 0.05$, $^{\#\#\#}P < 0.001$ vs. O mice.

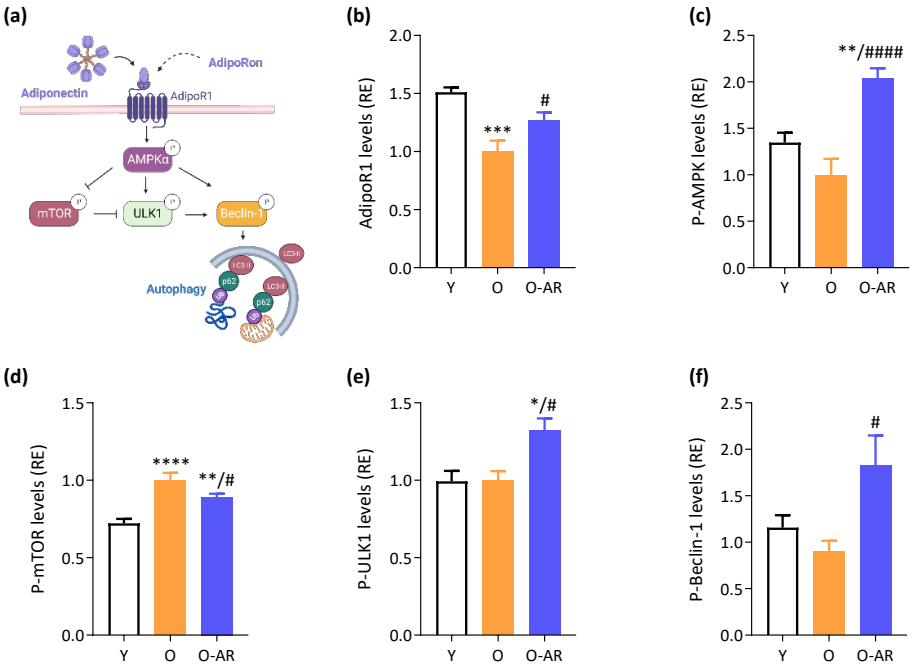

Figure 3. AdipoRon activates the AMPK pathway and promotes autophagy. (a) Proposed model for the effects of AdipoRon. Briefly, AdipoRon binds to AdipoR1 and activates the AMPK. AMPK plays a pivotal role in initiating autophagy by activating ULK1 and Beclin1, two critical regulators of the autophagic process. AMPK also exerts its regulatory influence by inhibiting mTOR, thereby alleviating mTOR-mediated inhibition of ULK1. LC3-II and p62, two important proteins in the

autophagy process. **(b)** AdipoR1 protein levels were measured by ELISA. Active phosphorylated forms of **(c)** AMPKα (P-AMPK), **(d)** mTOR (P-mTOR), **(e)** ULK1 (P-ULK1) and **(f)** Beclin-1 (P-Beclin-1) were quantified by ELISA. Absorbance data were presented as relative expression compared with O values. Data are means ± SEM for 6 Y, 6 O and 9 O-AR. Statistical analysis was performed using one-way ANOVA followed by Tukey's test to compare the 3 groups of mice. $^{*}P < 0.05$, $^{**}P < 0.01$, $^{***}P < 0.001$, $^{****}P < 0.0001$ vs. Y mice. $^{\#}P < 0.05$, $^{\#\#\#\#}P < 0.0001$ vs. O mice.

AdipoRon enhances mitochondrial content, function, and normalizes morphology

The content, function and morphology of mitochondria play a crucial role in skeletal muscle health. Notably, aging is associated with mitochondrial dysfunction, which contributes to muscle decline [34]. PGC-1α, a transcriptional co-activator controlled by AMPK is a master regulator of mitochondrial biogenesis and function (Figure 4a). Protein levels of PGC-1α were nearly halved in O-mice when compared to Y ones. However, a partial but significant restoration of PGC-1α was observed in O-AR mice (+36% vs. O mice) (Figure 4b).

Protein expression of Translocase of Outer Mitochondrial Membrane 20 (TOMM20) was measured to assess muscle mitochondrial content (Figure 4a). TOMM20 was slightly but significantly increased in O-AR mice compared to the other two groups (12%), suggesting a higher number of mitochondria (Figure 4c). Mitochondrial function was next studied by measuring Cytochrome C oxidase (COX) activity (Figure 4a, d, e). The proportion of dark fibers (i.e. with high activity of COX) was decreased in O mice compared to Y, indicating impaired mitochondrial activity with aging. By contrast, the proportion of dark fibers was higher in O-AR mice than in O ones (by ~2-fold) and reached values observed in Y mice, suggesting a protective effect of the treatment (Figure 4d, e).

Because abnormal mitochondrial ultrastructure is associated with impaired mitochondrial function, we analyzed mitochondrial morphology by TEM in the red G muscle of each group of mice. On transverse sections, each mitochondrion was manually circled within the subsarcolemmal region that was outlined in yellow (Figure 4f). Mean mitochondrion area was 20% larger in O than Y mice, but was corrected by AdipoRon (Figure 4g). In agreement with this result, the mitochondrial density (number/μm^2) was decreased in O mice, but restored in O-AR ones (Figure 4h). Mitochondria were subsequently classified as either "healthy" (painted in green) or "damaged" (in pink). Damaged mitochondria showed at least one of the following characteristics: disarticulated cristae and vacuolization, reduced electron density of the matrix or swollen appearance (Figure 4f inset) [18, 19]. Mitochondria with an area above the 90^{th} percentile of Y mice were considered as swollen [20]. The percentage of abnormal mitochondria increased considerably (by 2.4-fold) with aging, while it was normalized by AdipoRon treatment (Figure 4i). These observations indicate that with age, there is an increase in the size of subsarcolemmal mitochondria, a decrease in their number/μm^2, and an accumulation of abnormal mitochondria. However, the administration of AdipoRon counteracts all these age-induced alterations.

Oxidative stress in aging muscle is intricately linked to mitochondrial dysfunction [35]. Therefore, 4-hydroxynonenal (HNE), a marker of oxidative stress and a lipid peroxidation product, was also measured. HNE protein levels were increased in muscle of O mice, while being significantly reduced in O-AR mice, reaching levels similar to Y ones (Figure 4j). These findings suggest that AdipoRon could help to preserve mitochondrial function and then reduces oxidative stress.

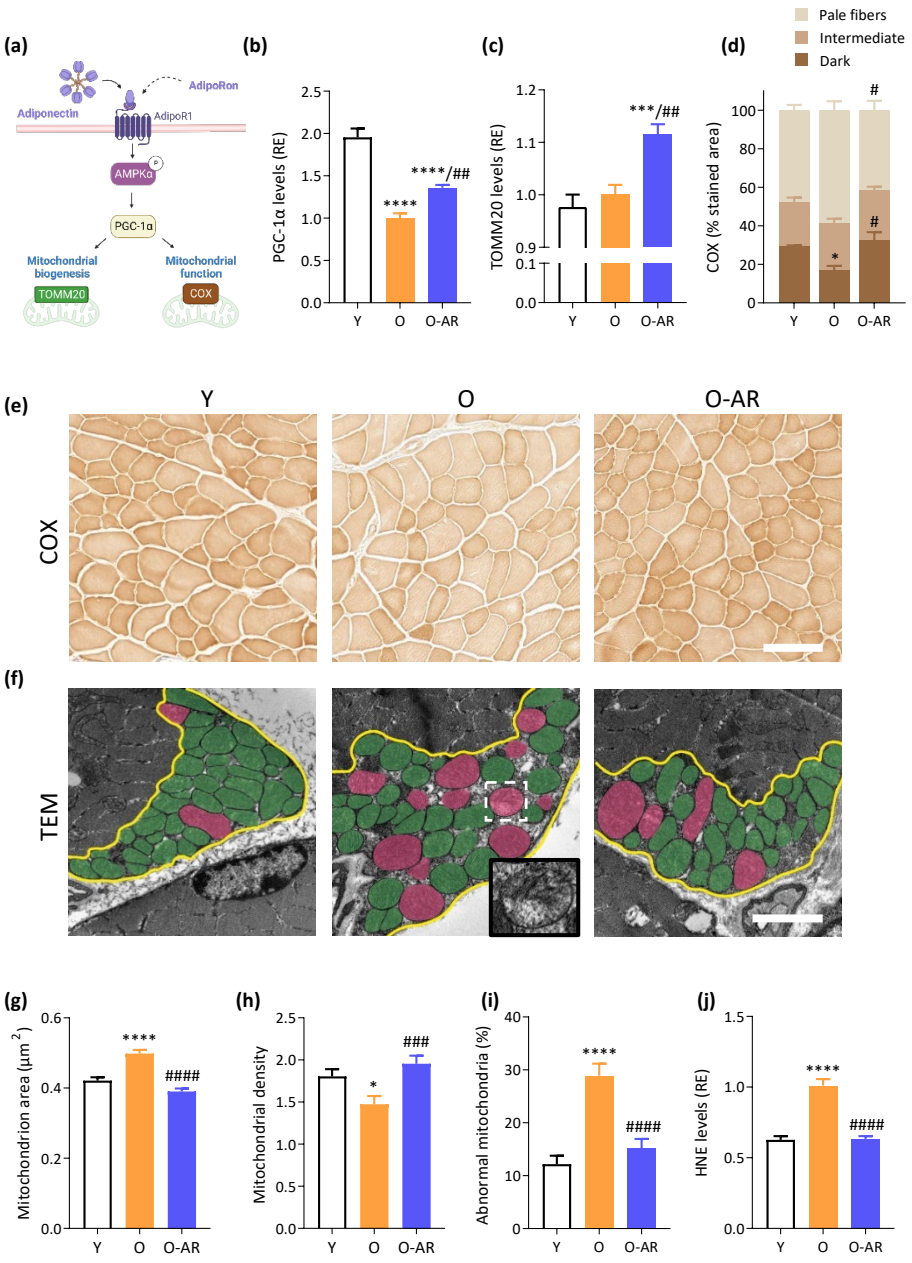

Figure 4. AdipoRon enhances mitochondrial biogenesis and function. (a) Activation of AMPK-PGC-1α signalling pathway by ApN stimulate mitochondrial biogenesis and function. TOMM20 is a marker of mitochondrial content, while COX activity reflects mitochondrial activity. **(b)** PGC-1α and **(c)** TOMM20 protein levels

quantified by ELISA. **(d)** Quantification of COX activity in the TA of the three groups of mice based on histochemistry staining, for which representative images are shown in **(e)**. Three staining intensities were defined as pale, intermediate or dark, the darkest color being associated with the highest activity. Activity was expressed as % of stained area (i.e. colored areas normalized to the cross-sectional area of the muscle). Scale bar = 100 µm. **(f)** Transmission electron micrographs of mitochondria in the subsarcolemmal region of G in the 3 groups of mice. The yellow line delimits the subsarcolemmal area. Abnormal mitochondria are false-colored in pink, while normal mitochondria are colored in green. Representative images of each group are shown. Scale bar = 2 µm. **(g)** The mitochondrion area and **(h)** the number of mitochondria per μm^2 in the subsarcolemmal region were calculated based on TEM images as depicted in (f). **(i)** Percentage of abnormal mitochondria out of the total number of mitochondria. (g-i) 1117, 1604 and 1435 subsarcolemmal mitochondria were sampled for Y, O and O-AR group, respectively. **(j)** HNE protein levels were quantified by ELISA. (b, c, j) Absorbance data were presented as relative expression compared with O values. Data are means ± SEM for 6 Y, 6 O and 9 O-AR (b-d, j). Statistical analysis was performed using one-way ANOVA followed by Tukey's test to compare the 3 groups of mice. $^{*}P < 0.05$, $^{***}P < 0.001$, $^{****}P < 0.0001$ vs. Y mice. $^{\#}P < 0.05$, $^{\#\#}P < 0.01$, $^{\#\#\#}P < 0.001$, $^{\#\#\#\#}P < 0.0001$ vs. O mice.

AdipoRon attenuates muscle age-related fibrosis and NF-κB overactivation

AMPK can be a potent suppressor of SMAD and NF-κB signaling, repressing the subsequent transcription of some pro-fibrotic, and pro-inflammatory genes (Figure 5a). We thus investigated fibrosis and found that O mice displayed a stronger picrosirius staining than Y mice (+70%). By contrast, the percentage of fibrotic areas was reduced by ~20 % in O-AR mice (Figure 5b, c). In addition, the active form of SMAD2 (P-SMAD2), a major downstream regulator that promotes TGF-β-mediated fibrosis, was also higher in O than in Y mice. However, P-SMAD2 was significantly reduced in O-AR mice and even reached Y values (Figure 5d). Lastly, we studied the potential anti-inflammatory effect of AdipoRon on the muscle via NF-κB. NF-κB is a

pleiotropic transcription factor modulating immune, inflammatory, survival, and proliferative responses [4]. NF-κB activity, assessed by the active and phosphorylated form of the p65-subunit, almost doubled with age in O mice, but was restored to basal levels with AdipoRon (Figure 5e). These data clearly indicate that treatment with AdipoRon could significantly repress NF-κB activity in aged skeletal muscle and protect it from fibrosis.

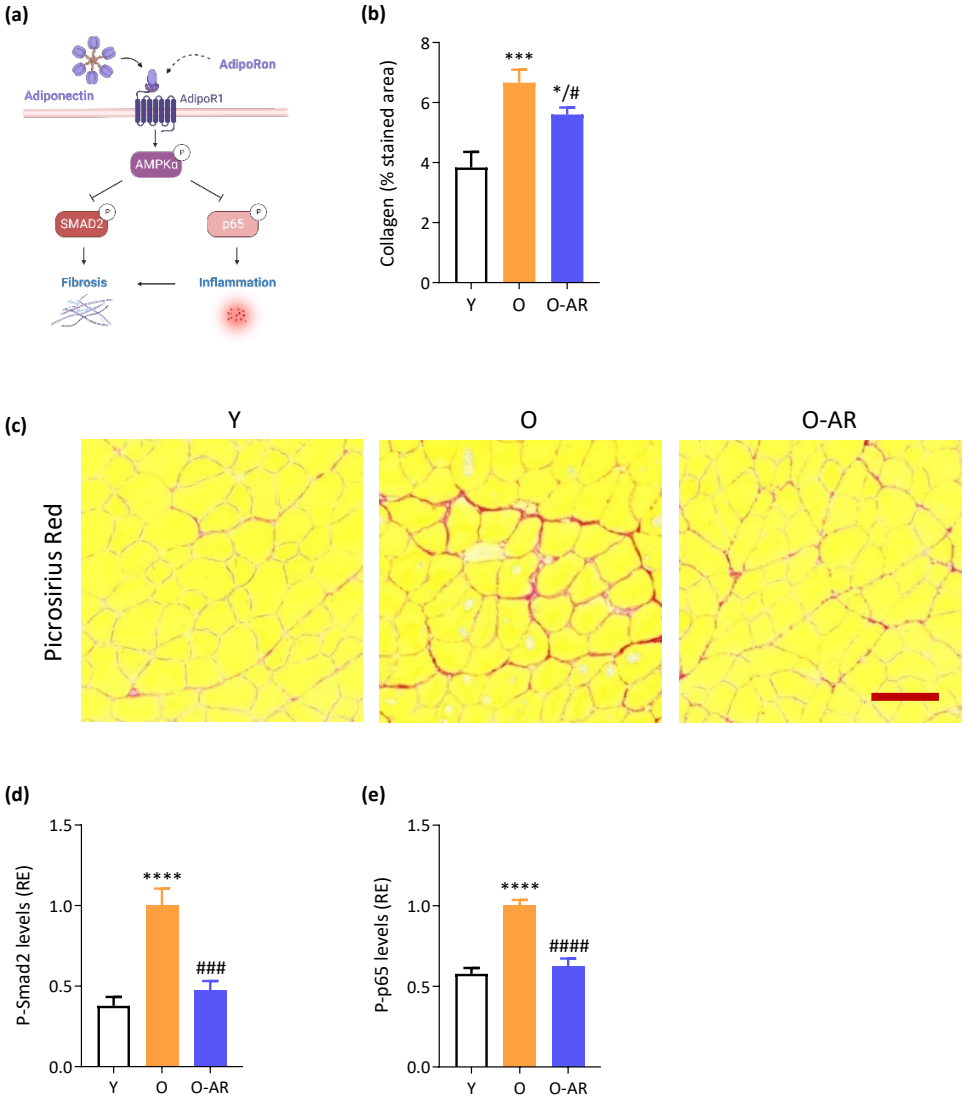

Figure 5. Treatment with AdipoRon limits age-related fibrosis and inflammation. **(a)** Activation of AMPK signalling pathway by ApN represses SMAD2 activity, an effector protein of the TGF-β pathway, and NF-κB activity (p65 subunit). **(b)** Quantification of picrosirius red expressed as % of collagen stained area, for which representative images are shown in **(c)**, scale bar = 100 µm. The active, phosphorylated forms of **(d)** SMAD2 (P-SMAD2) and **(e)** p65-subunit of NF-κB (P-p65) were measured by ELISA. Absorbance data were presented as relative expression compared with O values. Data are means ± SEM for 6 Y, 6 O and 9 O-AR. Statistical analysis was performed using one-way ANOVA followed by Tukey's test to compare the 3 groups of mice. $^{*}P < 0.05$, $^{***}P < 0.001$, $^{****}P < 0.0001$ vs. Y mice. $^{\#}P < 0.05$, $^{\#\#\#}P < 0.001$, $^{\#\#\#\#}P < 0.0001$ vs. O mice.

AdipoRon mitigates systemic inflammation

Senescence-Associated Secretory Phenotype (SASP) factors including circulating cytokines and chemokines increase in the bloodstream with aging [36, 37]. Accordingly, in this study, plasma levels of several cytokines (Figure 6a) and chemokines (Figure 6b) rose by 2- to 13-fold in O mice compared to Y one. Except for IL-6, all these factors tended to decrease or were significantly reduced by AdipoRon treatment. Some of them, like tumor necrosis factor α (TNF-α), interleukin-10 (IL-10), monocyte chemoattractant protein-1 (MCP-1) and macrophage inflammatory protein-2 (MIP-2) were even close to Y values (Figure 6a, b). Other factors such as fibroblast growth factor 21 (FGF21), eotaxin, granulocyte macrophage-colony stimulating factor (GM-CSF), IL-2, IL-15, IL-1β, MIP-3α were also measured, but did not differ between the 3 groups (not shown).

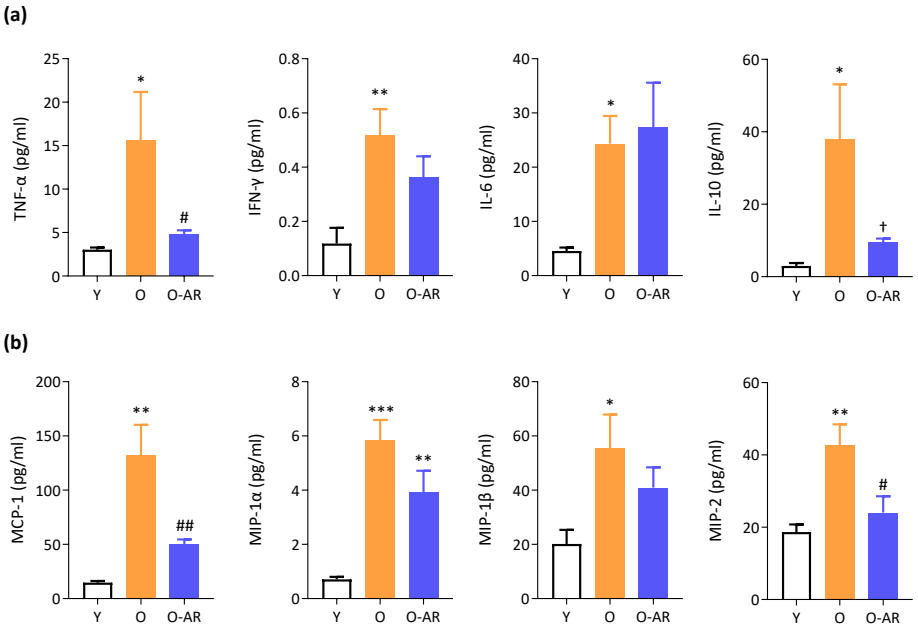

Figure 6. AdipoRon partially protects against age-related systemic inflammation. **(a-b)** A multiplex assay was performed to measure the concentrations of different cytokines (a) and chemokines (b) in the plasma of the three groups of mice. These can serve as markers of inflammaging/senescence associated secretory phenotype (SASP). Data are means ± SEM for 6 Y, 6 O and 9 O-AR. Statistical analysis was performed using one-way ANOVA followed by Tukey's test to compare the 3 groups of mice. $^{*}P < 0.05$, $^{**}P < 0.01$, $^{***}P < 0.001$ vs. Y mice. $^{\dagger}P = 0.07$, $^{\#}P < 0.05$, $^{\#\#}P < 0.01$ vs. O mice.

DISCUSSION

ApN is regarded as a unique and salutary adipokine exerting beneficial metabolic effects that could increase longevity. Accordingly, plasma ApN levels were higher among centenarians than in elderly individuals and these levels correlated with a favourable metabolic phenotype and a greater insulin sensitivity [38]. Additionally, in geriatric patients who are more likely to be functionally dependent, sarcopenia was associated with higher circulating inflammatory markers (CRP) and lower ApN levels [39]. Conversely, in some life-threatening conditions associated with muscle wasting such as chronic heart failure, ApN levels were paradoxically elevated. This elevation is however the result of both ApN resistance linked to downregulation of AdipoR1, and inactivation of AMPK signaling [40]. In this situation, high plasma ApN levels reflect a protective (yet unsuccessful) mechanism to counteract ApN resistance, insulin resistance, inflammation and oxidative stress [38, 40]. In our previous study, middle aged mice displayed decreased plasma ApN [12]. Here, in much older O mice, plasma ApN levels were normalized, but there was a significant downregulation of AdipoR1 protein and its two main downstream effectors, P-AMPK and PGC-1α were or tended to be decreased. Hence, this makes a strong case for the existence of ApN resistance in old O mice. Accordingly, these mice showed hyperglycemia possibly resulting from an age-related insulin resistance, as the insulin sensitizing effects of ApN were hindered [3]. Importantly, a novel finding of this study was to demonstrate that administration of an ApN receptor agonist is able to alleviate ApN resistance in aging, as this treatment rescued AdipoR1 expression and activated the ApN signaling cascade. These observations are consistent with those reported in diabetic mice [41]. ApN deficiency or resistance may thus prevail in aging, with the former possibly evolving into the latter, an ApN mimic may be useful. Consequently, there could be a rationale to therapeutically correcting ApN deficiency or resistance in the elderly.

A pioneering study by Balasubramanian *et al.*, conducted in old mice showed an improved muscle function after 6 weeks of i.v. treatment with AdipoRon, as well as a very slight increase in mitochondrial function [13]. However, because of the lack of a control group, sarcopenia couldn't be assessed accurately in old mice, and the effect of AdipoRon on muscle mass was not clearly established. In this study, we delve deeper into all the features of severe sarcopenia [2], namely: i) a decrease in muscle quantity as assessed by muscle weight and fiber number, ii) a decline in muscle quality as assessed by the accumulation of Tags, abnormal mitochondria and fibrosis, as well as iii) a marked reduction in muscle function as assessed by mitochondrial content and function, and endurance exercise. Furthermore, we unraveled in more detail the mechanisms of action of AdipoRon in sarcopenic muscle. We show unequivocally that all the abnormalities accompanying sarcopenia, as well as inflammaging, were rescued by three months' oral treatment with AdipoRon in aged mice, an action achieved primarily via the AdipoR1-AMPK axis.

In humans, the loss of muscle mass occurs incipiently from middle-age (∼1%/year) and may reach a loss of ~50% in the very old age [42]. In our 23-month-old mice, low muscle mass was assessed by the reduced sarcopenia index and by morphometric analysis, which was conducted over the whole muscle cross-section (*tibialis anterior*), to avoid biases due to selection of individual areas. This analysis showed an age-related decrease in the total number of fibers, with no change in size (Minimum Feret), as described [23]. These results are in line with the myofiber loss reported in humans by gold-standard measurements performed on cross-sections of autopsied thigh muscles [42]. In the present study, we showed that short-term treatment with AdipoRon protects mice against fiber loss due to aging.

Muscle quality was also compromised in old mice partly due to the abundance of TAgs. Protein aggregates may exert several adverse effects on cell function (lysosome and DNA damage, disruption of the membrane system and Ca^{2+} homeostasis, and induction of ROS) thereby accelerating in many ways aging [27]. TAgs are abnormal accumulation of ordered and tightly packed sarcoplasmic reticulum tubes [43, 44]. They were almost absent in young mice but accumulated in old ones, mainly within glycolytic fibers. In humans, the presence of TAgs defines a clinically heterogenous group of disorders termed TA myopathies (TAM) characterized by muscle weakness [43]. TAg abundance in old mice is accompanied by impaired ability to restore internal Ca^{2+} stores from extracellular space, which could contribute to muscle weakness [44]. We have previously shown that AdipoRon administered for ~1 yr in young obese mice prevented the development of TAgs [12]. Herein, we demonstrated that short term AdipoRon given to much older mice, once TAgs are already formed [12], reversed their accumulation.

Another key contributor to poor muscle quality is the age-related decline in mitochondrial function associated with mitochondrial damage [45]. This compromises the input of mitochondria to cellular bioenergetics, enhances the production of ROS, and may trigger accidental permeabilization of mitochondrial membranes causing inflammation and cell death [46], thereby hastening sarcopenia [34]. Accordingly, we observed a decrease in COX activity in the muscle of O mice, indicating impaired oxidative capacity and mitochondrial function. Ultrastructural analysis of electron microscopy images also revealed swollen and damaged mitochondria with age. Oxidative stress, reflected by HNE, was increased as well. All these abnormalities were completely corrected by AdipoRon treatment.

Because AdipoRon reduced the accumulation of TAgs as well as damaged mitochondria, we investigated whether this mimic could upregulate the pathways

involved in clearance of improperly assembled proteins. As reported in some [47], but not all studies [48], the ubiquitin-proteasome system was downregulated in sarcopenia and remained unmodified by AdipoRon. Moreover, this system is helpless when facing large misfolded proteins such as protein aggregates or damaged organelles [27]. We thus examined whether AdipoRon could stimulate the autophagy-lysosome system in the muscle of old mice. Different lines of evidence indicate that autophagy decline with aging, while autophagy stimulation may have beneficial effects on healthspan and lifespan [28, 49, 50]. Autophagy was impaired in our old mice as indicated by the increased levels of the p62 protein, an adaptator tethering ubiquitinated cargoes to the phagophore [28, 51]. By contrast, autophagy was stimulated by AdipoRon, which increased the ratio of LC3-II/LC3-I and blocked the accumulation of p62. This was explained by upstream overactivation of AMPK, which in turn phosphorylates and activates ULK1 and Beclin-1, two kinases that serve as initiators of autophagy [28, 52]. Autophagy is not only involved in proteostasis, but also affects entire organelles (including dysfunctional mitochondria targeted by ‘‘mitophagy,’’ a selective type of autophagy) [28, 46]. Mitophagy is also known to be impaired in aged skeletal muscle, leading to progressive accumulation of defective mitochondria [51-53]. In AdipoRon-treated mice, the presence of damaged/dysfunctional mitochondria was erased, indicating improved clearance of defective organelles. The higher mitochondrial content (see TOMM20) observed in treated mice, despite higher clearance, further suggests that AdipoRon could enhance mitochondrial biogenesis via PGC-1α. Taken together, our data indicate that AdipoRon could protect the muscle by hindering age-induced accumulation of TAgs and damaged mitochondria through stimulation of autophagy/mitophagy, and by possibly stimulating mitochondrial biogenesis.

Fibrosis is also a key contributor to poor muscle quality in the elderly. Fibrosis disrupts the muscle structural integrity, compromises muscle function and regenerative process, and stands out as a primary contributor to muscle weakness, stiffness and susceptibility to re-injury [54, 55]. O mice displayed fibrosis as shown by marked staining for Picrosirius Red, a marker of collagen deposition and doubling levels of P-SMAD2, an effector of TGF-β that regulates fibrosis. Under treatment, collagen accretion was attenuated and P-SMAD2 levels were normalized. AMPK can be a powerful suppressor of TGF-β/SMAD signalling [56-58]. Conversely, specific AMPK inhibition in mouse fibro-adipogenic progenitors has been shown to enhance TGF-β signalling and promote fibrosis in regenerated muscles [59]. This is explained by the potent repressive role of AMPK on NF-κB through the Sirtuin-1/ PGC1-α pathway [4, 60]. So, impaired AMPK results in enhanced NF-κB activity and subsequent transcription of pro-inflammatory and of some pro-fibrotic genes [59, 61]. Herein, O mice exhibited a ~2 fold-rise in NF-κB activity, to which mitochondrial dysfunction, oxidative stress and inflammation are likely to contribute [62]. Such a rise was completely abolished by AdipoRon treatment. Taken together, our data indicate that AdipoRon could be a therapeutic prospect to damper fibrosis in aged skeletal muscle.

Advancing age is accompanied by a chronic, low-grade and systemic inflammation, a processed termed inflammaging. Inflammaging is a recognized risk factor for several age-related diseases such as cardiovascular disease, cancer, type 2 diabetes, cognitive defects and sarcopenia/frailty [63]. Thus, overtime, the ongoing inflammation may render the muscle more vulnerable to developing sarcopenia, potentially by provoking protein degradation, impaired regeneration, mitochondrial dysregulation, and insulin resistance [64]. Inflammaging prevailed in O mice and was mitigated by AdipoRon. Except for IL-6, most cytokines and

chemokines were (or tended to be) decreased by the treatment, with a striking normalization for some of them (TNF-α, IL-10, MCP-1 or MIP-2). The surge of the anti-inflammatory cytokine IL-10 in O mice may be viewed as a compensatory mechanism to counterbalance systemic inflammation [63]. With regard to TNF-α, high circulating levels of this cytokine were associated with an 8-fold increased risk of sarcopenia in elderly subjects [65], while its pharmacological blockade prevented sarcopenia and extended survival in aged mice [66]. Moreover, circulating MCP-1 has been described as a measure of biological rather than chronological age both in mice and in humans. In mice, MCP-1 levels were significantly higher in progeroid animals than in control ones and in elderly humans, were higher in frail individuals compared to non-frail [67]. Our data demonstrate that AdipoRon is able to damper inflammaging, a root cause of many chronic diseases in elderly.

All these beneficial or protective effects of AdipoRon ultimately results in improved muscle function as shown by increased endurance during a treadmill test. We thus extend previous findings reporting a tendency to improved agility *in vivo* and a higher resistance to fatigue and recovery in a glycolytic muscle *ex vivo* after 6 wks of AdipoRon in old mice [13]. Here, the marked improvement in endurance was due to a striking increase in mitochondrial function. It was also due to strong reduction of dysfunctional SR proteins and subsequent improved capability of fibres to use extracellular Ca^{2+} [44]. Reduced fibrosis, oxidative stress and inflammaging could contribute as well. Taken together, these data are consistent with the exercise mimicker effect of AdipoRon [3, 7].

In this work, mice were studied in basal conditions only, to directly assess the effects of AdipoRon on age-related muscle changes. However, in basal state, some processes are weak or some cell types are scarce and need to be unveiled by muscle challenge (i.e. injury) [68, 69]. Therefore, in agreement with previous reports [68,

70], protein levels of p16 and p21, two markers of senescent cells, were undetectable. Additionally, gene expression of MyoD, Myf5, Myogenin, MRF4, markers of regeneration, was not different between the three groups of mice (not shown). More specifically, muscle injury is known to increase the number of senescent cells, which via their SASP, release factors that trigger inflammation and leading to the formation of fibrosis, preventing muscle regeneration [70]. Exploring the potential impact of AdipoRon on injured muscles of aged mice would be a valuable perspective. Additionally, tumor prevalence seemed to be higher in untreated old mice. Due to the anti-cancer properties of ApN [71], it would also be very important to treat larger cohorts of old mice possibly for a longer time in order to demonstrate a potential long-term protection of AdipoRon on cancer linked to aging. Eventually, effects on survival curves and lifespan could also be investigated.

Conclusively, a three-month administration of AdipoRon in aged mice yielded in notable improvements in muscle mass, quality, and function, effectively counteracting sarcopenia. By offsetting various hallmarks of aging, AdipoRon emerges as a promising anti-aging therapy for skeletal muscles, potentially extending healthspan.

Author contributions

Conception and design of the study: S.M.B., M.A.-S. and C.M.S. Protocol implementation: C.M.S. and L.N. Investigation: C.M.S., M.A.D.-L.d.C., R.V., L.N. and M.A.S. Formal analysis: C.M.S., M.A.D.-L.d.C., R.V., N.D., S.M.B and M.A.-S. Writing, review and editing: C.M.S., M.A.D.-L.d.C., R.V., N.D., S.M.B. and M.A.S. Supervision: M.A.-S. and S.M.B.

Acknowledgements

This work was supported by grants from Société Francophone du Diabète/Abott Diabetes Care 2020 and Fund for Scientific Research– FNRS (Research Credit 35275437, 2019). M.A.-S is Chargé de Recherches and C.M.S. has received a fellowship from the FRIA and from UCLouvain.

We are grateful to Caroline Bouzin and the IREC imaging platform for the use of the equipment and their aid, to Laura De Cock for her participation in mice experiments. We thank Peter Van den Bergh for his help in the interpretation of TEM images; Véronique Van Den Berge for her technical support. We also thank the personnel of the microscopy services (CITIUS, Universidad de Sevilla) for their technical support for transmission electron microscopy.

Ethical guidelines and consent

All procedures conducted in mice were approved by the Ethical Committee for Animal Experimentation from the Medical Sector at Université Catholique de Louvain (2019/UCL/MD/013).

Conflicts of interest

Authors declare that no conflict of interest exists.

References

1. Olshansky, S.J., *From Lifespan to Healthspan.* Jama, 2018. **320**(13): p. 1323-1324.
2. Cruz-Jentoft, A.J. and A.A. Sayer, *Sarcopenia.* Lancet, 2019. **393**(10191): p. 2636-2646.
3. Abou-Samra, M., et al., *Adiponectin and Its Mimics on Skeletal Muscle: Insulin Sensitizers, Fat Burners, Exercise Mimickers, Muscling Pills … or Everything Together?* Int J Mol Sci, 2020. **21**(7).
4. Abou-Samra, M., et al., *Involvement of adiponectin in the pathogenesis of dystrophinopathy.* Skelet Muscle, 2015. **5**: p. 25.
5. Otabe, S., et al., *Overexpression of human adiponectin in transgenic mice results in suppression of fat accumulation and prevention of premature death by high-calorie diet.* Am J Physiol Endocrinol Metab, 2007. **293**(1): p. E210-8.
6. Li, N., et al., *Adiponectin preserves metabolic fitness during aging.* Elife, 2021. **10**.
7. Okada-Iwabu, M., et al., *A small-molecule AdipoR agonist for type 2 diabetes and short life in obesity.* Nature, 2013. **503**(7477): p. 493-9.
8. Wang, Y., et al., *Hepatoprotective effects of AdipoRon against d-galactosamine-induced liver injury in mice.* Eur J Pharm Sci, 2016. **93**: p. 123-31.
9. Zhang, Y., et al., *AdipoRon, the first orally active adiponectin receptor activator, attenuates postischemic myocardial apoptosis through both AMPK-mediated and AMPK-independent signalings.* Am J Physiol Endocrinol Metab, 2015. **309**(3): p. E275-82.
10. Iwabu, M., et al., *AdipoR agonist increases insulin sensitivity and exercise endurance in AdipoR-humanized mice.* Commun Biol, 2021. **4**(1): p. 45.
11. Abou-Samra, M., et al., *AdipoRon, a new therapeutic prospect for Duchenne muscular dystrophy.* J Cachexia Sarcopenia Muscle, 2020. **11**(2): p. 518-533.
12. Selvais, C.M., et al., *AdipoRon enhances healthspan in middle-aged obese mice: striking alleviation of myosteatosis and muscle degenerative markers.* J Cachexia Sarcopenia Muscle, 2023. **14**(1): p. 464-478.
13. Balasubramanian, P., et al., *Adiponectin receptor agonist AdipoRon improves skeletal muscle function in aged mice.* Elife, 2022. **11**.
14. Ross, J.M., *Visualization of mitochondrial respiratory function using cytochrome c oxidase/succinate dehydrogenase (COX/SDH) double-labeling histochemistry.* J Vis Exp, 2011(57): p. e3266.
15. Schindelin, J., et al., *Fiji: an open-source platform for biological-image analysis.* Nat Methods, 2012. **9**(7): p. 676-82.
16. Selvais, C.M., et al., *Fiber Type and Subcellular-Specific Analysis of Lipid Droplet Content in Skeletal Muscle.* J Vis Exp, 2022(184).
17. Faitg, J., et al., *Effects of Aging and Caloric Restriction on Fiber Type Composition, Mitochondrial Morphology and Dynamics in Rat Oxidative and Glycolytic Muscles.* Front Physiol, 2019. **10**: p. 420.
18. Bonnard, C., et al., *Mitochondrial dysfunction results from oxidative stress in the skeletal muscle of diet-induced insulin-resistant mice.* J Clin Invest, 2008. **118**(2): p. 789-800.

19. Liu, Y., et al., *Adiponectin corrects high-fat diet-induced disturbances in muscle metabolomic profile and whole-body glucose homeostasis.* Diabetes, 2013. **62**(3): p. 743-52.
20. Leduc-Gaudet, J.P., et al., *Mitochondrial morphology is altered in atrophied skeletal muscle of aged mice.* Oncotarget, 2015. **6**(20): p. 17923-37.
21. Abou-Samra, M., et al., *Potential Therapeutic Action of Adiponectin in Duchenne Muscular Dystrophy.* Am J Pathol, 2017. **187**(7): p. 1577-1585.
22. Mathewson, M.A., et al., *Anatomical, architectural, and biochemical diversity of the murine forelimb muscles.* J Anat, 2012. **221**(5): p. 443-51.
23. Giacomello, E., et al., *Age Dependent Modification of the Metabolic Profile of the Tibialis Anterior Muscle Fibers in C57BL/6J Mice.* Int J Mol Sci, 2020. **21**(11).
24. Sander, H., et al., *Ponceau S waste: Ponceau S staining for total protein normalization.* Anal Biochem, 2019. **575**: p. 44-53.
25. Shavlakadze, T., J. McGeachie, and M.D. Grounds, *Delayed but excellent myogenic stem cell response of regenerating geriatric skeletal muscles in mice.* Biogerontology, 2010. **11**(3): p. 363-76.
26. Jortay, J., et al., *Adiponectin and skeletal muscle: pathophysiological implications in metabolic stress.* Am J Pathol, 2012. **181**(1): p. 245-56.
27. Wen, J.H., et al., *Cellular Protein Aggregates: Formation, Biological Effects, and Ways of Elimination.* Int J Mol Sci, 2023. **24**(10).
28. Hansen, M., D.C. Rubinsztein, and D.W. Walker, *Autophagy as a promoter of longevity: insights from model organisms.* Nat Rev Mol Cell Biol, 2018. **19**(9): p. 579-593.
29. Egan, D.F., et al., *Phosphorylation of ULK1 (hATG1) by AMP-activated protein kinase connects energy sensing to mitophagy.* Science, 2011. **331**(6016): p. 456-61.
30. Bujak, A.L., et al., *AMPK activation of muscle autophagy prevents fasting-induced hypoglycemia and myopathy during aging.* Cell Metab, 2015. **21**(6): p. 883-90.
31. Gwinn, D.M., et al., *AMPK phosphorylation of raptor mediates a metabolic checkpoint.* Mol Cell, 2008. **30**(2): p. 214-26.
32. Tang, H., J.B. Shrager, and D. Goldman, *Rapamycin protects aging muscle.* Aging (Albany NY), 2019. **11**(16): p. 5868-5870.
33. Park, J.M., et al., *ULK1 phosphorylates Ser30 of BECN1 in association with ATG14 to stimulate autophagy induction.* Autophagy, 2018. **14**(4): p. 584-597.
34. Picca, A., et al., *Update on mitochondria and muscle aging: all wrong roads lead to sarcopenia.* Biol Chem, 2018. **399**(5): p. 421-436.
35. Marzetti, E., et al., *Mitochondrial dysfunction and sarcopenia of aging: from signaling pathways to clinical trials.* Int J Biochem Cell Biol, 2013. **45**(10): p. 2288-301.
36. Coppé, J.P., et al., *The senescence-associated secretory phenotype: the dark side of tumor suppression.* Annu Rev Pathol, 2010. **5**: p. 99-118.
37. Liang, Z., et al., *Inflammaging: The ground for sarcopenia?* Exp Gerontol, 2022. **168**: p. 111931.
38. Arai, Y., K. Kamide, and N. Hirose, *Adipokines and Aging: Findings From Centenarians and the Very Old.* Front Endocrinol (Lausanne), 2019. **10**: p. 142.

39. Can, B., et al., *Serum markers of inflammation and oxidative stress in sarcopenia.* Aging Clin Exp Res, 2017. **29**(4): p. 745-752.
40. Van Berendoncks, A.M., et al., *Functional adiponectin resistance at the level of the skeletal muscle in mild to moderate chronic heart failure.* Circ Heart Fail, 2010. **3**(2): p. 185-94.
41. Kim, Y., et al., *The Adiponectin Receptor Agonist AdipoRon Ameliorates Diabetic Nephropathy in a Model of Type 2 Diabetes.* J Am Soc Nephrol, 2018. **29**(4): p. 1108-1127.
42. Wilkinson, D.J., M. Piasecki, and P.J. Atherton, *The age-related loss of skeletal muscle mass and function: Measurement and physiology of muscle fibre atrophy and muscle fibre loss in humans.* Ageing Res Rev, 2018. **47**: p. 123-132.
43. Brady, S., et al., *Tubular Aggregates and Cylindrical Spirals Have Distinct Immunohistochemical Signatures.* J Neuropathol Exp Neurol, 2016. **75**(12): p. 1171-1178.
44. Boncompagni, S., et al., *Long-Term Exercise Reduces Formation of Tubular Aggregates and Promotes Maintenance of Ca(2+) Entry Units in Aged Muscle.* Front Physiol, 2020. **11**: p. 601057.
45. Sebastián, D., et al., *Mfn2 deficiency links age-related sarcopenia and impaired autophagy to activation of an adaptive mitophagy pathway.* Embo j, 2016. **35**(15): p. 1677-93.
46. López-Otín, C., et al., *Hallmarks of aging: An expanding universe.* Cell, 2023. **186**(2): p. 243-278.
47. Edström, E., et al., *Atrogin-1/MAFbx and MuRF1 are downregulated in aging-related loss of skeletal muscle.* J Gerontol A Biol Sci Med Sci, 2006. **61**(7): p. 663-74.
48. Clavel, S., et al., *Atrophy-related ubiquitin ligases, atrogin-1 and MuRF1 are up-regulated in aged rat Tibialis Anterior muscle.* Mech Ageing Dev, 2006. **127**(10): p. 794-801.
49. Liu, Y., et al., *Adiponectin stimulates autophagy and reduces oxidative stress to enhance insulin sensitivity during high-fat diet feeding in mice.* Diabetes, 2015. **64**(1): p. 36-48.
50. Ahlstrom, P., et al., *Adiponectin improves insulin sensitivity via activation of autophagic flux.* J Mol Endocrinol, 2017. **59**(4): p. 339-350.
51. Palikaras, K., E. Lionaki, and N. Tavernarakis, *Mechanisms of mitophagy in cellular homeostasis, physiology and pathology.* Nat Cell Biol, 2018. **20**(9): p. 1013-1022.
52. Leduc-Gaudet, J.P., et al., *Mitochondrial Dynamics and Mitophagy in Skeletal Muscle Health and Aging.* Int J Mol Sci, 2021. **22**(15).
53. Drake, J.C. and Z. Yan, *Mitophagy in maintaining skeletal muscle mitochondrial proteostasis and metabolic health with ageing.* J Physiol, 2017. **595**(20): p. 6391-6399.
54. Mahdy, M.A.A., *Skeletal muscle fibrosis: an overview.* Cell Tissue Res, 2019. **375**(3): p. 575-588.
55. Wood, L.K., et al., *Intrinsic stiffness of extracellular matrix increases with age in skeletal muscles of mice.* J Appl Physiol (1985), 2014. **117**(4): p. 363-9.

56. Darmawan, C.C., et al., *Adiponectin-Based Peptide (ADP355) Inhibits Transforming Growth Factor-β1-Induced Fibrosis in Keloids.* Int J Mol Sci, 2020. **21**(8).
57. Marangoni, R.G., et al., *Adiponectin is an endogenous anti-fibrotic mediator and therapeutic target.* Sci Rep, 2017. **7**(1): p. 4397.
58. Wu, J., et al., *Ferulic Acid Ameliorates Hepatic Inflammation and Fibrotic Liver Injury by Inhibiting PTP1B Activity and Subsequent Promoting AMPK Phosphorylation.* Front Pharmacol, 2021. **12**: p. 754976.
59. Liu, X., et al., *AMP-activated protein kinase inhibition in fibro-adipogenic progenitors impairs muscle regeneration and increases fibrosis.* J Cachexia Sarcopenia Muscle, 2023. **14**(1): p. 479-492.
60. Salminen, A., J.M. Hyttinen, and K. Kaarniranta, *AMP-activated protein kinase inhibits NF-κB signaling and inflammation: impact on healthspan and lifespan.* J Mol Med (Berl), 2011. **89**(7): p. 667-76.
61. Xie, H., et al., *ROS/NF-κB Signaling Pathway-Mediated Transcriptional Activation of TRIM37 Promotes HBV-Associated Hepatic Fibrosis.* Mol Ther Nucleic Acids, 2020. **22**: p. 114-123.
62. Li, X., et al., *Mitochondrial dysfunction in fibrotic diseases.* Cell Death Discov, 2020. **6**: p. 80.
63. Dugan, B., J. Conway, and N.A. Duggal, *Inflammaging as a target for healthy ageing.* Age Ageing, 2023. **52**(2).
64. Wang, T., *Searching for the link between inflammaging and sarcopenia.* Ageing Res Rev, 2022. **77**: p. 101611.
65. Li, C.W., et al., *Circulating factors associated with sarcopenia during ageing and after intensive lifestyle intervention.* J Cachexia Sarcopenia Muscle, 2019. **10**(3): p. 586-600.
66. Sciorati, C., et al., *Pharmacological blockade of TNFα prevents sarcopenia and prolongs survival in aging mice.* Aging (Albany NY), 2020. **12**(23): p. 23497-23508.
67. Yousefzadeh, M.J., et al., *Circulating levels of monocyte chemoattractant protein-1 as a potential measure of biological age in mice and frailty in humans.* Aging Cell, 2018. **17**(2).
68. Moiseeva, V., et al., *Senescence atlas reveals an aged-like inflamed niche that blunts muscle regeneration.* Nature, 2023. **613**(7942): p. 169-178.
69. Tanaka, Y., et al., *Adiponectin promotes muscle regeneration through binding to T-cadherin.* Sci Rep, 2019. **9**(1): p. 16.
70. Glass, D.J., *Senescent cells damage the body throughout life.* Nature, 2023. **613**(7942): p. 30-31.
71. Nigro, E., et al., *AdipoRon and Other Adiponectin Receptor Agonists as Potential Candidates in Cancer Treatments.* Int J Mol Sci, 2021. **22**(11).

SUPPORTING INFORMATION

Supplementary Tables

Table S1. Circulating parameters in the three groups of mice at the end of the study.

	Y	O	O-AR
Circulating parameters			
Cholesterol (g/l)	0.86 ± 0.05	0.79 ± 0.09	0.85 ± 0.03
Triglycerides (g/l)	1.18 ± 0.14	0.76 ± 0.15	0.99 ± 0.11
NEFAs (mg/dl)	13.09 ± 1.70	10.03 ± 1.49	11.01 ± 1.00
ApN (µg/ml)	3.5 ± 0.1	3.5 ± 0.2	3.2 ± 0.2

Circulating parameters were collected from fed mice at the end of the study (at the age of 3 months for Y mice and 23 months for O/O-AR groups). NEFA, non-esterified fatty acids. Data are means ± SEM for 6Y, 6 O and 9 O-AR mice. Statistical analysis was performed using one-way ANOVA followed by Tukey's test to compare the 3 groups of mice.

Table S2. Body weight, adipose tissue weight and skeletal muscle weights in the three groups of mice at the end of the study.

	Y	O	O-AR
Body weight (BW) (g)	27.2 ± 0.7	35.9 ± 2.2 ***	35.7 ± 0.9 ****
White adipose tissue weight (g)	0.65 ± 0.04	0.75 ± 0.10	0.85 ± 0.09
White adipose tissue weight/BW(%)	2.39 ± 0.15	2.05 ± 0.15	2.39 ± 0.20
Skeletal muscle weight (mg)			
Tibialis anterior	101.8 ± 1.9	87.3 ± 4.3 **	90.6 ± 2.0 *
Gastrocnemius	325.7 ± 8.6	284.1 ± 16.9 *	295.8 ± 11.7
EDL	10.2 ± 0.4	10.8 ± 0.7	11.7 ± 1.2
Soleus	19.58 ± 0.5	17.9 ± 0.8	17.6 ± 0.8
Skeletal muscle weight/BW (%)			
Tibialis anterior	0.37 ± 0.01	0.25 ± 0.01 ****	0.25 ± 0.01 ****
Gastrocnemius	1.20 ± 0.01	0.81 ± 0.04 ****	0.83 ± 0.03 ****
EDL	0.04 ± 0.01	0.03 ± 0.01	0.03 ± 0.01
Soleus	0.07 ± 0.01	0.05 ± 0.01 ****	0.04 ± 0.01 ****
Skeletal muscle weight/tibia length (mg/mm)			
Tibialis anterior	5.84 ± 0.09	4.57 ± 0.23 ****	5.14 ± 0.09 **/ #
Gastrocnemius	18.67 ± 0.43	14.75 ± 0.74 ****	17.44 ± 0.20 ##
EDL	0.59 ± 0.02	0.61 ± 0.03	0.58 ± 0.04
Soleus	1.12 ± 0.03	0.97 ± 0.04 *	1.0 ± 0.05

Adipose tissue and muscle weights refer to pairs of fat pads (the sum of inguinal and epididymal) and skeletal muscles. Data are presented as absolute values and as a percentage of body weight. Additionally, a sarcopenia index was calculated by dividing muscle weight by tibia length. Data are means ± SEM for 6Y, 6 O and 9 O-AR mice. Statistical analysis was performed using one-way ANOVA followed by Tukey's test to compare the 3 groups of mice. $^{*}P < 0.05$, $^{**}P < 0.01$, $^{***}P < 0.001$, $^{****}P < 0.0001$ vs. Y mice. $^{\#}P < 0.05$, $^{\#\#}P < 0.01$ vs. O mice.

Supplementary Figures

Fig. S1

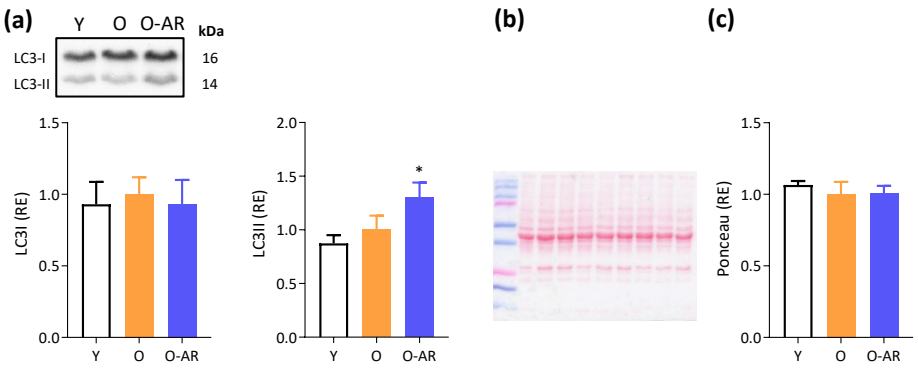

Figure S1. LC3I and LC3II protein levels and representative Ponceau staining. **(a)** LC3I and LC3II protein levels were analyzed by Western blotting. **(b)** The full ponceau-staining membrane from Western blotting with Y, O, O-AR (three animals for each condition but representative for all the animals studied). **(c)** Quantification of ponceau-staining. Results are presented as relative expression compared to O values. Data are means ± SEM for 6 Y, 6 O and 9 O-AR. Statistical analysis was performed using a one-way ANOVA followed by Tukey's test to compare the 3 groups of mice. *P < 0.05 vs. Y mice.

Fig. S2

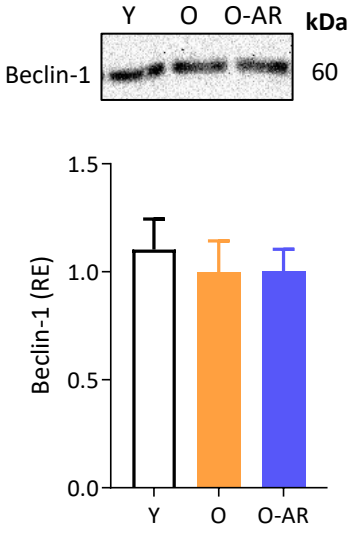

Figure S2. Beclin-1 protein levels analyzed by Western blotting. Results are presented as relative expression compared to O values. Data are means ± SEM for 6 Y, 6 O and 9 O-AR.

CHAPTER 4: GENERAL DISCUSSION AND PERSPECTIVES

CHAPTER 4: GENERAL DISCUSSION AND PERSPECTIVES

PART I: DISCUSSION

1. Bridging the Gaps in Age-related research and sarcopenia

By 2050, more than 20% of the world's population will be over the age of 60 years. While longevity has increased, the advantages of living longer are offset by the global surge in non-communicable diseases, including obesity, and age-related conditions [1]. The World Health Organization has recently implemented an Extension Code for 'Aging-related' (XT9T) diseases in the latest version of the International Classification of Diseases (ICD-11), defining them as those "caused by biological processes which persistently lead to the loss of organism's adaptation and progress in older ages" [1]. The inclusion of this code was intended to place a greater emphasis on the biological aspects of aging in global health policy and to create better opportunities for the development of therapeutic intervention and preventive strategies [1, 2].

Obesity among older adults has noticeably increased over the last decades on all continents. In the United States, obesity prevalence over 65 is reaching 35% and is expected to at least double by 2050 [3]. Obesity accelerates aging and predisposes individuals to age-related conditions and diseases. Obesity and aging are associated with loss of muscle function and endurance capacity, insulin resistance, and features of the metabolic syndrome [4]. Ectopic lipids play a key role in the development of myosteatosis and NAFLD, two severe burdens of aging and metabolic diseases [5, 6].

Sarcopenia is a generalized skeletal muscle disorder that commonly occurs as an age-related process. Sarcopenia is characterized by the accelerated loss of muscle mass, quality and function and is associated with adverse outcomes [7]. Considering the economic threat posed by an aging population, progress aimed at improving healthspan by limiting age-related diseases is vital.

Due to its potent metabolic benefits and its protective role in muscle [8] and lifespan [9], ApN appears to hold great promise as a strategy for extending healthspan. Circulating ApN levels are notably higher in centenarians than in the general elderly population and correlate with a more favorable metabolic profile [10]. In contrast, in the population aged around 80, ApN levels are lower in individuals with sarcopenia than in those without sarcopenia [11]. However, in certain life-threatening conditions associated with muscle wasting, such as chronic heart failure, ApN levels are paradoxically elevated. This elevation, however, results from both ApN resistance linked to downregulation of AdipoR1, and inactivation of AMPK signaling [12]. In this situation, high plasma ApN levels reflect a protective, albeit unsuccessful, mechanism that aimed to counteract ApN resistance, insulin resistance, inflammation, and oxidative stress [10, 12].

Two experimental designs were implemented to assess the effects of AdipoRon, an ApN mimic [13, 14]. In the first study [13], the approach was rather preventive, with a treatment starting early and of long duration (1 year). Importantly, it was the longest AdipoRon treatment ever reported so far. C57/BL6J mice received a high-fat diet to mimic the high prevalence of obesity in the elderly and to trigger metabolic complications such as myosteatosis and NAFLD. Mice were studied up to 62 weeks of age since the average lifespan of obese mice is shortened around 70 weeks [15, 16]. At the end of the protocol, these so-called "middle-aged" mice were already showing signs of aging, such as the hypertrophy of preputial and seminal

glands, which are common signs of aging in C57BL/6 mice [17]. In the second study [14], a later and shorter treatment (3 months) was initiated in older mice fed a standard diet, aligning it more with a curative approach in a non-obese model. Until now, the effects of AdipoRon in old wild-type mice have been poorly studied. Okada-Iwabu had shown an effect on longevity in a mouse model with a severe form of genetic diabetes (db/db). However, the marked alleviation of diabetes status provoked by AdipoRon was, in this case, a major confounding factor [18]. Recently, a short-term (6 weeks) intravenous administration of AdipoRon has also been tested in older and non-obese mice [19]. This treatment has been reported to enhance muscle function. However, the study lacked a control group of young mice, an evaluation of muscle mass (muscle weight and fiber counting), and muscle quality, and therefore it fell short in accurately assessing sarcopenia. Moreover, molecular and cellular mechanisms were not explored. Our last work was necessary to precisely demonstrate the effects of AdipoRon on sarcopenia and extend the scope of studies carried out to date.

2. Hallmarks of Aging under ApN/AdipoRon Spotlight

By using histology and electron microscopy, we found the presence of tubular aggregates (TAgs) in glycolytic myofibers of both middle-aged (obese or not) [13] and old mice [14], while these structures were nearly absent in young ones. TAgs are described as an abnormal accumulation of ordered and tightly packed sarcoplasmic reticulum tubes. In humans, they are found within a clinically heterogeneous group of TA myopathies (TAM), characterized by symptoms including pain, cramps, and muscle weakness [20, 21]. The presence of TAgs has not yet been studied in the elderly, but virtually identical TAgs to those in TAM patients have been found in aging mice [22]. The abundance of TAgs in old mice is associated with impaired ability to restore internal Ca^{2+} stores from the

extracellular space during repetitive muscle activity, which could contribute to muscle weakness [23]. In both studies, we have demonstrated that AdipoRon, whether administered in the long or short term, partially prevents or reverses the accumulation of Tags [13, 14]. These findings have also been observed with long-term regular physical exercise in old mice, which prevents the formation of TAgs and reduces muscle fatigue [23].

Because AdipoRon reduced the accumulation of TAgs, we speculated that this mimic could upregulate the pathways involved in clearance of improperly assembled proteins and aggregates. Different lines of evidence indicate that autophagy declines with aging, while autophagy stimulation may have beneficial effects [24-28]. Autophagy was actually impaired in the skeletal muscle of old mice [14], as shown by the increased levels of p62 protein, which serves as a receptor for cargo destined for clearance [27]. We found no changes in autophagy markers in the middle-aged mice [13] but such modifications are typically observed in older mice [29]. Nevertheless, in both studies, AdipoRon activated AMPK [13, 14], which has been recognized as an activator of autophagy through phosphorylation and activation of UNC-51 like kinase (ULK1) [27, 30, 31]. Accordingly, ULK-1 was phosphorylated and accumulation of p62 was decreased with the treatment [13, 14]. Furthermore, the ratio LC3-II/LC3-I and the activation of beclin-I, another kinase involved in phagophore formation, were increased in old treated mice [14]. AdipoRon therefore effectively stimulated autophagy clearance, in line with other studies performed with ApN [28, 32].

Mitochondrial function was impaired with aging [33] in middle-aged [13] and old mice [14], as evidenced by decreased cytochrome C oxidase (COX) activity. Likewise, analysis of mitochondrial ultrastructure revealed a greater abundance of swollen and damaged (presumably dysfunctional) mitochondria than in young

mice. Mitochondrial dysfunction is known to compromise ATP production and enhance oxidative stress [34], as reflected by elevated HNE levels [14]. Conversely, in mice treated with AdipoRon, damaged mitochondria and oxidative stress were reduced, while mitochondrial function was improved [13, 14]. This protection by AdipoRon could be explained by two different mechanisms. First, autophagy is not on only involved in proteostasis, but also affects entire organelles, including dysfunctional mitochondria targeted by “mitophagy”, a selective type of mitophagy [27, 34]. Mitophagy is also known to be impaired in aged skeletal muscle, leading to progressive accumulation of defective mitochondria [35-37]. In AdipoRon-treated mice, the presence of damaged/dysfunctional mitochondria was erased, indicating improved clearance of defective organelles [14]. Second, in both studies, AdipoRon stimulates PGC-1α signaling [13, 14]. PGC-1α regulates several transcription factors involved in mitochondrial biogenesis, function, fatty acid oxidation and energy dissipation. These factors were upregulated by AdipoRon [13], in line with a previous report [18]. Collectively, AdipoRon protects against the age-related decline in mitochondrial function and contributes to the reduction of myosteatosis through mitophagy, mitochondrial synthesis, and fatty-acid oxidation.

In the first study, middle-aged mice (obese or not) displayed decreased plasma ApN [13]. In the second one, conducted with much older mice, plasma ApN levels were normalized, but there was a significant downregulation of AdipoR1 protein [14]. In both studies, the two main downstream effectors of AdipoR1, namely P-AMPK and PGC-1α were (or tended to be) decreased with aging [13, 14], as previously described [38-42]. This collectively provides strong evidence for the existence of ApN deficiency or resistance in aging. Decreased ApN action prevents the insulin-sensitizing effects [8] and contributes to the hyperglycemia observed in obese

middle-aged [13] and old mice [14], which was reversed by AdipoRon. A novel and important finding of our second study was to demonstrate that administration of an ApN receptor agonist is able to alleviate ApN resistance in aging, as this treatment rescued AdipoR1 expression and activated the ApN signaling cascade [14]. These observations are consistent with those reported in diabetic mice [43]. ApN deficiency or resistance may thus prevail in aging, with the former possibly evolving into the latter. Consequently, there could be a rationale to therapeutically correcting ApN deficiency or resistance in the elderly with AdipoRon.

Finally, inflammaging was identified in old mice and mitigated by AdipoRon [14]. This result is interesting, as age-associated inflammation is a critical predictor of age-related morbidity and mortality [44]. For example, centenarians exhibit low levels of inflammation [45]. Low grade inflammation causes collateral damage to tissues and organs over time, including oxidative stress, and ultimately results in an increased risk of metabolic syndrome, types 2 diabetes, NAFLD and a myriad of other diseases [46]. Most circulating cytokines and chemokines were decreased by the treatment, with a striking normalization for some of them (TNF-α, IL-10, MCP-1 or MIP-2). Their harmful effects have been illustrated in different studies. For example, MCP-1 levels are considered a measure of biological age in mice and humans [47], while pharmacological inhibition of TNF-α prevents sarcopenia in mice and extends survival [48]. The surge of the anti-inflammatory cytokine IL-10 in old mice may be seen as a compensatory mechanism to counterbalance systemic inflammation [44]. Inflammaging could arise from several tissues [34] and is thought to be caused in part by the accumulation of senescent cells with aging. Senescent cells develop a senescence-associated secretory phenotype (SASP) characterized by increased secretion of pro-inflammatory cytokines, chemokines and other pro-inflammatory molecules, which contribute to inflammaging [46, 49,

50]. In our case, the mice were studied in basal conditions and senescence markers (p16, p21) were not detected [14]. This is consistent with the literature, which suggests that the accumulation of senescent cells in the skeletal muscle need to be unveiled by muscle challenge [51]. Upon injury, senescent cells through their SASP, release factors that trigger inflammation and lead to the formation of fibrosis, preventing muscle regeneration [52]. Markers of inflammation were also low in the muscle [14]. However, in middle-aged obese mice, the liver already showed noticeable signs of inflammation [13].

3. Potential of AdipoRon in preventing sarcopenia and preserving Health

Sarcopenia is defined by the accelerated loss of muscle mass and/or quality and function [7].

First, muscle quality.

Myosteatosis, fibrosis, TAgs, and abnormal mitochondria may contribute to impair muscle quality. The presence of TAgs and altered mitochondria have been discussed supra. Herein, I will focus on myosteatosis and fibrosis.

The protective effects of AdipoRon against myosteatosis have been poorly studied so far [18]. Yet, myosteatosis is emerging as a public health concern. It increases with age and obesity and is recognized to negatively correlate with muscle mass, strength and mobility, and disrupt metabolism (leading to insulin resistance and diabetes)[5]. Myosteatosis is also a negative prognostic factor for cancer [53], cardiovascular disease [54] and NAFLD [55]. By using Bodipy staining, we quantified IMCL content and analyzed LD size and subcellular distribution in a fibre-specific manner [13]. The study highlights the differential impact of aging and dietary fat

overload on IMCL content according to fibre type. Aging promotes accumulation of IMCLs in oxidative fibres while dietary fat overload promotes such an accumulation in glycolytic ones. A novel and important finding is that AdipoRon strikingly reverses IMCL accumulation whether due to aging in oxidative fibres (Types 1 and 2a) or to HFD in glycolytic ones (Types 2x and 2b). This correction occurs in both subsarcolemmal and central regions. The size of LDs, especially subsarcolemmal ones, is reduced as well. Besides being associated with adverse metabolic outcomes, large LDs could also affect muscle contractile capacity as previously suggested [56]. Even in single myofiber of older obese subjects, IMCL content is inversely related with fiber contraction, power and force development [57], raising the possibility of a vicious circle between IMCL accumulation and functional muscle impairment.

Fibrosis also contributes to poor muscle quality in the elderly by disrupting muscle structural integrity, compromising the regenerative process, and contributing to muscle weakness, stiffness, and susceptibility to re-injury [58, 59]. Levels of P-SMAD2, an effector of TGF-β that regulates fibrosis, were doubled in old mice, while being reversed by AdipoRon [14].

Second, muscle mass.

In middle-aged obese mice, in spite of unchanged muscle mass, fiber size and number, the true contractile mass was likely to be reduced by infiltration of IMCL and Tags, both abnormalities being reversed by Adiporon [13]. In much older mice, low muscle mass was evidenced by the reduced sarcopenia index (ratio of skeletal muscle weight to tibia length) and confirmed by morphometric analysis. Thus, an age-related decrease in the total number of muscle fibers, with no change in size was observed [14], in accordance with previous studies [60]. These results align

with myofiber loss observed in humans by gold-standard measurements performed on cross-sections of autopsied thigh muscles [61]. We showed that AdipoRon strikingly protected mice against the loss of muscle fibers due to aging.

Third, muscle function.

Ultimately, all these beneficial and protective effects of AdipoRon translated into enhanced muscle function in treated mice as shown during the treadmill tests [13, 14]. These findings extend previous works that reported increased endurance in mice fed a HFD after 10 days of treatment [18] and in mdx mice treated for 3 months [62]. There were also observations of improved agility and increased resistance to fatigue in a glycolytic muscle ex vivo after 6 weeks of AdipoRon treatment in old mice [19]. The improvement in muscle mass and quality is a major contributor to enhanced muscle function. Reduced inflammaging could participate as well. Moreover, we cannot exclude the possibility that effects of AdipoRon on other tissues (e.g. heart) could be involved [8]. Of note, the better performance of AdipoRon-treated mice does not appear to be linked to higher motivation: a panel of behavioral tests did not reveal any differences in attitudes between our middle-aged obese mice treated or not (not shown) [13], unlike data obtained in a mouse model of depression [63].

Importantly, AdipoRon exhibits additional health benefits. On one hand, AdipoRon prevents the progression of NAFLD into NASH in middle-aged obese mice [13]. NASH is the severe form of NAFLD characterized by lobular inflammation and hepatocyte ballooning and this stage has a clear potential for progression to cirrhosis and hepatocellular cancer [64]. On the other hand, old untreated mice displayed a higher tumor prevalence than treated ones [14]: 3 out of 9 mice from the untreated old group developed large intra-abdominal tumors, compared to

only 1 out of 10 mice in the treated group[1]. This observation raises possibilities about the broader healthspan benefits of AdipoRon beyond its effects on muscle [65].

Taken together, these findings support the idea that AdipoRon acts as an exercise mimicker, leading to notable improvements in muscle mass, quality, and function, and counteracts sarcopenia and promotes healthspan [8, 18] (Figure 1).

[1] All these mice were excluded from data analysis.

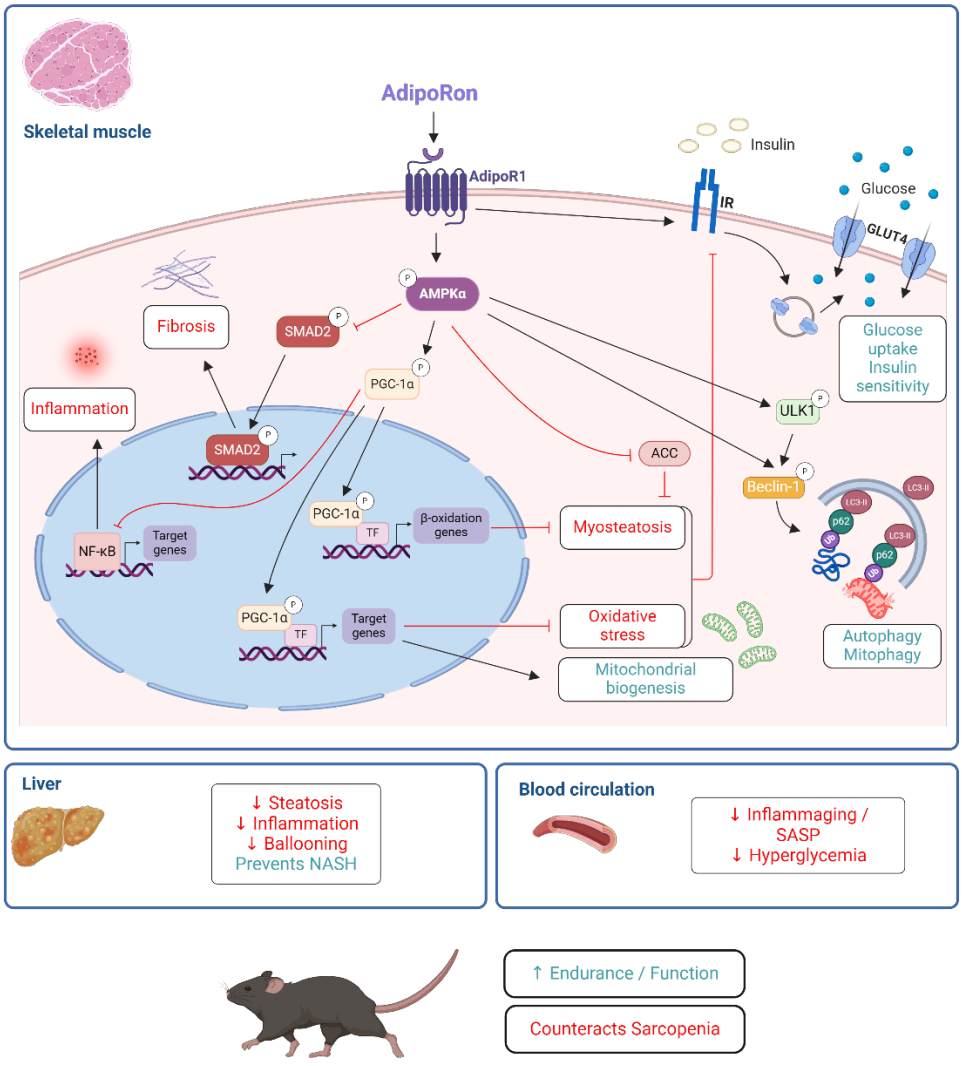

Figure 1. Proposed model summarizing the effects of AdipoRon on skeletal muscle, liver, circulating parameters, and function of middle-aged obese and old mice [13, 14]. Green boxes represent net beneficial effects of AdipoRon, while red boxes represent dysfunctions counteracted by AdipoRon. Figure drawn by Selvais C. with BioRender.

4. Other interventions for Aging and Sarcopenia

Regular physical activity preserves function, delays the onset of morbidity and disability, extends lifespan, and contributes to optimal longevity. Therefore, exercise is considered a powerful anti-aging strategy [66]. Conversely, physical inactivity is a major contributor to endocrine and metabolic diseases [67]. It can hasten muscle weakening and the progression toward functional impairment and disability, while exercise training intervention seem to slow or reverse these processes. To prevent or delay sarcopenia development, it is advised to maximize muscle in youth and young adulthood, maintain muscle in middle-age and minimize the loss in older age [68]. Evidence-based clinical practice provides strong recommendations for physical activity as the primary treatment of sarcopenia [7, 69, 70].

Exercise may sometimes be difficult to implement, and low adherence in older adults is a real issue [71]. This has led to global expectations for development of exercise mimics that effectively activate similar pathways [72, 73]. Exercise notably activates AMPK/SIRT1 and PGC-1α, enhancing mitochondrial function, muscle endurance and energy metabolism [74, 75]. Different pharmacological compounds are currently investigated with the intent to activate this pathway and improve healthspan. Among them, metformin is the most widely prescribed oral glucose-lowering agent for type 2 diabetes [76]. Its glucose-lowering effects are mainly ascribed to inhibition of hepatic glucose production, interactions with the gut and reduction of meta-inflammation, rather than to a direct action on skeletal muscle. Metformin operates via both AMPK-dependent and -independent mechanisms. Notably, metformin inhibits mitochondrial complex 1, leading to a decreased cellular energy charge and an elevated AMP/ATP ratio, thereby activating AMPK [76-78]. Metformin appears to offer beneficial effects beyond improving blood

sugar levels. In nematodes and mice, it extends both lifespan and healthspan. In humans, it reduces the mortality rate of diabetic patients independently of its effect on diabetes control [79]. However, before providing metformin as a targeted aging drug, further research is necessary to elucidate the mechanisms underlying metformin positive impact on aging and whether it could benefit individuals without diabetes [76]. Furthermore, responses to the treatment vary among individuals. Long-term treatment and potential off-target effects should also be thoroughly evaluated [76, 80]. Regarding its effects on sarcopenia, the current studies are too limited and controversial to draw firm conclusions [81].

Caloric restriction, which aims to reduce calorie intake without malnutrition is another intervention that has been identify to target aging [34, 82]. In mice, caloric restriction (~30% reduction of daily food intake) extends lifespan by at least 10% and up to 35%. It also attenuates age-related changes, notably by improving glucose homeostasis and delaying the increased expression of gene involved in immune processes and inflammation [82]. These health benefits are conserved in monkeys [83]. Observational and randomized clinical trials indicate that caloric restriction in humans results in some of the same metabolic and molecular adaptations [84, 85]. However, even if the results are appealing, there are several factors to consider. First, the ability to adhere to an intervention that imposes a calorie restriction of up to 25% over several months, or even years, requires a great deal of willpower and, in practice, is rarely, if ever, achievable [86]. Furthermore, caloric restriction induces weight loss and may result in a loss of muscle mass and bone mineral density. Therefore, decreasing caloric intake in older adults who are already exposed to compromised nutritional intake and at a high risk of sarcopenia does not seem to be a favorable approach [66, 80, 86]

Since the discovery that the removal of senescent cells can prevent or delay tissue dysfunction and extend healthspan [87], research for small chemical compounds that selectively kill senescent cells, referred to as “senolytics”, has intensified. These strategies have been extensively explored in a wide range of murine disease models associated with senescence and many clinical trials are underway [34, 50]. Following muscle injury, senescent cells accumulate in the skeletal muscle. Treatment with the senolytics Dasatinib and Quercetin in old mice was shown to improve regeneration, increase fiber cross-sectional area and enhanced physical function [88]. Administering these same senolytics also alleviates physical dysfunction and extends survival [89]. However, positive roles for senescent cells have also been proposed in exercised muscle [90]. There are still many unknowns about the relationship among senescent cells and skeletal muscle, requiring further study.

Efforts to find drugs that enhance healthspan by targeting the processes of aging have become a hot topic in the field. Resveratrol, a polyphenolic compound found in various plants, has garnered interest; however, its limited bioavailability restricts its potential. Rapamycin, an inhibitor of mTOR, is already FDA-approved for transplantation, and is also being explored in this context.

5. General conclusion

The results of these two studies collectively demonstrate the remarkable potential of AdipoRon as a therapeutic intervention for addressing age-related muscle decline and improving healthspan. AdipoRon leads to significant improvements in muscle mass, quality, and function, counteracting sarcopenia. Furthermore, AdipoRon provides protection against the metabolic and degenerative consequences of aging and excess calorie consumption. By offsetting various

hallmarks of aging, AdipoRon emerges as a promising anti-aging therapy for skeletal muscle and for promoting “healthy aging” (Figure 1).

PART II: PERSPECTIVES

1. Further explorations of AdipoRon in pre-clinical research

Senescent cells accumulate in multiple tissues with aging [50]. However, some studies suggest that senescent cells do not accumulate in resting skeletal muscle with aging, at least within the age ranges tested [51, 91, 92]. Accordingly, we did not detect markers of senescence (p16, p21) in the skeletal muscle of 23-month-old mice studied in the basal state. Conversely, in response to acute injury, senescent cells increase dramatically in the muscles of both young and old mice, as well as in humans [51]. Normally, their numbers later decrease as the injury heals, but this process is impaired with aging and senescent cells accumulate [51, 88, 92, 93]. Through their SASP, they release factors that trigger inflammation and lead to the formation of fibrosis, which hinders muscle regeneration [51, 52]. Therefore, investigating the potential impact of AdipoRon after muscle injury in mice would be a valuable perspective. The question would be to know whether AdipoRon, with its anti-inflammatory, antioxidant, and antifibrotic properties, can protect muscles against fibrosis and enhance muscle regeneration. The accumulation of senescent cells would be quantified, alongside various inflammatory and fibrotic markers of the SASP. Markers of regeneration (MyoD, Myf5, Myogenin, MRF4), which were not detected either in the basal state of our last study, would be thoroughly investigated. Muscle function would also be evaluated in vivo and ex vivo. Furthermore, effects of AdipoRon on senescence could be investigated in the mdx mouse model of Duchenne muscular dystrophy [94], characterized by continuous cycles of muscle necrosis and repair leading to fibrosis and weakness [8]. The potent effects of AdipoRon on improving the dystrophic phenotype have already been demonstrated by the laboratory [62], and these findings on senescence could provide additional insights into the underlying mechanisms.

Other treatment modalities with AdipoRon could also be explored. In the first study, the persisting effects of AdipoRon indicated that there was no habituation to this compound, and that the treatment was well-tolerated. An even longer treatment protocol, starting in adulthood and extending into old age, would be implemented and compared to that of an intermittent treatment. Throughout the protocol, we would perform whole-body computed tomography (CT) scans at different time points to non-invasively assess body composition and the muscle compartment. Additionally, blood samples will be taken to assess various SASP markers over the course of a lifetime. Tumor prevalence seemed to be higher in untreated old mice [14]. We would also determine the potential long-term protection of AdipoRon on cancer as ApN has been reported to exhibit anti-cancer properties, by reducing inflammation, oxidative stress, and cell proliferation [65]. Ideally, survival curves and lifespan could also be investigated. These studies will be conducted on a larger sample of animals. Firstly, because mouse attrition rates in these long-term studies tend to be higher. Additionally, to ensure an adequate quantity of materials for measuring the multiple parameters involved in aging. Finally, to mitigate the issue of age-induced variability in the results.

2. Other ApN receptors agonists

So far, the absence of clinical trials for AdipoRon is surprising: it is commercially available for a decade [18], tested successfully in multiple preclinical models and remains effective in humanized AdipoR1 mice [95]. Moreover, no side effects have been reported in rodents to date, including in our long-term study [13]. However, besides AdipoRon, several short peptides and small molecules have been identified to target AdipoRs and mimic some of ApN effects [8]. ALY688 (formerly known as ADP355) is one of those: it is a decapeptide AdipoRs agonist derived from the active site of human gApN, which acts preferentially through AdipoR1 [96]. This

compound is now developed by Allysta Pharmaceuticals with the hope of being a strong candidate for phase I clinical trials. Our group recently investigated a two-month treatment with ALY688 in dystrophic mice. ALY688 exerted protective anti-inflammatory, anti-oxidative and anti-fibrotic actions on the skeletal muscle and enhanced regeneration [97]. When we directly compared it *in vitro* to AdipoRon on human myotubes from patients with Duchenne muscular dystrophy, both exhibited similar protective effects. However, these effects were reached at much lower concentrations with ALY688 (100 nM vs 25 µM). Another difference is that, to date, AdipoRon has been used for research purposes only and no clinical trials are underway. With a step ahead in development, ALY688 could be a strong candidate for clinical evaluation in the near future.

3. Other potential effects of ApN mimics in aging

Adiponectin has pleiotropic effects, and the potential benefits of ApN replacement therapy with ApN mimetic drugs extend beyond skeletal muscle diseases/sarcopenia [14] and obesity-related disorders [13, 18]. AdipoRon penetrates the blood brain barrier, increases neurogenesis and reduces neuroinflammation and has therefore been proposed as a potential treatment for Alzheimer disease [98], depression [63] or anxiety [99]. ApN-based therapy is also regarded as a promising pharmacological approach in both cancer prevention and management [65], as mentioned *supra*. Last but not least, ApN mimetics are being studied as potential drugs to mimic some of the health benefits of exercise [72]. Of course, it is essential to recognize the intricate and complex physiological responses to exercise across various cells and organs. It's unlikely that any drug could ever fully replicate its broad effects [73], but it would actually offer a therapeutic option for people who are unable to engage in sufficient physical activity, for whatever reason. For instance, it might initiate a rehabilitation program for individuals with

morbid obesity or those recovering from severe injuries, at least until they are able to start exercising on their own [100].

Eventually, we could imagine a combination of several anti-aging strategies (diet, exercise, senolytics, ApN mimics and others) in order to promote and extend healthspan. Now that we live longer, the ultimate goal of this research is to add new life to years, not years to life, an idea which was already famously expressed by John Fitzgerald Kennedy in 1963.

REFERENCES

1. The Lancet Diabetes, E., *Opening the door to treating ageing as a disease.* Lancet Diabetes Endocrinol, 2018. **6**(8): p. 587.
2. Rabheru, K., J.E. Byles, and A. Kalache, *How "old age" was withdrawn as a diagnosis from ICD-11.* Lancet Healthy Longev, 2022. **3**(7): p. e457-e459.
3. Fakhouri, T.H., et al., *Prevalence of obesity among older adults in the United States, 2007-2010.* NCHS Data Brief, 2012(106): p. 1-8.
4. Tam, B.T., J.A. Morais, and S. Santosa, *Obesity and ageing: Two sides of the same coin.* Obes Rev, 2020. **21**(4): p. e12991.
5. Correa-de-Araujo, R., et al., *Myosteatosis in the Context of Skeletal Muscle Function Deficit: An Interdisciplinary Workshop at the National Institute on Aging.* Front Physiol, 2020. **11**: p. 963.
6. Alqahtani, S.A. and J.M. Schattenberg, *NAFLD in the Elderly.* Clin Interv Aging, 2021. **16**: p. 1633-1649.
7. Cruz-Jentoft, A.J. and A.A. Sayer, *Sarcopenia.* Lancet, 2019. **393**(10191): p. 2636-2646.
8. Abou-Samra, M., et al., *Adiponectin and Its Mimics on Skeletal Muscle: Insulin Sensitizers, Fat Burners, Exercise Mimickers, Muscling Pills … or Everything Together?* Int J Mol Sci, 2020. **21**(7).
9. Li, N., et al., *Adiponectin preserves metabolic fitness during aging.* Elife, 2021. **10**.
10. Arai, Y., K. Kamide, and N. Hirose, *Adipokines and Aging: Findings From Centenarians and the Very Old.* Front Endocrinol (Lausanne), 2019. **10**: p. 142.
11. Can, B., et al., *Serum markers of inflammation and oxidative stress in sarcopenia.* Aging Clin Exp Res, 2017. **29**(4): p. 745-752.
12. Van Berendoncks, A.M., et al., *Functional adiponectin resistance at the level of the skeletal muscle in mild to moderate chronic heart failure.* Circ Heart Fail, 2010. **3**(2): p. 185-94.
13. Selvais, C.M., et al., *AdipoRon enhances healthspan in middle-aged obese mice: striking alleviation of myosteatosis and muscle degenerative markers.* J Cachexia Sarcopenia Muscle, 2023. **14**(1): p. 464-478.
14. Selvais, C.M., et al., *Thwarting Sarcopenia: Exploring AdipoRon in aging skeletal muscle as a healthspan-Extending Shield.* Submitted.
15. List, E.O., et al., *The effects of weight cycling on lifespan in male C57BL/6J mice.* Int J Obes (Lond), 2013. **37**(8): p. 1088-94.
16. Otabe, S., et al., *Overexpression of human adiponectin in transgenic mice results in suppression of fat accumulation and prevention of premature death by high-calorie diet.* Am J Physiol Endocrinol Metab, 2007. **293**(1): p. E210-8.
17. Pettan-Brewer, C. and P.M. Treuting, *Practical pathology of aging mice.* Pathobiol Aging Age Relat Dis, 2011. **1**.
18. Okada-Iwabu, M., et al., *A small-molecule AdipoR agonist for type 2 diabetes and short life in obesity.* Nature, 2013. **503**(7477): p. 493-9.
19. Balasubramanian, P., et al., *Adiponectin receptor agonist AdipoRon improves skeletal muscle function in aged mice.* Elife, 2022. **11**.

20. Brady, S., et al., *Tubular Aggregates and Cylindrical Spirals Have Distinct Immunohistochemical Signatures.* J Neuropathol Exp Neurol, 2016. **75**(12): p. 1171-1178.
21. Schiaffino, S., *Tubular aggregates in skeletal muscle: just a special type of protein aggregates?* Neuromuscul Disord, 2012. **22**(3): p. 199-207.
22. Nishikawa, T., et al., *Tubular aggregates in the skeletal muscle of the senescence-accelerated mouse; SAM.* Mech Ageing Dev, 2000. **114**(2): p. 89-99.
23. Boncompagni, S., et al., *Long-Term Exercise Reduces Formation of Tubular Aggregates and Promotes Maintenance of Ca(2+) Entry Units in Aged Muscle.* Front Physiol, 2020. **11**: p. 601057.
24. Carnio, S., et al., *Autophagy impairment in muscle induces neuromuscular junction degeneration and precocious aging.* Cell Rep, 2014. **8**(5): p. 1509-21.
25. Zhou, J., et al., *Changes in macroautophagy, chaperone-mediated autophagy, and mitochondrial metabolism in murine skeletal and cardiac muscle during aging.* Aging (Albany NY), 2017. **9**(2): p. 583-599.
26. García-Prat, L., et al., *Autophagy maintains stemness by preventing senescence.* Nature, 2016. **529**(7584): p. 37-42.
27. Hansen, M., D.C. Rubinsztein, and D.W. Walker, *Autophagy as a promoter of longevity: insights from model organisms.* Nat Rev Mol Cell Biol, 2018. **19**(9): p. 579-593.
28. Liu, Y., et al., *Adiponectin stimulates autophagy and reduces oxidative stress to enhance insulin sensitivity during high-fat diet feeding in mice.* Diabetes, 2015. **64**(1): p. 36-48.
29. Huang, D.D., et al., *Nrf2 deficiency promotes the increasing trend of autophagy during aging in skeletal muscle: a potential mechanism for the development of sarcopenia.* Aging (Albany NY), 2020. **12**(7): p. 5977-5991.
30. Egan, D.F., et al., *Phosphorylation of ULK1 (hATG1) by AMP-activated protein kinase connects energy sensing to mitophagy.* Science, 2011. **331**(6016): p. 456-61.
31. Hurley, J.H. and L.N. Young, *Mechanisms of Autophagy Initiation.* Annu Rev Biochem, 2017. **86**: p. 225-244.
32. Ahlstrom, P., et al., *Adiponectin improves insulin sensitivity via activation of autophagic flux.* J Mol Endocrinol, 2017. **59**(4): p. 339-350.
33. Chistiakov, D.A., et al., *Mitochondrial aging and age-related dysfunction of mitochondria.* Biomed Res Int, 2014. **2014**: p. 238463.
34. López-Otín, C., et al., *Hallmarks of aging: An expanding universe.* Cell, 2023. **186**(2): p. 243-278.
35. Palikaras, K., E. Lionaki, and N. Tavernarakis, *Mechanisms of mitophagy in cellular homeostasis, physiology and pathology.* Nat Cell Biol, 2018. **20**(9): p. 1013-1022.
36. Leduc-Gaudet, J.P., et al., *Mitochondrial Dynamics and Mitophagy in Skeletal Muscle Health and Aging.* Int J Mol Sci, 2021. **22**(15).
37. Drake, J.C. and Z. Yan, *Mitophagy in maintaining skeletal muscle mitochondrial proteostasis and metabolic health with ageing.* J Physiol, 2017. **595**(20): p. 6391-6399.

38. Salminen, A. and K. Kaarniranta, *AMP-activated protein kinase (AMPK) controls the aging process via an integrated signaling network.* Ageing Res Rev, 2012. **11**(2): p. 230-41.
39. Reznick, R.M., et al., *Aging-associated reductions in AMP-activated protein kinase activity and mitochondrial biogenesis.* Cell Metab, 2007. **5**(2): p. 151-6.
40. Ghosh, S., et al., *Reduction in reactive oxygen species production by mitochondria from elderly subjects with normal and impaired glucose tolerance.* Diabetes, 2011. **60**(8): p. 2051-60.
41. Kang, C., et al., *Exercise training attenuates aging-associated mitochondrial dysfunction in rat skeletal muscle: role of PGC-1α.* Exp Gerontol, 2013. **48**(11): p. 1343-50.
42. Chabi, B., et al., *Mitochondrial function and apoptotic susceptibility in aging skeletal muscle.* Aging Cell, 2008. **7**(1): p. 2-12.
43. Kim, Y., et al., *The Adiponectin Receptor Agonist AdipoRon Ameliorates Diabetic Nephropathy in a Model of Type 2 Diabetes.* J Am Soc Nephrol, 2018. **29**(4): p. 1108-1127.
44. Dugan, B., J. Conway, and N.A. Duggal, *Inflammaging as a target for healthy ageing.* Age Ageing, 2023. **52**(2).
45. Arai, Y., et al., *Inflammation, But Not Telomere Length, Predicts Successful Ageing at Extreme Old Age: A Longitudinal Study of Semi-supercentenarians.* EBioMedicine, 2015. **2**(10): p. 1549-58.
46. Furman, D., et al., *Chronic inflammation in the etiology of disease across the life span.* Nat Med, 2019. **25**(12): p. 1822-1832.
47. Yousefzadeh, M.J., et al., *Circulating levels of monocyte chemoattractant protein-1 as a potential measure of biological age in mice and frailty in humans.* Aging Cell, 2018. **17**(2).
48. Sciorati, C., et al., *Pharmacological blockade of TNFα prevents sarcopenia and prolongs survival in aging mice.* Aging (Albany NY), 2020. **12**(23): p. 23497-23508.
49. Khosla, S., et al., *The role of cellular senescence in ageing and endocrine disease.* Nat Rev Endocrinol, 2020. **16**(5): p. 263-275.
50. Zhang, L., et al., *Cellular senescence: a key therapeutic target in aging and diseases.* J Clin Invest, 2022. **132**(15).
51. Moiseeva, V., et al., *Senescence atlas reveals an aged-like inflamed niche that blunts muscle regeneration.* Nature, 2023. **613**(7942): p. 169-178.
52. Glass, D.J., *Senescent cells damage the body throughout life.* Nature, 2023. **613**(7942): p. 30-31.
53. Aleixo, G.F.P., et al., *Myosteatosis and prognosis in cancer: Systematic review and meta-analysis.* Crit Rev Oncol Hematol, 2020. **145**: p. 102839.
54. Miljkovic, I., et al., *Greater Skeletal Muscle Fat Infiltration Is Associated With Higher All-Cause and Cardiovascular Mortality in Older Men.* J Gerontol A Biol Sci Med Sci, 2015. **70**(9): p. 1133-40.
55. Nachit, M. and I.A. Leclercq, *Emerging awareness on the importance of skeletal muscle in liver diseases: time to dig deeper into mechanisms!* Clin Sci (Lond), 2019. **133**(3): p. 465-481.

56. Andrich, D.E., et al., *Altered Lipid Metabolism Impairs Skeletal Muscle Force in Young Rats Submitted to a Short-Term High-Fat Diet.* Front Physiol, 2018. **9**: p. 1327.
57. Choi, S.J., et al., *Intramyocellular Lipid and Impaired Myofiber Contraction in Normal Weight and Obese Older Adults.* J Gerontol A Biol Sci Med Sci, 2016. **71**(4): p. 557-64.
58. Mahdy, M.A.A., *Skeletal muscle fibrosis: an overview.* Cell Tissue Res, 2019. **375**(3): p. 575-588.
59. Wood, L.K., et al., *Intrinsic stiffness of extracellular matrix increases with age in skeletal muscles of mice.* J Appl Physiol (1985), 2014. **117**(4): p. 363-9.
60. Giacomello, E., et al., *Age Dependent Modification of the Metabolic Profile of the Tibialis Anterior Muscle Fibers in C57BL/6J Mice.* Int J Mol Sci, 2020. **21**(11).
61. Wilkinson, D.J., M. Piasecki, and P.J. Atherton, *The age-related loss of skeletal muscle mass and function: Measurement and physiology of muscle fibre atrophy and muscle fibre loss in humans.* Ageing Res Rev, 2018. **47**: p. 123-132.
62. Abou-Samra, M., et al., *AdipoRon, a new therapeutic prospect for Duchenne muscular dystrophy.* J Cachexia Sarcopenia Muscle, 2020. **11**(2): p. 518-533.
63. Nicolas, S., et al., *Adiporon, an adiponectin receptor agonist acts as an antidepressant and metabolic regulator in a mouse model of depression.* Transl Psychiatry, 2018. **8**(1): p. 159.
64. Sheka, A.C., et al., *Nonalcoholic Steatohepatitis: A Review.* Jama, 2020. **323**(12): p. 1175-1183.
65. Nigro, E., et al., *AdipoRon and Other Adiponectin Receptor Agonists as Potential Candidates in Cancer Treatments.* Int J Mol Sci, 2021. **22**(11).
66. Seals, D.R., J.N. Justice, and T.J. LaRocca, *Physiological geroscience: targeting function to increase healthspan and achieve optimal longevity.* J Physiol, 2016. **594**(8): p. 2001-24.
67. Kerr, N.R. and F.W. Booth, *Contributions of physical inactivity and sedentary behavior to metabolic and endocrine diseases.* Trends Endocrinol Metab, 2022. **33**(12): p. 817-827.
68. Cruz-Jentoft, A.J., et al., *Sarcopenia: revised European consensus on definition and diagnosis.* Age Ageing, 2019. **48**(4): p. 601.
69. Dent, E., et al., *International Clinical Practice Guidelines for Sarcopenia (ICFSR): Screening, Diagnosis and Management.* J Nutr Health Aging, 2018. **22**(10): p. 1148-1161.
70. Cho, M.R., S. Lee, and S.K. Song, *A Review of Sarcopenia Pathophysiology, Diagnosis, Treatment and Future Direction.* J Korean Med Sci, 2022. **37**(18): p. e146.
71. Rivera-Torres, S., T.D. Fahey, and M.A. Rivera, *Adherence to Exercise Programs in Older Adults: Informative Report.* Gerontol Geriatr Med, 2019. **5**: p. 2333721418823604.
72. Iwabu, M., et al., *Elucidating exercise-induced skeletal muscle signaling pathways and applying relevant findings to preemptive therapy for lifestyle-related diseases.* Endocr J, 2022. **69**(1): p. 1-8.

73. Hawley, J.A., M.J. Joyner, and D.J. Green, *Mimicking exercise: what matters most and where to next?* J Physiol, 2021. **599**(3): p. 791-802.
74. Hawley, J.A., et al., *Integrative biology of exercise.* Cell, 2014. **159**(4): p. 738-49.
75. Campos, J.C., et al., *Exercise preserves physical fitness during aging through AMPK and mitochondrial dynamics.* Proc Natl Acad Sci U S A, 2023. **120**(2): p. e2204750120.
76. Soukas, A.A., H. Hao, and L. Wu, *Metformin as Anti-Aging Therapy: Is It for Everyone?* Trends Endocrinol Metab, 2019. **30**(10): p. 745-755.
77. Foretz, M., et al., *Metformin: from mechanisms of action to therapies.* Cell Metab, 2014. **20**(6): p. 953-66.
78. Foretz, M., B. Guigas, and B. Viollet, *Metformin: update on mechanisms of action and repurposing potential.* Nat Rev Endocrinol, 2023. **19**(8): p. 460-476.
79. Campbell, J.M., et al., *Metformin reduces all-cause mortality and diseases of ageing independent of its effect on diabetes control: A systematic review and meta-analysis.* Ageing Res Rev, 2017. **40**: p. 31-44.
80. Li, Z., et al., *Aging and age-related diseases: from mechanisms to therapeutic strategies.* Biogerontology, 2021. **22**(2): p. 165-187.
81. Song, Y., Z. Wu, and P. Zhao, *The Function of Metformin in Aging-Related Musculoskeletal Disorders.* Front Pharmacol, 2022. **13**: p. 865524.
82. Acosta-Rodríguez, V., et al., *Circadian alignment of early onset caloric restriction promotes longevity in male C57BL/6J mice.* Science, 2022. **376**(6598): p. 1192-1202.
83. Mattison, J.A., et al., *Caloric restriction improves health and survival of rhesus monkeys.* Nat Commun, 2017. **8**: p. 14063.
84. Longo, V.D. and R.M. Anderson, *Nutrition, longevity and disease: From molecular mechanisms to interventions.* Cell, 2022. **185**(9): p. 1455-1470.
85. Most, J., et al., *Calorie restriction in humans: An update.* Ageing Res Rev, 2017. **39**: p. 36-45.
86. Flanagan, E.W., et al., *Calorie Restriction and Aging in Humans.* Annu Rev Nutr, 2020. **40**: p. 105-133.
87. Baker, D.J., et al., *Clearance of p16Ink4a-positive senescent cells delays ageing-associated disorders.* Nature, 2011. **479**(7372): p. 232-6.
88. Dungan, C.M., et al., *Deletion of SA β-Gal+ cells using senolytics improves muscle regeneration in old mice.* Aging Cell, 2022. **21**(1): p. e13528.
89. Xu, M., et al., *Senolytics improve physical function and increase lifespan in old age.* Nat Med, 2018. **24**(8): p. 1246-1256.
90. Saito, Y., et al., *Exercise enhances skeletal muscle regeneration by promoting senescence in fibro-adipogenic progenitors.* Nat Commun, 2020. **11**(1): p. 889.
91. Dungan, C.M., et al., *Senolytic treatment rescues blunted muscle hypertrophy in old mice.* Geroscience, 2022. **44**(4): p. 1925-1940.
92. Dungan, C.M., J.M. Wells, and K.A. Murach, *The life and times of cellular senescence in skeletal muscle: friend or foe for homeostasis and adaptation?* Am J Physiol Cell Physiol, 2023. **325**(1): p. C324-c331.

93. Young, L.V., et al., *Muscle injury induces a transient senescence-like state that is required for myofiber growth during muscle regeneration.* Faseb j, 2022. **36**(11): p. e22587.
94. Sugihara, H., et al., *Cellular senescence-mediated exacerbation of Duchenne muscular dystrophy.* Sci Rep, 2020. **10**(1): p. 16385.
95. Iwabu, M., et al., *AdipoR agonist increases insulin sensitivity and exercise endurance in AdipoR-humanized mice.* Commun Biol, 2021. **4**(1): p. 45.
96. Otvos, L., Jr., et al., *Design and development of a peptide-based adiponectin receptor agonist for cancer treatment.* BMC Biotechnol, 2011. **11**: p. 90.
97. Dubuisson, N., et al., *The Adiponectin Receptor Agonist, ALY688: A Promising Therapeutic for Fibrosis in the Dystrophic Muscle.* Cells, 2023. **12**(16).
98. Ng, R.C., et al., *Chronic oral administration of adipoRon reverses cognitive impairments and ameliorates neuropathology in an Alzheimer's disease mouse model.* Mol Psychiatry, 2021. **26**(10): p. 5669-5689.
99. Sun, F., et al., *Adiponectin modulates ventral tegmental area dopamine neuron activity and anxiety-related behavior through AdipoR1.* Mol Psychiatry, 2019. **24**(1): p. 126-144.
100. Hunter, P., *Exercise in a bottle: Elucidating how exercise conveys health benefits might lead to new therapeutic options for a range of diseases from cancer to metabolic syndrome.* EMBO Rep, 2016. **17**(2): p. 136-8.
101. Tanabe, H., et al., *Crystal structures of the human adiponectin receptors.* Nature, 2015. **520**(7547): p. 312-316.

ANNEXES

ANNEX 1: LIST OF ABBREVIATIONS

4EBP1	Eukaryotic translation initiation factor 4E (eIF4E)-binding protein 1
ACC2	Acetyl-CoA carboxylase 2
ACO	Acyl-CoA oxidase
AdipoR1	Adiponectin receptor 1
AdipoR2	Adiponectin receptor 2
AMPK	AMP-activated protein kinase
ApN	Adiponectin
ATG	autophagy-related genes
ATP	Adenosin triphosphate
BMI	Body mass index
C/EBPα	CAAT/enhancer-binding protein alpha
Ca	Calcium
CaMK	Calcium/Calmodulin-Dependent Protein Kinase
CAMKK	Calmodulin-dependent protein kinase kinase beta
CD36	Cluster of differentiation 36
COX	Cytochrome C oxidase
CPT1	Carnitine palmitoyltransferase 1
CREB	cAMP response element-binding protein
DAG	Diacylglycerol
DMD	Duchenne muscular Dystrophy
EMCL	Extramyocellular lipids
ERRα	Estrogen-related receptor alpha
FAT/CD36	Fatty acid translocase
Fis1	Fission protein 1
FoxO3a	Forkhead box protein O3a
gAPN	Globular adiponectin

GLUT4	Glucose transporter type 4
HFD	High-fat diet
HMW	High-molecular-weight form
IGF1	Insulin-like growth factor 1
IMCL	Intramyocellular lipids
IMF	Intermyofibrillar
IRS-1	Insulin receptor substrate-1
LC3	Microtubule-associated protein 1A/1B-light chain 3 protein
LCA-COA	Long chain acyl-CoA
LDs	Lipid droplets
LIR	LC3-interacting region
LKB1	Liver kinase B1
LMW	Low-molecular-weight form
MAPK	p38 mitogen-activated protein kinase
Mff	Mitochondrial fission factor
MMW	Middle-molecular-weight form
mtDNA	Mitochondrial deoxyribonucleic acid
mTOR	Mammalian target of rapamycin
NAFLD	Non-alcoholic Fatty Liver Disease
NASH	Non-alcoholic steatohepatitis
nDNA	Nuclear deoxyribonucleic acid
NEFA	Non-esterified free fatty acids
NF-κB	Nuclear factor kappa B
NRF-1/2	Nuclear respiratory factor 1 and 2
OXPHOS	Oxidative phosphorylation
p16	p16INK4A
p21	p21Cip1
p62	Ubiquitin-binding protein p62

p70S6K1	Ribosomal protein S6 kinase beta-1
PGC-1α	Proliferator-activated receptor gamma coactivator 1-alpha
PI3KC3	Class III phosphatidylinositol-3 kinase
PINK1	Phosphatase and tensin homolog (PTEN)-induced kinase 1
PLIN	Perilipin
PPARα	Peroxisome proliferator-activated receptor alpha
PPARγ	Peroxisome proliferator-activated receptor gamma
ROS	Reactive oxygen species
SASP	Senescence-secretory associated phenotype
SIRT1	Sirtuin 1
SMAD2	SMAD Family Member 2
SREBP	Sterol regulatory element-binding protein
SS	Subsarcolemmal
T-tubule	Transverse tubular system
TAG	Triacyglycerol
TAgs	Tubular aggregates
TF	Transcription factors
TFAM	Mitochondrial transcription factor A
ULK1	Unc-51-like kinase 1
UPS	Ubiquitin proteasom system

ANNEX 2

Fiber type and subcellular-specific analysis of lipid droplet content in skeletal muscle with Bodipy.

Camille M. Selvais[1], Laura L. De Cock[1], Sonia M. Brichard[1] and Maria A. Davis-López de Carrizosa[1,3].

1. Endocrinology, Diabetes and Nutrition Unit, Institute of Experimental and Clinical Research, Medical Sector, Université Catholique de Louvain, 1200 Brussels, Belgium.
2. Departamento de Fisiología, Facultad de Biología, Universidad de Sevilla, 41012 Seville, Spain.

* Correspondence: María A. Davis-López de Carrizosa (mayadavis@us.es)

Fiber Type and Subcellular-Specific Analysis of Lipid Droplet Content in Skeletal Muscle

Camille M. Selvais[1], Laura L. De Cock[1], Sonia M. Brichard[1], María A. Davis-López de Carrizosa[1,2]

[1] Endocrinology, Diabetes and Nutrition Unit, Institute of Experimental and Clinical Research, Medical Sector, Université Catholique de Louvain [2] Departamento de Fisiología, Facultad de Biología, Universidad de Sevilla

Corresponding Author

María A. Davis-López de Carrizosa
mayadavis@us.es

Citation

Selvais, C.M., De Cock, L.L., Brichard, S.M., Davis-López de Carrizosa, M.A. Fiber Type and Subcellular-Specific Analysis of Lipid Droplet Content in Skeletal Muscle. *J. Vis. Exp.* (184), e63718, doi:10.3791/63718 (2022).

Date Published

June 8, 2022

DOI

10.3791/63718

URL

jove.com/video/63718

Abstract

Skeletal muscle lipid infiltration, known as myosteatosis, increases with obesity and ageing. Myosteatosis has also recently been discovered as a negative prognostic factor for several other disorders such as cardiovascular disease and cancer. Excessive lipid infiltration decreases muscle mass and strength. It also results in lipotoxicity and insulin resistance depending on total intramyocellular lipid content, lipid droplet (LD) morphology, and subcellular distribution. Fiber type (oxidative vs glycolytic) is also important, since oxidative fibers have a greater capacity to utilize lipids. Because of their crucial implications in pathophysiology, in-depth studies on LD dynamics and function in a fiber type-specific manner are warranted.

Herein, a complete protocol is presented for the quantification of intramyocellular lipid content and analysis of LD morphology and subcellular distribution in a fiber type-specific manner. To this end, serial muscle cryosections were stained with the fluorescent dye Bodipy and antibodies against myosin heavy chain isoforms. This protocol enables the simultaneous processing of different muscles, saving time and avoiding possible artifacts and, thanks to a personalized macro created in Fiji, the automatization of LD analysis is also possible.

Introduction

Skeletal muscle lipid infiltration, known as myosteatosis, increases with obesity and ageing. Myosteatosis is negatively correlated with muscle mass and strength and with insulin sensitivity[1]. Moreover, recent studies indicate that the degree of myosteatosis could be used as a prognostic factor for other conditions such as cardiovascular disease[2], non-alcoholic fatty liver disease[3], or cancer[4]. Lipids can accumulate in skeletal muscle between muscle fibers as extramyocellular lipids or within the fibers, as intramyocellular lipids (IMCLs). IMCLs are predominantly stored as triglycerides in lipid droplets (LDs) that are used as metabolic fuel during physical exercise[5,6]. However, when lipid supply exceeds demand, or when mitochondria become dysfunctional, IMCLs will be implicated in muscle insulin resistance, as seen

in metabolically unhealthy, obese individuals and in type 2 diabetes patients[7]. Intriguingly, endurance athletes have similar, if not higher, levels of IMCLs to those found in obese patients with type 2 diabetes mellitus, while maintaining high insulin sensitivity. This phenomenon is described as the "athlete's paradox"[8,9], and is explained by a more nuanced appraisal of muscle LDs, related to their size, density, localization, dynamics, and lipid species composition.

First, LD size is inversely correlated to insulin sensitivity and physical fitness[10,11]. In fact, smaller LDs exhibit a relatively greater surface area for lipase action and, thus, potentially have a greater capacity to mobilize lipids[12]. Second, LD density (number/surface) plays a controversial role in insulin action[8,10]; yet, it seems to be increased in athletes. Third, the subcellular localization of LDs is important, since LDs located just below the surface membrane (subsarcolemmal or peripheral) exert a more deleterious effect on insulin sensitivity than central ones[8,9,13]. The latter provide fuel to central mitochondria, which have a greater respiratory activity and are more specialized to meet the high energy demand required for contraction[14]. By contrast, peripheral LDs supply subsarcolemmal mitochondria, which are involved in membrane-related processes[8]. Finally, beyond triglycerides, specific complex lipids within the muscle may be more deleterious than others. For instance, diacylglycerol, long-chain acyl-CoA, and ceramides may accumulate in muscle when the triglyceride turnover rate is low, thereby impairing insulin signaling[9,15]. Returning to the "athlete's paradox," endurance athletes have a high number of smaller central LDs with elevated turnover rates in type I (oxidative) fibers, while obese and diabetic patients have larger peripheral LDs with low turnover rates in type II (glycolytic) fibers[8,15,16]. In addition to their role in energy storage and release, LDs *via* derived fatty acids (FA) and a coat protein (perilipin 5) could also function as critical players involved in the transcriptional regulation of FA oxidation and mitochondrial biogenesis[8]. Because of their crucial implications in physiology and pathophysiology, in-depth studies on LDs dynamics and functions are warranted.

Although there are several techniques to study IMCLs, they are not all suitable to accurately quantify LD size, density, and distribution in a fiber-specific manner. For example, the assessment of IMCLs by magnetic resonance spectroscopy, while being non-invasive, offers a level of resolution that is not sufficient to study the size and precise location of LDs within the fiber, and it is not fiber-type specific[17,18]. Likewise, biochemical techniques performed on whole-muscle homogenates[19] cannot assess the location and size of lipids. Consequently, the most adequate method to analyze LD morphology and location is quantitative transmission electronic microscopy[13], but this technique is expensive and time-consuming. Therefore, confocal fluorescence imaging on preparations with dyes such as Oil Red O (ORO)[20,21], monodansylpentane (MDH)[22], or Bodipy[23,24,25], has emerged as the best tool for these studies.

Here, a complete protocol is described, including tissue sampling and processing, Bodipy staining, and confocal image acquisition and analysis to quantify LD size, number, and localization in mouse muscle cryosections. Since IMCLs are not evenly distributed among oxidative and glycolytic fibers, and each fiber type regulates LD dynamics differently, the study of IMCLs must be fiber-type specific[16,25,26,27]. Therefore, this protocol uses immunofluorescence on serial sections to identify myosin heavy chain (MyHC) isoform(s) expressed by each fiber. Another advantage of this protocol is the simultaneous processing of a glycolytic

(extensor digitorum longus, EDL) and an oxidative (soleus) muscle placed side-by-side before freezing (**Figure 1**). This simultaneous processing not only saves time but also avoids variability due to separate processing of the samples.

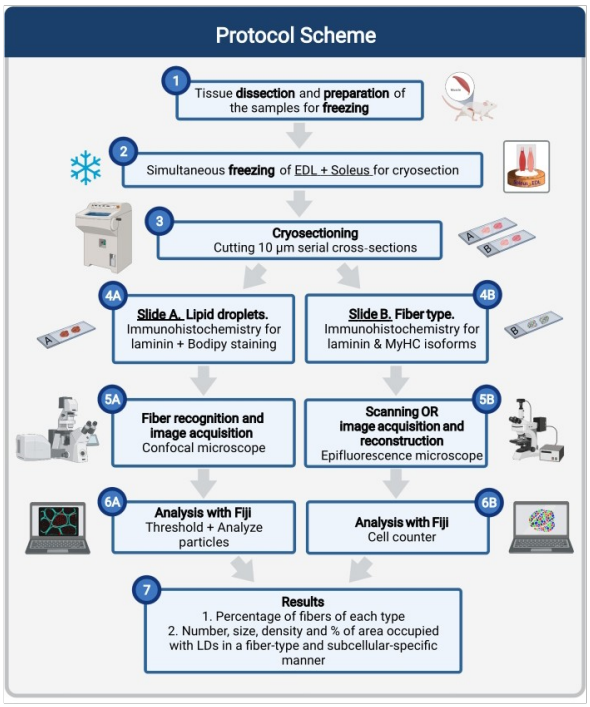

Figure 1: Schematic overview of the procedure. After muscle dissection (1), similar-size selected muscles are prepared and frozen together (2). Serial transverse sections of 10 µm are obtained using a cryostat and directly mounted on adhesion slides (3). From two serial slides, the first (4A) is immunolabeled for laminin and stained with Bodipy to recognize LDs and the second (4B) is immunostained with antibodies against MyHCs for the recognition of muscle fiber types. Images are acquired using a confocal microscope for Bodipy (5A) and an epifluorescence microscope for muscle fiber types (5B). Images are analyzed in Fiji by applying a threshold and quantifying particles (6A) to obtain the number, average size, density, and percentage of the total area occupied by LDs (7) or counting cells (6B) to obtain the percentage of fibers of each

type in the section (7). Abbreviations: LDs = lipid droplets; EDL = extensor digitorum longus; MyHCs = myosin heavy chain isoforms. Please click here to view a larger version of this figure.

Protocol

All procedures conducted on mice were approved by the Ethical Committee for Animal Experimentation from the Medical Sector at Université Catholique de Louvain (2019/UCL/MD/013).

1. Dissection and preparation of the samples for freezing

1. Label a 3 mm thick piece of cork for each pair of muscles.
2. Through a small incision made with a blade on the center of the cork, insert perpendicularly a rectangular piece of rigid plastic (0.5 cm W, 1 cm H) that will serve as support (**Figure 2B**).
   NOTE: The size of the rectangular plastic piece will depend on the size of the muscle. Here, the described dimensions are adapted to the size of the soleus (~9 mg, 1 cm L, 2-3 mm W) and EDL (~5 mg, 1 cm L, 2-3 mm W) of a 3-month-old C57BL/6J male mouse.
3. At the time of dissection, remove the soleus and EDL of the mouse hind limb. To prevent the samples from drying out during dissection, place them on a compress lightly moistened with saline solution in a Petri dish placed on ice.
   NOTE: See Wang et al.[28] for explanations on how to dissect these two limb muscles.
4. Place a small drop of Optimal Cutting Temperature compound (OCT) at the cork/plastic junction, avoiding air bubbles.
5. Eliminate excess moisture from the samples by gently drying them with a paper towel (**Figure 2A**) and place both muscles on the plastic perpendicular to the cork (**Figure 2C**).
6. Check the orientation of the muscle myofibers under a stereo microscope (**Figure 2D**).
   NOTE: It is important not to cover the muscle with OCT, since its insulating effect would prevent rapid freezing and will produce freezing artifacts.

2. Freezing skeletal muscle samples for cryosectioning

CAUTION: Freezing of the muscle must be done under a chemical hood, wearing appropriate personal protective equipment (see the **Table of Materials**).

1. Use a stainless-steel tumbler (~8 cm H, 6 cm Ø) with two side straps attached to it at least 25 cm long (**Figure 2F**), and fill the tumbler up to 2/3 of its capacity with isopentane.
2. Grabbing the tumbler by the straps, immerse it gently in a polystyrene box filled with liquid nitrogen so that the level of nitrogen outside the container is above the level of isopentane inside (**Figure 2F,G**).
   CAUTION: When the tumbler comes into contact with the nitrogen, the thermal shock may cause swirling. Ensure that the tumbler is sufficiently immersed but avoid the entry of nitrogen as this would cause isopentane precipitation. If this happens, let the isopentane cool down, fill the tumbler with new isopentane and start over.

3. When the inside of the tumbler is completely covered with a white solid layer of isopentane, take it out of the liquid nitrogen box (**Figure 2H**).

   NOTE: The melting temperature of isopentane being -159 °C, the edges of the tumbler will turn white when it is cold enough.

4. Gently stir the solid isopentane pieces into the remaining liquid isopentane with forceps until the entire volume becomes liquid again.

5. Re-immerse the tumbler in the liquid nitrogen until isopentane forms white pebbles all over the bottom and edges of the tumbler (**Figure 2G,H**).

   NOTE: This second cooling step ensures the appropriate freezing temperature of the isopentane.

6. Remove the tumbler from the liquid nitrogen and quickly dip the muscles in the bottom of the tumbler, holding the cork with rat tooth tweezers. Swirl the cork for 15 s in the isopentane and store it at -80 °C until processing (**Figure 2I**).

   NOTE: For short-term storage, the samples can be maintained in a -20 °C freezer. The complete protocol for rapid freezing of skeletal muscle has already been published elsewhere. For detailed references and troubleshooting, see: Meng et al.[29], Kumar et al.[30], and Leiva-Cepas et al.[31].

3. Cryosectioning

1. Bring the samples into the chamber of a cryostat previously cooled to -20 °C and the blade temperature set to -25 °C.

   NOTE: Transport samples from the -20 °C/-80 °C freezer to the cryostat in a polystyrene box filled with dry ice and allow the samples to equilibrate for at least 20-30 min to the chamber temperature before cutting.

2. Remove the plastic from the cork with fine tweezers and place the cryostat specimen disc on the quick freeze plate to cool. Once the plate has reached -50 °C, place some OCT on the disc and quickly place the cork on top of the disk, pressing firmly. Wait until the OCT solidifies and the cork is well fixed on the disc.

3. Place the disc on the object head in the desired cutting orientation (**Figure 2J,K**) and trim the muscle block beyond at least 1/3 of the length of the muscles and until both cross sections of the muscles are visible.

4. Set the cutting thickness to 10 µm and place one section on an adhesion slide to check the correct orientation of the fibers on a brightfield microscope.

   NOTE: Checking the transverse orientation of the fibers is critical. If the fibers are not adequately oriented, adjust the angle of the object head, cut another section and check again.

5. Place two serial cross-sections on two prelabeled adhesion slides: one slide to determine fiber types, the other to quantify lipid content (**Figure 2L**).

   NOTE: Additional serial cross sections can be obtained and kept at -80 °C for other histological studies. However, to avoid altering the lipid content and intracellular morphology[24], it is essential to process the first two slides immediately after cutting to prevent air-drying. Freezing and thawing the slides for LD quantification would have the same effect and is thus highly inadvisable.

4. Fiber typing and Bodipy staining

1. Immunohistochemical detection of muscle fiber type

NOTE: For the following protocol, a total solution volume of 250 µL is sufficient to cover the entire muscle section surrounded by a circle drawn with a hydrophobic pen the approximate size of a 1 cent coin.

1. Surround the sections with an outline drawn with a hydrophobic pen and rinse with ice-cold 0.1 M phosphate-buffered saline (PBS) for 1 min at room temperature (RT). Place the slide in a humid chamber and block for 90 min at 37 °C in blocking solution (10% normal goat serum (NGS) and 1:30 mouse on mouse (MOM) blocking reagent in PBS).

2. Remove the blocking solution and incubate the slides for 90 min at 37 °C with the solution containing the primary antibodies (5% NGS, 1:30 MOM blocking reagent, the mouse primary antibodies to recognize type I (IgG2b, at 1:10), type IIa (IgG1, at 1:10), and type IIx (IgM, at 1:5) fibers and a rat anti-laminin (α2 chain, 1:1,000) in PBS.

3. Wash the slides with PBS 3 x 5 min at RT.

4. Incubate the slides in the dark for 1 h at RT with the solution containing the secondary antibodies (goat anti-IgG2b AF405 (1:500), goat anti-IgG1 AF488 (1:500), goat anti-IgM AF568 (1:1,000), and goat anti-laminin AF647 (1:500) in PBS).
   CAUTION: For the rest of the protocol, make sure to keep the slides away from light to preserve the fluorescence.

5. Wash again 3 x 5 min in PBS, rinse in double-distilled H_2O, remove excess water, and mount with an antifade reagent.
   NOTE: Store the slides at 4 °C, protected from light to preserve the fluorescence until image acquisition. Since the slides are not fixed, it is recommended to use freshly made solutions for each experiment, autoclave the PBS, and acquire the images as soon as possible to avoid contamination of the sections.

2. Staining of LDs with Bodipy
   NOTE: Similar to step 4.1., a total solution volume of 250 µL is sufficient to cover the entire muscle section surrounded by a circle drawn with a hydrophobic pen the approximate size of a 1 cent coin.

   1. Surround the sections with an outline drawn by a hydrophobic pen and rinse with ice-cold 0.1 M PBS for 10 min at RT. Use ice-cold PBS for all the rinses and washes.

   2. Fix with cold 4% paraformaldehyde (PFA) without methanol for 10 min at RT. After a first quick rinse, wash the slides with PBS 3 x 5 min at RT.
      CAUTION: Perform this step under a chemical hood.

   3. Place the slide in a humid chamber and block for 1 h at RT with 5% NGS in PBS.

   4. Incubate the slides for 90 min at 37 °C with the solution of the primary antibody (2% NGS and rat anti-laminin (α2 chain, 1:1,000) in PBS). Wash the slides with PBS 3 x 5 min at RT.
      CAUTION: For the rest of the protocol, make sure to keep the slides away from light to preserve the fluorescence.

   5. Incubate for 1 h at RT with the secondary antibody solution containing goat anti-rat-AF647 antibody (1:500) in PBS. Wash the slides with PBS 3 x 5 min at RT.

   6. Incubate for 20 min at RT with a solution of 4',6-diamidino-2-phenylindole (DAPI, 0.5 µg/mL) and BODIPY (1 µg/mL) in PBS.

NOTE: To prepare BODIPY stock solution, dissolve it in DMSO at a concentration of 1 mg/mL. Different Bodipy formulations are commercially available for LD staining. Depending on the choice made, the staining method is the same (same steps, concentration, and incubation time); however, the acquisition method will be slightly different.

7. After a first quick rinse, wash the slides with PBS 3 x 5 min at RT, rinse in double-distilled H_2O, remove excess water, and mount with an antifade reagent.
   NOTE: Store the slides at 4 °C, protected from light, to preserve the fluorescence until image acquisition.

5. Acquisition of images

NOTE: Once the staining protocols have been completed, it is important to proceed immediately to image acquisition (within the following 24 h), not only to avoid contamination but also to preserve the morphology, size, and number of LDs.

1. Acquisition of images to assess the fiber-types of each muscle sampled
   NOTE: This step could be achieved with a whole-slide fluorescence scanning microscope or with a conventional epifluorescence microscope. With the latter, manual or automated stitching of the images must be done to reconstruct the section.
   1. For fiber-type recognition, use an epifluorescence microscope with a 10x/0.3 objective. Select excitation filters for DAPI (405 nm), FITC, TRITC, and Cy5 to detect type I, IIa, IIx fibers, and laminin, respectively.
      NOTE: Type IIb fibers will not be immunolabeled. They will be recognized as fibers stained by laminin on the limits of the sarcolemma with a black sarcoplasm.
   2. Adjust the appropriate exposure time for each channel.
   3. When using a conventional epifluorescence microscope, always acquire the images of the entire muscle following the same order to facilitate muscle reconstruction. Make sure that the fibers on the right edge of one image also appear on the left edge of the following image. The same applies for the top and the bottom parts of the images (**Figure 3A**).
      NOTE: As a reference, for a section of the EDL or the soleus dissected from a 3-month-old mouse, an average of six and eight images, respectively, will cover the entire muscle cross-section.
   4. After the muscle is scanned, upload the captured digital images into any image-processing software for reconstruction (stitching), based on the fiber morphology (laminin) and the histology of the muscle section, and save it as a TIFF, PNG, or JPG file with all the channels (colors) merged (**Figure 3A**).
2. Acquisition of images with laminin and Bodipy co-staining
   NOTE: To recognize the fiber type and have an estimate of the number of fibers for each type captured, it is essential to have the fiber-type section already scanned and the muscles reconstructed before starting the image acquisition of Bodipy-laminin (**Figure 3B**).
   1. For Bodipy image observation and acquisition, use a confocal microscope with a 40x oil immersion objective lens with a numerical aperture of 1.4.
   2. Use the following settings: pinhole at 1 AU, 2,048 pixel x 2,048 pixel resolution, pixel size at 0.08 µm,

unidirectional mode, scan speed at 4 (~4 µs/pixel), line averaging set to 4x, and digital zoom set to 1.

3. To avoid cross-talk between Bodipy-558/568 and laminin-AF647, use the sequential scan mode on the confocal software.

   NOTE: When the dye chosen is Bodipy-493/503, simultaneous confocal laser scanning is possible with no crosstalk between the Bodipy channel and laminin-AF647 channel. This will speed up the acquisition of images.

4. Excite Bodipy-493/503 using the 488 nm laser line or argon laser line, and excite Bodipy-555/568 using the 561 nm diode laser line. Finally, detect laminin-AF647 with a 640 nm diode laser line.

   CAUTION: Bear in mind that Bodipy molecules are very sensitive to photobleaching, so avoid unnecessary laser scanning. To recognize fibers, use only the laser for laminin.

5. Depending on the dye chosen, set the emission ranges at 570-650 nm for Bodipy-493/503[24] and at 565-620 nm for Bodipy-558/568. Set the emission range for laminin at 656-700 nm.

6. Set the gain and digital gain appropriately so no saturated pixels are detected on the range indicator. Correct the background signal by adjusting the offset.

   NOTE: Filter selection and other above-mentioned scanning parameters must be optimized for each confocal microscope. It is important that all the above-mentioned settings are kept constant for all the images captured from samples to be compared.

7. To identify the type of fiber among those visualized on the confocal microscope, use a personal laptop on which the image of the section reconstructed after fiber-type immunodetection is checked (**Figure 3B**).

8. Once a group of fibers is correctly identified, acquire the image with the Bodipy and laminin channels.

   NOTE: It is recommended to note the Bodipy-laminin image name on the region of the muscle where these fibers are located on the image acquired for MyHC recognition to facilitate the later fiber-specific analysis of LDs.

6. Analysis of images

1. Analysis of the fiber-types on each muscle sample

   1. In Fiji (or ImageJ)[32], open the TIFF, PNG, or JPG file with the reconstructed muscle obtained from the merge of all the channels used to detect the fiber isoforms.

   2. To start the **Cell Counting** tool, click on **Plugins | Analyze | Cell counter | Cell counter**.

   3. On the **Cell counter** window, click on **Actions | Initialize**.

   4. Under **Counters** in the same window, select **Type 1**.

   5. On the Fiji main window, select the **Wand** tool.

   6. To quantify the number of fibers of each type, click on each fiber of the same type, so that the program records the number of fibers clicked.

   7. Once finished, select the next type of fiber and repeat the same steps.

   8. When all fibers of the image have been assigned to a given fiber type, click on **Results** on the **Cell Counter** window to display the results in a table.

   9. Save this table as a spreadsheet table by clicking on **File | Save As** on the **Results** window.

10. Save and reload the selections on the same image at any time by clicking on **Save Markers** or **Load Markers**, respectively, on the **Cell Counting** window.

2. Analysis of lipid droplets in a fiber-type-dependent manner

    1. Analyze the images of Bodipy and laminin obtained on the confocal using Fiji for the quantification of LDs.

        NOTE: The authors designed a customized macro to automatize the analysis. This macro, along with a step-by-step explanation on how to use it, is available as **Supplemental File 1** and **Supplemental File 2**, respectively.

    2. Open each image with the aid of the **Bio-Formats Importer** from Fiji. Under the **View Stack with** option, select **Hyperstack | Color mode, Default**. Make sure that the **Autoscale** window is selected.

        NOTE: The following steps will describe the protocol for the analysis of one fiber on the image, but it must be repeated as many times as the number of entire fibers appear on the image.

    3. Use the **freehand selection** tool to manually select the sarcolemma of the fiber based on the laminin channel (**Figure 4A**) and press T on the keyboard to record the selection or Region of Interest (ROI) on the **ROI** window.

    4. Go to Fiji's **main** window and click on **Analyze | Set Measurements**, and on the pop-up window, select **Area** and **Feret's diameter**. Leave the remaining boxes unchecked and other parameters as they appear by default.

    5. Click on **Measure** on the **ROI** window to obtain the Area and Minimal Feret's Diameter (MF) of the fiber selected, and note them for later use.

        NOTE: When analyzing LDs, it is important to have in mind that their size and density vary between the center and the periphery (subsarcolemmal region-SS) of the fiber. Therefore, the analysis must be done separately.

    6. Calculate the value of 1/6 of the MF to delimit the central part of the fiber.

        NOTE: In the macro, the default MF value is set to 6, which means that the reduction applied will be set as 1/6 of the MF. This value was chosen based on the empirical data obtained from the soleus of animals fed a high-fat diet. However, each researcher must change this number based on the empirical data and the muscle analyzed, the type of fiber, and the animal condition.

    7. On the **ROI** window, click on **Add** to have a duplicate of the first ROI and select the second ROI that appears on the window.

    8. On Fiji's main window, click on **Edit | Selection | Enlarge** and introduce the previously calculated value (from step 6.2.6.) with a minus sign before the number and click on **OK**. On the ROI window, click on **Add[t]** (a third ROI must appear) and **Delete**, to delete the second ROI.

        NOTE: The researcher can check the results by clicking on the **Show All** box on the **ROI** window. At this point, two ROIs must appear, one that surrounds the entire perimeter of the fiber (**Figure 4B**) and another one that is placed in the center (**Figure 4C**).

9. Select both ROIs on the **ROI** window and click on **More | XOR | Add[t]**. Wait for a third ROI to appear, which corresponds to the periphery of the fiber (**Figure 4D**).

10. Save the ROIs by clicking on **More | Save** to save the ROIs in case a later reanalysis of the same fibers is needed.

11. Select the **Bodipy channel** and open the **Threshold** tool by clicking on **Image | Adjust | Threshold** on Fiji's **main** window.

12. On the **Threshold** pop-up window, set the values to **70/255**, select **Yen | B&W method**, and click on **Dark background | Apply**.
    NOTE: The values applied on the **Threshold** may vary depending on the conditions of the experiment and the threshold must be appropriately set to optimize the analysis. A B&W window with the Bodipy signal above the threshold limit shown in white and the background in black must appear (compare the original Bodipy image in **Figure 4E** with the one in **Figure 4F**).

13. Go to Fiji's **main** window and click on **Analyze | Set Measurements** and on the pop-up window, select **Area, Area fraction,** and **Limit to threshold**. Leave the remaining boxes unchecked and other parameters as they appear by default.
    NOTE: If the researcher wants to analyze the "circularity" of LDs, which is an index of the spherical morphology that ranges from 1 for a perfect sphere to 0 for a line, click on the **Shape descriptors** box of the **Set Measurements** pop-up window.

14. Go to the **ROI** window and select the first ROI. On Fiji's **main** window, click on **Analyze | Analyze particles tool**.
    NOTE: This tool quantifies the number, size, area covered, and percentage of the total area covered by particles on each selection and saves the results as a spreadsheet file.

15. Set the values from **2** to **Infinity** (**2-Infinity**) on the **Analyze Particles** window, check the **Pixels** box, maintain the default circularity values, select **Summarize**, and click on **OK**.
    NOTE: To check the results on the fiber, under the **Show** option, select any of the available options. To have the information of each LD recognized on the selection in a table, check the **Display results** option on the **Analyze Particles** window. The results from the analysis of the total area of the fiber are averaged and summarized in a table with several columns (Count, Total Area, Average size, % Area; these correspond to the number of particles [LDs], the area occupied by these particles, their average size, and the percentage of the total area of the selection occupied by particles, respectively). To calculate the density, divide the number of particles by the total area of each selection.

16. To obtain the values of the center and the periphery of the fiber, repeat steps 6.2.14 and 6.2.15, selecting the second (center) and the third ROI (periphery) each time.

17. Save the results by clicking on **File | Save as** on the **Summary** window.
    NOTE: Include the type of fiber, the condition, and the image name on the assigned name of the results

to facilitate later unification and statistical analysis of the data. To analyze the rest of the fibers in the same image, repeat steps 6.2.3 to 6.2.17. For the statistical analysis, at least 10-15 fibers of each type must be analyzed per animal.

Representative Results

The protocol described herein provides an efficient method to easily quantify LDs in a fiber type and subcellular-specific manner. It shows how, by freezing together two muscles of similar size, such as the EDL and the soleus, the time and resources spent on the following steps are reduced by half.

A complete protocol is provided for immunostaining, image acquisition, and analysis of the different MyHC isoforms expressed in adult mouse muscles. This protocol is based on the one first designed by Schiaffino et al. in 1989[3 3], with some adjustments such as the use of an additional antibody to label laminin. This later modification is critical for the location of type IIb fibers, which will be black as they are not stained with any antibody. As shown in **Figure 5**, this immunohistochemical protocol not only permits the recognition of mouse slow-oxidative (type I and IIa) and fast-glycolytic (type IIx and IIb) fibers, but also the presence of hybrid fibers (see asterisk in **Figure 5D**). Moreover, having the cross sections of both muscles on the same slide permits the comparison of the proportions of each fiber-type between the two selected muscles, ensuring that the experimental conditions were identical on both sections.

For LD labeling, the results presented here are based on the use of Bodipy-558/568 C_{12} as a lipid dye; however, the reader is referred to an excellent protocol paper detailing the use of the classical dye Bodipy-493/503 on muscle sections[23]. The protocol presented combined the staining of LDs based on immunohistochemistry against α2-laminin to distinguish the fiber sarcolemma. As with the fiber-type experiment, this step is essential, not only for the recognition of individual fibers, but also for subsequent analysis of lipids in both the central and peripheral regions of fibers (**Figure 4**). One of the critical steps of this protocol is the identification and tagging of the same fibers on the two slides. As explained before, it is important to scan the slide with fiber types and have the reconstruction of muscle cross-sections with the merged colors before the acquisition of images for LDs (**Figure 3B**). Remarkable structures of each muscle section, such as axon twigs or muscle spindles, are good landmarks that could help the researcher locate the same fibers on both slides (**Figure 6**). Remember that because the slide is placed upside down on most confocal microscopes, it is recommended to invert the fiber-type-reconstructed image on the personal computer to facilitate the location task.

The settings described for the acquisition of Bodipy-laminin staining by confocal microscopy allow the visualization and later analysis of the size, number, and distribution of LDs from three to six fibers simultaneously (**Figure 6** and **Figure 7**). A detailed step-by-step protocol to analyze LDs with the image analysis software Fiji is also provided here. As shown in the protocol, the full analysis of each of the fibers present on an image is long and tedious. However, Fiji has the advantage of permitting the design of customized programs, called *macros*, based on the Java language. The authors designed a macro that enables the automation of the series of individual commands described above that is automatically run in a loop to analyze in a few minutes-not only each of the fibers present on an image but also a large set of images. The only input from the researcher is the manual selection of the perimeter of the fiber to be analyzed each time, the selection of the fiber

type, and the visual inspection of the resulting image after applying the threshold and quantifying the particles.

Here, the analysis of LDs in a location-dependent manner is implemented. By previously measuring the area and MF diameter of the fiber, a size-dependent (non-fixed as described by Strauss et al.[25]) reduction is applied to obtain the central and the peripheral areas of each fiber (**Figure 4** and **Figure 7**). As seen in the histograms of **Figure 7**, this method allows the quantification of three important parameters: the percentage of the fiber area occupied by LDs (**Figure 7E**), the density of LDs-the number of LDs per μm^2 (**Figure 7F**), and the average size of LDs (**Figure 7G**). As a result, in 3-month-old mice (N = 5), type IIa (green outline) and type IIx (red outline) fibers present the largest proportion of area occupied by LDs in the periphery (**Figure 7E**). With respect to the density of particles, EDL fibers always show higher density than soleus fibers independently of the subcellular location (**Figure 7F**). Finally, the average size of those LDs is always larger in the periphery than in the center (**Figure 7G**).

The different methods used by other groups to assess the accumulation of LDs in rodent skeletal muscle[34, 35] make it difficult to compare these results with those of previous studies. However, in line with the results from Komiya et al.[34], the percentage of fiber area occupied by LDs is higher in soleus type IIa and EDL type IIx fibers. Most importantly, type IIb fibers presented the lowest percentage of area occupied by LDs (**Figure 7E**, grey histograms). Since fiber type IIb is the most predominant fiber type of the EDL (75%, **Figure 5E**), these results confirm what other groups have previously described: the overall accumulation of lipids is lower in EDL than in the soleus[34, 35].

Contrary to what has been described in humans[25], and also in line with the results of Komiya et al.[34], the results presented here show that the accumulation of LDs in soleus type I fibers is relatively low. This could be explained by fiber-type interspecies differences between mice and humans[36], since the metabolic properties of human type I fibers are more similar to those of rodent type IIa and IIx, while those of human type IIx fibers are close to rodent type IIb[37]. In summary, the different techniques described here provide a reproducible, reliable, and time-efficient method to study and compare several parameters related to LDs and their distribution within the cell in a fiber type-dependent manner.

Suboptimal experiments

If the freezing procedure is not performed correctly and isopentane is not at the right temperature, **ice crystals** will form inside the fibers (**Figure 8A**). These freezing artifacts are detectable only after the histological preparation of the sample and can be recognized as holes in the fibers. For proper quantification of LDs, these artifacts must be avoided. It has been demonstrated that thawing and refreezing the muscle block appropriately can significantly reduce these artifacts[29].

Another problem is encountered when **fibers are not cut perpendicular to the longitudinal axis** (**Figure 8B**). LD quantification and comparison between fibers, muscles, or animals cannot be done when sections are not transverse. For this reason, it is essential to place the muscles correctly on the cork with the aid of a stereo microscope before freezing and have a brightfield microscope close to the cryostat. The latter will allow the researcher to find the correct alignment of the sample on the cryostat.

In some rare occasions, the **labeling of MyHC isoforms is very weak** on one or more fiber types (**Figure 8C**). If

this happens, the analysis of LDs will be incomplete. In this case, the experiment has to be repeated starting from the cutting of the muscles. Finally, **Bodipy could accumulate in the periphery of the muscle cross section** (**Figure 8D**). If this happens, the staining will be very strong on those fibers producing an artifactual result. Avoid the acquisition of images from these fibers.

Figure 2: Preparation of the samples for freezing and cryosectioning. (**A-D**) Mouse soleus and EDL muscles are dissected and placed on a cork held by a rigid plastic with a drop of OCT. (**E-G**) A stainless steel tumbler is filled with isopentane and cooled to its melting temperature in liquid nitrogen. (**H,I**) The tumbler with the cold isopentane is taken out of the liquid nitrogen, and the sample is immersed up to the bottom of the tumbler, swirling for 15 s. (**J-L**) The cork with the samples is placed on the cryostat holder disk without the plastic support, and serial transverse sections of 10 µm are directly mounted on adhesion slides. Two adjacent serial cross-sections are immediately processed for the staining of LDs and the detection of MyHCs. Abbreviations: LDs = lipid droplets; EDL = extensor digitorum longus; MyHCs = myosin heavy chain isoforms; OCT = optimum cutting temperature. Please click here to view a larger version of this figure.

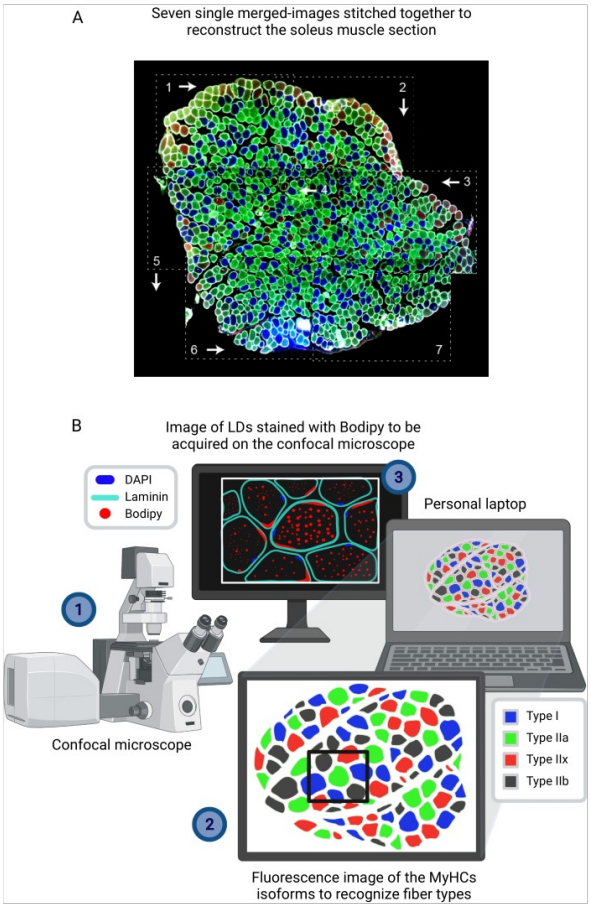

Figure 3: Bodipy image acquisition after identifying the type of fiber from the reconstructed composite image seen on another computer. (**A**) Reconstruction of the entire soleus section immunolabeled for fiber type (MyHCs) from seven independent merged images (dashed rectangles) stitched together using image processing software. The white arrows and the numbers represent the order followed during image acquistion using a conventional epifluorescence microscope. (**B**) For Bodipy image acquisition, (**1**) a field containing the muscle section immunostained with laminin-AF647 and Bodipy-555/568 is visualized on the screen of a computer connected to the confocal microscope. (**2**) Those fibers are located on the reconstructed image of the muscle section immunostained to detect the type of fibers (MyHCs). (**3**) The image is acquired using a confocal microscope. Abbreviations: LDs = lipid droplets; DAPI = 4',6-diamidino-2-phenylindole; MyHCs = myosin heavy chain isoforms. Please click here to view a larger version of this figure.

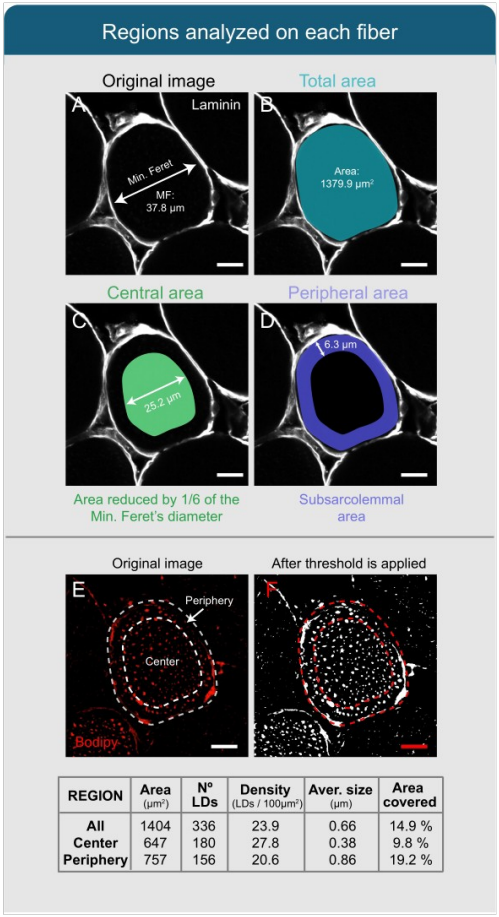

REGION	Area (µm²)	N° LDs	Density (LDs / 100µm²)	Aver. size (µm)	Area covered
All	1404	336	23.9	0.66	14.9 %
Center	647	180	27.8	0.38	9.8 %
Periphery	757	156	20.6	0.86	19.2 %

Figure 4: Analysis of lipid droplets with Fiji. (**A**,**B**) The sarcolemma of the fiber is recognized based on the laminin image and selected as the ROI. Total area and MF are measured. (**C**) To recognize the central part of the fiber, the selection is reduced by 1/6 of the value of the MF. (**D**) The area between the central and the total selection is set as the periphery or the subsarcolemmal area. (**E**) For the analysis of LDs stained with Bodipy, a threshold is applied, (**F**) and the **Analyze Particles** tool is used to quantify different parameters related to the LDs (see table). These values are obtained for the complete fiber (All), for the central part (Center), and for the subsarcolemmal area (Periphery), independently. Scale bars = 12 µm. Abbreviations: LDs = lipid droplets; ROI = region of interest; MF = Minimal Feret's diameter. Please click here to view a larger version of this figure.

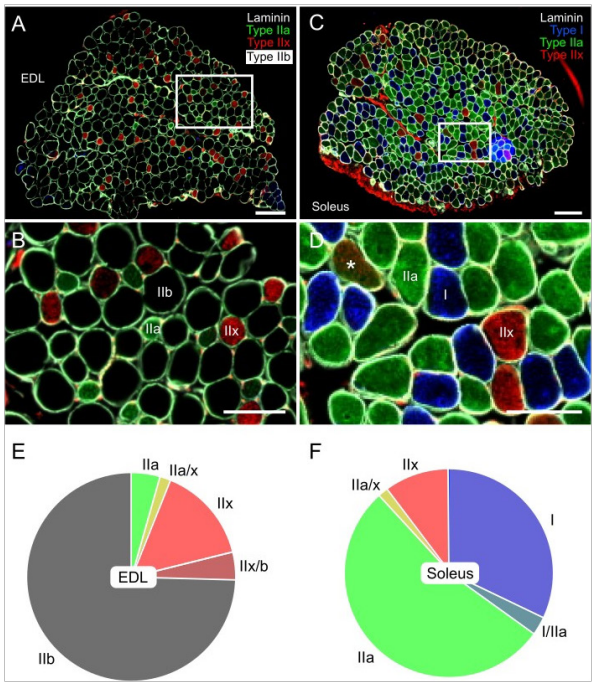

Figure 5: Representative immunostaining of fiber types in EDL (glycolytic) and soleus (oxidative) mouse muscle. Merged fluorescence images of EDL (**A**,**B**) and soleus (**C**,**D**) obtained with a digital, whole-slide fluorescence microscope. Antibodies against type I (blue-AF405), type IIa (green-AF488), type IIx (red-AF568), and laminin (white-AF647) were used. Black fibers correspond to fiber type IIb. **B** and **D** show details of the fibers inside the white rectangles of panels **A** and **C**, respectively. The asterisk (*) in panel **D** shows a IIa/IIx hybrid fiber. (**E**,**F**) Representative quantification of fiber type distribution in EDL and soleus from 3-month-old mice (N = 5). EDL was mainly composed of type IIb, then IIx, and IIa fibers (~75%, 15%, and 5%, respectively). By contrast, soleus was mainly composed of type IIa (>50%) and type I fibers (30%). The proportions of type IIx fibers were rather similar in both muscles, while those of hybrid fibers were very low. Scale bars = 200 µm (**A**,**C**), 100 µm (**B**,**D**). Abbreviation: EDL = extensor digitorum longus. Please click here to view a larger version of this figure.

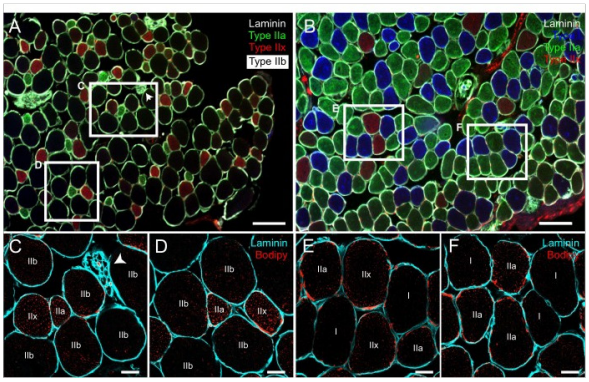

Figure 6: Representative staining of LDs with Bodipy on serial cross sections previously immunolabeled for MyHC isoforms. Fluorescence merged images of mouse EDL (**A**) and soleus (**B**) acquired using an epifluorescence microscope showing type I (blue), IIa (green), IIx (red), IIb (black) fibers, and laminin (white signal surrounding the fibers). (**C-F**) Confocal fluorescence images from the EDL (**C,D**) and the soleus (**E,F**) co-labeled with laminin (cyan) and Bodipy (red). Note that fibers shown in **C-F** are the same as those inside the white rectangles on panels **A** and **B**. On the right corner of the white rectangle in **A**, an axon twig can be distinguished (white arrowhead). Scale bars = 200 µm (**A,B**), 20 µm (**C-F**). Abbreviations: LDs = lipid droplets; EDL = extensor digitorum longus; MyHCs = myosin heavy chain isoforms. Please click here to view a larger version of this figure.

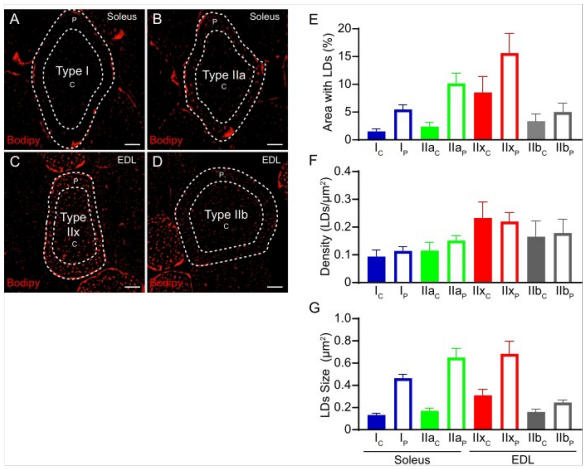

Figure 7: Quantification of LDs in a fiber-type- and subcellular-specific manner. Representative fluorescence confocal images of type I and type IIa fibers from soleus (**A**,**B**) and type IIx and type IIb fibers from EDL (**C**,**D**) obtained after co- labeling with Bodipy (red) and α2-laminin (not shown). LD content (% of the area occupied by Bodipy and density) and morphology (size) were analyzed in a subcellular-specific manner. Fiber perimeter was defined by laminin staining and the central or peripheral areas were set based on the MF diameter. Percentage of fiber area occupied by Bodipy (LDs) (**E**), LD density (number/µm^2) (**F**), or average LD size (**G**) in central or peripheral regions for each fiber type. Results are represented as mean ± SEM. Scale bars = 10 µm. Abbreviations: LDs = lipid droplets; EDL = extensor digitorum longus; C = central; P = peripheral.
Please click here to view a larger version of this figure.

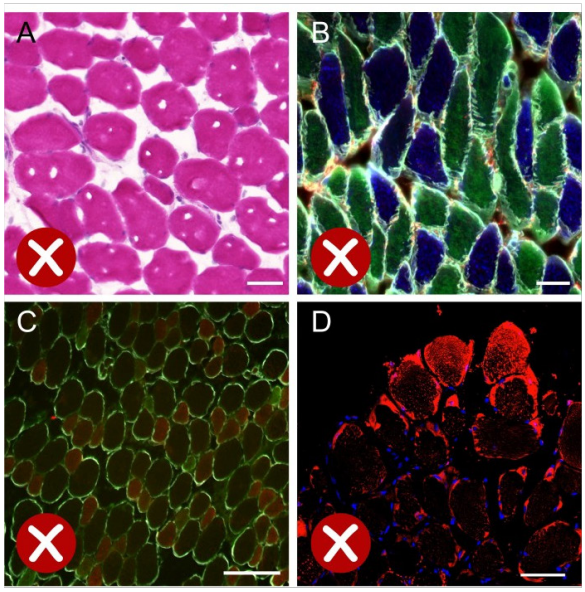

Figure 8: Images corresponding to suboptimal results. (**A**) Brightfield image of muscle cross-section stained for hematoxylin-eosin showing ice crystals formed during the freezing process. (**B**) Fluorescence merged image of a soleus section immunostained for MyHCs and laminin, showing that the majority of fibers are cut along the longitudinal axis. (**C**) Fluorescence image of an EDL section immunostained for MyHCs and laminin. The weak staining of fiber type IIa (green) hinders the correct quantification of each fiber type. (**D**) Confocal image showing a strong artifactual staining of Bodipy (red) on fibers located at the periphery of the muscle cross section. Scale bars = 50 µm (**A**,**B**), 200 µm (**C**,**D**). Abbreviations: EDL = extensor digitorum longus; MyHCs = myosin heavy chain isoforms. Please click here to view a larger version of this figure.

Supplemental Figure S1: LD staining with Oil Red O on muscle cross sections. (**A**,**B**) Confocal images showing the pattern of staining obtained with Oil Red O in the soleus and EDL, respectively. The protocol used for this staining is described in detail by Prats et al.[24]. Note that accumulation of LDs is higher in the subsarcolemmal region of the myofibers, as previously described for Bodipy. Scale bars = 20 µm. Abbreviations: LD = lipid droplet; EDL = extensor digitorum longus. Please click here to download this File.

Supplemental Figure S2: Co-staining of LDs and mitochondria in the soleus muscle. (**A**) Confocal merged image showing the immunolabeling of Tomm20, a protein

present on the mitochondrial membrane (green), DAPI (blue), and Bodipy-558/568 labeled LDs (red). The inset in **A** shows several mitochondria (green) bound to LDs (red). This image was obtained by applying Airyscan confocal superresolution microscopy. (**B**,**C**) Corresponding single-channel images of LDs and mitochondria, respectively. Scale bars = 10 µm (**A-C**), 5 µm (**A, inset**). Abbreviations: LDs = lipid droplets; DAPI = 4',6-diamidino-2-phenylindole. Please click here to download this File.

Supplemental File 1: Fiji macro for the automated analysis of LDs on multiple laminin+Bodipy images. Please click here to download this File.

Supplemental File 2: Step-by-step explanation of how to work with the macro Bodipy_JoVE.ijm. Please click here to download this File.

Discussion

The protocol detailed here describes an efficient method to quantify LDs tagged with Bodipy on a fiber-type- and subcellular-specific basis. In recent years, classical lipid dyes, such as ORO or Sudan Black B, have been substituted with a new array of cell-permeable, lipophilic, fluorescent dyes that bind to neutral lipids (e.g., Bodipy). Available as different conjugates, Bodipy has been proven very effective at tagging LDs to study their morphology, dynamics, and interaction with other organelles, not only in different fixed tissues and cells[23,38,39,40] but also in living cells[41,42].

Within the protocol, there are several critical aspects that the researcher must consider to obtain optimal results. It is essential to place the chosen muscles correctly on the cork to ensure perfect alignment and orientation of muscle myofibers, since once frozen, only slight readjustments of the holder can be made on the cryostat. Moreover, it is critical to start the immunostaining protocol immediately after the sections are cut, since air-drying cryosections (for only 15 min) has severe adverse effects on LDs, resulting in a 66% decrease in LD density and a 37% decrease in the average size[24]. Similarly, freezing and thawing the slides would have adverse effects and are therefore not recommended. A third important feature of this protocol is related to the fixation of samples. For the identification of the different MyHC isoforms with the antibodies cited here, tissue fixation must be avoided as it disrupts the binding of the chosen antibodies to their epitopes. If the muscle samples have been previously fixed, the reader is referred to a recently published paper using different antibodies[43]. Only PFA without methanol is recommended for the labeling and quantification of LDs, because the use of methanol or acetone disrupts the morphology of LDs[23,44]. Furthermore,a permeabilization step is not necessary for the quantification of LDs on slides immunolabeled with laminin. Since some groups have shown that permeabilization with detergents such as TritonX-100, saponin, or glycine can reduce the size or number of LDs[44,45], permeabilization is highly discouraged. Finally, the fine-tuning of the confocal microscope settings is crucial to recognize only the neutral lipids present in LDs and not those in membranes of other organelles[24].

Here, Bodipy-558/568 C_{12} was used as a LD marker. However, the most frequently Bodipy used for tagging LDs and studying their morphology and location within the skeletal muscle myofibers is Bodipy-493/503. Both dyes are similar in their incubation time, working concentration, and their narrow emission spectra, although their excitation and emission ranges are slightly different. For a complete protocol on the use of Bodipy-493/503, the reader is referred to the work of Listenberger and Brown[46] or Spangenburg et al.[23]. Bodipy-558/568 C_{12} has been used

for staining LDs in other tissues such as adipose tissue[47], degenerating retina[48], fibrotic kidneys[49], or fibroblasts[50]. This Bodipy yields a similar staining to the one obtained with ORO (see **Supplemental Figure S1**) but with considerably less technical burden and more specificity[24, 51]. Moreover, Bodipy-558/568 C_{12} has the advantage of enabling the quantification of LDs in combination with the detection of proteins or organelles tagged with a green-spectrum secondary antibody (see **Supplemental Figure S2** and Yan et al.[49]) or with GFP-genetically modified models[52]. These two applications are very powerful tools to unravel the dynamics and interactions of LDs with other cell organelles and proteins. Nevertheless, when no colabeling of proteins within the cells is intended, the authors recommend the use of the best-characterized LD dye Bodipy-493/503.

One of the limitations of this protocol is related to the acquisition of images and the quantification of LD morphological characteristics. Technological advances in confocal laser scanning microscopy have greatly improved the plane resolution compared with wide-field microscopes and permit 3D reconstruction of objects when scanning the sample in the Z plane. This has been very useful for the study of LD morphology[24] and interaction with other proteins in skeletal myofibers[38, 53], but has increased the image acquisition and processing time, since each 3D-reconstructed image is composed of several independent 2D images. In the above protocol, confocal images were acquired with a 40x objective lens and only in 2D. This method allows the acquisition of three to six myofibers per image instead of only one as it would be when using a 63x objective. This results in lower resolution and an overall estimation of the LD size and morphology that is not completely accurate. Nevertheless, it permits the analysis of a greater number of fibers per sample, which is also an important fact to consider, especially in animal experiments, in which a high number of muscles and conditions must be compared.

Here, it is shown that, by freezing two muscles of similar size that are adjacent to each other[34], the processing time of the samples is considerably decreased, and possible artifactual differences derived from their independent processing are reduced. Moreover, this method of analyzing LDs takes into consideration the differences between the subcellular distribution of LDs within and among fiber types[54]. Selecting the perimeter of the myofiber and reducing this selection in relation to the fiber's Minimal Feret's diameter facilitates the study of the size and density of central and peripheral (subsarcolemmal) LDs independently. Applying this method is extremely important since it has been demonstrated that the subsarcolemmal accumulation of LDs directly contributes to insulin resistance. While some reports in humans have studied LDs in a fiber type- and location-dependent fashion[11, 16, 25], this is the first time, to our knowledge, that this method has been applied to muscles from rodents. Moreover, the quantification of LDs with the aid of a self-designed macro for Fiji significantly reduced and simplified the image analysis time. Both the macro and a step-by-step explanation on how to use it are available as **Supplemental File 1** and **Supplemental File 2**, respectively.

Overall, the authors consider that the protocol described herein could be a useful tool for other researchers studying lipid metabolism in skeletal muscle. The techniques explained may be applied to different muscles and under distinct conditions (fasted/overfed, trained/sedentary, young/aged, lean/obese) and will hopefully help to better comprehend the dynamics of LDs, the importance of their interactions with other components of the cell, how lipids are stored and

metabolized in glycolytic and oxidative fibers, and their role in the onset of insulin resistance in type 2 diabetes.

Disclosures

The authors have no conflicts of interest to declare.

Acknowledgments

This work was supported by grants from the *Fonds National de la Recherche Scientifique* (FNRS-Crédit de Recherche J.0022.20) and the *Société Francophone du Diabète* (SFD-Roche Diabetes Care).C.M.S. is the recipient of a Ph.D. fellowship from the FRIA (FNRS). M.A.D.-L.d.C. received a fellowship from the Wallonie-Bruxelles International Excellence Program.

The authors thank Alice Monnier for her contribution to the development of this protocol and Caroline Bouzin for her expertise and technical help in the image acquisition process. We also thank the 2IP-IREC imaging platform for access to the cryostat and the microscopes (2IP-IREC Imaging Platform, Institute of Experimental and Clinical Research, Université Catholique de Louvain, 1200 Brussels, Belgium). Finally, the authors would like to thank Nicolas Dubuisson, Romain Versele, and Michel Abou-Samra for constructive criticism of the manuscript. Some of the figures of these article were created with BioRender.com.

References

1. Correa-de-Araujo, R. et al. Myosteatosis in the context of skeletal muscle function deficit: an interdisciplinary workshop at the National Institute on Aging. *Frontiers in Physiology.* **11**, 963 (2020).
2. Miljkovic, I. et al. Greater skeletal muscle fat infiltration is associated with higher all-cause and cardiovascular mortality in older men. *Journals of Gerontology Series A: Biomedical Sciences and Medical Sciences.* **70** (9), 1133-1140 (2015).
3. Nachit, M. et al. Myosteatosis rather than sarcopenia associates with non-alcoholic steatohepatitis in non-alcoholic fatty liver disease preclinical models. *Journal of Cachexia, Sarcopenia, and Muscle.* **12** (1), 144-158 (2021).
4. Aleixo, G. F. P. et al. Myosteatosis and prognosis in cancer: Systematic review and meta-analysis. *Critical Reviews in Oncology/Hematolgoy.* **145**, 102839 (2020).
5. Gemmink, A., Schrauwen, P., Hesselink, M. K. C. Exercising your fat (metabolism) into shape: a muscle-centred view. *Diabetologia.* **63** (8), 1453-1463 (2020).
6. van Loon, L. J. Use of intramuscular triacylglycerol as a substrate source during exercise in humans. *Journal of Applied Physiology.* **97** (4), 1170-1187 (2004).
7. Coen, P. M., Goodpaster, B. H. Role of intramyocelluar lipids in human health. *Trends in Endocrinology and Metabolism.* **23** (8), 391-398 (2012).
8. Seibert, J. T., Najt, C. P., Heden, T. D., Mashek, D. G., Chow, L. S. Muscle lipid droplets: cellular signaling to exercise physiology and beyond. *Trends in Endocrinology and Metabolism.* **31** (12), 928-938 (2020).
9. Bergman, B. C., & Goodpaster, B. H. Exercise and muscle lipid content, composition, and localization: influence on muscle insulin sensitivity. *Diabetes.* **69** (5), 848-858 (2020).
10. Nielsen, J., Christensen, A. E., Nellemann, B., Christensen, B. Lipid droplet size and location in human skeletal muscle fibers are associated with insulin sensitivity. *American Journal of Physiology-*

Endocrinology and Metabolism. **313** (6), E721-E730 (2017).

11. Covington, J. D. et al. Intramyocellular lipid droplet size rather than total lipid content is related to insulin sensitivity after 8 weeks of overfeeding. *Obesity (Silver Spring).* **25** (12), 2079-2087 (2017).
12. Bosma, M. Lipid droplet dynamics in skeletal muscle. *Experimental Cell Research.* **340** (2), 180-186 (2016).
13. Nielsen, J. et al. Increased subsarcolemmal lipids in type 2 diabetes: effect of training on localization of lipids, mitochondria, and glycogen in sedentary human skeletal muscle. *American Journal of Physiology-Endocrinology and Metabolism.* **298** (3), E706-713 (2010).
14. Ferreira, R. et al. Subsarcolemmal and intermyofibrillar mitochondria proteome differences disclose functional specializations in skeletal muscle. *Proteomics.* **10** (17), 3142-3154 (2010).
15. Barrett, J. S., Whytock, K. L., Strauss, J. A., Wagenmakers, A. J. M., Shepherd, S. O. High intramuscular triglyceride turnover rates and the link to insulin sensitivity: influence of obesity, type 2 diabetes and physical activity. *Applied Physiology, Nutrition and Metabolism.* 1-14 (2022).
16. Daemen, S. et al. Distinct lipid droplet characteristics and distribution unmask the apparent contradiction of the athlete's paradox. *Molecular Metabolism.* **17**, 71-81 (2018).
17. Bredella, M. A., Ghomi, R. H., Thomas, B. J., Miller, K. K., Torriani, M. Comparison of 3.0 T proton magnetic resonance spectroscopy short and long echo-time measures of intramyocellular lipids in obese and normal-weight women. *Journal of Magnetic Resonance Imaging.* **32** (2), 388-393 (2010).
18. Schrauwen-Hinderling, V. B., Hesselink, M. K., Schrauwen, P., Kooi, M. E. Intramyocellular lipid content in human skeletal muscle. *Obesity (Silver Spring).* **14** (3), 357-367 (2006).
19. De Bock, K. et al. Evaluation of intramyocellular lipid breakdown during exercise by biochemical assay, NMR spectroscopy, and Oil Red O staining. *American Journal of Physiology-Endocrinology and Metabolism.* **293** (1), E428-434 (2007).
20. Koopman, R., Schaart, G., Hesselink, M. K. Optimisation of oil red O staining permits combination with immunofluorescence and automated quantification of lipids. *Histochemistry and Cell Biology.* **116** (1), 63-68 (2001).
21. Gueugneau, M. et al. Skeletal muscle lipid content and oxidative activity in relation to muscle fiber type in aging and metabolic syndrome. *Journal of Gerontology Series A: Biomedical Sciences and Medical Sciences.* **70** (5), 566-576 (2015).
22. Gemmink, A. et al. Super-resolution microscopy localizes perilipin 5 at lipid droplet-mitochondria interaction sites and at lipid droplets juxtaposing to perilipin 2. *Biochimica et Biophysica Acta-Molecular and Cell Biology of Lipids.* **1863** (11), 1423-1432 (2018).
23. Spangenburg, E. E., Pratt, S. J. P., Wohlers, L. M., Lovering, R. M. Use of BODIPY (493/503) to visualize intramuscular lipid droplets in skeletal muscle. *Journal of Biomedicine and Biotechnology.* 598358 (2011).
24. Prats, C. et al. An optimized histochemical method to assess skeletal muscle glycogen and lipid stores reveals two metabolically distinct populations of type I muscle fibers. *PLoS One.* **8** (10), e77774 (2013).

25. Strauss, J. A., Shepherd, D. A., Macey, M., Jevons, E. F. P., Shepherd, S. O. Divergence exists in the subcellular distribution of intramuscular triglyceride in human skeletal muscle dependent on the choice of lipid dye. *Histochemistry and Cell Biology*. **154** (4), 369-382 (2020).

26. Shepherd, S. O. et al. Sprint interval and traditional endurance training increase net intramuscular triglyceride breakdown and expression of perilipin 2 and 5. *Journal of Physiology*. **591** (3), 657-675 (2013).

27. Whytock, K. L. et al. A 7-day high-fat, high-calorie diet induces fibre-specific increases in intramuscular triglyceride and perilipin protein expression in human skeletal muscle. *Journal of Physiology*. **598** (6), 1151-1167 (2020).

28. Wang, C., Yue, F., Kuang, S. Muscle histology characterization using h&e staining and muscle fiber type classification using immunofluorescence staining. *Bio-Protocol*. **7** (10) (2017).

29. Meng, H. et al. Tissue triage and freezing for models of skeletal muscle disease. *Journal of Visualized Experiments: JoVE*. (89) (2014).

30. Kumar, A., Accorsi, A., Rhee, Y., Girgenrath, M. Do's and don'ts in the preparation of muscle cryosections for histological analysis. *Journal of Visualized Experiments: JoVE*. (99), e52793 (2015).

31. Leiva-Cepas, F. et al. Laboratory methodology for the histological study of skeletal muscle. *Archivos de Medicina del Deporte*. **35** (186), 254-262 (2018).

32. Schindelin, J. et al. Fiji: an open-source platform for biological-image analysis. *Nature Methods*. **9** (7), 676-682 (2012).

33. Schiaffino, S. et al. Three myosin heavy chain isoforms in type 2 skeletal muscle fibres. *Journal of Muscle Research & Cell Motility*. **10** (3), 197-205 (1989).

34. Komiya, Y. et al. Mouse soleus (slow) muscle shows greater intramyocellular lipid droplet accumulation than EDL (fast) muscle: fiber type-specific analysis. *Journal of Muscle Research & Cell Motility*. **38** (2), 163-173 (2017).

35. Andrich, D. E. et al. Altered lipid metabolism impairs skeletal muscle force in young rats submitted to a short-term high-fat diet. *Frontiers in Physiology*. **9**, 1327 (2018).

36. Schiaffino, S. Fibre types in skeletal muscle: a personal account. *Acta Physiologica*. **199** (4), 451-463 (2010).

37. Bloemberg, D., Quadrilatero, J. Rapid determination of myosin heavy chain expression in rat, mouse, and human skeletal muscle using multicolor immunofluorescence analysis. *PLoS One*. **7** (4), e35273 (2012).

38. Gemmink, A. et al. Decoration of intramyocellular lipid droplets with PLIN5 modulates fasting-induced insulin resistance and lipotoxicity in humans. *Diabetologia*. **59** (5), 1040-1048 (2016).

39. Askinas, C. et al. in *Biophotonics Congress: Biomedical Optics Congress 2018 (Microscopy/Translational/Brain/ OTS)*. JTu3A.4 (Optical Society of America) (2018).

40. Morén, B. et al. EHD2 regulates adipocyte function and is enriched at cell surface-associated lipid droplets in primary human adipocytes. *Molecular Biology of the Cell*. **30** (10), 1147-1159 (2019).

41. Benador, I. Y. et al. Mitochondria bound to lipid droplets have unique bioenergetics, composition, and dynamics that support lipid droplet expansion. *Cell Metabolism*. **27** (4), 869-885.e866 (2018).

42. de la Rosa Rodriguez, M. A. et al. Hypoxia-inducible lipid droplet-associated induces DGAT1 and promotes lipid storage in hepatocytes. *Molecular Metabolism.* **47**, 101168 (2021).

43. Jevons, E. F. P., Gejl, K. D., Strauss, J. A., Ørtenblad, N., Shepherd, S. O. Skeletal muscle lipid droplets are resynthesized before being coated with perilipin proteins following prolonged exercise in elite male triathletes. *American Journal of Physiology-Endocrinology and Metabolism.* **318** (3), E357-E370, (2020).

44. Ohsaki, Y., Maeda, T., Fujimoto, T. Fixation and permeabilization protocol is critical for the immunolabeling of lipid droplet proteins. *Histochemistry and Cell Biology.* **124** (5), 445-452 (2005).

45. Prats, C. et al. Decrease in intramuscular lipid droplets and translocation of HSL in response to muscle contraction and epinephrine. *Journal of Lipid Research.* **47** (11), 2392-2399 (2006).

46. Listenberger, L. L., Brown, D. A. Fluorescent detection of lipid droplets and associated proteins. *Current Protocols in Cell Biology.* **Chapter 24** (Unit 24.22) (2007).

47. Xue, Y., Lim, S., Bråkenhielm, E., Cao, Y. Adipose angiogenesis: quantitative methods to study microvessel growth, regression and remodeling in vivo. *Nature Protocols.* **5** (5), 912-920 (2010).

48. Muliyil, S. et al. ADAM17-triggered TNF signalling protects the ageing Drosophila retina from lipid droplet-mediated degeneration. The *EMBO Journal.* **39** (17), e104415 (2020).

49. Yan, Q. et al. Autophagy activation contributes to lipid accumulation in tubular epithelial cells during kidney fibrosis. *Cell Death Discovery.* **4**, 2 (2018).

50. Coassin, S. et al. Investigation and functional characterization of rare genetic variants in the adipose triglyceride lipase in a large healthy working population. *PLoS Genetics.* **6** (12), e1001239 (2010).

51. Daemen, S., van Zandvoort, M., Parekh, S. H., Hesselink, M. K. C. Microscopy tools for the investigation of intracellular lipid storage and dynamics. *Molecular Metabolism.* **5** (3), 153-163 (2016).

52. Chen, Q. et al. Rab8a deficiency in skeletal muscle causes hyperlipidemia and hepatosteatosis by impairing muscle lipid uptake and storage. *Diabetes.* **66** (9), 2387-2399 (2017).

53. Gemmink, A. et al. Decoration of myocellular lipid droplets with perilipins as a marker for in vivo lipid droplet dynamics: A super-resolution microscopy study in trained athletes and insulin resistant individuals. *Biochimica et Biophysica Acta (BBA)-Molecular and Cell Biology of Lipids.* **1866** (2), 158852 (2021).

54. Bergman, B. C., Hunerdosse, D. M., Kerege, A., Playdon, M. C., Perreault, L. Localisation and composition of skeletal muscle diacylglycerol predicts insulin resistance in humans. *Diabetologia.* **55** (4), 1140-1150 (2012).

ANNEX 3

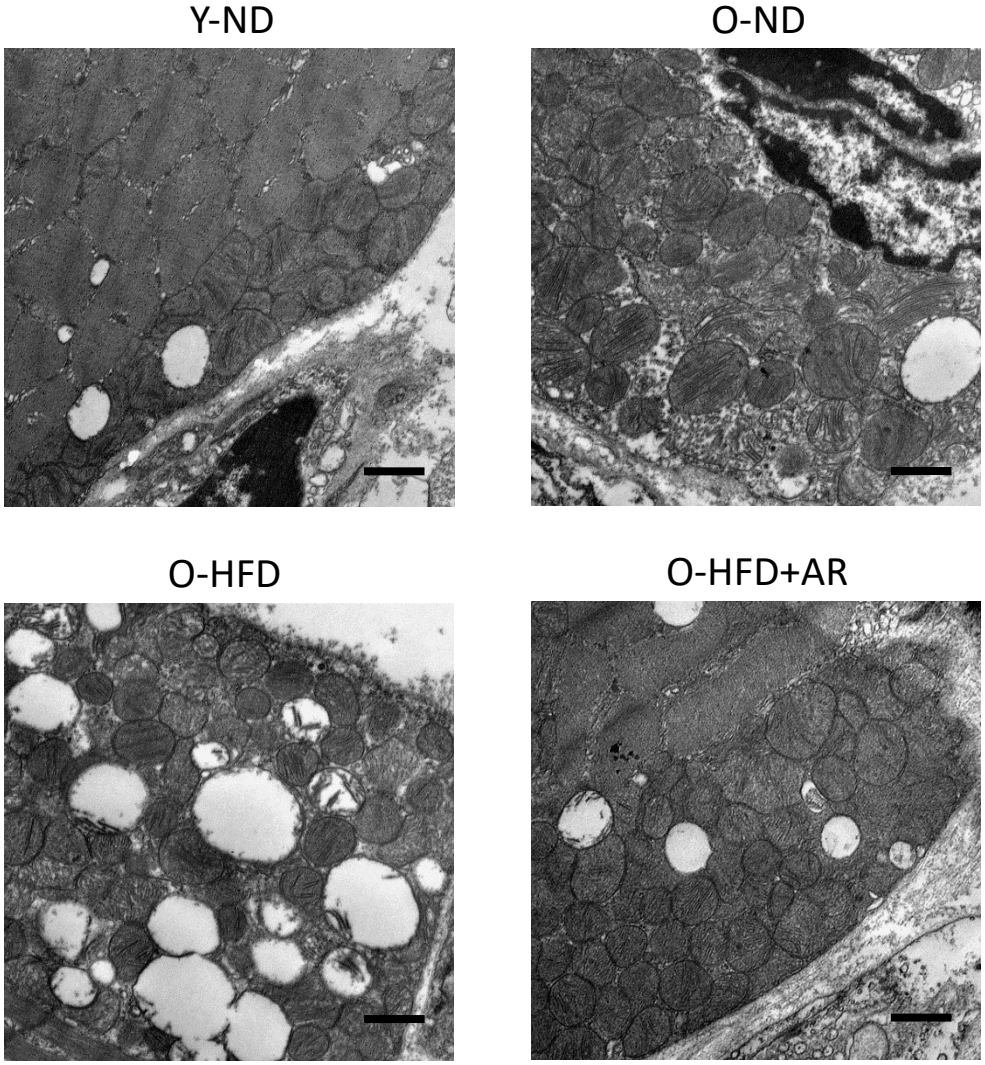

Annex 3. Uncolored transmission electron micrographs of mitochondria in the subsarcolemmal region of rectus femoris in the 4 groups of mice of Study 1. Representative images of each group are shown. Scale bar = 1 µm.